




12-2023

The Identification of Small Molecule Inhibitors to *Candida albicans* Phosphatidylserine Synthase

Yue Zhou

University of Tennessee, Knoxville, yzhou58@vols.utk.edu

Follow this and additional works at: https://trace.tennessee.edu/utk_graddiss

 Part of the [Biochemistry Commons](#), [Molecular Biology Commons](#), [Pathogenic Microbiology Commons](#), and the [Structural Biology Commons](#)

Recommended Citation

Zhou, Yue, "The Identification of Small Molecule Inhibitors to *Candida albicans* Phosphatidylserine Synthase. " PhD diss., University of Tennessee, 2023.
https://trace.tennessee.edu/utk_graddiss/9164

This Dissertation is brought to you for free and open access by the Graduate School at TRACE: Tennessee Research and Creative Exchange. It has been accepted for inclusion in Doctoral Dissertations by an authorized administrator of TRACE: Tennessee Research and Creative Exchange. For more information, please contact trace@utk.edu.

To the Graduate Council:

I am submitting herewith a dissertation written by Yue Zhou entitled "The Identification of Small Molecule Inhibitors to *Candida albicans* Phosphatidylserine Synthase." I have examined the final electronic copy of this dissertation for form and content and recommend that it be accepted in partial fulfillment of the requirements for the degree of Doctor of Philosophy, with a major in Microbiology.

Todd B. Reynolds, Major Professor

We have read this dissertation and recommend its acceptance:

Barry D. Bruce, Elizabeth M. Fozo, Erik R. Zinser

Accepted for the Council:

Dixie L. Thompson

Vice Provost and Dean of the Graduate School

(Original signatures are on file with official student records.)

**The Identification of Small Molecule Inhibitors to *Candida albicans*
Phosphatidylserine Synthase**

**A Dissertation Presented for the
Doctor of Philosophy
Degree
The University of Tennessee, Knoxville**

**Yue Zhou
December 2023**

Copyright © 2023 by Yue Zhou
All rights reserved.

DEDICATION

This dissertation is dedicated to my wife, Yiqun (Yuki) Liu. I can't do it without you. I want to quote this poem from over 2,000 years ago for you:

“山无陵，江水为竭，冬雷震震，夏雨雪，天地合，乃敢与君绝”

"Only when mountains have no peaks, rivers run dry, thunder rumbles in winter, snow falls in summer, and heaven and earth become one, would I part from you."

ACKNOWLEDGMENTS

Firstly, I'd like to express my deep gratitude to my Ph.D. mentor, Dr. Todd Reynolds. I can't remember how many times I stumbled and fell in research, or just had a terrible day, you always encouraged me and showed your kindness so I could move on. Your guidance, patience, and insight throughout my Ph.D. journey are invaluable to me, and I'm spoiled for having a PI like you. Being a member of your team has been a privilege that I'll always cherish. I'm also grateful for the research opportunities, conference trips, and the freedom to explore my research ideas. Also, thank you for always pointing me to the right person for help. My Ph.D. project would not be so successful without any of the collaborations. A special thanks to Dr. Barry Bruce and my go-to Ph.D. advisor when I need advice in biochemistry experiments. I remember being in your office twice a week when I started to deal with detergents. Your availability for insightful discussions, as well as consistent advice, have been pivotal, which made me a proud membrane biochemist today. I'm also grateful to Dr. Elizabeth Fozo and Dr. Erik Zinser for being my doctoral committee members. Your invaluable guidance and insights helped me re-think the Chol project left by Chelsi and push it in my own direction. To Dr. Melanie Ohi, thank you for accommodating me in your lab for the whole summer of 2022, this experience has sparked my interest in pursuing a career in the field of structural biology and potentially becoming a structural biologist in the future.

I'm grateful to all my lab-mates, past and current, for being such an incredible group. Starting with the senior ones, I would like to thank Dr. Tian Chen and Dr. Bob Tams for helping me familiarize the lab during my rotation, and for being role models in doing research. Andy Wagner, I will always thank you for the questions that helped me

think through my experiments and projects. We both like to push each other to the limit, and that's what is needed to be a great scientist. Big thanks to Elise Philips for being so considerate and kind, and always showing optimism when things do not go well. To new people in the lab, Jordan Cannon, Ainsley King, Jemma McLeish and Mikayla Mangrum, I really appreciate your help and support for the projects. Science thrives on teamwork, and our lab was blessed with a cooperative and helpful bunch. Outside our lab, I would like to thank Dr. Jeff Rybak and Greg Phelps. The drug screening project worked so well because of your input. Also, to folks in the Ohi lab at the University of Michigan, thank you for leading my way into structure biology.

To all my friends outside academia, thank you for bringing laughter into daily life and for spotting me during the workouts. My "Big Three" exercises (bench, deadlift and squat) can't exceed 1,200 lbs. without your support. Special thanks to my wife, Yuki. I do not think a simple "Thank you" is enough, and to be honest, I owe at least half of this dissertation to you. You always made sure that I was not hungry after extensive experiments and that I was mentally healthy during these five tough years. Sorry for making you a "protein purification widow" and "PS synthase assay widow", and I feel blessed that you do understand experiments and science take time. Also, a big thanks to my parents, as well as Charlie Wagner (a cute little corgi), for the emotional support throughout these years. You made me who I am today.

ABSTRACT

Candida albicans phosphatidylserine (PS) synthase, encoded by the *CHO1* gene, has been identified as a potential drug target for new antifungals against systemic candidiasis due to its importance in virulence, absence in the host and conservation among fungal pathogens. This dissertation is focused on the identification of inhibitors for this membrane enzyme. Cho1 has two substrates: cytidyldiphosphate-diacylglycerol (CDP-DAG) and serine. Previous studies identified a conserved CDP-alcohol phosphotransferase (CAPT) binding motif present within Cho1, and here we revealed that mutations in all but one conserved amino acid within the CAPT motif resulted in decreased Cho1. For serine, we have predicted a serine-binding site based on sequence alignment and found that some of the residues in this putative serine-binding site are required for Cho1 function. One residue, R189, is particularly interesting because it was suggested to be involved in serine binding.

Then, we attempted to perform a small molecule screening on *C. albicans* Cho1, which will be facilitated by purified Cho1 protein. Due to the transmembrane nature, several solubilizing reagents were used to solubilize Cho1 protein. Digitonin was determined to be the best detergent as it retained the most PS synthase activity. Pull-downs of HA-tagged Cho1 in the digitonin-solubilized fraction reveal an apparent MW of Cho1 consistent with a hexamer. Biochemical and electron microscopy analysis suggest that the hexamer is composed of a trimer of dimers. Cho1 protein was then purified to near-homogeneity as a hexamer and was optimized for high activity to be used in the small drug screening.

For the screening, we developed a nucleotidase-coupled malachite green-based screen against purified Cho1. Over 7,300 molecules curated from repurposing chemical libraries were interrogated in primary and dose-responsivity assays using this platform, and seven compounds were identified to inhibit purified Cho1. Among all, compound CBR-5884 disrupted *in vivo* Cho1 function by inducing phenotypes consistent with the *cho1ΔΔ* mutant, including a reduction of cellular PS levels. Kinetic curves and computational docking suggest that CBR-5884 competes with serine for binding of Cho1 with a K_i of $1,550 \pm 245.6$ nM, thus this compound has the potential for further drug design.

TABLE OF CONTENTS

CHAPTER 1 MEMBRANE ENZYMES AS ANTIFUNGAL TARGETS	1
Introduction.....	2
Cell wall biosynthesis enzymes	3
Cell membrane biosynthesis enzymes	12
Summary.....	35
References.....	36
CHAPTER 2 MAPPING THE SUBSTRATE-BINDING SITES IN THE PHOSPHATIDYLSERINE SYNTHASE IN <i>CANDIDA ALBICANS</i>	52
Publication Note.....	53
Abstract.....	54
Introduction.....	55
Materials and Methods.....	61
Results.....	76
Discussion.....	97
Conflict of Interest	101
Acknowledgements.....	101
References.....	102
Supplementary Figures	107
CHAPTER 3 SOLUBILIZATION, PURIFICATION, AND CHARACTERIZATION OF THE HEXAMERIC FORM OF PHOSPHATIDYLSERINE SYNTHASE FROM <i>CANDIDA ALBICANS</i>	112
Publication Note.....	113
Abstract.....	114
Introduction.....	115
Results.....	119
Discussion.....	142
Experimental Procedures	145
Acknowledgments.....	156
References.....	157
Supplementary Figures	163
CHAPTER 4 IDENTIFICATION OF SMALL MOLECULE INHIBITORS TO <i>CANDIDA ALBICANS</i> PHOSPHATIDYLSERINE SYNTHASE VIA A TARGET- BASED SCREEN.....	170
Abstract.....	172
Introduction.....	173
Results.....	176
Discussion.....	195
Materials and Methods.....	199
References.....	210
Supplementary Figures	218
CHAPTER 5 FUTURE DIRECTIONS	225
Introduction.....	226
Conclusion	236

APPENDIX RECONSTITUTION OF PURIFIED HEXAMERIC CHO1 FROM
CANDIDA ALBICANS INTO LIPID NANODISC FOR STRUCTURE

DETERMINATION	237
Introduction.....	239
Method	239
Results and Discussion	240
VITA.....	245

LIST OF TABLES

Table 1.1. Potential phospholipid biosynthesis enzymes as drug targets and inhibitors. .	31
Table 2.1 The CAPT motif for binding CDP-alcohols is mostly conserved across domains	58
Table 2.2. Strains produced in this study	62
Table 2.3. Plasmids Used in this Study.....	64
Table 2.4 Primers Used in this Study.....	67
Table 2.5. Normalized densitometry values (NDVs) via western blotting for CAPT motif (left) and serine binding motif (right) mutants.....	73
Table 2.6 The k_{cat} , K_M and k_{cat}/K_M of HA1, L184A and R189A for both serine and CDP- DAG	94
Table 3.1. Strains used and produced in this study	146
Table 3.2. Primers used in this study	148
Table 4.1. Primers used in this study	201

LIST OF FIGURES

Figure 1.1. The interaction between nikkomycin Z and <i>Phytophthora sojae</i> Chs1.	7
Figure 1.2. Bind models of UDP-GlcNAc, Nikkomycin Z and Polyoxin D to <i>CaChs2</i>	8
Figure 1.3. Chemical structures of the three FDA-approved echinocandins.....	11
Figure 1.4. Structural interpretation of echinocandin-resistant mutations in <i>ScFKS1</i> structure.....	13
Figure 1.5 Binding of itraconazole to <i>S. cerevisiae</i> Erg11.	15
Figure 1.6. Binding model of terbinafine to squalene epoxidase.	18
Figure 1.7. <i>De novo</i> synthesis of sphingolipids in <i>S. cerevisiae</i> and known inhibitors targeting each enzyme.....	22
Figure 1.8. The active site of ceramide synthase is depicted in a model that illustrates how FB ₁ (right) mimics both the sphingoid base and the fatty acyl-CoA substrates (left).....	25
Figure 1.9. Phospholipid biosynthesis pathways for <i>C. albicans</i> (A) and mammals/parasites (B).....	28
Figure 2.1 Expression and activity of Cho1-HAx3 under the <i>ENO1</i> promoter.....	78
Figure 2.2. Most conserved CAPT mutants displayed defects in ethanolamine-dependent growth.	80
Figure 2.3. Most of the conserved CAPT motif residues are required for PS synthase activity.....	83
Figure 2.4. CAPT mutant G129P and R133E displayed decreased Cho1 function.....	84
Figure 2.5. Sequence alignment reveals a possible serine binding motif.....	86
Figure 2.6. Mutations in the putative serine binding site reduce <i>in vivo</i> Cho1 function ..	88
Figure 2.7. Enzyme activity decreases in some putative serine binding site mutants	90
Figure 2.8. Michaelis-Menten kinetics showed decreased serine binding capacity of R189A.....	92
Figure 2.9. Location of CDP-DAG and putative serine binding residues on a predicted structure of Cho1 based on homology modeling.....	96
Figure S2.1. The 36 kDa and 29 kDa band of Cho1 protein contains phosphorylated population.	108
Figure S2.2. The elevated growth of L184A is not due to a spurious mutation.	109
Figure S2.3. Alignment of CAPT motifs from <i>S. cerevisiae</i> Cpt1 and <i>C. albicans</i> Cho1	110
Figure S2.4. Alignment of several previously reviewed PS synthase with PI synthase sequences from different species reveals part of the putative serine binding site in <i>C.</i> <i>albicans</i> Cho1.....	111
Figure 3.1. Solubilization of HAx3-tagged Cho1 using six popular non-ionic detergents.	120
Figure 3.2. Optimization of digitonin, DDM and styrene maleic acid (SMA) 2000 for solubilization and activity.....	123
Figure 3.3. The solubilized native Cho1 complex appears to be a hexamer.	126
Figure 3.4. His-, GST- and MBP-tagged Cho1 construct express active enzyme.....	131
Figure 3.5. Tag-free hexameric Cho1 was purified to homogeneity using affinity chromatography and AcTEV treatment.....	133

Figure 3.6. Effects of temperature, manganese concentration, pH and detergents on purified hexameric Cho1 enzyme activity.	135
Figure 3.7. Kinetic curves suggest a cooperative serine binding in the purified hexameric Cho1.	137
Figure 3.8. Hexameric Cho1 is likely made of a trimer of dimers.	139
Figure S3.1. HAx3-tagged Cho1 protein was solubilized in SMA1000, 2000 and 3000164	
Figure S3.2. BN-PAGE of the pulled-down HAx3-tagged Cho1 protein from the solubilized fractions.	165
Figure S3.3. BN-PAGE gel of cobalt resin flowthrough (FT), washes 1, 2, & 3, and elutions 1, 2, & 3.....	166
Figure S3.4. Data processing pathway for the negative staining TEM of the Cho1 micelles.	167
Figure S3.5. The structure prediction model of the Cho1 dimer using AlphaFold2	168
Figure S3.6. Superposition of AlphaFold2-predicted Cho1 structure with <i>Methanocaldococcus jannaschii</i> PS synthase structure.....	169
Figure 4.1. A malachite-green-based nucleotidase-coupled assay measures the activity of purified Cho1 protein.....	178
Figure 4.2. Seven Cho1-specific inhibitors were identified from the high-throughput malachite green screen.....	180
Figure 4.3. Ebselen, LOC14 and CBR-5884 inhibited cell growth of <i>C. albicans</i>	183
Figure 4.4. Ethanolamine supplementation can mitigate the inhibitory impact of CBR-5884.....	185
Figure 4.5 CBR-5884 interferes with <i>in vivo</i> PS synthesis.....	188
Figure 4.6 CBR-5884 may function as a competitive inhibitor occupying the serine binding site of Cho1.....	192
Figure S4.1. Dose-response curve of AB-680 compound..	219
Figure S4.2. Avasimibe, tideglusib and CBR-5884 precipitated at high concentrations220	
Figure S4.3. The PS synthase activity of crude membrane containing Cho1 was measured b in the presence of different inhibitors at 1 mM.....	221
Figure S 4.4. Superposition of <i>C. albicans</i> AlphaFold Cho1 model with <i>Methanocaldococcus jannaschii</i> PS synthase222	
Figure S4.5. Overlay of ligand interactions between top five poses of CBR-5884 with <i>C. albicans</i> AlphaFold Cho1 model.	223
Figure S4.6. Growth curve of wildtype and <i>cho1ΔΔ</i> <i>C. albicans</i> strains in YPD	224
Figure A1. Purified Cho1 was successfully reconstituted into lipid nanodisc.	241
Figure A2. Purified Cho1-filled nanodiscs showed high homogeneity	243
Figure A3. Enzyme activity of Cho1 in the micelle form and Cho1 in the lipid nanodiscs measured by malachite green.....	244

CHAPTER 1 MEMBRANE ENZYMES AS ANTIFUNGAL TARGETS

Introduction

Over the past three decades, systemic fungal infections in humans, primarily caused by *Candida* species, have surged due to a rise in immunocompromised patients (1-3). *Candida* species are the leading cause of fungal infections in humans. Among all *Candida* spp., *Candida albicans* (*C. albicans*) is the most common cause of fungal infections in humans, capable of causing mucosal, cutaneous and bloodstream infections (2, 4, 5). Effective treatment requires antifungal therapy, with the main classes being azoles, echinocandins, and polyenes. Each antifungal class targets specific fungal cellular components, but they face challenges like growing drug resistance and patient toxicity (6-10). Hence, there is a pressing need for new antifungals.

In the quest to address this challenge, various strategies have been exploited to develop new drugs. High-throughput screening (HTS) and rational drug design are two ways to identify leads for drug development (11, 12). For HTS, target-based and whole-cell-based screenings are two major types, and both require the efforts of screening thousands of compounds (13). On the contrary, rational drug design develops drugs based on the information about the structure and function of the target protein and can also aid in optimizing hits identified from HTS (11). Rational drug design also comes in two types: ligand-based and structure-based approaches. The former depends on understanding the structure of existing ligands that can bind to a target, while the latter focuses on designing inhibitors using the structural details of target proteins (14). The rational drug design process typically involves multiple rounds of design, synthesis and evaluation to yield compounds potent and specific enough for preclinical trials (15). The atomic structures, as well as predicted structures from various methods, of the target

proteins have been shown to be useful in drug design (16, 17). Dorzolamide, used for treating glaucoma (15), and saquinavir, an HIV protease inhibitor (18), are two market drugs refined or conceived through the structure-based method.

In recent years, minimal progress has been made to identify new antifungals because of the relatively high gene homology (~40%) and conservation of fundamental biochemical pathways between fungi and humans, prohibiting easy identification of drugs that are selectively toxic to fungi (19). To this end, it is important to identify new fungal-specific targets that are absent in mammals, or at least share little homology with mammals, and can thus provide selective inhibition for antifungal therapies. Among all current and potential antifungal drug targets, membrane enzymes present valuable targets for the development of novel antifungal agents due to their essential nature in fungal survival, proliferation, pathogenicity, and resistance to antifungal drugs. In addition, some of these enzymes are absent in humans. Here, we provide an overview of the structural knowledge of several membrane enzymes considered current or potential antifungal targets, as well as known inhibitors, and their potential use in rational drug design. These targets all affect the cell envelope of fungi, which comprises cell wall and cell membrane.

Cell wall biosynthesis enzymes

The fungal cell wall is an ideal target for antifungal drugs as it is an organelle that is not conserved in mammals. The cell wall shields fungi from environmental threats and prevents harmful macromolecules from entering the cell (20). The fungal cell wall accounts for around 40% of the entire cell volume and is made of polysaccharides

(mainly glucan and chitin) and glycoproteins (21). Structurally, chitin and β -1,3-glucan are the primary constituents of most fungal cell walls, and they are embedded within a gel-like matrix mainly made up of α -1,3-glucans and galactomannoproteins. The synthesis of chitin and glucan is mediated by chitin synthases and glucan synthases, respectively, which are promising targets for antifungal drugs.

Chitin synthases

Chitin accounts for 1–2% of the dry weight of the yeast cell wall and could reach up to 10–20% in filamentous fungi (22). In *C. albicans*, chitin content in the hyphae wall is three times higher than that of yeast form (23). Chitin is a long-chain polymer consisting of β -(1,4)-linked N-acetylglucosamine (GlcNAc), and because of its absence in plants and vertebrates, the biosynthesis of chitin is considered a promising target for antifungal drugs (24). The chitin layer is formed by large families of plasma membrane-bound chitin synthases, which catalyze the formation of β (1-4) bonds using UDP-GlcNAc as the sugar source (25, 26). There are a total of seven classes of chitin synthases, and class IV enzymes often make the most amounts of cell wall chitin and are generally associated with virulence (26-28). *S. cerevisiae* has three chitin synthase genes (*CHS1*, *CHS2* and *CHS3*) and *C. albicans* has four (*CHS1*, *CHS2*, *CHS3* and *CHS8*), while *Aspergillus nidulans*, *Aspergillus fumigatus* and *Cryptococcus neoformans* are known to have eight (26).

Polyoxin B (PolyB) is a type of peptidyl nucleoside that acts against chitin synthases as a competitive inhibitor (29). It has been employed for many years in the fields of agriculture and forestry to combat fungal plant pathogens and harmful

arthropods (which have chitinous exoskeletons) (29, 30). Similarly, Nikkomycin Z (NikkoZ) is another peptidyl nucleoside that inhibits chitin synthase, and it has demonstrated substantial positive effects in treating fungal infections in mammals (31) (32). In 2000, a range of new inhibitors for *CaChs1* was discovered through an extensive screening process, which led to the discovery of compound RO-09-3024, a very effective chitin synthase inhibitor with an IC_{50} value of 0.14 nM *invitro* and an EC_{50} of 0.07 mg/ml against *C. albicans* (CY1002) (33). However, many fungal pathogens containing *CHS* genes are less sensitive to these inhibitors, stressing the need to optimize these molecules via further drug design, which requires chitin synthase structures (34, 35). However, as a multi-transmembrane enzyme, chitin synthases have proven challenging for protein expression, solubilization, and crystallization, hindering structural analysis (36). For this reason, a bacterial glycosyltransferase from *Sinorhizobium meliloti*, *SmNodC*, was shown to be an appropriate model to study the general structure and reaction mechanism of chitin synthases due to the fact that (i) *SmNodC* has catalytic core the conserved with chitin synthases (37, 38) and (ii) *SmNodC* is inhibited by Nikkomycin Z (36). The homology models of *SmNodC* and *ScChs2* were made based on the structure of bacterial cellulose synthase from *Rhodobacter sphaeroides* (39), and have shown overall similar structure architectures with one difference that *SmNodC* is missing the chitin transport channel from *ScChs2* (36). A detailed display of the active site and product-binding site of *SmNodC* are shown in (36).

The first atomic structure of chitin synthase was solved from the soybean root rot pathogenic oomycete *Phytophthora sojae* in 2022 via cryo-EM (40). The structure of chitin synthase was solved in apo-, GlcNAc-bound, UDP-bound (post-synthesis), nascent

chitin oligomer-bound, and most importantly, the nikkomyacin Z-bound forms (Figure 1.1). The *PsChs* shares great sequence and architectural similarity with *ScChs*, but with an elevated K_i value for nikkomyacin Z (40). This could represent the binding mode of nikkomyacin Z to fungal chitin synthase. As a substrate analog, nikkomyacin Z binds to the uridine-binding tub via its uridine segment in the same way as the substrate UDP-GlcNAc does (Figure 1.1B). The hydroxypyridine moiety of nikkomyacin Z occupies a significant portion of the reaction chamber and translocating channel. This restricts the donor substrate from accessing the reaction area required for chitin synthesis. The hydroxypyridine ring also forms hydrophobic interactions with Leu412, Tyr433, Val452, Pro454 and Trp539 from the conserved motifs in *PsChs*. Mutation of these residues impairs activity but, in the meantime, reduces inhibition from nikkomyacin Z (40).

The structure of *C. albicans* chitin synthase 2 was recently solved (35). Structures were solved for the apo-, substrate-bound, nikkomyacin Z-bound, and polyoxin D-bound forms of *CaChs2*. Similarly, nikkomyacin Z and polyoxin D occupy the substrate binding site of *CaChs2*, and an overlay of bound UDP-GlcNAc and polyoxin D with nikkomyacin Z is shown in Figure 1.2. For nikkomyacin Z, the aminohexuronic acid moiety (in the red square has an overall similar position to that from the UDP-GlcNAc (Figure 1.2A). However, nikkomyacin Z gains interactions with residues Y571 and W647 on the pyridinyl ring, which is absent in UDP-GlcNAc, but loses or severely decreases the interaction with residue D465 as this residue rotates away when bound to nikkomyacin Z. In contrast, polyoxin D adapts a slightly different binding mode compared to nikkomyacin Z. The critical residue involved in polyoxin D binding is Q643, forming two hydrogen bonds with hydroxyl groups on polyoxin (Figure 1.2A). Residue K440 also rotates to

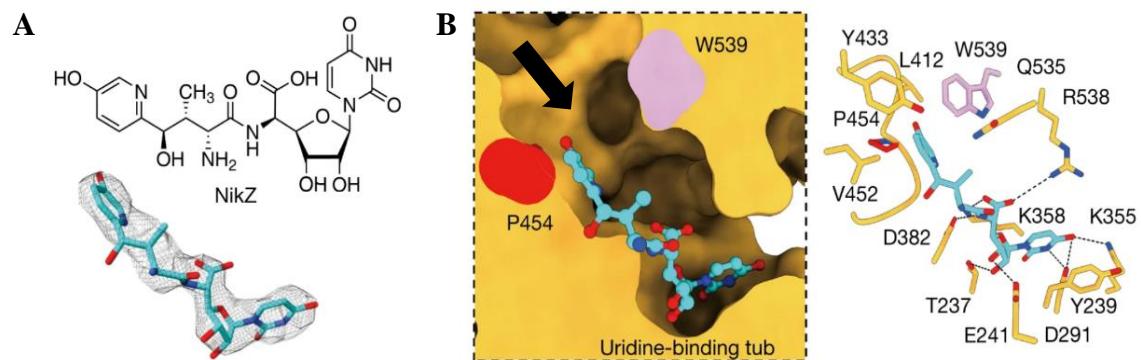


Figure 1.1. The interaction between nikkomycin Z and *Phytophthora sojae* Chs1.

(A) Chemical and 3D structure of nikkomycin Z (NikZ). (B) The left is the sliced-surface view of the NikZ-binding site of *PsChs* and the right is detailed interactions between NikZ and *PsChs*1. The reaction chamber and translocating channel are pointed by the arrow. The hydrogen bonds are labeled as black dashed lines. Figures are adapted from (40).

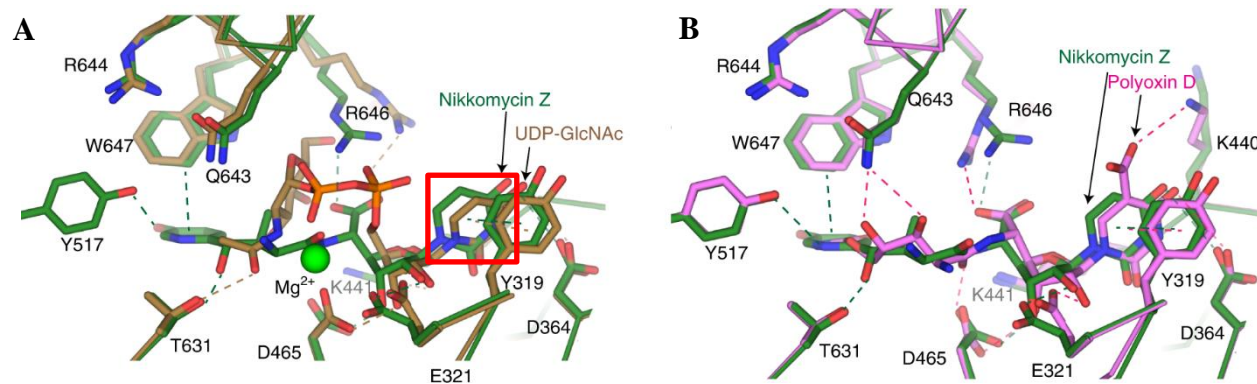


Figure 1.2. Bind models of UDP-GlcNAc, Nikkomycin Z and Polyoxin D to *CaChs2*.

(A) Overlay of substrate binding sites: one with UDP-GlcNAc-bound (in brown) and the other with nikkomycin Z-bound (in green) in *CaChs2*. The aminohexuronic acid moiety is highlighted in red square. (B) Overlay of the substrate binding sites of *CaChs2*: one bound with nikkomycin Z (in green) and the other with polyoxin D (in magenta). Hydrogen bond and π - π stacking interactions between the substrate or ligand and *CaChs2* are marked with dashed lines in their respective colors. Figures are adapted from (35).

interact with polyoxin D, which is not seen in either nikkomycin- or UDP-GlcNAc-bound forms. This interaction between K440 and the 5-carboxyl of the uracil base is suggested to be the addition inhibition mechanism that polyoxin has on *CaChs2* activity (35). Overall, it was suggested that the stronger inhibitory effect of nikkomycin Z on *CaChs2* compared to polyoxin D probably results from the enhanced interaction via the pyridinyl ring. The presence of the 5-carboxyl in polyoxin D and its interaction with K440 somewhat makes up for the absence of interactions associated with the pyridinyl ring (35).

The third and most current structure of chitin synthase is the *S. cerevisiae* Chs1 from the Bai group (41). Again, the structures of substrate-, polyoxin D- and nikkomycin Z-bound *ScChs1* were determined using cryo-EM, and the mechanism of the chitin synthesis initiation, extension and transport was described in (41). One unique finding on the mode of polyoxin D and nikkomycin Z binding is that besides the competition from the nucleoside moiety on the UDP, the peptidyl moiety of polyoxin D and nikkomycin Z opens the switch loop and thus keeps the gate of chitin transport channel blocked (41). This unique mechanism of inhibition can potentially be used in future rational drug design.

β -1,3-glucan synthase

Glucan is the foundational polysaccharide in the fungal cells, constituting ~50-60% of its dry weight (22). Predominantly, 65-90% of these glucan polymers have a 1,3 linkage, but there exist other linkage types like β -1,6 (in *Candida* spp.), β -1,4, α -1,3, and α -1,4. Among those different linkage glucans, the most structurally significant

component is β -1,3-D-glucan, which serves as the anchor for other covalent attachments within the wall (22, 42). β -1,3-D-glucan is synthesized by glucan synthases, a group of membrane enzymes located in the plasma membrane. Glucan synthases have a conserved catalytic domain (Fks), serving the function of glucan biosynthesis, and are regulated by GTPase Rho1 subunits (43, 44). The genes *FKS1* and *FKS2*, responsible for producing β -1,3-D-glucan synthases, were first discovered in *Saccharomyces cerevisiae* (44, 45), and later the orthologs were identified in other fungal species. Disruption of one *FKS* gene leads to cell growth perturbation and disruption of both causes cell death (20, 45, 46), indicating a promising drug target.

Echinocandins, derivatives of the secondary metabolites from *Aspergillus nidulans* and *Aspergillus rugulosus* (47), act as a noncompetitive inhibitor of β (1-3)-glucan synthase and are the most recent class of antifungal agents approved by the US Food and Drug Agency in 2001 (9). The primary *in vitro* mode of action of echinocandins is associated with the disorganized fungal cell wall, which is then vulnerable to osmotic imbalances, leading to the death of the fungal cell and a reduction in damage to the host tissue (48, 49). The *in vivo* mode of action of echinocandins may be associated with the host immune response, specifically increased dectin-1 detection (50). The FDA-approved echinocandin-class drugs are caspofungin, micafungin, and anidulafungin (9, 51) (Figure 1.3). Structurally, they are all lipopeptides with similar cores, and one noticeable difference among them is the side chain. The long fatty acid chain was hypothesized to disrupt the membrane and thus inhibit glucan synthase activity (9, 51), and the resistant mutations of echinocandins often occur at the highly conserved hot spot 1 (HS1, residue 641-649), hot spot 2 (HS2, residue 1345–1365) and hot spot 3

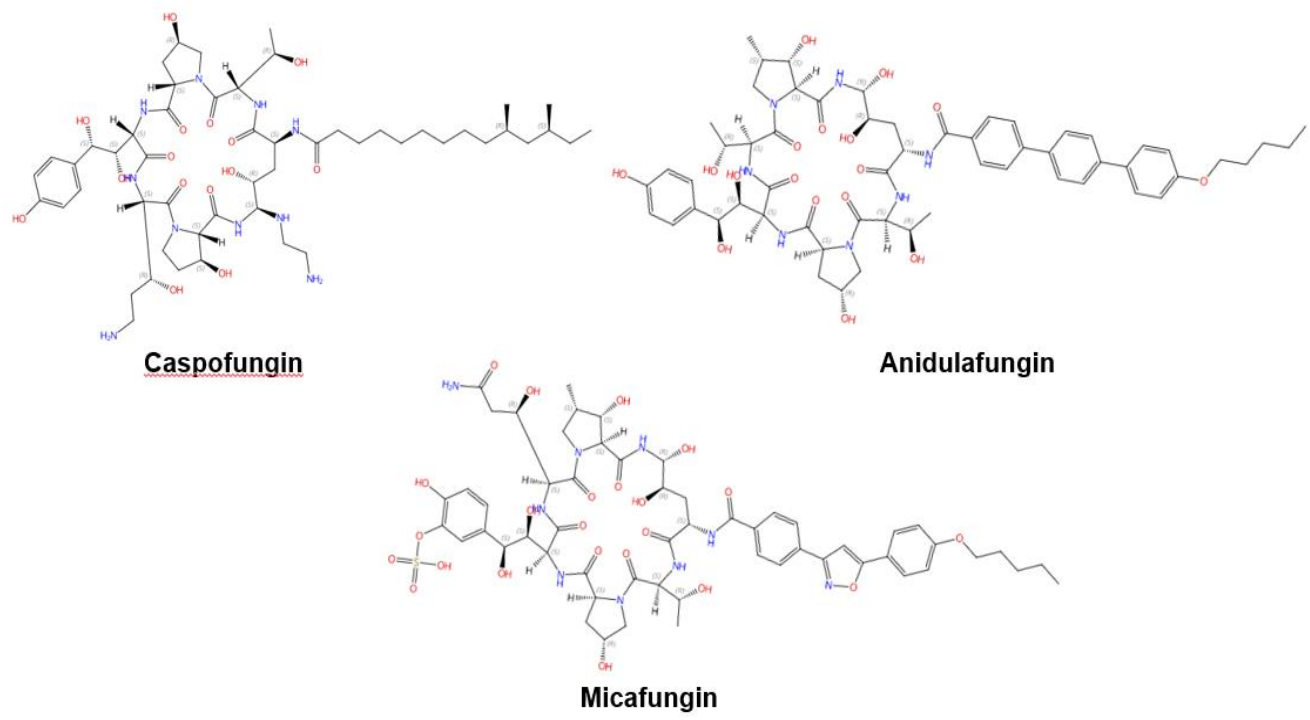


Figure 1.3. Chemical structures of the three FDA-approved echinocandins.

(HS3, 690–700) (52-54). In 2023, the structures of the *Saccharomyces cerevisiae* FKS1 and the echinocandin-resistant mutant, S643P FKS1, were determined using cryo-EM (55), providing structural insights into the mechanism of echinocandin resistance. In ScFKS1 the active site is located in the interface between the cytoplasm and plasma membrane, with a putative path for glucan translocation spanning across the membrane layers (55). HS 1,2 and 3 were shown in Figure 1.4A and are spatially located very close to each other. In wildtype ScFKS1, the residues F639 and S643 from the HS1 region play roles in lipid binding, as the side chain of F639 has direct interactions with three lipid molecules, while the side chain of S643 seems to stabilize the lipid-binding residue Y638 (Figure 1.4B). However, in the echinocandin-resistant S643P mutant, the side chains of both F639 and Y638 rotate significantly, leading to the re-orientation of bound lipids (Figure 1.4C). Therefore, the echinocandin resistance mechanism was hypothesized to be the re-oriented amino acid side chains and corresponding lipid movement that lead to change in [i] the binding site of echinocandins or [ii] ScFKS1's response to membrane perturbation caused by echinocandin (55). Evidence of more direct drug/protein interactions will help determine the mechanism of echinocandin inhibition and resistance, aiding in designing more potent echinocandin-class drugs.

Cell membrane biosynthesis enzymes

Drugs that impact cell membrane integrity have seen significant success (56). For example, drugs targeting ergosterol synthesis, such as imidazoles and triazoles, are especially effective. While many new antifungal triazole compounds have been introduced recently, they still have a long journey before being recognized as successful

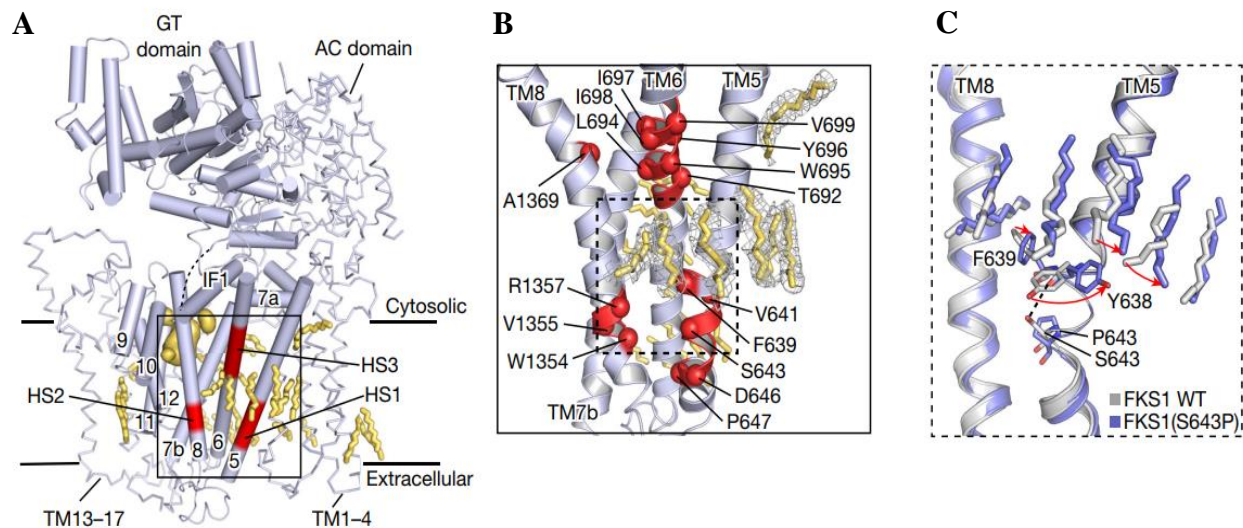


Figure 1.4. Structural interpretation of echinocandin-resistant mutations in *ScFKS1* structure.

(A) The *ScFKS1* structure with three distinct hotspot regions (colored in red) labeled as HS1–3. These regions are associated with mutations that confer resistance to echinocandins. (B) A detailed view of echinocandin-resistant mutations is provided, as referenced in (A). The mutations' alpha carbon ($C\alpha$) atoms are illustrated as red spheres. (C) Conformational changes and lipid re-arrangements, marked by red arrows, in wildtype *ScFKS1* (grey) and drug-resistant mutation S643P *ScFKS1* (blue). Potential polar interaction is indicated by the black dashed line. Figures are adapted from (55).

antifungals (57). Beyond sterols, the membrane also contains essential components like phospholipids and sphingolipids, which are crucial for cellular operations and signaling pathways. Here, we will summarize current and potential membrane enzyme antifungal targets involved in ergosterol, sphingolipid and phospholipid biosynthesis, with their available structures and inhibitors.

Ergosterol biosynthesis enzymes

Lanosterol 14 α -demethylase (Erg11)

Ergosterol is a major component of fungal cell membranes and plays a role similar to cholesterol in human cell membranes (58-60). Its biosynthesis pathway in fungi is a prime target for antifungal drug development, and a detailed ergosterol biosynthesis pathway including all involving enzymes and the sites of inhibition was summarized in (58). These enzymes, residing in the endoplasmic reticulum and other organelles, are crucial for the synthesis of ergosterol, the main sterol in fungal cell membranes. For example, Lanosterol 14 α -demethylase (known as Erg11 or CYP51) is a single-pass membrane-bound cytochrome P450 enzyme and is a well-studied drug target of azoles (61, 62). Erg11 is responsible for the demethylation of lanosterol, a step vital for the subsequent conversion of lanosterol to ergosterol, inhibition upon which leads to the accumulation of toxic intermediates, thus compromising cell membrane integrity (62). The structures and the interactions with different azoles were identified using X-ray crystallography for *Saccharomyces cerevisiae*, *Aspergillus fumigatus*, *Candida albicans*, and *Candida glabrata* Erg11 (61, 63-65). Like other members within the P450 enzyme family, Erg11 has a thiolate-heme iron center, the active site where oxidation reactions occur (Figure 1.5B). Also, it contains hydrophobic pockets and channels that

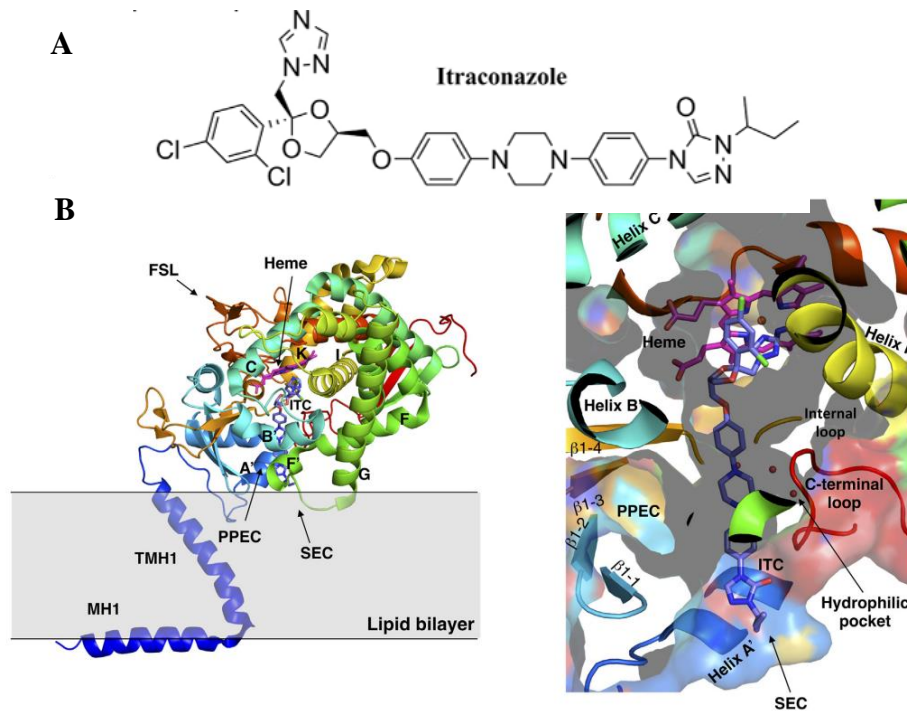


Figure 1.5 Binding of itraconazole to *S. cerevisiae* Erg11.

(A) Structure of itraconazole. (B) *S. cerevisiae* Erg11 structure adapted from (66). The Left shows the cartoon representation of the overall fold of *S. cerevisiae* Erg11 and its predicted position in the lipid (PDBID:5EQB). The right shows the binding of itraconazole within the *S. cerevisiae* Erg11. Itraconazole is shown in purple and heme moiety is shown in pink. (ITC: itraconazole).

accommodate the lipid substrate and facilitate its access to the catalytic center (61, 63-65). The interaction between itraconazole and *C. albicans* Erg11 shows that on a molecular scale, one of the nitrogen atoms in the azole ring binds as the sixth coordinating ligand to the heme iron, preventing oxygen activation (Figure 1.5B) (66). The interaction of the azole ring with the heme is crucial in determining the binding of azole drugs to Erg11 targets in other structures as well (63-65). With the detailed structural information of Erg11 available, structure-directed drug discovery can be performed, which involves virtually screening compound libraries for molecules that might bind more effectively to Erg11, even in resistant strains, or designing new molecules based on insights from the enzyme's structure (66).

Squalene synthase (Erg9)

Besides Erg11, other membrane-bound enzymes are also involved in ergosterol biosynthesis. For example, squalene synthase (Erg9), an enzyme that catalyzes the conversion of two molecules of farnesyl pyrophosphate to squalene, is also a potential drug target due to the functional difference between animal and fungal counterparts (67-69). The structures of Erg9 homologs from a trypanosomatid parasite, *Trypanosoma cruzi*, and humans were first determined via X-ray crystallography, and this could aid in the development of anti-Chagas disease and the cholesterol-lowering drugs (70-72). Zaragozic acids are potent competitive inhibitors of rat liver squalene synthases and potentially treat hypercholesterolemia (73). Malwal et al. reported the first fungal Erg9 structure from *Aspergillus flavus* in both apo- and substrate-bound forms, and compared it to the previous structures (67). The transmembrane domains of *A. flavus* Erg9 have similar architectures compared to their human counterpart, but the B-helix is significantly

shorter in the human Erg9 (67). This difference might lead to different ligand/inhibitor binding between human and pathogen proteins and could be used in antifungal design.

Squalene epoxidase (Erg1)

Following the formation of squalene, squalene epoxidase (also known as Erg1) adds an epoxide group to squalene to form 2,3-oxidosqualene (58, 67). Erg1 is also a membrane-bound enzyme located in the ER membrane and its reaction is the rate-limiting step of ergosterol biosynthesis in fungi and cholesterol biosynthesis in mammals. It is predicted to form a complex with Erg9 in the microsomal fraction (74, 75).

Terbinafine, one of the allylamine drugs (Figure 1.6A), inhibits Erg1 and leads to ergosterol depletion and accumulation of squalene, which is fungicidal for filamentous fungi but fungistatic for most *Candida* species (76-78). The human Erg1 structure was solved with an N-terminally truncated enzyme [118–574] in the presence of a known inhibitor NB-598 (79). The terbinafine molecule was superposed with NB-598 to show the potential mode of inhibition of the molecule (Figure 1.6B). The conserved residues of human Erg1, L326, L473, F477, F492, F495, L508, P505, and H522, are predicted to form the non-polar interactions with the inhibitor, and the mutations of these equivalent residues lead to terbinafine-resistance in fungi (79-82). Furthermore, a homology model of *S. cerevisiae* Erg1 was made and compared to its human counterpart (74). The *S. cerevisiae* Erg1 possesses an extended loop between β -strands 6 and 7 (residues 109–139, based on *S. cerevisiae*, pointed by one arrow), while the human homolog has a much shorter loop (residues 210–220) (Figure 1.6C). This compact loop in the human version might aid in crystal formation and the extended loop in *S. cerevisiae* Erg1 might obstruct this process (74). Currently, the function of the extended loop in *S. cerevisiae* Erg1 is

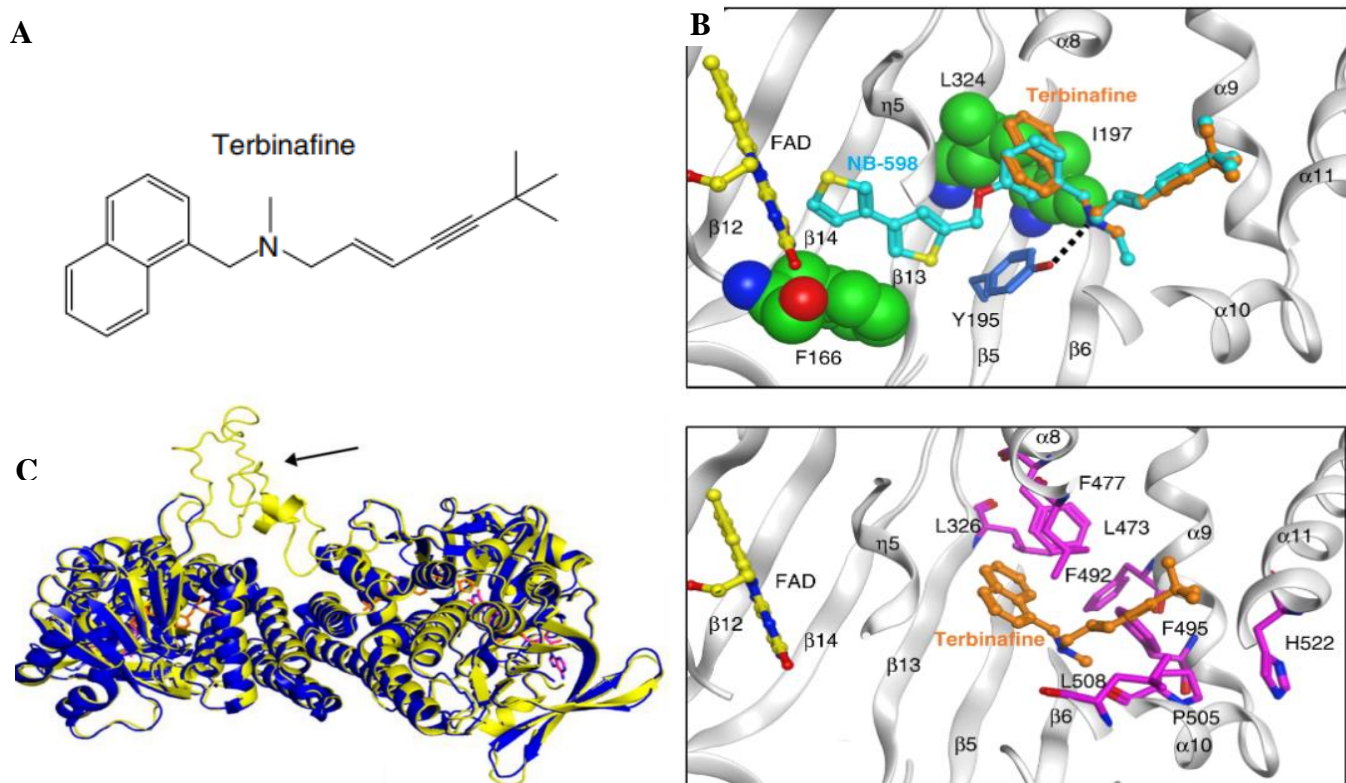


Figure 1.6. Binding model of terbinafine to squalene epoxidase.

(A) structure of terbinafine. (B) The upper panel shows the superposition of terbinafine (orange) with NB-598 (cyan) in human squalene epoxidase (PDBID:6C6P). The lower panel shows the positions of the known terbinafine-resistant mutations (pink) with respect to terbinafine (orange) in the human squalene epoxidase with a superposed terbinafine model. (C) Superposition of human squalene epoxidase structure (blue) and the *S. cerevisiae* squalene epoxidase homology model (yellow). Figures (A) and (B) are adapted from (79), and Figure (C) is adapted from (74). The extended loop on *S. cerevisiae* Erg1 was pointed by an arrow.

unknown, but may be targeted to develop molecules that destabilize the protein or disrupt potential protein-protein interactions.

C-24 sterol methyltransferase (Erg6)

C-24 sterol methyltransferase (known as Erg6) is also a membrane enzyme involved in the ergosterol biosynthesis, which was suggested to be an antifungal target due to its absence in mammals (58, 83). Erg6 catalyzes the methylation of the 24th carbon in the sterol side chain in the later stages of ergosterol biosynthesis, disruption of which reduced mating capability, diminished tryptophan uptake, increased permeability and susceptibility to cations and antifungals in *S. cerevisiae* (84-86). In *C. albicans*, the disruption of Erg6 leads to increased sensitivity to cycloheximide, terbinafine, fenpropiomorph, and tridemorph, but not to azoles, while showing resistance to amphotericin B (87). Interestingly, deletion of Erg6 leads to reduced virulence but not cell growth (88).

Several sterol analogs were determined to suppress Erg6 activity due to their structural resemblance to the substrate or product of Erg6 (89). Other inhibitors to Erg6, such as tomatidine and arylguanidines, effectively hinder the growth of *C. albicans*, might target other cellular targets since disruption of Erg6 did not lead to a growth defect (88, 90-92). Recently, an antipyrine derivative H55, identified from screening, showed low cytotoxicity and effectively inhibits *C. albicans* hyphal formation under various conditions, and also exhibited therapeutic efficacy in mouse models of azole-resistant candidiasis (93). Later, various assays supported H55 as an allosteric inhibitor for Erg6, and a molecular dynamic simulation predicted that binding of H55 prevents the binding of Erg6's substrate S-adenosylmethionine (93). More structural information is needed to

validate or provide more insight into the interaction between Erg6 and H55.

There are currently no structures experimentally solved for Erg6 to our knowledge, but Azam et al. modeled a C-24 sterol methyltransferase from *Leishmania infantum* and identified relevant residues that interact with itraconazole and amphotericin B (83). Since the substrate-binding sites and active sites are conserved between *L. infantum* and *S. cerevisiae* C-24 sterol methyltransferase, the ligand/protein interaction information from *L. infantum* homolog can be potentially applied to antifungal design (83).

Sterol C-14 reductase (Erg24) and sterol C-8,7 isomerase (Erg2)

Morpholines are known to inhibit sterol C-14 reductase (known as Erg24) and sterol C-8,7 isomerase (Erg2), which are two membrane-bound enzymes involved in ergosterol biosynthesis (58, 94, 95). Fenpropimorph as well as its analogs, fenpropidin and amorolfine, exhibited potent antifungal effects against different human fungal pathogens (96). Erg24 catalyzes the reduction of the C14=15 double bond of sterol intermediates which cannot be recognized by the downstream enzymes thus perturbing the membrane (58), and a *erg24*ΔΔ mutant has reduced virulence in a mouse model of disseminated candidiasis (97). Erg2 facilitates the double bond from the 8 to the 7 position in sterol the intermediate fecosterol, and this enzyme has a polyvalent high-affinity drug binding site similar to that in mammalian sigma receptors (98). Currently, neither the structures of Erg24 and Erg2 nor their interactions with morpholines have been characterized. The Erg2 homolog from human has a solved structure, and its interaction with the anti-breast cancer drug tamoxifen and the cholesterol biosynthesis inhibitor U18666A have been studied (99). Similarly, one Erg23 homolog,

Methylomicrobium alcaliphilum sterol C-14 reductase, shows an interesting arrangement of ten transmembrane domains, with the catalytic domain localized in the carboxy-terminal half (TM6–10). This domain surrounds two linked pockets with one facing the cytoplasm, which accommodates NADPH, and the second pocket accessible from the lipid bilayer (100). However, neither the structure of human sterol C-14 reductase nor the *Methylomicrobium alcaliphilum* sterol C-14 reductase has direct use in the antifungal design, and efforts are needed in the structure determination of their fungal counterparts.

Sphingolipid biosynthesis enzymes

Sphingolipid production is crucial for the growth and survival of various human fungal pathogens such as *S. cerevisiae*, *Histoplasma capsulatum* and *C. albicans* (101, 102). Therefore, using a drug to obstruct this process could effectively halt their growth and trigger cell death. The sphingolipid biosynthesis pathway in *S. cerevisiae* is depicted in Figure 1.7 from the first step to the formation of the major sphingolipid mannose-(inositol-P)₂-ceramide (M(IP)₂C) (103-105). Three membrane-bound enzymes involved in sphingolipid synthesis have been suggested to be potential antifungal targets --- Serine palmitoyltransferase (SPT), ceramide synthase and Inositol phosphorylceramide (IPC) synthase. In addition, these all have their respective inhibitors.

Serine palmitoyltransferase (SPT)

SPT catalyzes the condensation of serine and palmitoyl-CoA, which is the first and rate-limiting enzyme in the biosynthesis of sphingolipids (106, 107). SPT uses pyridoxal phosphate (PLP) as a cofactor for catalysis, and belongs to the allene oxide synthase (AOS) family (108). The active yeast SPT enzyme is a heterodimer made from

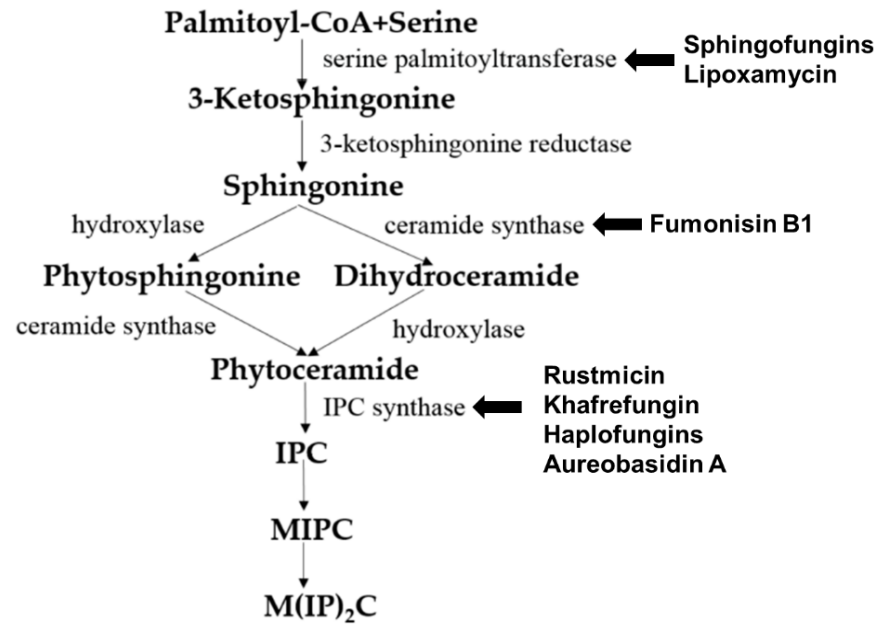


Figure 1.7. *De novo* synthesis of sphingolipids in *S. cerevisiae* and known inhibitors targeting each enzyme.

This figure is adapted and modified from (60). Inositolphosphatylceramide (IPC); mannose inositol-P-ceramide (MIPC); mannose-(inositol-P)₂-ceramide (M(IP)₂C).

subunits encoded by *lcb1* or *lcb2* (109, 110), and a third subunit Tsc3p is required for high-level SPT activity (111). The protein structure of the SPT complex was first solved in bacteria (112-114), but since the bacterial SPT homologs are soluble homodimers, they provided limited insights into the catalytic mechanism of eukaryotic SPT. In 2021, structures of a human SPT–ORMDL3 complex (ORMDL proteins function as regulatory subunits) in different catalytic states were solved (115, 116), and later the ceramide-sensing mechanism of SPT-ORMDL3 complex was studied using the ceramide-bound structure (117). Due to the high sequence similarity between fungal and mammalian SPT subunits (118), the human SPT-ORMDL3 complex can be used to study the mechanism of unknown SPT inhibitors such as sphingofungins (119, 120) and lipoxamycin (121, 122).

Ceramide synthase

Ceramide synthase, another membrane-bound enzyme involved in sphingolipid biosynthesis, adds a fatty acyl chain from fatty acyl–coenzyme A (CoA) to the sphingoid base of sphinganine to form ceramide (105). Mammals possess six ceramide synthase isoforms that differ in their tissue distribution and substrate specificity, and each isoform is known to produce ceramides with different acyl chain lengths (123, 124). Currently, there is no structure available for any fungal ceramide synthase homologs to our knowledge, but there are some studies available to provide structure-function characterization of ceramide synthases. Ceramide synthase belongs to the longevity assurance gene 1 (Lag1) protein family, which has a stretch of 52 amino acids as a highly conserved Lag1p motif (125). Two conserved histidine residues within this Lag1p motif were shown to be crucial for catalysis and binding of the substrates, the alteration of

which negatively impacts the enzymatic function of mammalian and yeast ceramide synthases (125-127). Fumonisin is a group of mycotoxins that have a striking structural resemblance to sphingolipids and are known to be carcinogenic (128). Notably, fumonisin B1 (FB₁), among many fumonisins, effectively inhibits ceramide synthase, conferring toxicity and carcinogenic properties. Though neither the protein structure of ceramide synthase nor the FB₁/protein binding is known, an inhibition mechanism model of FB₁ was proposed (129) (Figure 1.8). Briefly, concentrations of both substrates affected the potency of FB₁, thus FB₁ appeared as a competitive inhibitor binding in the active site of ceramide synthase (130). Then, it was later found that the tricarballic acid sidechains (in the red boxes) play essential roles in the inhibition of FB₁, as eliminating tricarballic acid sidechains reduces the strength of ceramide synthase inhibition *in vitro* by 10 fold (129, 131). Moreover, this model was further supported by the observation that the FB₁ derivative without tricarballic acid sidechains can be used as a substrate by ceramide synthase, indicating those side chains directly interact with the active site of ceramide synthase (132). Further structure investigation is needed to validate this model, and will also help optimize FB₁ to act specifically against fungi.

Inositol phosphorylceramide (IPC) synthase

Unlike serine palmitoyltransferase or ceramide synthase, which has homologs in mammalian cells, inositol phosphorylceramide (IPC) synthase, catalyzes a reaction unique to plants and some microbial eukaryotes, such as fungi and kinetoplastids. This reaction is the transfer of phosphoinositol from phosphatidylinositol to phytoceramide (105). Following its discovery in *S. cerevisiae*, IPC synthases have been characterized in various protozoans causing neglected tropical diseases, such as Chagas disease and

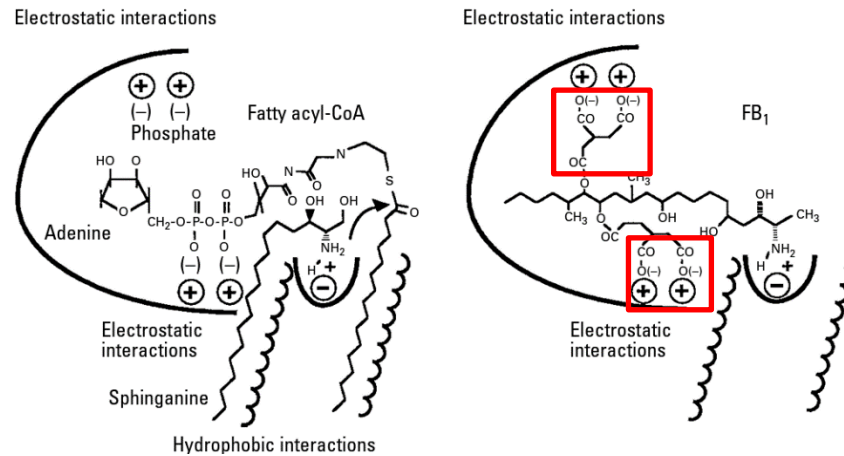


Figure 1.8. The active site of ceramide synthase is depicted in a model that illustrates how FB₁ (right) mimics both the sphingoid base and the fatty acyl-CoA substrates (left).

Potential interaction sites between the ceramide synthase and its substrates or inhibitors are represented by bold lines. The tricarballylic acid sidechains are highlighted in the red boxes. This figure is adapted and modified from (129).

leishmaniasis (133-137), and it has also been characterized in plants (138-140). An alignment of trypanosomatid IPC synthases showed conserved arginine, histidine and aspartate residues in the active site and their contributions in a predicted catalysis transfer of the phosphoryl group was shown in *Leishmania major* IPC synthase (137).

A couple of inhibitors have been identified to act specifically against IPC synthases. Rustmicin, a 14-membered macrolide, was identified as a potent inhibitor against IPC synthase. It is especially potent against *C. neoformans*, where it inhibits the growth of *C. neoformans* and its sphingolipid synthesis at concentrations <1 ng/ml with an IC₅₀ of 70 pM to solubilized *C. neoformans* IPC synthase (141, 142). The compound khafrefungin, isolated from a Costa Rican plant, displayed antifungal effects against *C. albicans* and *C. neoformans*, and was determined to inhibit *C. albicans* IPC synthase with an IC₅₀ of 0.6 nM, but with no effects on mammalian sphingolipids (143). Another compound, aureobasidin A, a natural compound from the fungus *Aureobasidium pullulans*, has very low (sub- μ g /mL) MIC values for *S. cerevisiae*, *C. albicans*, and *C. neoformans* with IC₅₀ values for IPC synthase activities ranging from 0.2 to 4.9 nM (105, 144). Then, haplofungins, a phytoceramide mimic isolated from the fungus *Lauriomyces bellulus*, also showed potent inhibitory activities against fungal IPC synthases (145, 146). However, despite the fact that several potent IPC synthase inhibitors have been identified, the atomic structure of this protein is missing. The *Arabidopsis thaliana* IPC synthase monomer is predicted with six transmembrane domains with a flexible N-terminal region (AlphaFoldDB: Q9SH93), and further structure–activity relationship study will be helpful for optimizing or designing new antifungal drugs.

Phospholipid biosynthesis enzymes

Phospholipids, accounting for 40-60% of lipids in eukaryotic cells, are the predominant lipids present in most organisms' membranes (147). The four major phospholipids in eukaryotes are phosphatidylserine (PS), phosphatidylcholine (PC), phosphatidylethanolamine (PE), and phosphatidylinositol (PI) (148). PC and PE constitute the majority of phospholipids in yeasts and are required for functional membrane construction in eukaryotic organisms, which are involved in membrane integrity and mitochondrial function, respectively (149, 150); PI species are involved in various cellular signal transduction pathways (151). PS is enriched in the plasma membrane (148) and is known to activate protein kinase C, which is involved in various signaling pathways and also affects a variety of other signaling cascades (152-154). PS also plays important roles in apoptosis and blood clotting (155-157) and is associated with virulence of *C. albicans* (150, 158).

Phospholipid biosynthesis in cells is intricate, with distinct variations between fungal and mammalian cells. The phospholipid biosynthesis pathways of *C. albicans* (A) and mammals/parasites (B) are shown in Figure 1.9, adapted from (159). The biosynthesis of phospholipids in *C. albicans* differs from the mammalian cell in several steps. First, mammalian cells encode one *PSD* gene for PS decarboxylase (160), which converts PS to PE, while yeast has two distinct proteins with little similarity, *PSD1* and *PSD2*. Each of these genes has PS decarboxylase activity (161, 162). Also, the production of PS uses a different mechanism in mammalian versus fungal cells. In mammalian cells, PS is produced through a base-exchange reaction catalyzed by the mammalian phosphatidylserine synthase-1 (PSS1) and phosphatidylserine synthase-2

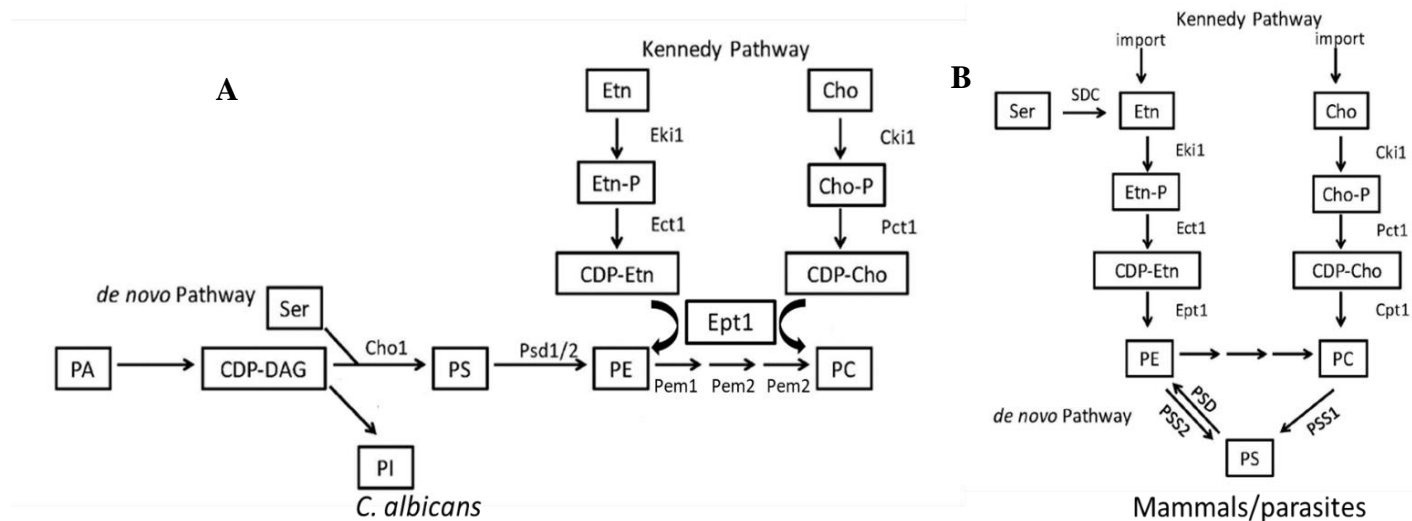


Figure 1.9. Phospholipid biosynthesis pathways for *C. albicans* (A) and mammals/parasites (B).

Both *de novo* pathway and Kenney pathway exist in each scenario. PA: phosphatidic acid; CDP-DAG: cytidine diphosphate diacylglycerol; Ser: serine; Cho1/PSS1/PSS2: PS synthase; PI: phosphatidylinositol; PS: phosphatidylserine; PE: phosphatidylethanolamine; PC: phosphatidylcholine; Etn: ethanolamine; Cho: choline; Etn-P: phosphoethanolamine; Cho-P: phosphocholine; CDP-Etn: cytidyldiphosphate-ethanolamine; CDP-Cho: cytidyldiphosphatecholine; PSD: PS decarboxylase; Eki: ethanolamine kinase; Ect: ethanolamine-phosphate cytidylyltransferase; Ept: ethanolamine phosphotransferase; Cki: choline kinase; Pct: choline-phosphate cytidylyltransferase; SDC: serine decarboxylase; Cpt: choline phosphotransferase. This figure is adapted and modified from (159).

(PSS2), in which the headgroups of existing PC and PE, respectively, are cleaved off and replaced with serine to produce PS (163). On the contrary, fungal cells condense cytidine diphosphate diacylglycerol (CDP-DAG) and serine into PS via phosphatidylserine synthase (PS synthase), using a different catalytic mechanism compared to the mammalian PSS1/PSS2 enzymes (148, 163). Here, we will discuss the current inhibitors and structure studies of PS decarboxylase and PS synthase.

PS decarboxylases (PSD)

In both yeast and mammals, PE is synthesized through the *de novo* pathway by decarboxylating PS or through the Kennedy pathway by using exogenous ethanolamine (Figure 1.9). Even if the Kennedy pathway was suggested to contribute to the majority of PE in some mammalian cells (164-166), in yeast, the majority of PE is generated by the decarboxylation of PS (160, 162, 167). Also, research has shown that while the elimination of the Kennedy pathway does not impact yeast cell survival, disruption of the *PSD1* gene leads to ethanolamine auxotrophy and mitochondrial instability (162). PSDs are evolutionarily conserved across a wide range of organisms, and most are membrane-associated enzymes relying on a covalently attached pyruvoyl moiety for their activities (168). Membrane bound PSDs are synthesized as a single polypeptide proenzyme, which undergoes self-cleavage at a highly conserved LGST motif (169, 170). The a and b chains from the cleavage assemble into a mature homodimer PSD, with each protomer having one a and one b chain. The a chains function as the catalytic domains and b chains are in charge of membrane association (168). Recently, the structures of apo and PE-

bound *E. coli* PSDs were solved, and structural insight into detailed mechanisms of membrane-binding, PS-recognition, self-cleavage and catalysis were provided (171, 172). Several PSD inhibitors have been proposed and shown in Table 1.1. In 1970s, hydroxylamine was found to inhibit the enzymatic activity of PSD and PE synthesis, and induce a compensatory accumulation of PS (173, 174). The effects of hydroxylamine are similar when incubated with *S. cerevisiae* and *C. albicans*, which lead to an accumulation in the PS level and decreased PE and PC level, but the PC and PE levels were much lower in *C. albicans* compared to *S. cerevisiae* (175). Similarly, serine hydroxamate, a serine analog, was also found to inhibit the conversion from PS to PE in *E. coli* and with an accumulation in PS, indicating targeting PS decarboxylase (176). However, due to the simple and small sizes of these molecules and lack of enzymatic studies, neither specificity nor the inhibition mechanism is known for hydroxylamine and serine hydroxamate. In 2007, a screen with direct measurements of PS and PE was performed with a collection of 9,920 molecules against the human inner mitochondrial membrane containing PISD enzyme, and it identified 54 molecules that exhibited inhibition in a dose-dependent manner (177). More recently, one molecule was identified from a cell-based screening and it is 7-chloro-N-(4-ethoxyphenyl)-4-quinolinamin (MMV007285), which has potent inhibition of *P. falciparum* PSD with low toxicity toward mammalian cells (178). An analog of this compound, 7CPQA, showed inhibition on the PfPSD activity (178). Later, two compounds, YU253467 and YU254403, discovered from a target-based screen, and they inhibit both native *C. albicans* growth and PSD mitochondrial activity (179). The molecules identified from these different screens are

Table 1.1. Potential phospholipid biosynthesis enzymes as drug targets and inhibitors.

Compound	Site of action	Organism	References
Hydroxylamine	PS decarboxylase	<i>E.coli</i>	(173, 174)
Hydroxylamine	PS decarboxylase	<i>S. cerevisiae</i> and <i>C. albicans</i>	(175)
Serine hydroxamate	PS decarboxylase	<i>E.coli</i>	(176)
7CPQA	PS decarboxylase	<i>P. falciparum</i>	(178)
YU253467and YU254403	PS decarboxylase	<i>C. albicans</i>	(179)
Validamycin A	PI synthesis	<i>R. cerealis</i>	(210)
Ethionine	PE methylation	<i>S. cerevisiae</i>	(212)
2-hydroxyethyl- hydrazine	PE methylation	<i>S. cerevisiae</i>	(211)
BR23 and BR25	Choline kinase	<i>P. falciparum</i>	(213)

promising, but the addition of detailed protein structure and ligand interactions would improve optimization efforts for higher specificity and potency.

PS synthase

Fungi use PS synthase to catalyze the formation of PS from CDP-DAG and serine, and both the enzyme and the reaction are absent in mammals (148, 163, 180), indicating a potential antifungal target. Furthermore, deleting the PS synthase in *Candida albicans* prevents it from causing disease in mouse models of oral or systemic candidiasis (150, 181). PS synthase is also crucial for the growth of the major fungal pathogen *Cryptococcus neoformans* (182) and also is highly conserved across various fungal species (180); These reasons make PS synthase an excellent drug target.

PS synthases were first characterized in bacteria. The PS synthases from Gram-negative bacteria such as *E.coli*, *Salmonella typhimurium* and *Enterobacter aerogenes* are tightly associated with ribosomes, and perform catalysis when they bind to the plasma membrane (183). Gram-positive bacteria such as *B. megaterium*, *Bacillus subtilis* and *Clostridium perfringens* have membrane-associated PS synthase, which have conserved motifs and belong to the protein family that includes eukaryotic counterparts (184). The first eukaryotic PS synthase was identified in *Saccharomyces cerevisiae* (185, 186). Since then, characterization of *S. cerevisiae* PS synthase (Cho1) included understanding the regulation of Cho1 (187-191), identifying the localization of the enzyme (192, 193), protein solubilization and purification (194, 195), and determination of Michaelis-Menton kinetics (187, 194, 195). The *C. albicans* PS synthase was first characterized in 2010, with the finding that it is crucial for systemic *Candida* infections in mouse experiments (150). Michaelis Menten kinetics of *C. albicans* PS synthase were described,

and its conserved CAPT motif for binding CDP-DAG was identified (196-198). Later, *C. albicans* PS synthase was solubilized and purified, but surprisingly formed a hexamer, which is unique among the known structures of the same family of membrane bound phospholipid synthases (199).

PS synthase belongs to the CDP-alcohol phosphatidyltransferase (CDP-AP) protein family, and six prokaryotic (200-205) and two eukaryotic (206, 207) members have solved structures to date. Among these, there is only one PS synthase structure, and it is from the archaean *Methanocaldococcus jannaschii*, and has 8 transmembrane domains (205). This is different from the homology model of *C. albicans* PS synthase with 6 transmembrane domains. In addition, some key residues involved in catalytic activity of *C. albicans* PS were lacking functions in the *M. jannaschii* PS synthase (199, 205). A structure of fungal PS synthase will reconcile this discrepancy and also provide insights into the mechanisms of *C. albicans* PS synthase.

Currently, despite the fact that PS synthase is a promising drug target, no molecule has been reported to inhibit it. Two cell-based screens were conducted to identify inhibitors of *C. albicans* PS synthase, but both attempts were unsuccessful (208, 209). One screen pinpointed the compound SB-224289. However, it was later determined that SB-224289 only acts on PS synthase-related physiological pathways rather than the enzyme directly (208). The other screen identified bleomycin, but it was also found that this compound affects phospholipid-associated processes rather than targeting *C. albicans* PS synthase directly (209). A target-based screening using purified PS synthase is needed for specific inhibitors.

Finally, besides PS decarboxylase and PS synthase, several inhibitors have been identified to target the phospholipid biosynthesis pathway. For example, it was suggested that validamycin A might hinder the incorporation of inositol into PI in *Rhizoctonia cerealis*, a process driven by the membrane-associated enzyme PI synthase (210), but a detailed enzymatic characterization is missing. For *de novo* PC biosynthesis, where PE is methylated three times into PC (Figure 1.9), ethionine and 2-hydroxyethyl-hydrazine were shown to inhibit the PE methylation and thus resulted in low PC levels (211, 212). Moreover, the anti-cancer compounds BR23 and BR25, known to inhibit human choline kinase, directly inhibited the ethanolamine activity from *P. falciparum* choline kinase, thus significantly reducing PE levels in *P. falciparum* without affecting PC (213). This led to halted growth of the parasite due to the depletion of membrane PE, and was ultimately lethal (213). These observations underscore the significance of phospholipid biosynthesis in certain microbes' survival and pathogenicity and thus drug development.

The essential nature of the fungal cell wall and cell membrane makes them prime targets for antifungal agents. Although current antifungals and novel drugs target various membrane enzymes on the cell wall or membrane, a deeper understanding of the inhibition mechanism provided by protein structures and ligand/protein interactions may lead to the optimization of current drugs and development of new drugs. The popularization of the single-particle cryo-EM approach has added many atomic-scale protein structures into the database, which aids in drug development. The Bioinformatics tools, like homology modeling and newly-developed AlphFold, may also predict the structures of target enzymes when the experimental structures are not available, as well as the resistance mechanisms linked to structural changes. This can deepen our knowledge

of the structure-activity relationship, refining antifungal drug design strategies and speeding exploration of new antifungals.

Summary

Among all these potential membrane-bound antifungal targets, I will focus on the PS synthase from *C. albicans* for this dissertation. Efforts facilitating rational drug design of *C. albicans* PS synthase are described in Chapter two, where critical substrate-binding residues from this enzyme have been predicted and characterized. Chapter three describes the purification and enzymatic characterization of *C. albicans* PS synthase, revealing a unique hexameric assembly of this protein and also leading the way for target-based drug screening. For Chapter four, we adapted a novel assay to screen small molecules against the purified *C. albicans* PS synthase, and identified several interesting inhibitors. One of these inhibitors, CBR-5884, has a great potential to be developed into a new class of antifungals upon optimization. Appendix I describes the methods for reconstructing purified *C. albicans* PS synthase into lipid nanodisc for structure determination, which also provided information for further drug design. In summary, this dissertation not only advances our understanding of *C. albicans* PS synthase as a promising antifungal target but also sets the stage for the future development of innovative antifungal therapies.

References

1. Kullberg, B., Filler, S., and Calderone, R. (2002) *Candida and candidiasis* ASM Press, Washington, DC,
2. Cassone, A., and Cauda, R. (2012) *Candida and candidiasis in HIV-infected patients: where commensalism, opportunistic behavior and frank pathogenicity lose their borders* *Aids* 26, 1457-1472
3. Brown, G. D., Denning, D. W., Gow, N. A., Levitz, S. M., Netea, M. G., and White, T. C. (2012) *Hidden killers: human fungal infections* *Science translational medicine* 4, 165rv113 10.1126/scitranslmed.3004404
4. Morrell, M., Fraser, V. J., and Kollef, M. H. (2005) *Delaying the empiric treatment of Candida bloodstream infection until positive blood culture results are obtained: a potential risk factor for hospital mortality* *Antimicrobial agents and chemotherapy* 49, 3640-3645
5. Wisplinghoff, H., Bischoff, T., Tallent, S. M., Seifert, H., Wenzel, R. P., and Edmond, M. B. (2004) *Nosocomial bloodstream infections in US hospitals: analysis of 24,179 cases from a prospective nationwide surveillance study* *Clinical infectious diseases* 39, 309-317
6. Pfaller, M., Neofytos, D., Diekema, D., Azie, N., Meier-Kriesche, H.-U., Quan, S.-P. *et al.* (2012) *Epidemiology and outcomes of candidemia in 3648 patients: data from the Prospective Antifungal Therapy (PATH Alliance®) registry, 2004–2008* *Diagnostic microbiology and infectious disease* 74, 323-331
7. Holeman Jr, C. W., and Einstein, H. (1963) *The toxic effects of amphotericin B in man* *California medicine* 99, 90
8. Ghannoum, M. A., and Rice, L. B. (1999) *Antifungal Agents: Mode of Action, Mechanisms of Resistance, and Correlation of These Mechanisms with Bacterial Resistance* *Clinical Microbiology Reviews* 12, 501-517 10.1128/cmr.12.4.501
9. Odds, F. C., Brown, A. J., and Gow, N. A. (2003) *Antifungal agents: mechanisms of action* *Trends in microbiology* 11, 272-279 10.1016/s0966-842x(03)00117-3
10. Whaley, S. G., Berkow, E. L., Rybak, J. M., Nishimoto, A. T., Barker, K. S., and Rogers, P. D. (2016) *Azole Antifungal Resistance in Candida albicans and Emerging Non-albicans Candida Species* *Front Microbiol* 7, 2173 10.3389/fmicb.2016.02173
11. Mandal, S., Moudgil, M. n., and Mandal, S. K. (2009) *Rational drug design* *European Journal of Pharmacology* 625, 90-100 <https://doi.org/10.1016/j.ejphar.2009.06.065>
12. Macarron, R., Banks, M. N., Bojanic, D., Burns, D. J., Cirovic, D. A., Garyantes, T. *et al.* (2011) *Impact of high-throughput screening in biomedical research* *Nature Reviews Drug Discovery* 10, 188-195 10.1038/nrd3368
13. Butts, A., DeJarnette, C., Peters, T. L., Parker, J. E., Kerns, M. E., Eberle, K. E. *et al.* (2017) *Target Abundance-Based Fitness Screening (TAFiS) Facilitates Rapid Identification of Target-Specific and Physiologically Active Chemical Probes* *mSphere* 2, 10.1128/mSphere.00379-17
14. Klebe, G. (2000) *Recent developments in structure-based drug design* *Journal of molecular medicine* 78, 269-281

15. Greer, J., Erickson, J. W., Baldwin, J. J., and Varney, M. D. (1994) Application of the Three-Dimensional Structures of Protein Target Molecules in Structure-Based Drug Design *Journal of Medicinal Chemistry* 37, 1035-1054
10.1021/jm00034a001
16. Cavasotto, C. N., and Phatak, S. S. (2009) Homology modeling in drug discovery: current trends and applications *Drug Discovery Today* 14, 676-683
<https://doi.org/10.1016/j.drudis.2009.04.006>
17. Doytchinova, I. (2022) Drug design—Past, present, future *Molecules* 27, 1496
18. Vacca, J. P., and Condra, J. H. (1997) Clinically effective HIV-1 protease inhibitors *Drug Discovery Today* 2, 261-272 [https://doi.org/10.1016/S1359-6446\(97\)01053-2](https://doi.org/10.1016/S1359-6446(97)01053-2)
19. Galao, R. P., Scheller, N., Alves-Rodrigues, I., Breinig, T., Meyerhans, A., and Díez, J. (2007) *Saccharomyces cerevisiae*: a versatile eukaryotic system in virology *Microbial Cell Factories* 6, 32 10.1186/1475-2859-6-32
20. Bowman, S. M., and Free, S. J. (2006) The structure and synthesis of the fungal cell wall *Bioessays* 28, 799-808
21. Klis, F. M. (1994) Cell wall assembly in yeast *Yeast (Chichester, England)* 10, 851-869
22. Garcia-Rubio, R., de Oliveira, H. C., Rivera, J., and Trevijano-Contador, N. (2020) The Fungal Cell Wall: *Candida*, *Cryptococcus*, and *Aspergillus* Species *Frontiers in Microbiology* 10, 10.3389/fmicb.2019.02993
23. Chattaway, F., Holmes, M. R., and Barlow, A. (1968) Cell wall composition of the mycelial and blastospore forms of *Candida albicans* *Microbiology* 51, 367-376
24. Chaudhary, P. M., Tupe, S. G., and Deshpande, M. V. (2013) Chitin synthase inhibitors as antifungal agents *Mini Rev Med Chem* 13, 222-236
10.2174/138955713804805256
25. Duran, A., Cabib, E., and Bowers, B. (1979) Chitin synthetase distribution on the yeast plasma membrane *Science* 203, 363-365
26. Lenardon, M. D., Munro, C. A., and Gow, N. A. (2010) Chitin synthesis and fungal pathogenesis *Curr Opin Microbiol* 13, 416-423 10.1016/j.mib.2010.05.002
27. Bulawa, C. E., Miller, D. W., Henry, L. K., and Becker, J. M. (1995) Attenuated virulence of chitin-deficient mutants of *Candida albicans* *Proceedings of the National Academy of Sciences* 92, 10570-10574
28. Nino-Vega, G., Carrero, L., and San-Blas, G. (2004) Isolation of the CHS4 gene of *Paracoccidioides brasiliensis* and its accommodation in a new class of chitin synthases *Sabouraudia* 42, 51-57
29. Hori, M., Eguchi, J., Kakiki, K., and Misato, T. (1974) Studies on the mode of action of polyoxins. VI Effect of polyoxin B on chitin synthesis in polyoxin-sensitive and resistant strains of *Alternaria kikuchiana* *The Journal of Antibiotics* 27, 260-266
30. Jackson, K. E., Pogula, P. K., and Patterson, S. E. (2013) Polyoxin and nikkomycin analogs: recent design and synthesis of novel peptidyl nucleosides *Heterocyclic Communications* 19, 375-386

31. McCARTHY, P. J., TROKE, P. F., and GULL, K. (1985) Mechanism of action of nikkomycin and the peptide transport system of *Candida albicans* *Microbiology* 131, 775-780
32. Larwood, D. J. (2020) Nikkomycin Z-Ready to Meet the Promise? *J Fungi (Basel)* 6, 10.3390/jof6040261
33. Masubuchi, K., Taniguchi, M., Umeda, I., Hattori, K., Suda, H., Kohchi, Y. *et al.* (2000) Synthesis and structure–activity relationships of novel fungal chitin synthase inhibitors *Bioorganic & medicinal chemistry letters* 10, 1459-1462
34. Draelos, M., Yokoyama, K., Liu, H., and Begley, T. (2020) *Comprehensive Natural Products III*
35. Ren, Z., Chhetri, A., Guan, Z., Suo, Y., Yokoyama, K., and Lee, S.-Y. (2022) Structural basis for inhibition and regulation of a chitin synthase from *Candida albicans* *Nature Structural & Molecular Biology* 29, 653-664 10.1038/s41594-022-00791-x
36. Dorfmüller, H. C., Ferenbach, A. T., Borodkin, V. S., and van Aalten, D. M. F. (2014) A structural and biochemical model of processive chitin synthesis *J Biol Chem* 289, 23020-23028 10.1074/jbc.M114.563353
37. Atkinson, E., and Long, S. (1992) Homology of *Rhizobium meliloti* NodC to polysaccharide polymerizing enzymes *Molecular Plant Microbe Interactions* 5, 439-439
38. Debelle, F., Rosenberg, C., and Denarie, J. (1992) The *Rhizobium*, *Bradyrhizobium*, and *Azorhizobium* NodC proteins are homologous to yeast chitin synthases *MOLECULAR PLANT MICROBE INTERACTIONS* 5, 443-443
39. Morgan, J. L., Strumillo, J., and Zimmer, J. (2013) Crystallographic snapshot of cellulose synthesis and membrane translocation *Nature* 493, 181-186
40. Chen, W., Cao, P., Liu, Y., Yu, A., Wang, D., Chen, L. *et al.* (2022) Structural basis for directional chitin biosynthesis *Nature* 610, 402-408 10.1038/s41586-022-05244-5
41. Chen, D.-D., Wang, Z.-B., Wang, L.-X., Zhao, P., Yun, C.-H., and Bai, L. (2023) Structure, catalysis, chitin transport, and selective inhibition of chitin synthase *Nat Commun* 14, 4776 10.1038/s41467-023-40479-4
42. Aimanianda, V., Clavaud, C., Simenel, C., Fontaine, T., Delepierre, M., and Latgé, J.-P. (2009) Cell wall β -(1, 6)-glucan of *Saccharomyces cerevisiae*: structural characterization and in situ synthesis *Journal of Biological Chemistry* 284, 13401-13412
43. Grün, C. H., Hochstenbach, F., Humbel, B. M., Verkleij, A. J., Sietsma, J. H., Klis, F. M. *et al.* (2005) The structure of cell wall α -glucan from fission yeast *Glycobiology* 15, 245-257
44. Qadota, H., Python, C. P., Inoue, S. B., Arisawa, M., Anraku, Y., Zheng, Y. *et al.* (1996) Identification of yeast Rho1p GTPase as a regulatory subunit of 1, 3- β -glucan synthase *Science* 272, 279-281
45. Douglas, C. M., Foor, F., Marrinan, J. A., Morin, N., Nielsen, J. B., Dahl, A. M. *et al.* (1994) The *Saccharomyces cerevisiae* FKS1 (ETG1) gene encodes an

- integral membrane protein which is a subunit of 1, 3-beta-D-glucan synthase
Proceedings of the National Academy of Sciences 91, 12907-12911
46. Mazur, P., Morin, N., Baginsky, W., El-Sherbeini, M., Clemas, J. A., Nielsen, J. B. *et al.* (1995) Differential expression and function of two homologous subunits of yeast 1, 3- β -D-glucan synthase *Molecular and cellular biology* 15, 5671-5681
 47. Nyfeler, R. (1974) A novel polypeptide-antibiotic from *Aspergillus nidulans* var. *echinulatus*: isolation and structural components *Helv Chim Acta* 57, 2459-2477
 48. Kathiravan, M. K., Salake, A. B., Chothe, A. S., Dudhe, P. B., Watode, R. P., Mukta, M. S. *et al.* (2012) The biology and chemistry of antifungal agents: a review *Bioorganic & medicinal chemistry* 20, 5678-5698
 49. Song, J. C., and Stevens, D. A. (2016) Caspofungin: pharmacodynamics, pharmacokinetics, clinical uses and treatment outcomes *Critical reviews in microbiology* 42, 813-846
 50. Marakalala, M. J., Vautier, S., Potrykus, J., Walker, L. A., Shepardson, K. M., Hopke, A. *et al.* (2013) Differential adaptation of *Candida albicans* in vivo modulates immune recognition by dectin-1 PLoS pathogens 9, e1003315
 51. Hasim, S., and Coleman, J. J. (2019) Targeting the fungal cell wall: current therapies and implications for development of alternative antifungal agents *Future Medicinal Chemistry* 11, 869-883 10.4155/fmc-2018-0465
 52. Perlin, D. S. (2015) Mechanisms of echinocandin antifungal drug resistance *Ann N Y Acad Sci* 1354, 1-11 10.1111/nyas.12831
 53. Johnson, M. E., Katiyar, S. K., and Edlind, T. D. (2011) New Fks hot spot for acquired echinocandin resistance in *Saccharomyces cerevisiae* and its contribution to intrinsic resistance of *Scedosporium* species *Antimicrobial agents and chemotherapy* 55, 3774-3781
 54. Carolus, H., Pierson, S., Muñoz, J. F., Subotić, A., Cruz, R. B., Cuomo, C. A. *et al.* (2021) Genome-wide analysis of experimentally evolved *Candida auris* reveals multiple novel mechanisms of multidrug resistance *MBio* 12, 10.1128/mbio.03333-03320
 55. Hu, X., Yang, P., Chai, C., Liu, J., Sun, H., Wu, Y. *et al.* (2023) Structural and mechanistic insights into fungal β -1,3-glucan synthase FKS1 *Nature* 616, 190-198 10.1038/s41586-023-05856-5
 56. Müller, C., Staudacher, V., Krauss, J., Giera, M., and Bracher, F. (2013) A convenient cellular assay for the identification of the molecular target of ergosterol biosynthesis inhibitors and quantification of their effects on total ergosterol biosynthesis *Steroids* 78, 483-493 10.1016/j.steroids.2013.02.006
 57. Ostrosky-Zeichner, L., Casadevall, A., Galgiani, J. N., Odds, F. C., and Rex, J. H. (2010) An insight into the antifungal pipeline: selected new molecules and beyond *Nat Rev Drug Discov* 9, 719-727 10.1038/nrd3074
 58. Akins, R. A. (2005) An update on antifungal targets and mechanisms of resistance in *Candida albicans* *Medical mycology* 43, 285-318
 59. Sant, D. G., Tupe, S. G., Ramana, C. V., and Deshpande, M. V. (2016) Fungal cell membrane—promising drug target for antifungal therapy *Journal of Applied Microbiology* 121, 1498-1510 <https://doi.org/10.1111/jam.13301>

60. Pan, J., Hu, C., and Yu, J.-H. (2018) Lipid biosynthesis as an antifungal target *Journal of Fungi* 4, 50
61. Keniya, M. V., Sabherwal, M., Wilson, R. K., Woods, M. A., Sagatova, A. A., Tyndall, J. D. *et al.* (2018) Crystal structures of full-length lanosterol 14 α -demethylases of prominent fungal pathogens *Candida albicans* and *Candida glabrata* provide tools for antifungal discovery *Antimicrobial agents and chemotherapy* 62, 10.1128/aac.01134-01118
62. Lepesheva, G. I., Hargrove, T. Y., Kleshchenko, Y., Nes, W. D., Villalta, F., and Waterman, M. R. (2008) CYP51: A Major Drug Target in the Cytochrome P450 Superfamily *Lipids* 43, 1117-1125 <https://doi.org/10.1007/s11745-008-3225-y>
63. Monk, B. C., Tomasiak, T. M., Keniya, M. V., Huschmann, F. U., Tyndall, J. D. A., O'Connell, J. D. *et al.* (2014) Architecture of a single membrane spanning cytochrome P450 suggests constraints that orient the catalytic domain relative to a bilayer *Proceedings of the National Academy of Sciences* 111, 3865-3870 [10.1073/pnas.1324245111](https://doi.org/10.1073/pnas.1324245111)
64. Hargrove, T. Y., Wawrzak, Z., Lamb, D. C., Guengerich, F. P., and Lepesheva, G. I. (2015) Structure-functional characterization of cytochrome P450 sterol 14 α -demethylase (CYP51B) from *Aspergillus fumigatus* and molecular basis for the development of antifungal drugs *Journal of Biological Chemistry* 290, 23916-23934
65. Hargrove, T. Y., Friggeri, L., Wawrzak, Z., Qi, A., Hoekstra, W. J., Schotzinger, R. J. *et al.* (2017) Structural analyses of *Candida albicans* sterol 14 α -demethylase complexed with azole drugs address the molecular basis of azole-mediated inhibition of fungal sterol biosynthesis *Journal of Biological Chemistry* 292, 6728-6743
66. Monk, B. C., Sagatova, A. A., Hosseini, P., Ruma, Y. N., Wilson, R. K., and Keniya, M. V. (2020) Fungal Lanosterol 14 α -demethylase: A target for next-generation antifungal design *Biochim Biophys Acta Proteins Proteom* 1868, 140206 [10.1016/j.bbapap.2019.02.008](https://doi.org/10.1016/j.bbapap.2019.02.008)
67. Malwal, S. R., Shang, N., Liu, W., Li, X., Zhang, L., Chen, C.-C. *et al.* (2022) A Structural and Bioinformatics Investigation of a Fungal Squalene Synthase and Comparisons with Other Membrane Proteins *ACS omega* 7, 22601-22612
68. Kribii, R., Arró, M., Del Arco, A., González, V., Balcells, L., Delourme, D. *et al.* (1997) Cloning and characterization of the *Arabidopsis thaliana* SQS1 gene encoding squalene synthase: involvement of the C-Terminal region of the enzyme in the channeling of squalene through the sterol pathway *European journal of biochemistry* 249, 61-69
69. Linscott, K. B., Niehaus, T. D., Zhuang, X., Bell, S. A., and Chappell, J. (2016) Mapping a kingdom-specific functional domain of squalene synthase *Biochimica et Biophysica Acta (BBA)-Molecular and Cell Biology of Lipids* 1861, 1049-1057
70. Shang, N., Li, Q., Ko, T.-P., Chan, H.-C., Li, J., Zheng, Y. *et al.* (2014) Squalene Synthase As a Target for Chagas Disease Therapeutics *PLOS Pathogens* 10, e1004114 [10.1371/journal.ppat.1004114](https://doi.org/10.1371/journal.ppat.1004114)

71. Pandit, J., Danley, D. E., Schulte, G. K., Mazzalupo, S., Pauly, T. A., Hayward, C. M. *et al.* (2000) Crystal structure of human squalene synthase: a key enzyme in cholesterol biosynthesis *Journal of Biological Chemistry* 275, 30610-30617
72. Stein, E. A., Bays, H., O'Brien, D., Pedicano, J., Piper, E., and Spezzi, A. (2011) Lapaquistat acetate: development of a squalene synthase inhibitor for the treatment of hypercholesterolemia *Circulation* 123, 1974-1985
73. Bergstrom, J. D., Kurtz, M. M., Rew, D. J., Amend, A. M., Karkas, J. D., Bostedor, R. G. *et al.* (1993) Zaragozic acids: a family of fungal metabolites that are picomolar competitive inhibitors of squalene synthase *Proc Natl Acad Sci U S A* 90, 80-84 10.1073/pnas.90.1.80
74. Sagatova, A. A. (2021) Strategies to Better Target Fungal Squalene Monooxygenase *J Fungi (Basel)* 7, 10.3390/jof7010049
75. M'Baya, B., and Karst, F. (1987) In vitro assay of squalene epoxidase of *Saccharomyces cerevisiae* *Biochemical and biophysical research communications* 147, 556-564
76. Ryder, N. S., Wagner, S., and Leitner, I. (1998) In vitro activities of terbinafine against cutaneous isolates of *Candida albicans* and other pathogenic yeasts *Antimicrobial agents and chemotherapy* 42, 1057-1061
77. Ryder, N. (1999) Activity of terbinafine against serious fungal pathogens *Mycoses* 42, 115-119
78. RYDER, N. S. (1989) The mechanism of action of terbinafine *Clinical and Experimental Dermatology* 14, 98-100 10.1111/j.1365-2230.1989.tb00900.x
79. Padyana, A. K., Gross, S., Jin, L., Cianchetta, G., Narayanaswamy, R., Wang, F. *et al.* (2019) Structure and inhibition mechanism of the catalytic domain of human squalene epoxidase *Nat Commun* 10, 97
80. Osborne, C. S., Leitner, I., Hofbauer, B., Fielding, C. A., Favre, B., and Ryder, N. S. (2006) Biological, biochemical, and molecular characterization of a new clinical *Trichophyton rubrum* isolate resistant to terbinafine *Antimicrobial agents and chemotherapy* 50, 2234-2236
81. Leber, R., Fuchsbichler, S., Klobučníková, V., Schweighofer, N., Pitters, E., Wohlfarter, K. *et al.* (2003) Molecular mechanism of terbinafine resistance in *Saccharomyces cerevisiae* *Antimicrobial agents and chemotherapy* 47, 3890-3900
82. Klobučníková, V., Kohut, P., Leber, R., Fuchsbichler, S., Schweighofer, N., Turnowsky, F. *et al.* (2003) Terbinafine resistance in a pleiotropic yeast mutant is caused by a single point mutation in the ERG1 gene *Biochemical and biophysical research communications* 309, 666-671
83. Azam, S. S., Abro, A., Raza, S., and Saroosh, A. (2014) Structure and dynamics studies of sterol 24-C-methyltransferase with mechanism based inactivators for the disruption of ergosterol biosynthesis *Molecular biology reports* 41, 4279-4293
84. Gaber, R. F., Copple, D. M., Kennedy, B. K., Vidal, M., and Bard, M. (1989) The yeast gene ERG6 is required for normal membrane function but is not essential for biosynthesis of the cell-cycle-sparking sterol *Molecular and cellular biology* 9, 3447-3456

85. Kleinhans, F., Lees, N., Bard, M., Haak, R., and Woods, R. (1979) ESR determinations of membrane permeability in a yeast sterol mutant *Chemistry and physics of lipids* 23, 143-154
86. Bard, M., Lees, N., Burrows, L., and Kleinhans, F. (1978) Differences in crystal violet uptake and cation-induced death among yeast sterol mutants *Journal of bacteriology* 135, 1146-1148
87. Jensen-Pergakes, K., Kennedy, M., Lees, N., Barbuch, R., Koegel, C., and Bard, M. (1998) Sequencing, disruption, and characterization of the *Candida albicans* sterol methyltransferase (ERG6) gene: drug susceptibility studies in *erg6* mutants *Antimicrobial Agents and Chemotherapy* 42, 1160-1167
88. Becker, J. M., Kauffman, S. J., Hauser, M., Huang, L., Lin, M., Sillaots, S. *et al.* (2010) Pathway analysis of *Candida albicans* survival and virulence determinants in a murine infection model *Proceedings of the National Academy of Sciences* 107, 22044-22049 doi:10.1073/pnas.1009845107
89. Ganapathy, K., Kanagasabai, R., Nguyen, T. T. M., and Nes, W. D. (2011) Purification, characterization and inhibition of sterol C24-methyltransferase from *Candida albicans* *Archives of biochemistry and biophysics* 505, 194-201
90. Dorsaz, S., Snäkä, T., Favre-Godal, Q., Maudens, P., Boulens, N., Furrer, P. *et al.* (2017) Identification and mode of action of a plant natural product targeting human fungal pathogens *Antimicrobial agents and chemotherapy* 61, 10.1128/aac.00829-00817
91. Borelli, C., Schaller, M., Niewerth, M., Nocker, K., Baasner, B., Berg, D. *et al.* (2008) Modes of action of the new arylguanidine abafungin beyond interference with ergosterol biosynthesis and in vitro activity against medically important fungi *Chemotherapy* 54, 245-259
92. Wang, J., and Wu, J. (2008) Antifungal activity of 25-azalanosterol against *Candida* species *European journal of clinical microbiology & infectious diseases* 27, 1131-1136
93. Jin, X., Hou, X., Wang, X., Zhang, M., Chen, J., Song, M. *et al.* (2023) Characterization of an allosteric inhibitor of fungal-specific C-24 sterol methyltransferase to treat *Candida albicans* infections *Cell Chemical Biology* 30, 553-568. e557
94. K Mazu, T., A Bricker, B., Flores-Rozas, H., and Y Ablordeppey, S. (2016) The mechanistic targets of antifungal agents: an overview *Mini reviews in medicinal chemistry* 16, 555-578
95. Kelly, D. E., Rose, M. E., and Kelly, S. L. (1994) Investigation of the role of sterol $\Delta 8 \rightarrow 7$ -isomerase in the sensitivity of *Saccharomyces cerevisiae* to fenpropimorph *FEMS microbiology letters* 122, 223-226
96. Jachak, G. R., Ramesh, R., Sant, D. G., Jorwekar, S. U., Jadhav, M. R., Tupe, S. G. *et al.* (2015) Silicon incorporated morpholine antifungals: design, synthesis, and biological evaluation *ACS Medicinal Chemistry Letters* 6, 1111-1116
97. Jia, N., Arthington-Skaggs, B., Lee, W., Pierson, C., Lees, N., Eckstein, J. *et al.* (2002) *Candida albicans* sterol C-14 reductase, encoded by the ERG24 gene, as a potential antifungal target site *Antimicrobial agents and chemotherapy* 46, 947-957

98. Moebius, F. F., Bermoser, K., Reiter, R. J., Hanner, M., and Glossmann, H. (1996) Yeast Sterol C8–C7 Isomerase: Identification and Characterization of a High-Affinity Binding Site for Enzyme Inhibitors *Biochemistry* 35, 16871-16878 10.1021/bi961996m
99. Long, T., Hassan, A., Thompson, B. M., McDonald, J. G., Wang, J., and Li, X. (2019) Structural basis for human sterol isomerase in cholesterol biosynthesis and multidrug recognition *Nat Commun* 10, 2452 10.1038/s41467-019-10279-w
100. Li, X., Roberti, R., and Blobel, G. (2015) Structure of an integral membrane sterol reductase from *Methylomicrobium alcaliphilum* *Nature* 517, 104-107 10.1038/nature13797
101. Lester, R., and Dickson, R. (1993) Sphingolipids with inositolphosphate-containing head groups *Advances in lipid research* 26, 253-274
102. Wells, G. B., Dickson, R. C., and Lester, R. L. (1996) Isolation and composition of inositolphosphorylceramide-type sphingolipids of hyphal forms of *Candida albicans* *Journal of bacteriology* 178, 6223-6226
103. Steiner, S., Smith, S., Waechter, C., and Lester, R. L. (1969) Isolation and partial characterization of a major inositol-containing lipid in baker's yeast, mannosyl-diinositol, diphosphoryl-ceramide *Proceedings of the National Academy of Sciences* 64, 1042-1048
104. Smith, S. W., and Lester, R. L. (1974) Inositol phosphorylceramide, a novel substance and the chief member of a major group of yeast sphingolipids containing a single inositol phosphate *Journal of Biological Chemistry* 249, 3395-3405
105. Nagiec, M. M., Nagiec, E. E., Baltisberger, J. A., Wells, G. B., Lester, R. L., and Dickson, R. C. (1997) Sphingolipid synthesis as a target for antifungal drugs: complementation of the inositol phosphorylceramide synthase defect in a mutant strain of *Saccharomyces cerevisiae* by the AUR1 gene *Journal of Biological Chemistry* 272, 9809-9817
106. Hanada, K. (2003) Serine palmitoyltransferase, a key enzyme of sphingolipid metabolism *Biochimica et Biophysica Acta (BBA)-Molecular and Cell Biology of Lipids* 1632, 16-30
107. Lowther, J., Naismith, J. H., Dunn, T. M., and Campopiano, D. J. (2012) Structural, mechanistic and regulatory studies of serine palmitoyltransferase *Biochemical Society Transactions* 40, 547-554
108. Harrison, P. J., Dunn, T. M., and Campopiano, D. J. (2018) Sphingolipid biosynthesis in man and microbes *Natural product reports* 35, 921-954
109. Pinto, W., Srinivasan, B., Shepherd, S., Schmidt, A., Dickson, R., and Lester, R. (1992) Sphingolipid long-chain-base auxotrophs of *Saccharomyces cerevisiae*: genetics, physiology, and a method for their selection *Journal of bacteriology* 174, 2565-2574
110. Gable, K., Han, G., Monaghan, E., Bacikova, D., Natarajan, M., Williams, R. *et al.* (2002) Mutations in the yeast LCB1 and LCB2 Genes, including those corresponding to the hereditary sensory neuropathy type I mutations, dominantly inactivate serine palmitoyltransferase *Journal of Biological Chemistry* 277, 10194-10200

111. Gable, K., Slife, H., Bacikova, D., Monaghan, E., and Dunn, T. M. (2000) Tsc3p is an 80-amino acid protein associated with serine palmitoyltransferase and required for optimal enzyme activity *Journal of Biological Chemistry* 275, 7597-7603
112. Yard, B. A., Carter, L. G., Johnson, K. A., Overton, I. M., Dorward, M., Liu, H. *et al.* (2007) The structure of serine palmitoyltransferase; gateway to sphingolipid biosynthesis *Journal of molecular biology* 370, 870-886
113. Raman, M. C., Johnson, K. A., Clarke, D. J., Naismith, J. H., and Campopiano, D. J. (2010) The serine palmitoyltransferase from *Sphingomonas wittichii* RW1: an interesting link to an unusual acyl carrier protein *Biopolymers* 93, 811-822
114. Ikushiro, H., Islam, M. M., Okamoto, A., Hoseki, J., Murakawa, T., Fujii, S. *et al.* (2009) Structural Insights into the Enzymatic Mechanism of Serine Palmitoyltransferase from *Sphingobacterium multivorum* *The Journal of Biochemistry* 146, 549-562 10.1093/jb/mvp100
115. Li, S., Xie, T., Liu, P., Wang, L., and Gong, X. (2021) Structural insights into the assembly and substrate selectivity of human SPT-ORMDL3 complex *Nature Structural & Molecular Biology* 28, 249-257 10.1038/s41594-020-00553-7
116. Wang, Y., Niu, Y., Zhang, Z., Gable, K., Gupta, S. D., Somashekarappa, N. *et al.* (2021) Structural insights into the regulation of human serine palmitoyltransferase complexes *Nature Structural & Molecular Biology* 28, 240-248 10.1038/s41594-020-00551-9
117. Xie, T., Liu, P., Wu, X., Dong, F., Zhang, Z., Yue, J. *et al.* (2023) Ceramide sensing by human SPT-ORMDL complex for establishing sphingolipid homeostasis *Nat Commun* 14, 3475 10.1038/s41467-023-39274-y
118. Hanada, K., Hara, T., Nishijima, M., Kuge, O., Dickson, R. C., and Nagiec, M. M. (1997) A mammalian homolog of the yeast LCB1 encodes a component of serine palmitoyltransferase, the enzyme catalyzing the first step in sphingolipid synthesis *Journal of Biological Chemistry* 272, 32108-32114
119. VANMIDDLESWORTH, F., GIACOBBE, R. A., LOPEZ, M., GARRITY, G., BLAND, J. A., Bartizal, K. *et al.* (1992) SPHINGOFUNGINS A, B, C, AND D; A NEW FAMILY OF ANTIFUNGAL AGENTS I. FERMENTATION, ISOLATION, AND BIOLOGICAL ACTIVITY *The Journal of Antibiotics* 45, 861-867
120. HORN, W. S., SMITH, J. L., BILLS, G. F., RAGHOOBAR, S. L., HELMS, G. L., KURTZ, M. B. *et al.* (1992) Sphingofungins E and F: Novel serinepalmitoyl trans-ferase inhibitors from *Paecilomyces variotii* *The Journal of Antibiotics* 45, 1692-1696
121. Mandala, S. M., Frommer, B. R., Thornton, R. A., KURTZ, M. B., Young, N. M., Cabello, M. A. *et al.* (1994) Inhibition of serine palmitoyl-transferase activity by lipoxamycin *The Journal of antibiotics* 47, 376-379
122. Whaley, H. A. (1971) Structure of lipoxamycin, a novel antifungal antibiotic *Journal of the American Chemical Society* 93, 3767-3769
123. Pewzner-Jung, Y., Ben-Dor, S., and Futerman, A. H. (2006) When do Lasses (longevity assurance genes) become CerS (ceramide synthases)? Insights into the

- regulation of ceramide synthesis *Journal of Biological Chemistry* 281, 25001-25005
124. Levy, M., and Futerman, A. H. (2010) Mammalian ceramide synthases *IUBMB Life* 62, 347-356 10.1002/iub.319
 125. Spassieva, S., Seo, J.-G., Jiang, J. C., Bielawski, J., Alvarez-Vasquez, F., Jazwinski, S. M. *et al.* (2006) Necessary role for the Lag1p motif in (dihydro) ceramide synthase activity *Journal of Biological Chemistry* 281, 33931-33938
 126. Winter, E., and Ponting, C. P. (2002) TRAM, LAG1 and CLN8: members of a novel family of lipid-sensing domains? *Trends in biochemical sciences* 27, 381-383
 127. Kageyama-Yahara, N., and Riezman, H. (2006) Transmembrane topology of ceramide synthase in yeast *Biochemical Journal* 398, 585-593
 128. Riley, R. T., Enongene, E., Voss, K. A., Norred, W. P., Meredith, F. I., Sharma, R. P. *et al.* (2001) Sphingolipid perturbations as mechanisms for fumonisin carcinogenesis *Environmental health perspectives* 109, 301-308
 129. Merrill Jr, A. H., Sullards, M. C., Wang, E., Voss, K. A., and Riley, R. T. (2001) Sphingolipid metabolism: roles in signal transduction and disruption by fumonisins *Environmental health perspectives* 109, 283-289
 130. Merrill Jr, A. H., Van Echten, G., Wang, E., and Sandhoff, K. (1993) Fumonisin B1 inhibits sphingosine (sphinganine) N-acyltransferase and de novo sphingolipid biosynthesis in cultured neurons in situ *Journal of Biological Chemistry* 268, 27299-27306
 131. Merrill Jr, A. H., Wang, E., Gilchrist, D., and Riley, R. (1993) Fumonisin and other inhibitors of de novo sphingolipid biosynthesis *Advances in lipid research* 26, 215-234
 132. Humpf, H.-U., Schmelz, E.-M., Meredith, F. I., Vesper, H., Vales, T. R., Wang, E. *et al.* (1998) Acylation of naturally occurring and synthetic 1-deoxysphinganine by ceramide synthase: formation of N-palmitoyl-aminopentol produces a toxic metabolite of hydrolyzed fumonisin, API, and a new category of ceramide synthase inhibitor *Journal of Biological Chemistry* 273, 19060-19064
 133. Figueiredo, J. M., Dias, W. B., Mendonça-Previato, L., Previato, J. O., and Heise, N. (2005) Characterization of the inositol phosphorylceramide synthase activity from *Trypanosoma cruzi* *Biochemical Journal* 387, 519-529
 134. Figueiredo, J. M., Rodrigues, D. C., Silva, R. C., Koeller, C. M., Jiang, J. C., Jazwinski, S. M. *et al.* (2012) Molecular and functional characterization of the ceramide synthase from *Trypanosoma cruzi* *Molecular and biochemical parasitology* 182, 62-74
 135. Denny, P. W., Shams-Eldin, H., Price, H. P., Smith, D. F., and Schwarz, R. T. (2006) The protozoan inositol phosphorylceramide synthase: a novel drug target that defines a new class of sphingolipid synthase *Journal of Biological Chemistry* 281, 28200-28209
 136. Koeller, C. M., and Heise, N. (2011) The sphingolipid biosynthetic pathway is a potential target for chemotherapy against Chagas disease *Enzyme Research* 2011,
 137. Mina, J. G., Mosely, J. A., Ali, H. Z., Denny, P. W., and Steel, P. G. (2011) Exploring *Leishmania major* inositol phosphorylceramide synthase (Lmj IPCS):

- insights into the ceramide binding domain *Organic & Biomolecular Chemistry* 9, 1823-1830
138. Bromley, P. E., Li, Y. O., Murphy, S. M., Sumner, C. M., and Lynch, D. V. (2003) Complex sphingolipid synthesis in plants: characterization of inositolphosphorylceramide synthase activity in bean microsomes *Archives of biochemistry and biophysics* 417, 219-226
 139. Wang, W., Yang, X., Tangchaiburana, S., Ndeh, R., Markham, J. E., Tsegaye, Y. *et al.* (2008) An inositolphosphorylceramide synthase is involved in regulation of plant programmed cell death associated with defense in *Arabidopsis* *The Plant cell* 20, 3163-3179
 140. Mangwanda, R., Myburg, A. A., and Naidoo, S. (2015) Transcriptome and hormone profiling reveals *Eucalyptus grandis* defence responses against *Chrysosporthe austroafricana* *BMC genomics* 16, 1-13
 141. Mandala, S. M., Thornton, R. A., Milligan, J., Rosenbach, M., Garcia-Calvo, M., Bull, H. G. *et al.* (1998) Rustmicin, a potent antifungal agent, inhibits sphingolipid synthesis at inositol phosphoceramide synthase *Journal of Biological Chemistry* 273, 14942-14949
 142. TAKATSU, T., NAKAYAMA, H., SHIMAZU, A., FURIHATA, K., IKEDA, K., FURIHATA, K. *et al.* (1985) Rustmicin, a new macrolide antibiotic active against wheat stem rust fungus *The Journal of Antibiotics* 38, 1806-1809
 143. Mandala, S. M., Thornton, R. A., Rosenbach, M., Milligan, J., Garcia-Calvo, M., Bull, H. G. *et al.* (1997) Khafrefungin, a Novel Inhibitor of Sphingolipid Synthesis * *Journal of Biological Chemistry* 272, 32709-32714
10.1074/jbc.272.51.32709
 144. Zhong, W., Jeffries, M. W., and Georgopapadaku, N. H. (2000) Inhibition of inositol phosphorylceramide synthase by aureobasidin A in *Candida* and *Aspergillus* species *Antimicrobial agents and chemotherapy* 44, 651-653
 145. Ohnuki, T., Yano, T., Ono, Y., Kozuma, S., Suzuki, T., Ogawa, Y. *et al.* (2009) Haplofungins, novel inositol phosphorylceramide synthase inhibitors, from *Lauriomyces bellulus* SANK 26899 I. Taxonomy, fermentation, isolation and biological activities *The Journal of Antibiotics* 62, 545-549
 146. Ohnuki, T., Yano, T., Furukawa, Y., and Takatsu, T. (2009) Haplofungins, novel inositol phosphorylceramide synthase inhibitors, from *Lauriomyces bellulus* SANK 26899 III. Absolute structure of haplofungin A *The Journal of Antibiotics* 62, 559-563 10.1038/ja.2009.74
 147. van Meer, G., Voelker, D. R., and Feigenson, G. W. (2008) Membrane lipids: where they are and how they behave *Nat Rev Mol Cell Biol* 9, 112-124
10.1038/nrm2330
 148. Vance, J. E., and Steenbergen, R. (2005) Metabolism and functions of phosphatidylserine *Prog Lipid Res* 44, 207-234 10.1016/j.plipres.2005.05.001
 149. Atkinson, K. D., Jensen, B., Kolat, A. I., Storm, E. M., Henry, S. A., and Fogel, S. (1980) Yeast mutants auxotrophic for choline or ethanolamine *J Bacteriol* 141, 558-564
 150. Chen, Y. L., Montedonico, A. E., Kauffman, S., Dunlap, J. R., Menn, F. M., and Reynolds, T. B. (2010) Phosphatidylserine synthase and phosphatidylserine

- decarboxylase are essential for cell wall integrity and virulence in *Candida albicans* *Mol Microbiol* 75, 1112-1132 10.1111/j.1365-2958.2009.07018.x
151. Michell, R. (1979) Inositol phospholipids in membrane function *Trends in biochemical sciences* 4, 128-131
 152. Dey, P., Su, W. M., Han, G. S., and Carman, G. M. (2017) Phosphorylation of lipid metabolic enzymes by yeast protein kinase C requires phosphatidylserine and diacylglycerol *Journal of lipid research* 58, 742-751 10.1194/jlr.M075036
 153. Burstyn-Cohen, T., and Maimon, A. (2019) TAM receptors, Phosphatidylserine, inflammation, and Cancer *Cell Communication and Signaling* 17, 1-9
 154. N'Guessan, K. F., Patel, P. H., and Qi, X. (2020) SapC-DOPS—a Phosphatidylserine-targeted Nanovesicle for selective Cancer therapy *Cell Communication and Signaling* 18, 1-5
 155. Bevers, E. M., Comfurius, P., and Zwaal, R. F. (1983) Changes in membrane phospholipid distribution during platelet activation *Biochimica et Biophysica Acta (BBA)-Biomembranes* 736, 57-66
 156. Fadok, V. A., Voelker, D. R., Campbell, P. A., Cohen, J. J., Bratton, D. L., and Henson, P. M. (1992) Exposure of phosphatidylserine on the surface of apoptotic lymphocytes triggers specific recognition and removal by macrophages *Journal of immunology (Baltimore, Md: 1950)* 148, 2207-2216
 157. Erwig, L., and Henson, P. (2008) Clearance of apoptotic cells by phagocytes *Cell Death & Differentiation* 15, 243-250
 158. Davis, S. E., Hopke, A., Minkin, S. C., Montedonico, A. E., Wheeler, R. T., and Reynolds, T. B. (2014) Masking of $\beta(1-3)$ -Glucan in the Cell Wall of *Candida albicans* from Detection by Innate Immune Cells Depends on Phosphatidylserine *Infection and immunity* 82, 4405-4413 10.1128/iai.01612-14
 159. Cassilly, C. D., and Reynolds, T. B. (2018) PS, It's Complicated: The Roles of Phosphatidylserine and Phosphatidylethanolamine in the Pathogenesis of *Candida albicans* and Other Microbial Pathogens *J Fungi (Basel)* 4, 10.3390/jof4010028
 160. Kuge, O., Nishijima, M., and Akamatsu, Y. (1991) A cloned gene encoding phosphatidylserine decarboxylase complements the phosphatidylserine biosynthetic defect of a Chinese hamster ovary cell mutant *Journal of Biological Chemistry* 266, 6370-6376
 161. Trotter, P. J., Pedretti, J., and Voelker, D. (1993) Phosphatidylserine decarboxylase from *Saccharomyces cerevisiae*. Isolation of mutants, cloning of the gene, and creation of a null allele *Journal of Biological Chemistry* 268, 21416-21424
 162. Trotter, P. J., and Voelker, D. R. (1995) Identification of a Non-mitochondrial Phosphatidylserine Decarboxylase Activity (PSD2) in the Yeast *Saccharomyces cerevisiae* (*) *Journal of Biological Chemistry* 270, 6062-6070
 163. Kuge, O., and Nishijima, M. (1997) Phosphatidylserine synthase I and II of mammalian cells *Biochim Biophys Acta* 1348, 151-156 10.1016/s0005-2760(97)00137-9
 164. Zelinski, T. A., and Choy, P. C. (1982) Phosphatidylethanolamine biosynthesis in isolated hamster heart *Canadian Journal of Biochemistry* 60, 817-823

165. Tijburg, L. B., Geelen, M. J., and Van Golde, L. M. (1989) Biosynthesis of phosphatidylethanolamine via the CDP-ethanolamine route is an important pathway in isolated rat hepatocytes *Biochemical and biophysical research communications* 160, 1275-1280
166. Bleijerveld, O. B., Brouwers, J. F., Vaandrager, A. B., Helms, J. B., and Houweling, M. (2007) The CDP-ethanolamine pathway and phosphatidylserine decarboxylation generate different phosphatidylethanolamine molecular species *Journal of Biological Chemistry* 282, 28362-28372
167. Nerlich, A., von Orlow, M., Rontein, D., Hanson, A. D., and Dörmann, P. (2007) Deficiency in phosphatidylserine decarboxylase activity in the *psd1 psd2 psd3* triple mutant of *Arabidopsis* affects phosphatidylethanolamine accumulation in mitochondria *Plant physiology* 144, 904-914
168. Voelker, D. R. (1997) Phosphatidylserine decarboxylase *Biochimica et Biophysica Acta (BBA) - Lipids and Lipid Metabolism* 1348, 236-244 [https://doi.org/10.1016/S0005-2760\(97\)00101-X](https://doi.org/10.1016/S0005-2760(97)00101-X)
169. Choi, J.-Y., Duraisingh, M. T., Marti, M., Mamoun, C. B., and Voelker, D. R. (2015) From protease to decarboxylase: the molecular metamorphosis of phosphatidylserine decarboxylase *Journal of Biological Chemistry* 290, 10972-10980
170. Ogunbona, O. B., Onguka, O., Calzada, E., and Claypool, S. M. (2017) Multitiered and cooperative surveillance of mitochondrial phosphatidylserine decarboxylase 1 *Molecular and cellular biology* 37, e00049-00017
171. Watanabe, Y., Watanabe, Y., and Watanabe, S. (2020) Structural basis for phosphatidylethanolamine biosynthesis by bacterial phosphatidylserine decarboxylase *Structure* 28, 799-809. e795
172. Cho, G., Lee, E., and Kim, J. (2021) Structural insights into phosphatidylethanolamine formation in bacterial membrane biogenesis. *Sci Rep* 11: 5785
173. Wickner, W., and Kennedy, E. (1971) ISOLATION OF A MEMBRANE-BOUND ENZYME (PHOSPHATIDYLSERINE DECARBOXYLASE) FROM *ESCHERICHIA-COLI* In *Federation Proceedings, FEDERATION AMER SOC EXP BIOL* 9650 ROCKVILLE PIKE, BETHESDA, MD 20814-3998, 1119-&
174. Cronan Jr, J. E., and Vagelos, P. R. (1972) Metabolism and function of the membrane phospholipids of *Escherichia coli* *Biochimica et Biophysica Acta (BBA)-Reviews on Biomembranes* 265, 25-60
175. Trivedi, A., Singhal, G. S., and Prasad, R. (1983) Effect of phosphatidylserine enrichment on amino acid transport in yeast *Biochimica et Biophysica Acta (BBA)-Biomembranes* 729, 85-89
176. Pizer, L. I., and Merlie, J. P. (1973) Effect of serine hydroxamate on phospholipid synthesis in *Escherichia coli* *Journal of Bacteriology* 114, 980-987
177. Forbes, C. D., Toth, J. G., Özbal, C. C., Lamarr, W. A., Pendleton, J. A., Rocks, S. *et al.* (2007) High-throughput mass spectrometry screening for inhibitors of phosphatidylserine decarboxylase *Journal of biomolecular screening* 12, 628-634
178. Choi, J. Y., Kumar, V., Pachikara, N., Garg, A., Lawres, L., Toh, J. Y. *et al.* (2016) Characterization of *Plasmodium* phosphatidylserine decarboxylase

- expressed in yeast and application for inhibitor screening *Molecular microbiology* 99, 999-1014
179. Hendricson, A., Umlauf, S., Choi, J. Y., Thekkiniath, J., Surovtseva, Y. V., Fuller, K. K. *et al.* (2019) High-throughput screening for phosphatidylserine decarboxylase inhibitors using a distyrylbenzene-bis-aldehyde (DSB-3)-based fluorescence assay *J Biol Chem* 294, 12146-12156 10.1074/jbc.RA119.007766
 180. Braun, B. R., van Het Hoog, M., d'Enfert, C., Martchenko, M., Dungan, J., Kuo, A. *et al.* (2005) A human-curated annotation of the *Candida albicans* genome *PLoS Genet* 1, 36-57 10.1371/journal.pgen.0010001
 181. Davis, S. E., Tams, R. N., Solis, N. V., Wagner, A. S., Chen, T., Jackson, J. W. *et al.* (2018) *Candida albicans* cannot acquire sufficient ethanolamine from the host to support virulence in the absence of de novo phosphatidylethanolamine synthesis *Infection and immunity* 86, e00815-00817
 182. Konarzewska, P., Wang, Y., Han, G.-S., Goh, K. J., Gao, Y.-G., Carman, G. M. *et al.* (2019) Phosphatidylserine synthesis is essential for viability of the human fungal pathogen *Cryptococcus neoformans* *The Journal of biological chemistry* 294, 2329-2339 10.1074/jbc.RA118.006738
 183. Raetz, C. R., and Kennedy, E. P. (1972) The association of phosphatidylserine synthetase with ribosomes in extracts of *Escherichia coli* *J Biol Chem* 247, 2008-2014
 184. Matsumoto, K. (1997) Phosphatidylserine synthase from bacteria *Biochim Biophys Acta* 1348, 214-227 10.1016/s0005-2760(97)00110-0
 185. Atkinson, K., Fogel, S., and Henry, S. A. (1980) Yeast mutant defective in phosphatidylserine synthesis *Journal of Biological Chemistry* 255, 6653-6661
 186. Kovac, L., Gbelska, I., Poliachova, V., Subik, J., and Kovacova, V. (1980) Membrane mutants: a yeast mutant with a lesion in phosphatidylserine biosynthesis *Eur J Biochem* 111, 491-501 10.1111/j.1432-1033.1980.tb04965.x
 187. Carson, M. A., Atkinson, K. D., and Waechter, C. J. (1982) Properties of particulate and solubilized phosphatidylserine synthase activity from *Saccharomyces cerevisiae*. Inhibitory effect of choline in the growth medium *Journal of Biological Chemistry* 257, 8115-8121
 188. Poole, M. A., Homann, M. J., Bae-Lee, M. S., and Carman, G. M. (1986) Regulation of phosphatidylserine synthase from *Saccharomyces cerevisiae* by phospholipid precursors *Journal of Bacteriology* 168, 668-672 10.1128/jb.168.2.668-672.1986
 189. Bailis, A. M., Poole, M. A., Carman, G. M., and Henry, S. A. (1987) The membrane-associated enzyme phosphatidylserine synthase is regulated at the level of mRNA abundance *Molecular and Cellular Biology* 7, 167-176 10.1128/mcb.7.1.167
 190. Kelley, M. J., Bailis, A. M., Henry, S. A., and Carman, G. M. (1988) Regulation of phospholipid biosynthesis in *Saccharomyces cerevisiae* by inositol. Inositol is an inhibitor of phosphatidylserine synthase activity *J Biol Chem* 263, 18078-18085

191. Kinney, A. J., and Carman, G. M. (1988) Phosphorylation of yeast phosphatidylserine synthase in vivo and in vitro by cyclic AMP-dependent protein kinase *Proc Natl Acad Sci U S A* 85, 7962-7966
192. Kuchler, K., Daum, G., and Paltauf, F. (1986) Subcellular and submitochondrial localization of phospholipid-synthesizing enzymes in *Saccharomyces cerevisiae* *J Bacteriol* 165, 901-910
193. Kohlwein, S. D., Kuchler, K., Sperka-Gottlieb, C., Henry, S. A., and Paltauf, F. (1988) Identification of mitochondrial and microsomal phosphatidylserine synthase in *Saccharomyces cerevisiae* as the gene product of the CHO1 structural gene *J Bacteriol* 170, 3778-3781
194. Carman, G. M., and Matas, J. (1981) Solubilization of microsomal-associated phosphatidylserine synthase and phosphatidylinositol synthase from *Saccharomyces cerevisiae* *Can J Microbiol* 27, 1140-1149
195. Bae-Lee, M. S., and Carman, G. M. (1984) Phosphatidylserine synthesis in *Saccharomyces cerevisiae*. Purification and characterization of membrane-associated phosphatidylserine synthase *J Biol Chem* 259, 10857-10862
196. Cassilly, C. D., Farmer, A. T., Montedonico, A. E., Smith, T. K., Campagna, S. R., and Reynolds, T. B. (2017) Role of phosphatidylserine synthase in shaping the phospholipidome of *Candida albicans* *FEMS Yeast Res* 17, 10.1093/femsyr/fox007
197. Zhou, Y., Cassilly, C. D., and Reynolds, T. B. (2021) Mapping the Substrate-Binding Sites in the Phosphatidylserine Synthase in *Candida albicans* *Frontiers in Cellular and Infection Microbiology* 11, 10.3389/fcimb.2021.765266
198. Zhou, Y., and Reynolds, T. (2021) Identification of the substrate-binding sites in the phosphatidylserine synthase from *Candida albicans* *The FASEB Journal* 35, <https://doi.org/10.1096/fasebj.2021.35.S1.02666>
199. Zhou, Y., Syed, J. H., Semchonok, D. A., Wright, E., Kyrilis, F. L., Hamdi, F. *et al.* (2023) Solubilization, purification, and characterization of the hexameric form of phosphatidylserine synthase from *Candida albicans* *Journal of Biological Chemistry* 299, 10.1016/j.jbc.2023.104756
200. Nogly, P., Gushchin, I., Remeeva, A., Esteves, A. M., Borges, N., Ma, P. *et al.* (2014) X-ray structure of a CDP-alcohol phosphatidyltransferase membrane enzyme and insights into its catalytic mechanism *Nat Commun* 5, 4169 10.1038/ncomms5169
201. Sciara, G., Clarke, O. B., Tomasek, D., Kloss, B., Tabuso, S., Byfield, R. *et al.* (2014) Structural basis for catalysis in a CDP-alcohol phosphotransferase *Nat Commun* 5, 4068 10.1038/ncomms5068
202. Clarke, O. B., Tomasek, D., Jorge, C. D., Dufrisne, M. B., Kim, M., Banerjee, S. *et al.* (2015) Structural basis for phosphatidylinositol-phosphate biosynthesis *Nat Commun* 6, 8505 10.1038/ncomms9505
203. Dufrisne, M. B., Jorge, C. D., Timóteo, C. G., Petrou, V. I., Ashraf, K. U., Banerjee, S. *et al.* (2020) Structural and Functional Characterization of Phosphatidylinositol-Phosphate Biosynthesis in *Mycobacteria* *Journal of Molecular Biology*

204. Gråve, K., Bennett, M. D., and Högbom, M. (2019) Structure of Mycobacterium tuberculosis phosphatidylinositol phosphate synthase reveals mechanism of substrate binding and metal catalysis *Communications Biology* 2, 175
10.1038/s42003-019-0427-1
205. Centola, M., van Pee, K., Betz, H., and Yildiz, Ö. (2021) Crystal structures of phosphatidyl serine synthase PSS reveal the catalytic mechanism of CDP-DAG alcohol O-phosphatidyl transferases *Nat Commun* 12, 6982 10.1038/s41467-021-27281-w
206. Wang, L., and Zhou, M. (2023) Structure of a eukaryotic cholinephosphotransferase-1 reveals mechanisms of substrate recognition and catalysis *Nat Commun* 14, 2753 10.1038/s41467-023-38003-9
207. Wang, Z., Yang, M., Yang, Y., He, Y., and Qian, H. (2023) Structural basis for catalysis of human choline/ethanolamine phosphotransferase 1 *Nat Commun* 14, 2529 10.1038/s41467-023-38290-2
208. Cassilly, C. D., Maddox, M. M., Cherian, P. T., Bowling, J. J., Hamann, M. T., Lee, R. E. *et al.* (2016) SB-224289 Antagonizes the Antifungal Mechanism of the Marine Depsipeptide Papuamide A *PLoS One* 11, e0154932
10.1371/journal.pone.0154932
209. Pokharel, M., Konarzewska, P., Roberge, J. Y., Han, G.-S., Wang, Y., Carman, G. M. *et al.* (2022) The Anticancer Drug Bleomycin Shows Potent Antifungal Activity by Altering Phospholipid Biosynthesis *Microbiology Spectrum* 10, e00862-00822 doi:10.1128/spectrum.00862-22
210. Robson, G. D., Kuhn, P. J., and Trinci, A. P. (1989) Effect of validamycin A on the inositol content and branching of *Rhizoctonia cerealis* and other fungi *Microbiology* 135, 739-750
211. Jun-Ichi, N., and Satoshl, Y. (1983) 2-Hydroxyethylhydrazine as a potent inhibitor of phospholipid methylation in yeast *Biochimica et Biophysica Acta (BBA)-Lipids and Lipid Metabolism* 751, 201-209
212. Chin, J., and Bloch, K. (1988) Phosphatidylcholine synthesis in yeast *Journal of lipid research* 29, 9-14
213. Serrán-Aguilera, L., Denton, H., Rubio-Ruiz, B., López-Gutiérrez, B., Entrena, A., Izquierdo, L. *et al.* (2016) *Plasmodium falciparum* Choline Kinase Inhibition Leads to a Major Decrease in Phosphatidylethanolamine Causing Parasite Death *Scientific Reports* 6, 33189 10.1038/srep33189

**CHAPTER 2 MAPPING THE SUBSTRATE-BINDING SITES IN THE
PHOSPHATIDYLSERINE SYNTHASE IN *CANDIDA ALBICANS***

Publication Note

A version of this chapter has been previously published by Yue Zhou, Chelsi D. Cassilly, and Todd B. Reynolds:

Zhou, Y., Cassilly, C. D., & Reynolds, T. B. (2021). Mapping the substrate-binding sites in the phosphatidylserine synthase in *Candida albicans*. *Frontiers in Cellular and Infection Microbiology*, 11, 1281.

Contribution in the paper: Conceived and designed the experiments: YZ, CC, and TR. Performed the experiments: YZ and CC. Analyzed the data: YZ and TR. Contributed reagents/materials/analysis tools: TR. Wrote the paper: YZ, CC, and TR.

Specifically, Chelsi Cassilly made the strain expressing HA-tagged Cho1 and the CAPT mutants. Yue Zhou made all the putative serine-binding mutants. All the Western blot, PS synthase assays, spot dilution assay, growth curves, kinetic curves and homology modeling were done by Yue Zhou. The manuscript was written by Yue Zhou and edited by Todd Reynolds and Chelsi Cassilly.

Abstract

The fungal phosphatidylserine (PS) synthase, a membrane protein encoded by the *CHO1* gene, is a potential drug target for pathogenic fungi, such as *Candida albicans*. However, both substrate-binding sites of *C. albicans* Cho1 have not been characterized. Cho1 has two substrates: cytidyldiphosphate-diacylglycerol (CDP-DAG) and serine. Previous studies identified a conserved CDP-alcohol phosphotransferase (CAPT) binding motif, which is present within Cho1. We tested the CAPT motif for its role in PS synthesis by mutating conserved residues using alanine substitution mutagenesis. PS synthase assays revealed that mutations in all but one conserved amino acid within the CAPT motif resulted in decreased Cho1 function. In contrast, there were no clear motifs in Cho1 for binding serine. Therefore, to identify the serine binding site, PS synthase sequences from three fungi were aligned with sequences of a similar enzyme, phosphatidylinositol (PI) synthase, from the same fungi. This revealed a motif that was unique to PS synthases. Using alanine substitution mutagenesis, we found that some of the residues in this motif are required for Cho1 function. Two alanine substitution mutants, L184A and R189A, exhibited contrasting impacts on PS synthase activity, and were characterized for their Michaelis-Menten kinetics. The L184A mutant displayed enhanced PS synthase activity and showed an increased V_{\max} . In contrast, R189A showed decreased PS synthase activity and increased K_M for serine, suggesting that residue R189 is involved in serine binding. These results help to characterize PS synthase substrate binding, and should direct rational approaches for finding Cho1 inhibitors that may lead to better antifungals.

Introduction

Candida spp. are the most common causes of fungal infections in humans and are a major cause of fungi-associated mortality worldwide (1). These species are versatile pathogens, with *C. albicans* being the most common. While they can infect almost all body sites, they are most prevalently seen in infections of the oral mucosa, vaginal mucosa, and bloodstream/deep organs (*i.e.*, invasive mycoses) (2). The latter is of greatest concern because they are associated with a high (~40%) mortality rate (3, 4). There are only three classes of antifungals that are commonly used to treat systemic infections: echinocandins (e.g., caspofungin), azoles (e.g., itraconazole), and polyenes (e.g., amphotericin B) (5). However, these all have limitations, which include drug resistance for the echinocandins and azoles and patient toxicity for the polyene amphotericin B (6-9). Thus, there is an urgent need to discover new drugs. One classic approach is to identify virulence-related proteins within *C. albicans* that are not conserved in humans and exploit them as drug targets.

The phosphatidylserine (PS) synthase in *C. albicans* represents a potential drug target for three reasons: 1) It is required for virulence (10), indicating that inhibitors of this enzyme would render the organism incapable of causing infection; 2) it is absent in humans (11), so inhibitors potentially would have no toxic side effects for the host; and 3) it is conserved among many fungi, so a drug could potentially be effective against multiple fungal pathogens. Recently, deletion of PS synthase in *Cryptococcus neoformans* was shown to be lethal, suggesting phosphatidylserine synthesis is also essential for the viability of some fungi (12). This observation further strengthens the potential of PS synthase as a broad antifungal drug target.

The PS synthase enzyme (originally denoted as: cytidine 5'-diphospho-1,2-diacyl-sn-glycerol: L-serine O-phosphatidyltransferase, gene name: *CHO1*) was first identified in *Saccharomyces cerevisiae* (13-15). Since then, characterization of *S. cerevisiae* Cho1 included protein solubilization and purification (16, 17), determination of Michaelis-Menton kinetics (16-18), understanding regulation of Cho1 (18-22), and identifying the localization of the enzyme (23, 24). The function of the first fungal pathogen Cho1 homolog was described in *C. albicans* and this protein was shown to be required for both systemic and oral *Candida* infection in the mouse model (10, 25). Later, the Michaelis-Menten kinetics of the wildtype *C. albicans* Cho1 were biochemically determined, which yielded a millimolar-scale K_M for serine, similar to that reported for *S. cerevisiae* Cho1 (17, 26). These findings again highlight the enzyme's potential as a drug target for *Candida* infections.

The long-term goal of characterizing Cho1 is to discover a small molecule inhibitor of *C. albicans* Cho1 that can be used as a lead compound for drug development. Small molecule screening is a very effective approach to identify inhibitors of enzymes, but another strategy is to use a rational approach for identifying inhibitors (27). Ligand-based drug design for *C. albicans* Cho1 is limited because of the small number of known PS synthase ligands or ligand analogs, as well as the ubiquitous nature of its natural substrates. In addition, neither the three-dimensional structure nor the binding sites for substrates of *C. albicans* Cho1 are available, which hinders structure-based design. Thus, it is critical to the foundation of these approaches that the binding sites for the two substrates, cytidyldiphosphate-diacylglycerol (CDP-DAG) and serine, are described. Here, we biochemically identified potential substrate binding motifs in the enzyme. Identification

of these sites in the protein will facilitate a more directed approach to discovering small molecules that might interact with *C. albicans* Cho1.

Previously, a highly conserved motif, D-(X)₂-D-G-(X)₂-A-R-(X)₂-N-(X)₅-G-(X)₂-L-D-(X)₃-D, was identified from the alignment of yeast phosphatidylinositol synthase (PI synthase), phosphatidylserine synthase, and the *E. coli* phosphatidylglycerophosphate synthase (PGP synthase) (28). This motif has been further identified in yeast cholinephosphotransferase (Cpt1) and ethanolaminephosphotransferase (Ept1) (29, 30). All of these enzymes bind a CDP-linked molecule and a second small alcohol and catalyze the formation of a phosphodiester bond between the two. Since these initial studies, this CDP-alcohol phosphatidyltransferase (CAPT) motif was narrowed to D-G-(X)₂-A-R-(X)₈-G-(X)₃-D-(X)₃-D, and was identified to be almost invariably conserved in numerous other lipid biosynthetic enzymes, including those of Gram positive and Gram negative bacteria, archaea, fungi, plants, and mammals (12, 31-36). The CAPT motif in yeast Cpt1 was characterized by alanine substitution mutagenesis, providing information on the importance of specific residues within the conserved motif (37).

More recently, two enzymes from the CDP-alcohol phosphatidyltransferase family from *Archaeoglobus fulgidus* were shown to contain this motif on helices TM2 and TM3 of the solved crystal structures (38, 39). In these studies, the CAPT motif was also widened to include an extra aspartic acid, generating the current, more general motif: D₁xxD₂G₁xxAR...G₂xxxD₃xxxD₄ (Table 2.1). This was further confirmed in the phosphatidylinositol-phosphate synthase from *Renibacterium salmoninarum*, *Mycobacterium tuberculosis*, and *Mycobacterium kansasii*, where the CAPT motif was again found within TM2 and TM3 of the solved crystal structures (35, 40, 41). To our

Table 2.1 The CAPT motif for binding CDP-alcohols is mostly conserved across domains. * Gray highlighted residues represent the conserved amino acids

Organism	Enzyme	CDP-Binding Motif	Reference
<i>C. albicans</i>	PS Synthase	¹²⁵ DFFDGRVARLRNKSSLMGQELDSLAD ¹⁵⁰	This research
<i>S. cerevisiae</i>	PS Synthase	¹²⁷ DFLDGRVARLRNRSSLMGQELDSLAD ¹⁵²	(51)
<i>S. cerevisiae</i>	Cholinephosphotransferase (Cpt1)	¹¹⁰ DMHDGMHARRTGQQGPLGELFDHCID ¹³⁵	(37)
<i>S. pombe</i>	PS Synthase	⁹² DFLDGKVARWRGKSSLMGQELDSLAD ¹¹⁷	(34)
<i>B. subtilis</i>	PS Synthase	⁴² DFFDGMAARKLNAVSDMGRELDSFAD ⁶⁷	(52)
<i>S. meliloti</i>	Phosphatidylcholine (PC) Synthase	⁵⁶ DGIDGPIARKVQVKEVLPNWSGDTLDNVID ⁸⁵	(53)
<i>A. fulgidus</i>	CDP-alcohol phosphotransferase AF2299	²¹⁴ DGCDGEIARLKFMESKYGAWLDGVLD ²³⁹	(39)
<i>A. fulgidus</i>	CDP-alcohol phosphotransferase IPCT-DIPPS	³⁵⁷ DGCDGEIARASLKMSKGGYVDSILD ³⁸²	(38)
<i>R. salmoninarum</i>	PIP synthase	⁶⁶ DIIDGLMARLLFREGPWGAFLDSYLD ⁹¹	(40)

Table 2.1 continued

<i>M. tuberculosis</i>	PIP synthase	⁶⁸ DMLDGAMARERGGGTRFGAVLDATCD ₉₃	(35)
<i>M. kansasii</i>	PIP synthase	⁶⁸ DMLDGAMARLRSGGTRFGAVLDAACD ₉₃	(41)
		DFFDGRVARLRNKS----SLMGQELDSLAD DFLDGRVARLRNRS----SLMGQELDSLAD DMHDGMHARRTGQQ---- GPLGELFDHCID DFLDGKVARWRGKS---- SLMGQELDSLAD DFFDGMAARKLNAV---- SDMGRELDSFAD DGIDGPIARKVQVKEVLPNWSGDTLDNV ID DGCDGEIARLKFME---- SKYGAWLDGVLD DGCDGEIARASLKM----SKKGGYVDSILD DIIDGLMARLLFRE----GPWGAFLD SYLD DMLDGAMARERGGG---- TRFGAVLDATCD DMLDGAMARLRSGG---- TRFGAVLDAACD D ₁ xxD ₂ G ₁ xxAR.....G ₂ xxxD ₃ xxxD ₄	
	<i>C. albicans</i> PS Synthase		
	<i>S. cerevisiae</i> PS Synthase		
	<i>S. cerevisiae</i> Cpt1		
	<i>S. pombe</i> PS Synthase		
	<i>B. subtilis</i> PS Synthase		
	<i>S. meliloti</i> PC Synthase		
	<i>A. fulgidus</i> AF2299		
	<i>A. fulgidus</i> IPCT-DIPPS		
	<i>R. salmoninarum</i> PIP synthase		
	<i>M. tuberculosis</i> PIP synthase		
	<i>M. kansasii</i> PIP synthase		
	CAPT motif		

knowledge, these are the five CDP-alcohol phosphatidyltransferase enzymes with solved crystal structures, and there is currently no eukaryotic counterpart solved.

Based on the above studies, there is sequence homology to guide a search for the CAPT motif in Cho1, but the motif specific for the other substrate, serine, is unknown. In fact, for many of the CDP-DAG binding enzymes, such as PI synthase and PGP synthase, the binding sites for the non-CDP substrates are unclear. Furthermore, some important residues involved in serine binding or recognition from other serine-utilizing enzymes have been identified, but these residues are unlikely to inform our search as these enzymes catalyze very different reactions and the equivalent residues are absent in Cho1 (42, 43). Thus, identification of the serine binding site—or some residues involved in serine binding, even if it is not the full motif—in Cho1 will facilitate a better understanding of this class of enzymes which are crucial for phospholipid biosynthesis in all domains of life.

Previously, we described the apparent K_M and V_{max} for *C. albicans* PS synthase, as well as its role in the phospholipidome of *C. albicans* (26). Furthermore, we probed the specificity of the active site of this protein for L-serine by competition assays with the closely related amino acids L-threonine and D-serine by an *in vitro* assay (26). We found that only very high concentrations of these substrates could compete with L-serine, indicating that the enzyme seems to be specific for L-serine, which agrees with previous studies in *S. cerevisiae* and *E. coli* (18, 44). To further reveal insights into the active sites in the present communication, we mapped and characterized residues that affect binding for both substrates in Cho1.

Materials and Methods

Strains and media

In this study, we used the *cho1* $\Delta\Delta$ mutant (YLC337) and *cho1* $\Delta\Delta::CHO1$ strain created from the SC5314 (wildtype) strain of *C. albicans*, which have been described previously (10). The *cho1* $\Delta\Delta$ strain was used to generate the *cho1* $\Delta\Delta P_{ENO1}-CHO1-HAx3$ strain (HA1) and its binding site mutant derivatives (Table 2.2). The media used to culture strains were YPD or minimal medium (0.67% yeast nitrogen base, 2% dextrose) \pm 1 mM ethanolamine, where indicated.

Genetic cloning and site-directed mutagenesis

The plasmid containing *CHO1-HAx3* is called pCDC31 and was generated as follows: The plasmid pBT1, containing the *ENO1* promoter (P_{ENO1}) and the *SAT1* marker (45), was used as a vector. The *CHO1* gene was amplified from SC5314 genomic DNA using primers CCO160, which sits upstream of the *CHO1* start site and includes a 5' *NotI* cut site, and CCO55 which sits at the 3' end of *CHO1* just upstream of the stop codon and includes a 3' 2x HA tag followed by an *AatII* cut site. The 3' untranslated region (3'UTR) of *CHO1* was amplified using CCO56, which sits immediately downstream of the *CHO1* stop codon and contains a 5' *AatII* cut site followed by a 1x HA tag before the downstream sequence, and CCO163, which sits 500 bp downstream of the *CHO1* stop codon and includes a 3' *SacI* cut site. The 3'UTR was included in the construct to increase the stability of the transcripts (46). Once amplified, both fragments were double digested with their respective enzyme combinations. The plasmid pBT1 was digested with *NotI* and *SacI* and all three fragments were ligated together to create pCDC31. All plasmids are listed in Table 2.3.

Table 2.2. Strains produced in this study

Organism	Strain	Plasmid	Gene/Mutation	Genotype
<i>Candida albicans</i>	HA1	pCDC4	<i>CHO1-HAx3</i>	<i>cho1ΔΔP_{ENO1}-CHO1-HAx3</i>
<i>Candida albicans</i>	CDCS60	pCDC15	<i>CHO1^{D125A}-HAx3</i>	<i>cho1ΔΔP_{ENO1}-CHO1^{D125A}-HAx3</i>
<i>Candida albicans</i>	CDCS61	pCDC8	<i>CHO1^{D128A}-HAx3</i>	<i>cho1ΔΔP_{ENO1}-CHO1^{D128A}-HAx3</i>
<i>Candida albicans</i>	CDCS62	pCDC14	<i>CHO1^{G129A}-HAx3</i>	<i>cho1ΔΔP_{ENO1}-CHO1^{G129A}-HAx3</i>
<i>Candida albicans</i>	CDCS63	pCDC10	<i>CHO1^{R133A}-HAx3</i>	<i>cho1ΔΔP_{ENO1}-CHO1^{R133A}-HAx3</i>
<i>Candida albicans</i>	CDCS64	pCDC12	<i>CHO1^{G142A}-HAx3</i>	<i>cho1ΔΔP_{ENO1}-CHO1^{G142A}-HAx3</i>
<i>Candida albicans</i>	CDCS65	pCDC11	<i>CHO1^{D146A}-HAx3</i>	<i>cho1ΔΔP_{ENO1}-CHO1^{D146A}-HAx3</i>
<i>Candida albicans</i>	CDCS66	pCDC9	<i>CHO1^{D150A}-HAx3</i>	<i>cho1ΔΔP_{ENO1}-CHO1^{D150A}-HAx3</i>
<i>Candida albicans</i>	YZ 7	pYZ2	<i>CHO1^{V180A}-HAx3</i>	<i>cho1ΔΔP_{ENO1}-CHO1^{V180A}-HAx3</i>
<i>Candida albicans</i>	YZ 8	pYZ3	<i>CHO1^{L181A}-HAx3</i>	<i>cho1ΔΔP_{ENO1}-CHO1^{L181A}-HAx3</i>
<i>Candida albicans</i>	YZ 9	pYZ4	<i>CHO1^{C182A}-HAx3</i>	<i>cho1ΔΔP_{ENO1}-CHO1^{C182A}-HAx3</i>
<i>Candida albicans</i>	YZ 10	pYZ5	<i>CHO1^{G183A}-HAx3</i>	<i>cho1ΔΔP_{ENO1}-CHO1^{G183A}-HAx3</i>
<i>Candida albicans</i>	YZ 11	pYZ6	<i>CHO1^{L184A}-HAx3</i>	<i>cho1ΔΔP_{ENO1}-CHO1^{L184A}-HAx3</i>
<i>Candida albicans</i>	CDCS67	pCDC23	<i>CHO1^{R186A}-HAx3</i>	<i>cho1ΔΔP_{ENO1}-CHO1^{R186A}-HAx3</i>
<i>Candida albicans</i>	CDCS68	pCDC24	<i>CHO1^{L187A}-HAx3</i>	<i>cho1ΔΔP_{ENO1}-CHO1^{L187A}-HAx3</i>

Table 2.2 continued

<i>Candida albicans</i>	CDCS69	pCDC22	<i>CHO1^{R189A}-HAx3</i>	<i>cho1ΔΔP_{ENO1}-CHO1^{R189A}-HAx3</i>
<i>Candida albicans</i>	CDCS70	pCDC25	<i>CHO1^{F190A}-HAx3</i>	<i>cho1ΔΔP_{ENO1}-CHO1^{F190A}-HAx3</i>
<i>Candida albicans</i>	YZ32	pYZ32	<i>CHO1^{R133E}-HAx3</i>	<i>cho1ΔΔP_{ENO1}-CHO1^{R133E}-HAx3</i>
<i>Candida albicans</i>	YZ57	pYZ50	<i>CHO1^{G129P}-HAx3</i>	<i>cho1ΔΔP_{ENO1}-CHO1^{G129P}-HAx3</i>

Table 2.3. Plasmids Used in this Study.

*All CHO1 constructs are tagged on the 3'-terminus with the HAx3 epitope tag sequence

Plasmid	Inserts *	Source
pYLC314-TBR	NAT ^R , Amp ^R	(45)
pCDC31	NAT ^R , Amp ^R , <i>CHO1</i>	This study
pCDC15	NAT ^R , Amp ^R , <i>CHO1</i> ^{D125A}	This study
pCDC8	NAT ^R , Amp ^R , <i>CHO1</i> ^{D128A}	This study
pCDC14	NAT ^R , Amp ^R , <i>CHO1</i> ^{G129A}	This study
pCDC10	NAT ^R , Amp ^R , <i>CHO1</i> ^{R133A}	This study
pCDC12	NAT ^R , Amp ^R , <i>CHO1</i> ^{G142A}	This study
pCDC11	NAT ^R , Amp ^R , <i>CHO1</i> ^{D146A}	This study
pCDC9	NAT ^R , Amp ^R , <i>CHO1</i> ^{D150A}	This study
pYZ2	NAT ^R , Amp ^R , <i>CHO1</i> ^{V180A}	This study
pYZ3	NAT ^R , Amp ^R , <i>CHO1</i> ^{L181A}	This study
pYZ4	NAT ^R , Amp ^R , <i>CHO1</i> ^{C182A}	This study
pYZ5	NAT ^R , Amp ^R , <i>CHO1</i> ^{G183A}	This study
pYZ6	NAT ^R , Amp ^R , <i>CHO1</i> ^{L184A}	This study
pCDC23	NAT ^R , Amp ^R , <i>CHO1</i> ^{R186A}	This study
pCDC24	NAT ^R , Amp ^R , <i>CHO1</i> ^{L187A}	This study

Table 2.3 continued

pCDC22	NAT ^R , Amp ^R , <i>CHO1</i> ^{R189A}	This study
pCDC25	NAT ^R , Amp ^R , <i>CHO1</i> ^{F190A}	This study
pYZ32	NAT ^R , Amp ^R , <i>CHO1</i> ^{R133E}	This study
pYZ50	NAT ^R , Amp ^R , <i>CHO1</i> ^{G129P}	This study

Site-directed mutagenesis was performed using a primer-based method. Each residue was mutated to alanine in the *CHOI-HAx3* allele carried on the pCDC31 plasmid. Forward and reverse primers approximately 35-40 bp in length were made for each mutation where the codon of interest was modified as conservatively as possible to produce alanine (Table 2.4). Sanger sequencing was used to confirm the alanine substitution on the plasmids generated. The plasmids were then linearized with *MscI* (within the *ENO1* promoter (P_{ENO1}) sequence) prior to transformation, and integrated into the P_{ENO1} region in the chromosomal DNA of the *choI* $\Delta\Delta$ mutant by electroporation. Transformant colonies were selected on YPD plates containing 100 $\mu\text{g/ml}$ nourseothricin. A total of six candidates were chosen for each mutation, and subjected to colony PCR for correct integration. In addition, products from colony PCR for all site-directed mutant candidates were sequenced again to ensure that no spurious mutations had arisen during the transformation.

Spot dilution assay and growth curves

To determine ethanolamine auxotrophy, mutant and wildtype (HA1) strains were cultured overnight in liquid YPD medium. The next day, cells were centrifuged and washed three times with water to remove residual nutrients. For spot dilution assays, cells were diluted to $\text{OD}_{600} = 0.1$ using water before three consecutive five-fold dilutions. Then, 10 μl of each dilution was plated onto both minimal medium and minimal medium supplemented with 1 mM ethanolamine. Photos were taken after 24 h incubation at 30°C. For the growth curve, washed cells were diluted to $\text{OD}_{600} = 0.1$ in both liquid minimal medium and minimal medium supplemented with 1 mM ethanolamine. OD_{600} was measured at 2, 4, 6, 8, 10, 12, 24 and 48 hour time points for the growth curve. A total of six biological replicates were

Table 2.4 Primers Used in this Study

Oligonucleotide	Sequence	Function/Mutation
CCO25	CAGTAAGTTCTTTTAGACTC	Sequencing primer
YZO1	TCAACCACCTTACTCCCTTTATTG	Sequencing primer
CCO160	aaaaGCGGCCGCATGACAGACTCATCAGCTAC	Amplifying <i>CHO1</i> gene
CCO55	aaaaGACGTCATAGGGATAGCCGGCATAGTCAGG AACATCGTATGGGTAAACGGCCGCTGGTTTAGGA ATTTTTAAAGAT	Amplifying <i>CHO1</i> gene
CCO56	aaaaGACGTCCCGGACTATGCAGGATCCTATCCAT ATGACGTTCCAGATTACGCTCCGGCCGCCTAGAG ATGATTCTAAAATAGAAT	Amplifying HA tag
CCO163	aaaaGAGCTCCAGAACCAGAATTATTGTTTC	Amplifying HA tag
CCO58	GGGGTATTTTTTCGATTTTTTTTGCTGGTAGAGTT GCAAG	D128A
CCO59	CTTGCAACTCTACCAGCAAAAAAATCGAAAAAT AACCCC	D128A
CCO60	ATTTTTTCGATTTTTTTTGATGCTAGAGTTGCAAGA TTAAG	G129A
CCO61	CTTAATCTTGCAACTCTAGCATCAAAAAAATCG AAAAAT	G129A

Table 2.4 continued

CCO62	TTTTTGATGGTAGAGTTGCAGCTTTAAGAAATAA ATCATC	R133A
CCO63	GATGATTTATTTCTTAAAGCTGCAACTCTACCAT CAAAAA	R133A
CCO64	ATAAATCATCATTAAATGGCTCAAGAGTTAGATTC ATTAG	G142A
CCO65	CTAATGAATCTAACTCTTGAGCCATTAATGATGA TTTAT	G142A
CCO66	TAATGGGACAAGAGTTAGCTTCATTAGCTGATTT GGTATC	D146A
CCO67	GATACCAAATCAGCTAATGAAGCTAACTCTTGT CCCATTA	D146A
CCO68	GTTAGATTCATTAGCTGCTTTGGTATCATTTGGG GTATC	D150A
CCO69	GATACCCCAAATGATACCAAAGCAGCTAATGAA TCTAAC	D150A
CCO82	GTTGGGGTTATTTTTTCGCTTTTTTTGATGGTAGA GTTG	D125A
CCO83	CAACTCTACCATCAAAAAAAGCGAAAAATAACC CCAAC	D125A
CCO164	TTTTTGGCCTTTTGGGCTTTATGTGGATTAACAA G	V180A
CCO165	CTTGTTAATCCACATAAAGCCCAAAGGCCAAA AA	V180A

Table 2.4 continued

CCO166	TTGGCCTTTTGGGTTGCATGTGGATTAACAAGAT T	L181A
CCO167	AATCTTGTTAATCCACATGCAACCCAAAAGGCC AA	L181A
CCO168	GCCTTTTGGGTTTTAGCTGGATTAACAAGATTGG C	C182A
CCO169	GCCAATCTTGTTAATCCAGCTAAAACCCAAAAG GC	C182A
CCO170	CTTTTGGGTTTTATGTGCATTAACAAGATTGGCT A	G183A
CCO171	TAGCCAATCTTGTTAATGCACATAAAACCCAAA AG	G183A
CCO172	TTGGGTTTTATGTGGAGCAACAAGATTGGCTAG AT	L184A
CCO173	ATCTAGCCAATCTTGTTGCTCCACATAAAACCCA A	L184A
CCO88	GGTTTTATGTGGATTAACAGCTTTGGCTAGATTT AATATC	R186A
CCO89	GATATTAATCTAGCCAAAGCTGTTAATCCACAT AAAACC	R186A
CCO90	GATTAACAAGATTGGCTGCTTTTAATATCTCCGT C	R189A
CCO91	GACGGAGATATTAAGCAGCCAATCTTGTTAA TC	R189A

Table 2.4 continued

CC094	GGTTTTATGTGGATTAACAAGAGCTGCTAGATTT AATATC	L187A
CC095	GATATTAATCTAGCAGCTCTTGTTAATCCACAT AAAACC	L187A
CC096	CAAGATTGGCTAGAGCTAATATCTCCGTCAATA AC	F190A
CC097	GTTATTGACGGAGATATTAGCTCTAGCCAATCTT G	F190A
YZ028	ATTTTTCGATTTTTTTTGATCCAAGAGTTGCAAGA TTAAG	G129P
YZ029	CTTAATCTTGCAACTCTTGGATCAAAAAATCGA AAAAT	G129P
YZ030	TTTTTGATGGTAGAGTTGCAGAATTAAGAAATA AATCATC	R133E
YZ031	GATGATTTATTTCTTAATTCTGCAACTCTACCAT CAAAAA	R133E
CC0161	CTTCACTCGATAAGGTGC	Colony PCR
CC0162	AAAAGAGCTCCTAGGCGGCCGGAGCGTAATC	Colony PCR

measured for OD₆₀₀ for each time point. Doubling time was calculated from the exponential (Malthusian) growth (2-8 h) via Graphpad Prism 9.1.

Western blots

Protein isolation and western blotting were performed with some modifications to previously published methods (47) and according to the manufacturers' protocols (LI-COR). Cultures were grown overnight in 5 ml YPD, diluted to 0.1 OD₆₀₀/ml in 25 ml of YPD and allowed to grow until reaching early log phase (0.7 – 1 OD₆₀₀/ml). Cultures were centrifuged, washed with water and frozen overnight at -80°C. Pellets were then thawed on ice, resuspended in 1x phosphate buffered saline containing a protease inhibitor cocktail (Roche 4693124001) and lysed with a 200 µl volume of glass beads (Sigma G1145-500G) in a bead-beater at 4°C. Samples were centrifuged at 2,400 x g for 1 minute to clear debris and transferred to a new tube on ice. Again, samples were cleared by centrifuging at 2,400 x g for 8 minutes. This twice-cleared supernatant was moved to fresh tubes on ice and a Bradford assay (Bio-Rad, 5000006) was performed to determine protein concentration.

Proteins were separated by SDS-PAGE (6% stacking/12% separating gel), followed by transfer to PVDF membranes (926-31099 LI-COR). Membranes were dried at room temperature, blocked using TBS: Odyssey Blocking Buffer (1:1) (927-50100 LI-COR) for one hour and incubated overnight at 4°C in TBS: Odyssey Blocking Buffer (1:1) with primary antibodies (HA-tag monoclonal antibody (26183) and tubulin alpha antibody (MCA78G)) (1:10,000). The following day, after 4 washes in TBST (0.1% Tween 20) at room temperature, membranes were incubated with secondary antibodies (IRDye® 680RD Goat-anti-Rat (926-68076) and IRDye® 800CW Goat-anti-Mouse (926-32210)) (1:10,000) at room temperature for at least one hour. Membranes were then washed 4x

with TBST and imaged using a LI-COR Odyssey scanner. To compare the protein expression of different mutants with respect to HA1, densitometry values from per mutant were quantified against tubulin standards using ImageJ. These tubulin-adjusted densitometry values were further normalized to that of the three HA1 bands together to generate the normalized densitometry values (NDV) of different mutants. The average and standard deviation of the NDVs from two western blots were calculated and shown in Table 2.5.

***In vitro* PS synthase assay and calculation of the adjusted PS synthase activity**

The cells were grown and broken as previously described in (26). All strains were grown to OD₆₀₀ between 1.5-2.0 prior to lysis. The cell lysate was cleared by centrifuging at 2000 x g, 4°C for 5 min, then the crude membrane was collected by centrifuging at 27,000 x g, 4°C for 30 min. The pellets were resuspended in 0.1 M Tris-Cl pH 7.5, 5 mM BME, 10% glycerol and protease inhibitors, and the total protein concentration was measured using a Bradford assay.

The PS synthase assay reaction was performed as described in (26) with the exception that 100 mM Tris-HCl (pH=7.5) and 0.5 mg crude protein were used, and incubation times were set to 30 min. A thirty-minute time point was chosen for single point assays because PS was produced at a constant rate from 0 to 45 min (data not shown), thus a thirty-minute time point allows us to determine the enzymatic activity of Cho1. Briefly, PS synthase activity (nmol/(mg*min)) was measured by monitoring the incorporation of 0.5 mM L-serine spiked with 5% (by volume) L-[³H]-serine (30,500 cpm/nmol) in the chloroform phase (for product phosphatidylserine). In an effort to calculate the adjusted PS synthase activity, Cho1 protein expression in the isolated crude membrane was determined

Table 2.5. Normalized densitometry values (NDVs) via western blotting for CAPT motif and serine binding motif mutants. * NDV 1 and NDV 2 were measured from two western blots using Image J.

Strain	NDV 1	NDV 2	Average ± Standard deviation
HA1	1.0	1.0	1.0 ± 0.0
D125A	2.5	1.9	2.2 ± 0.4
D128A	1.8	1.8	1.8 ± 0.1
G129A	2.4	1.7	2.1 ± 0.5
R133A	2.5	1.2	1.9 ± 0.9
G142A	1.6	0.9	1.3 ± 0.5
D146A	1.7	2.0	1.9 ± 0.3
D150A	1.4	1.6	1.5 ± 0.1
G129P	0.6	0.9	0.7 ± 0.2
R133E	1.3	0.8	1.1 ± 0.3
HA1	1.0	1.0	1.0 ± 0.0
V180A	0.9	1.0	1.0 ± 0.1
L181A	1.1	0.7	0.9 ± 0.3
C182A	1.6	0.9	1.3 ± 0.5
G183A	1.8	0.9	1.3 ± 0.6
L184A	1.0	1.2	1.1 ± 0.2
R186A	1.2	1.7	1.5 ± 0.3
L187A	3.4	4.4	3.9 ± 0.7
R189A	1.1	2.3	1.7 ± 0.9
F190A	2.5	2.7	2.6 ± 0.1

using western blotting and was used for normalizing the PS synthase activity. Specifically, the radioactive counts from each mutant, subtracted by the radioactive counts of the *cho1* $\Delta\Delta$ mutant (as the background), were converted to nmol based on the radioactive counts of 1 nmol L-[³H]-Serine, and then normalized to 0.5 mg total membrane protein and 30-min reaction time (nmol/(mg*min)). Then this normalized activity of each mutant was further normalized to the relative densitometry values of the Cho1 bands for the final adjusted PS synthase activity. The relative densitometry values were calculated from the densitometry values of each mutant measured from the total membrane prep on the western blot adjusted against that of HA1 via ImageJ. Each adjusted PS synthase activity was measured in duplicate with a total of six biological replicates.

Michaelis-Menten curves

The Michaelis-Menten curves were generated experimentally based on the *in vitro* PS synthase assay. For the serine Michaelis-Menten curves, the concentration of CDP-DAG was kept at 0.1 mM, and only the initial velocity (calculated based on the rate of linear PS production within 30 min) of Cho1 protein was measured at the serine concentrations of 0.1, 0.5, 1.0, 2.5, 5.0, 7.5, 10 and 15 mM, and then normalized to the relative densitometry values of the Cho1 bands, which are measured from the total membrane prep on the western blot and then adjusted to HA1 via ImageJ, for the adjusted specific activity (nmol/(mg*min)). For the CDP-DAG Michaelis-Menten curves, the concentration of serine was kept at 2.5 mM, and the initial velocity of Cho1 protein was measured at the CDP-DAG concentrations of 25, 50, 100, 200, 500, and 1000 μ M, and then normalized to the relative densitometry values from the western blotting for the adjusted specific activity. The initial velocity was measured in duplicate with a total of six biological duplicates. The

curves were generated and the apparent K_M and V_{max} were estimated using Graphpad Prism 9.1. The statistical comparison of the apparent K_M and V_{max} values were also conducted with Graphpad Prism 9.1 using extra sum-of-squares F test. The k_{cat} was calculated using Graphpad Prism 9.1 with the total crude membrane protein serving as the enzyme concentration.

Homology modeling

The homology model was produced using Molecular Operating Environment (MOE) software. A Protein Data Bank (PDB) search was performed using the *C. albicans* Cho1 protein sequence and was found to have at least 25% sequence similarity to the four published crystal structures in (35, 38-40). Several homology models were produced using each of the four crystal structures as templates. The final homology model of Cho1 presented in this manuscript was produced by using the template of the phosphatidylinositolphosphate (PIP) synthase from *Renibacterium salmoninarum* (PDB: 5D92), a CDP-alcohol phosphotransferase, which had approximately 35.3% sequence similarity and 23.1% sequence identity with Cho1 (using the EMBOSS Stretcher alignment tool).

Statistical analysis

Statistical analysis for *in vitro* PS synthase assays was performed on Graphpad Prism 9.1 using Brown-Forsythe and Welch ANOVA tests (Assume unequal SDs), and the post hoc analysis compares each group to control HA1. Doubling time and the corresponding 95% asymmetrical (profile-likelihood) confidence intervals were calculated by Graphpad Prism 9.1. The best-fit values of the K_M and V_{max} were calculated and compared using Graphpad Prism 9.1.

Results

The CDP-alcohol phosphatidyltransferase (CAPT) binding motif (D₁xxD₂G₁xxAR...G₂xxxD₃xxxD₄) is highly conserved in enzymes binding CDP-alcohols, even across domains (Table 2.1), indicating the importance of this motif in the function of this type of enzyme. One exception lies in some Gram negative bacteria, such as *E. coli*, where this motif is not present within certain enzymes binding CDP-DAG (e.g., *E. coli* phosphatidylserine synthase, PssA), indicating divergence (32).

Detailed site-directed mutagenesis of the CAPT motif in the *CPT1* cholinephosphotransferase in *S. cerevisiae* (Table 2.1) showed that mutation of Gly114 (G₁), Gly127 (G₂), Asp131 (D₃), or Asp135 (D₄) caused loss of activity while mutations of Ala117 or Arg118 showed a decrease in activity, and Asp113 (D₂) showed wildtype activity (37). Using *S. cerevisiae* Cpt1 as a guide, we tested whether mutations in amino acids conserved in the CAPT motif of multiple enzymes shown in Table 2.1 were important for catalysis in the *C. albicans* PS synthase by mutating them to alanine using site-directed mutagenesis.

We generated a C-terminally HAX3-tagged version of *C. albicans* *CHO1* that is transcribed downstream of a constitutive yeast *ENO1* promoter on a SAT1 marked plasmid (pCDC31), and integrated it into the *cho1ΔΔ* mutant genome at the *ENO1* locus. Transformants were then screened for expression of Cho1-HAX3 by western blotting, and a successful transformant hereafter known as HA1 (Fig. 2.1A) was chosen as the reference strain for this study. It should be noted that three bands (36, 34, and 29 kDa) were observed that were recognized by the anti-HA antibody, but none of these were present in the *cho1ΔΔ* control (Fig. 2.1A). We suspect that the band at 34 kDa is the full-length protein, which

correlates with the predicted molecular weight of 34.8 kDa for Cho1-HAx3 protein. The 36 kDa and 29 kDa bands were shown to contain a phosphorylated protein population as Lambda phosphatase (NEB) decreased the abundance of both bands (Fig. 2.5). In addition, the 29 kDa band is likely to be the proteolytic product, as proteolytic maturation of enzymes is a well-documented phenomenon and previous studies reported similar findings with the PS synthase in *S. cerevisiae* (21, 23). These previous studies found that the 30 kDa band was likely proteolytically degraded to produce the 23 kDa band, but both forms of the protein were active (21, 23).

To determine the activity of HAx3-tagged Cho1 under the *ENO1* promoter, PS synthase enzyme activity was directly measured. Membranes were isolated from SC5314 (WT strain), the *CHO1* re-integrated strain (*cho1ΔΔ::CHO1*), the HA1 strain, and the *cho1ΔΔ* null mutant. Among these strains, HA1 has restored PS synthase activity compared to the *cho1ΔΔ* strain, and showed ~6 times higher activity than the strain bearing native *CHO1* expressed from its own promoter (*cho1ΔΔ::CHO1*) (Fig. 2.1B), indicating that the constitutive *P_{ENO1}* promoter significantly increases the expression of Cho1 protein. However, it is noticeable that HA1 strain still has significantly decreased PS synthase activity compared to the WT strain, and the underlying reason is unknown.

Confirmation of the CAPT Motif's importance in enzyme activity

We performed alanine substitution mutagenesis on the conserved non-alanine residues in the CAPT motif to confirm their importance and identify the key residues (Table 2.1, row 1, conserved residues are highlighted in gray). CAPT mutants were made, and a resulting western blot showed that all of the CAPT mutants have comparable Cho1

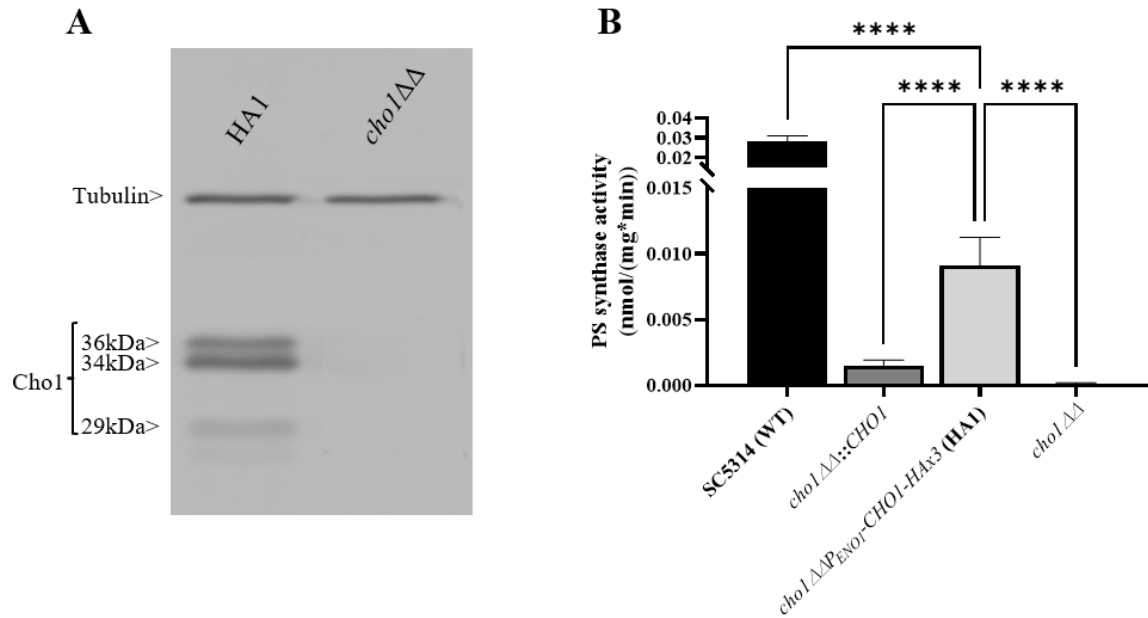


Figure 2.1 Expression and activity of Cho1-HAx3 under the *ENO1* promoter

(A) Proteins were extracted from the *cho1ΔΔ P_{ENO1}-CHO1-HAx3* (HA1) and *cho1ΔΔ* negative control strains, separated on SDS-PAGE and blotted with anti-HA and anti-tubulin (loading control) antibodies. Three bands (36 kDa, 34 kDa and 29 kDa) are present in the HA1 strain, in addition to the tubulin loading control. (B) Total membranes were collected from wildtype strain SC5314 (WT), the *CHO1* re-integrated strain where *CHO1* is expressed from its native promoter (*cho1ΔΔ::CHO1*), the HA1 strain, and the *cho1ΔΔ* negative control strain. PS synthase activity (nmol/(mg*min)) was measured from 0.5 mg crude membrane protein for 30 min. Statistics were conducted using one-way ANOVA (**** p < 0.0001). For each strain, PS synthase activity was measured in duplicate with a total of six biological replicates.

protein expression to the HA1 wildtype control (Fig. 2.2A; Table 2.5). To probe the activities of these mutants, assays were performed to measure PS synthase-dependent phenotypes, including ethanolamine-dependent growth and *in vitro* PS synthase activity.

Mutants that lack the PS synthase have a disruption of the *de novo* pathway for synthesizing phosphatidylethanolamine (PE), an essential phospholipid. In the *de novo* pathway, PE is made by decarboxylating PS; thus, the *choI* $\Delta\Delta$ mutant relies on exogenous ethanolamine to make PE by a salvage pathway called the Kennedy pathway (10). Therefore, these strains show a strong growth perturbation on minimal media with no ethanolamine supplement. For the CAPT mutants, if a mutant grows similarly to the wildtype in the absence of ethanolamine, then its Cho1 function is not disturbed due to the alanine substitution mutations, which indicates that the corresponding original residue is not important in Cho1 function, and *vice versa*. The CAPT mutants, the HA1 strain (positive control), and the *choI* $\Delta\Delta$ strain (negative control) were plated on minimal medium without ethanolamine. The R133A mutant grew similarly to HA1, but the other mutants, D125A, D128A, G129A, G142A, D146A and D150A, showed growth perturbations at all cell densities (Fig. 2.2B, -ETA). To confirm the growth perturbation is due to the lack of ethanolamine, the CAPT mutants were again grown on minimal medium supplemented with 1 mM ethanolamine, which should give a modest return of growth to the mutants. In the presence of ethanolamine, D125A, D128A, G129A, G142A, D146A and D150A gained obvious growth (Fig. 2.2B, +ETA), suggesting the absence of ethanolamine contributes to growth perturbation. However, these mutants still did not grow as well as HA1, which may be explained by inefficient transport of ethanolamine (25). To better quantify the impact of Cho1 activity on growth, cells were grown in liquid cultures

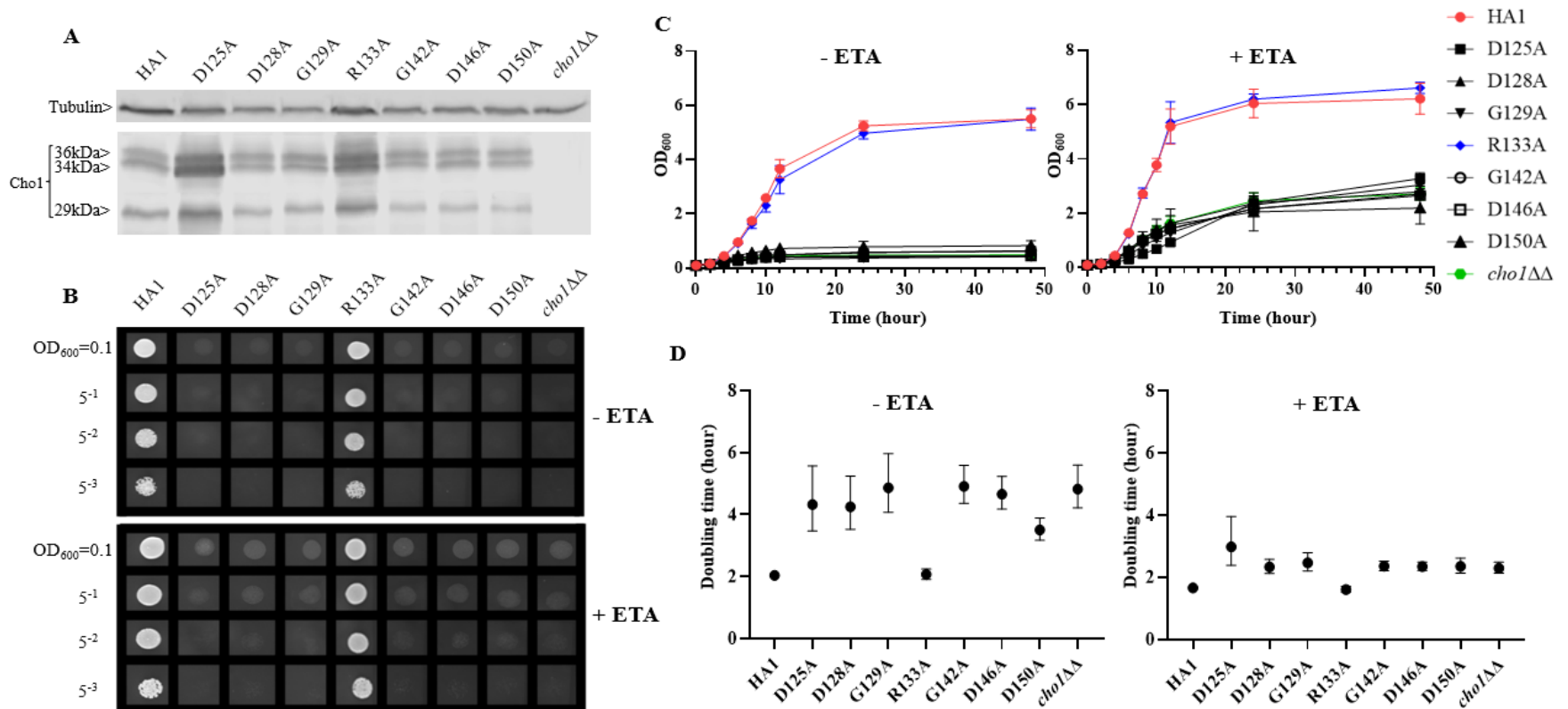


Figure 2.2. Most conserved CAPT mutants displayed defects in ethanolamine-dependent growth.

(A) Cho1 protein expression was measured from the cell lysates of *cho1ΔΔ*, HA1, and the CAPT motif mutant strains via western blotting. The impact of CAPT mutations on ethanolamine-dependent growth was measured by (B) spot dilution assays, (C) growth curves, and (D) doubling times from corresponding growth curves. Error bars in (D) represent the 95% asymmetrical (profile-likelihood) confidence intervals of each doubling time from a total of six replicates. (+ETA, minimal media+1 mM ethanolamine; -ETA, minimal media).

in the same minimal medium \pm 1 mM ethanolamine, and OD₆₀₀ was measured at successive time points (Fig. 2.2C). Furthermore, growth curves in the exponential phase (from 2h to 8h) were used to calculate doubling times (Fig. 2.2D). Consistent with Fig. 2.2B, mutant R133A showed similar growth dynamics to HA1 at different time points and a similar doubling time in the presence and absence of ethanolamine, while the other CAPT mutants had poor growth similar to the *cho1* $\Delta\Delta$ strain.

Alanine substitution of the conserved CAPT residues did not significantly reduce Cho1 protein expression (Fig. 2.2A; Table 2.5), but did cause growth perturbations (Figs. 2.2B-D) in mutants D125A, D128A, G129A, G142A, D146A and D150A. It was hypothesized that these decreases were due to decreased *in vivo* Cho1 protein function. To test this hypothesis, PS synthase enzyme activities of the CAPT mutants were directly measured. Membranes were isolated from each of the CAPT mutants, along with HA1 and *cho1* $\Delta\Delta$ controls, to assess the enzyme activity of each mutant Cho1 protein using an *in vitro* PS synthase assay. For these reactions, the concentration of crude membrane proteins used from each strain was compared to the estimated level of Cho1 protein expression measured by western blotting to generate a final adjusted PS synthase activity (nmol/(mg*min)). The adjusted PS synthase activities should more accurately reflect the intrinsic enzymatic activity of Cho1 in different strains compared to HA1. In Fig. 2.3, the D125A, D128A, G142A, and D150A CAPT mutants showed almost 0% of the activity of the HA1 control while D146A displayed 5-fold lower activity, consistent with the *in vivo* growth assay results (Fig. 2.2B-D). R133A mutant retained HA1-level activity which is consistent with its similar growth phenotype compared to HA1 (Fig. 2.2B-D). G129A, however, retained almost half the level of adjusted PS synthase activity, which contrasts

with its poor growth (Fig. 2.2B-D). A possible explanation for this discrepancy is that the level of retained enzymatic activity of G129A is not enough to support the growth under our *in vivo* assay conditions, but it remains detectable in the *in vitro* assay with higher concentrations of protein.

The data from Figs. 2.2&2.3 demonstrate that the CAPT motif is crucial for PS synthase function. However, there were two main discrepancies in our study compared to previous analyses of the CAPT motif residues: G129 and R133. Our R133A mutant retains HA1-level activity, in contrast with previous studies of similar enzymes bearing CAPT motifs, where the substitution of the conserved arginine residue with either methionine or alanine severely reduced activity (37, 38). In addition, previous alanine substitution of the first conserved glycine in the CAPT motif in the *S. cerevisiae* cholinephosphotransferase (G129 in *C. albicans* PS synthase numbering) abolished protein expression (37), but the *C. albicans* Cho1 G129A protein is expressed and retains partial *in vitro* activity (Figs. 2.2A&2.3). To better understand a role for these residues, more drastic substitutions were chosen to replace the two original residues: a negatively charged glutamate substitution was chosen for positively charged arginine (R133), and a rigid proline was chosen for the flexible glycine (G129). We hypothesized that these mutations would result in a marked reduction in Cho1 activity. Hence, mutants R133E and G129P were constructed using the same method above, followed by confirmation of protein expression via western blotting (Fig. 2.4A). Then, R133E and G129P strains were subjected to subsequent spot dilution assays, growth curve measurements, and *in vitro* PS synthase assays. As predicted, the R133E mutant displayed slower growth compared to HA1 in the absence of ethanolamine (Figs. 2.4B&2.4C), in contrast to the R133A mutant (Figs. 2.2B&2.2C). The negative

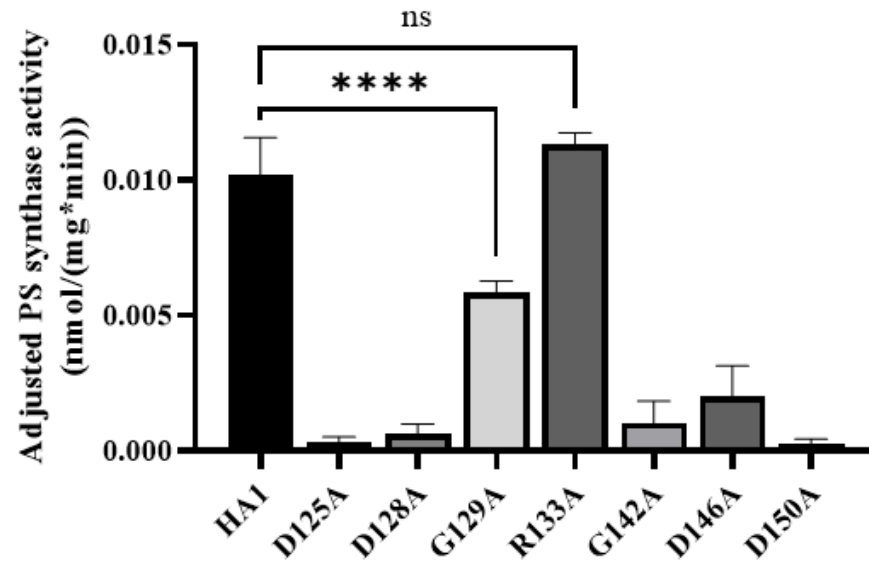


Figure 2.3. Most of the conserved CAPT motif residues are required for PS synthase activity.

Total membranes were collected from *cho1* $\Delta\Delta$, HA1, and each CAPT motif mutant and tested in an *in vitro* PS synthase assay. Adjusted PS synthase activity was measured for each total membrane prep. Statistics were conducted using one-way ANOVA, and all mutants were compared to HA1 (**** $p < 0.0001$; ns=not significant). For each strain, the adjusted PS synthase activity was measured in duplicate with a total of six biological replicates.

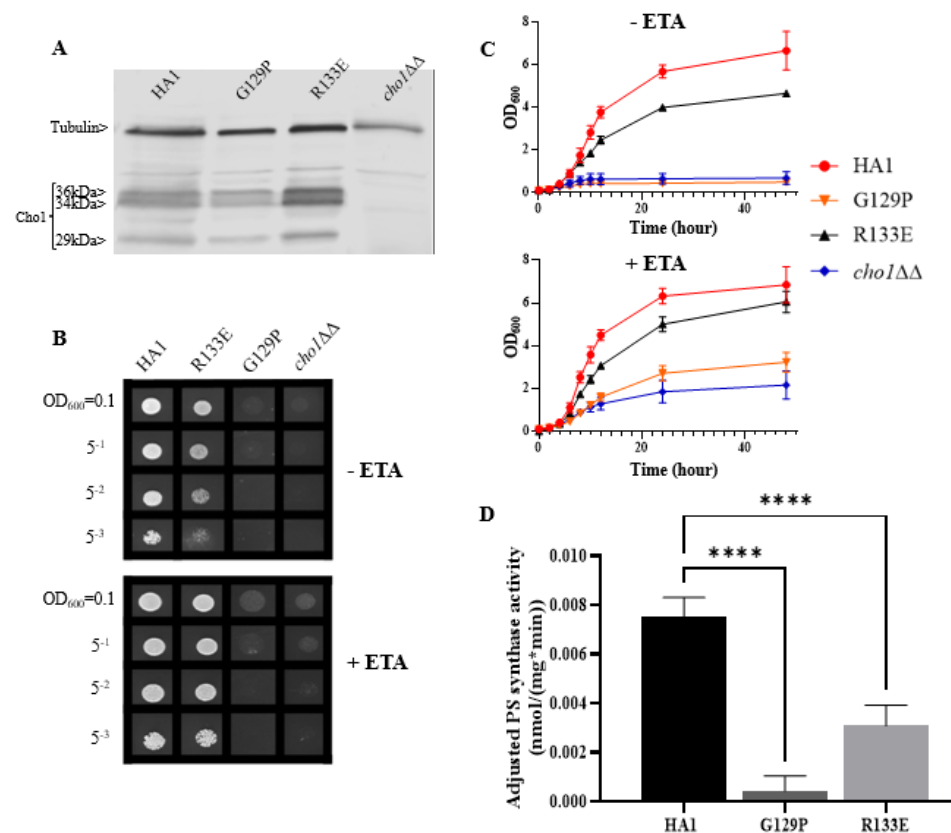


Figure 2.4. CAPT mutant G129P and R133E displayed decreased Cho1 function

(A) Proteins were collected from *cho1ΔΔ*, HA1, G129P and R133E strains, and Cho1 expression was measured using a western blot. Growth was measured by (B) spot dilution assays and (C) growth curves. (D) Adjusted PS synthase activity was measured by the *in vitro* PS synthase assay. Each adjusted PS synthase activity was measured in duplicate with a total of six biological replicates. Statistics was conducted using one-way ANOVA, and all mutants were compared to HA1. **** p < 0.0001 (+ETA, minimal media+1 mM ethanolamine; -ETA, minimal media)

effect of R133E is further corroborated by a significant decrease (more than 50%) in adjusted PS synthase activity in the *in vitro* PS synthase assay (Fig. 2.4D). The G129P mutation also had a greater impact than the G129A mutation, as the G129P mutant was 17-fold less active than HA1 (Fig. 2.4D) compared to G129A, which retained ~50% activity compared to the HA1 strain (Fig. 2.3). Thus, these more contrasting substitution mutations suggest that G129 and R133 also play a role in the CAPT motif, but may participate in more flexible interactions with CDP-DAG.

Analysis of a predicted serine binding motif

In addition to CDP-DAG, Cho1 also binds serine as a substrate. The serine binding site is more challenging to define compared to the CDP-DAG binding motif since the CDP-DAG motif is common to several other enzymes that bind CDP-alcohols (Table 2.1), whereas the serine binding site is more specific to the Cho1 protein, so limited information is available. Here, we took advantage of the fact that the phosphatidylinositol (PI) synthase (Pis1) and PS synthase from yeast are similar enzymes that both bind two substrates: CDP-DAG and a small molecule that serves as the head group of the phospholipid product. Also, PI synthase and PS synthase are reported to use the same sequential reaction mechanism for catalysis (16, 48). *C. albicans* Pis1 shares 37.2% amino acid similarity (using the EMBOSS Stretcher alignment tool) with Cho1 and only differs enzymatically in binding to inositol instead of serine. We hypothesized that alignment and comparison of sequences between these two genes might reveal a conserved serine binding site in Cho1. Thus, we aligned the Pis1 amino acid sequences from *C. albicans*, *Saccharomyces cerevisiae*, and *Schizosaccharomyces pombe* with the Cho1 amino acid sequence from the same organisms (Fig. 2.5). From this alignment, we found a highly conserved sequence in all of the PS

SpPps1	TFLDTVILSLEFVLCGLTRLARFNVSVNSIPKDG-SGKSQ-----FFEGTPIPTTLSLVTV	189
CaChol	TTVDVLFLLAFWVLCGLTRLARFNISVNNIPKDK-HGKSQ-----YFEGLP IPTNLFWVGF	222
ScChol	TTFDVMILSFFVLCGLTRLARFNVTVAQLPKDSSTGKSK-----YFEGLPMP TTLALVLG	225
SpPis1	LLVSLDLASH-----YMHMYSTLHQGASSHKT VTKKHNWMLRLYYGNNKVL FIF	149
CaPis1	ILVSLDLSSH-----YMHMYAMLSAGSTSHKNVDETQSKLLS LYNNRLV LFFV	167
ScPis1	LMLGLDITSH-----YMHMYASLSAGKTS HKSVGEGES RLLHLYYTRRDV LFTI	153

Figure 2.5. Sequence alignment reveals a possible serine binding motif

Alignment of the PS synthases (Chol or Pps1) and PI synthases (Pis1) from *C. albicans* (Ca), *S. cerevisiae* (Sc), and *S. pombe* (Sp) was conducted using Clustal Omega. A highly conserved sequence that is present in Chol homologs, but not in the Pis1 homologs, is hypothesized to be part of the serine binding site in PS synthases and is highlighted in yellow in the *C. albicans* sequence. Conserved non-alanine residues in the putative serine binding site are shown in the red boxes.

synthase amino acid sequences that was absent from the Pis1 sequences (X-V-L-C-G-L-X-R-L-A-R-F). We predicted that this motif might represent part of the serine binding site.

Alanine substitution mutagenesis was conducted on the conserved non-alanine residues (Fig. 2.5, red boxes) in the putative serine binding site. Putative serine binding site mutants, V180A, L181A, C182A, G183A, L184A, R186A, L187A, R189A and F190A, were constructed and all showed protein expression that is greater than or equal to HA1 (Fig. 2.6A; Table 2.5). These mutants were then subjected to *in vivo* spot dilution assays and growth curves. Among all the serine binding site mutants, V180A and C182A had similar growth to HA1 in the absence and presence of ethanolamine, and L181A displayed diminished growth in the absence of ethanolamine, but exhibited restored growth similar to HA1 with the addition of 1 mM ethanolamine (Figs. 2.6B-D). The G183A, R186A, L187A, R189A and F190A mutants all displayed diminished growth compared to HA1 in both conditions, but R189A had a greater improvement than the others in the presence of ethanolamine (Figs. 2.6B-D). The growth perturbation of these mutants is likely due to significantly decreased *in vivo* Cho1 function. The growth curves and doubling times correlate with the spot dilution assays, where mutants V180A, L181A and C182A showed similar patterns compared to HA1; mutants G183A, R186A, L187A and F190A grew similarly to the *cho1* $\Delta\Delta$ negative control strain, and mutant R189A had intermediate phenotypes (Figs. 2.6B-D).

Surprisingly, L184A demonstrated increased growth in both conditions when compared with HA1 (Figs. 2.6B). To rule out the possibility that a spurious mutation might account for the increased growth, several L184A transformation colony candidates were subjected to spot dilution assays and all of them displayed a similar phenotype (Fig. S2.2),

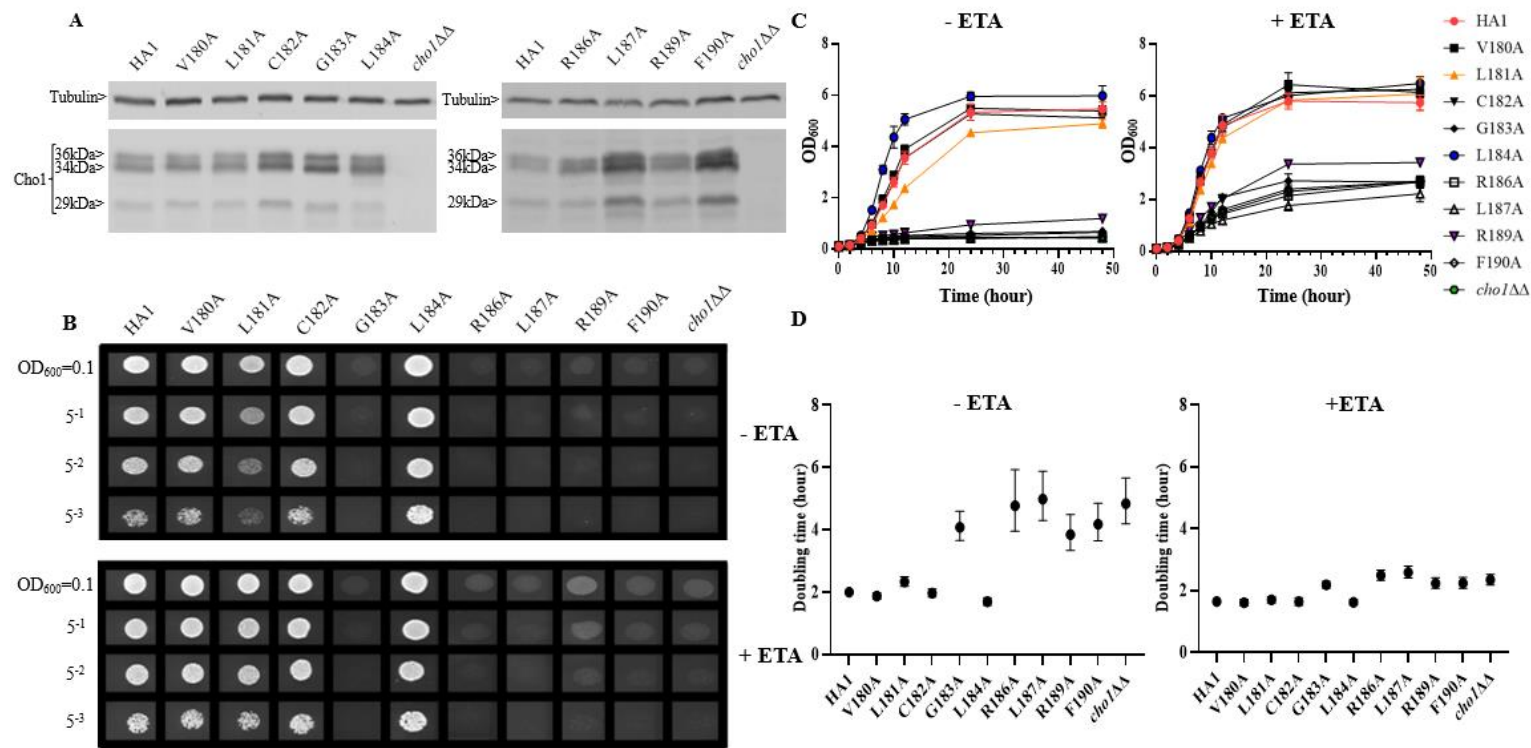


Figure 2.6. Mutations in the putative serine binding site reduce *in vivo* Cho1 function

(A) Cho1 expression from *cho1ΔΔ*, HA1 and each of the putative serine binding site mutants was checked using western blotting. *In vivo* activities were measured in (B) spot dilution assays and (C) growth curves. (D) Doubling times for each strain were calculated from growth curves. Error bars represent the 95% asymmetrical (profile-likelihood) confidence intervals of each doubling time from a total of six replicates. (+ETA, minimal medium+1 mM ethanolamine; -ETA, minimal medium).

indicating that the mutation L184A is responsible for the elevated growth. Furthermore, growth curve patterns and shorter doubling times, especially in the absence of ethanolamine (-ETA), are consistent with the spot dilution assay, further supporting the conclusion that L184A leads to elevated growth when compared with HA1 (Figs. 2.6C&D). Since mutant L184A does not significantly increase Cho1 expression (Fig. 6A; Table 2.5), the increased growth of L184A suggests that this mutation increases protein function.

To further assess these putative serine binding site mutants, we performed the *in vitro* PS synthase assay to measure their adjusted PS synthase activities (Fig. 2.7). Consistent with our *in vivo* results, C182A displayed a similar level of activity compared to HA1, while R189A displayed significantly decreased activity. G183A, R186A, L187A and F190A retained almost no activity. In contrast, the hyperactive mutant, L184A, showed significantly enhanced (~5 fold) *in vitro* activity compared to HA1, corroborating the *in vivo* results that mutation L184A increases intrinsic Cho1 activity (Figs. 2.6&S2.2).

However, there were two discrepancies between the *in vivo* and *in vitro* results. V180A grew similarly to HA1 in spot assays and growth curves, but yielded significantly lower adjusted PS synthase activity. This discrepancy is likely due to a decreased stability of the V180A mutant protein so that it cannot function properly under our *in vitro* assay conditions. The other inconsistency is L181A, which displayed higher *in vitro* adjusted PS synthase activity but grew similarly to HA1. This can be explained by a more sensitive nature of our *in vitro* PS synthase assay, which is able to detect elevated enzyme activity that is not high enough to support faster growth. Further studies will be needed to conclude

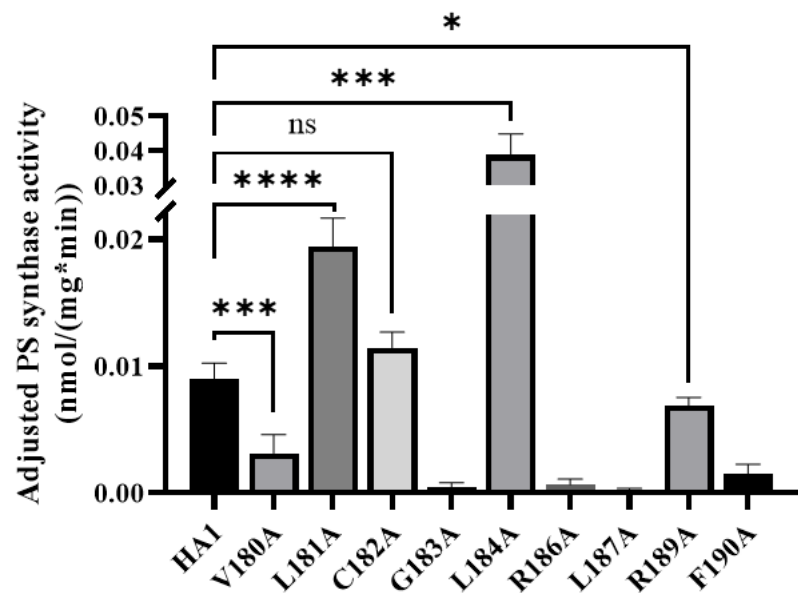


Figure 2.7. Enzyme activity decreases in some putative serine binding site mutants

Total membranes were collected from *cho1* $\Delta\Delta$, HA1 and each of the putative serine binding site mutants and tested in an *in vitro* PS synthase assay. Adjusted PS synthase activity was measured from each total membrane. Statistics were calculated using one-way ANOVA, and all mutants were compared to HA1 (* $p < 0.05$; *** $p < 0.001$; **** $p < 0.0001$; ns=not significant). Each adjusted PS synthase activity was measured in duplicate with a total of six biological replicates.

the exact nature of these differences. In sum, the putative serine binding site residues, especially the more C-terminal ones, play a role in Cho1 function.

Enzyme kinetics reveal residue R189 is involved in serine binding, and L184A mutation has increased V_{\max} .

Among the residues in the putative serine binding motif, L184 and R189 are particularly interesting because L184A increases Cho1 activity *in vivo* and *in vitro*, while R189A diminishes activity (Figs. 2.6 and 2.7, respectively). The other mutations: 1) retain original enzyme activity, 2) abolish activity, or 3) display inconsistencies between *in vivo* and *in vitro* activities. Thus, it is of interest to investigate how L184A and R189A alter enzyme kinetics of the Cho1 protein, specifically in regard to the K_M for serine. For this, Michaelis-Menten curves were produced and kinetic values, apparent K_M and V_{\max} , of HA1, L184A and R189A were calculated for serine (Fig. 2.8A). L-serine, when the concentration of CDP-DAG was held at 0.1 mM, yielded an apparent K_M of 8.43 ± 3.68 mM and an apparent V_{\max} of 0.058 ± 0.013 nmol/(mg*min) for HA1, an apparent K_M of 16.85 ± 7.11 mM and an apparent V_{\max} of 0.12 ± 0.03 nmol/(mg*min) for L184A, and an apparent K_M of 28.94 ± 10.04 mM and an apparent V_{\max} of 0.080 ± 0.021 nmol/(mg*min) for R189A. For comparison, the best-fit values from Graphpad Prism 9.1 of the K_M and V_{\max} for HA1, L184A and R189A were used to make bar graphs, with the error bars representing standard errors. Statistics conducted from Graphpad Prism 9.1 (Extra sum-of-squares F test) shows there is a significant increase in the L-serine K_M for R189A compared to HA1, indicating decreased L-serine binding affinity (Fig. 2.8B). This elevated apparent K_M can also explain the decreased activity of R189A. On the contrary, the increased activity of L184A is not

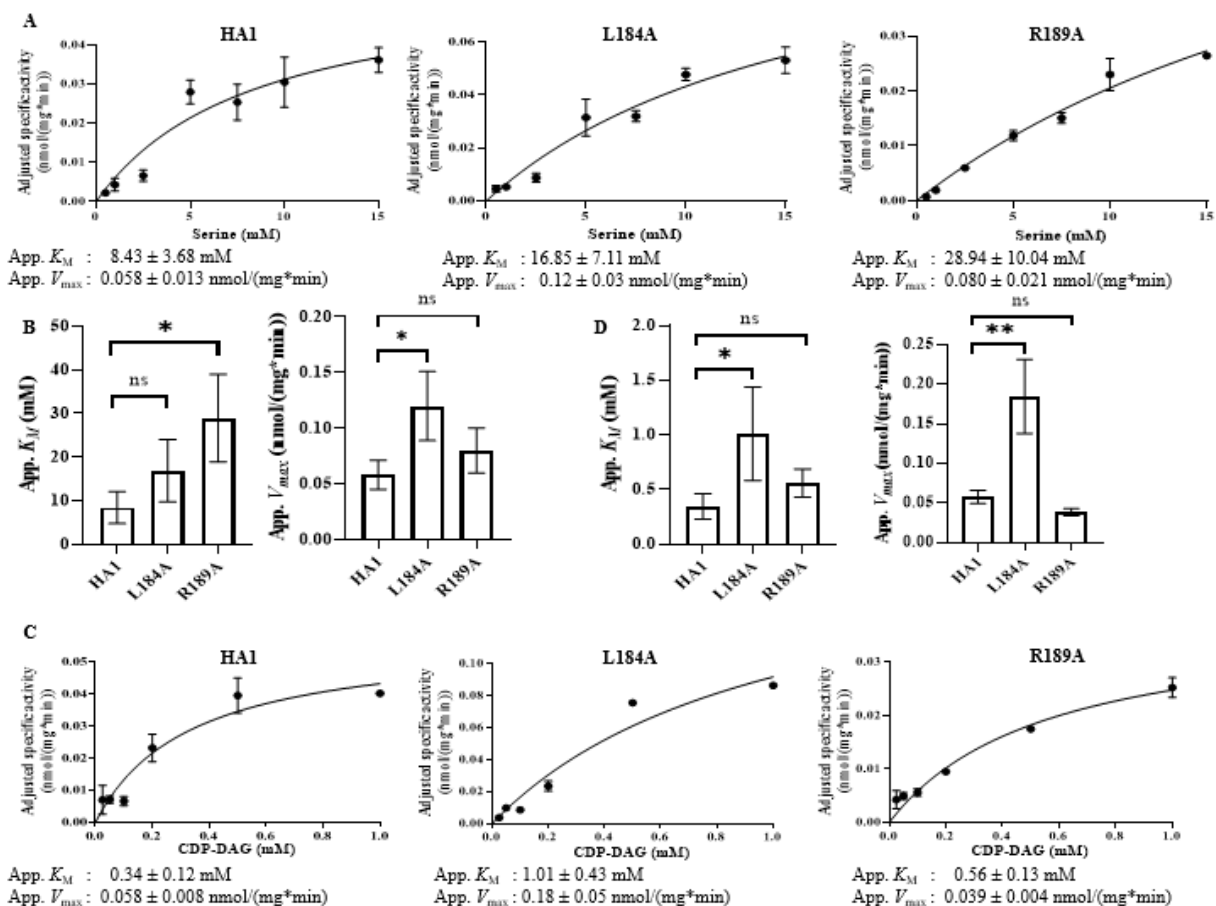


Figure 2.8. Michaelis-Menten kinetics showed decreased serine binding capacity of R189A. The *in vitro* PS synthase assay was performed with varying concentrations of CDP-DAG and serine, and the Michaelis-Menten kinetics curves of HA1, L184A and R189A were shown in (A) for serine and (C) for CDP-DAG. The apparent K_M and V_{max} estimated are below the corresponding curves, and are fit into bar graphs (B) for serine and (D) for CDP-DAG. Statistical comparisons were conducted using extra sum-of-squares F test (* p < 0.1; ** p < 0.01; ns=not significant). All adjusted specific activity was measured in duplicate with a total of six biological replicates.

due to a decreased K_M (thus enhanced L-serine binding), rather it is because of significantly increased apparent V_{max} under this condition.

To test whether L184A and R189A affect CDP-DAG binding, Michaelis-Menten kinetics including K_M and apparent V_{max} of HA1, L184A and R189A were calculated for CDP-DAG, where L-serine was held constant at 2.5 mM (Fig. 2.8C). Surprisingly, the apparent K_M for CDP-DAG of L184A was significantly elevated compared to HA1 (Fig. 2.8D), indicating a weaker binding. However, the negative effect of L184A for CDP-DAG binding is offset by an elevated k_{cat} , which leads to a similar k_{cat}/K_M compared to HA1 (Table 2.5). In sum, an elevated apparent V_{max} of L184A indicates this mutation increases the turnover number, while the increased K_M of R189A for serine suggests that residue R189 is involved in L-serine binding.

Homology modeling indicates that the CDP-DAG and L-serine binding motifs are in close proximity

Although the mutational evidence suggests that we have identified a motif involved in L-serine binding, its proximity to the CDP-DAG binding CAPT motif was not evident from the primary sequence. Cho1 is a membrane protein and has not yet been crystallized. However, there are several CDP-alcohol phosphotransferase (CDP-AP) proteins containing the CAPT motif from archaea and bacteria that have been crystallized (Table 2.1), and it has been previously suggested that the location of the substrate-binding pocket for the small alcohol molecule is in the proximity of the CAPT motif in the structure (35, 39-41). Four published crystal structures were found via Protein Data Bank (PDB) searches using the *C. albicans* PS synthase protein sequence as the query (PDB: 4O6N, 5D92, 6H53 and 4MND) and they all belong to the CDP-AP family (35, 38-40). An alignment of the

Table 2.6 The k_{cat} , K_M and k_{cat}/K_M of HA1, L184A and R189A for both serine and CDP-DAG

	Serine				CDP-DAG		
	HA1	L184A	R189A		HA1	L184A	R189A
k_{cat} (h^{-1})	0.12	0.23	0.16	k_{cat} (h^{-1})	0.12	0.37	0.077
K_M (mM)	8.43	16.85	28.94	K_M (mM)	0.34	1.01	0.56
k_{cat}/K_M ($h^{-1} * mM^{-1}$)	0.014	0.014	0.0055	k_{cat}/K_M ($h^{-1} * mM^{-1}$)	0.35	0.37	0.138

four published proteins showed a conserved CAPT binding motif and a similar distribution of secondary structures (data not shown), suggesting high conservation of structure and topology for proteins within this family. Using Molecular Operating Environment software (MOE, Chemical Computing Group, Ltd, Montreal, Canada), the homology model of the *C. albicans* PS synthase was built based on the phosphatidylinositolphosphate (PIP) synthase from *Renibacterium salmoninarum* (PDB: 5D92), which has 35.3% sequence similarity and 23.1% sequence identity with *C. albicans* PS synthase (using the EMBOSS Stretcher alignment tool). The model indicates that *C. albicans* Cho1 forms a homodimer (Fig. 2.9A), consistent with the four known CDP-APs (35, 38-40). Six transmembrane helices (TM1-TM6) are indicated with arrows and an N-terminal cytosolic domain that is connected to TM1. Both the CAPT motif (cyan) and the putative serine binding site (yellow) are highlighted in the red monomer. Specifically, residues L184 and R189 are highlighted in purple and their sidechains are shown (Fig. 2.9B). The residues of the putative serine binding site (yellow) in *C. albicans* PS synthase, similarly to the binding pockets of the second small molecules from the four known CDP-APs, are in close enough proximity to the CAPT motif (cyan) to interact during catalysis (Fig. 2.9A), further supporting our identified region as the putative serine binding site. Specifically, the side chain of residue R189 projects towards the CAPT motif (Fig. 2.9B), and the C α atomic distance of residue R189 to residue D150 (D₄), which serves as the catalytic core in some other CDP-APs (35, 39), is only 12.92Å, indicating it could coordinate serine and bring it closer to the active site. However, it is likely that other parts of the protein also help to coordinate serine, and this represents only part of the overall serine binding site. Further studies will be

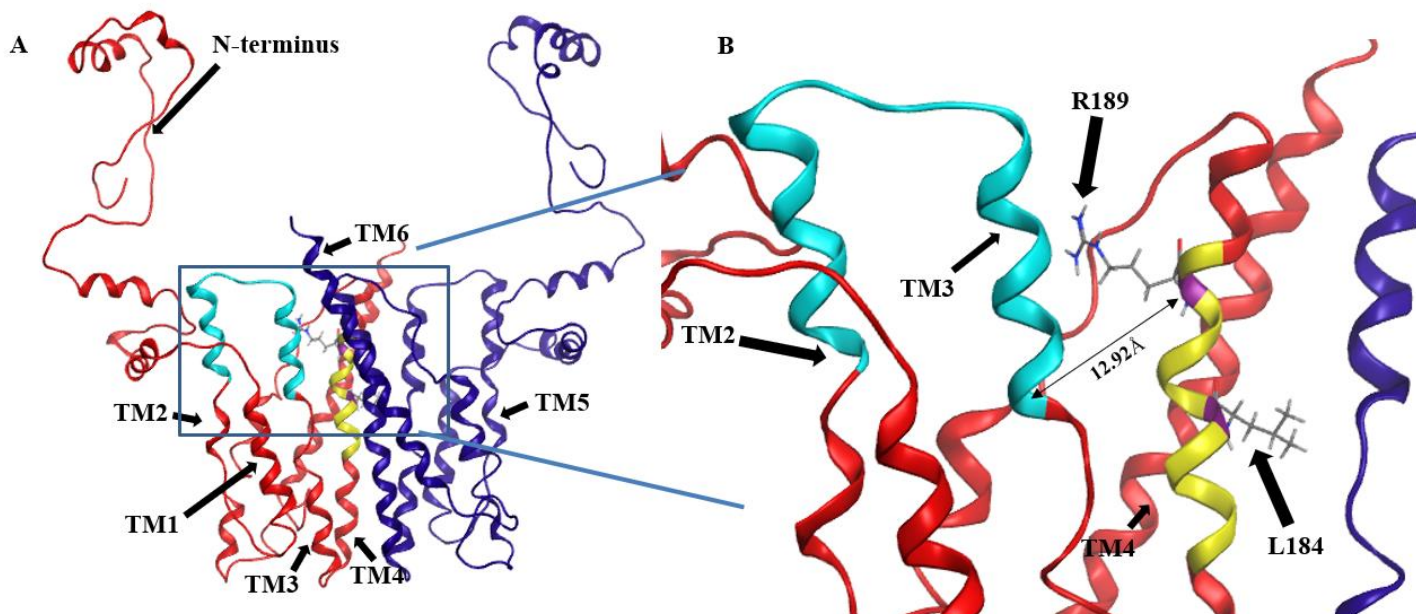


Figure 2.9. Location of CDP-DAG and putative serine binding residues on a predicted structure of Cho1 based on homology modeling

(A) The homology model for the Cho1 protein was built based on the structure of the phosphatidylinositolphosphate (PIP) synthase from *Renibacterium salmoninarum* (PDB: 5D92) using Molecular Operating Environment 2019 software. The two Cho1 monomers are shown in red and dark blue, respectively. The CAPT motif is shown in cyan and the predicted serine binding motif is shown in yellow in the red monomer. TM1, TM2, TM3 and TM4 are indicated in the red monomer, while TM5 and TM6 are indicated in the blue monomer. (B) A zoomed-in image of the predicted active site of Cho1 and the locations of residues R189 and L184 on the red monomer is shown. The distance between C α atoms of residues R189 and D150 is measured at 12.92Å using Molecular Operating Environment (MOE) 2019 software.

required to provide greater insight into all residues involved in the binding and positioning of serine during catalysis.

Discussion

In this study, we found that most of the conserved amino acids (Table 2.1) in the CAPT motif in *C. albicans* Cho1 are necessary for PS synthesis (Figs. 2.2&2.3). However, there were differences from what has been observed in the CAPT motif for some other enzymes. For example, as opposed to the findings in *S. cerevisiae* Cpt1 (Figure S2.3), mutations of G129 and D146 showed a severe to a modest decrease in activity, and R133 showed nearly wildtype level activity (Fig. 2.3). In the Cpt1 enzyme from *S. cerevisiae*, replacing G114 (equivalent to G129) and D131 (equivalent to D146) with alanine abolished enzyme activity, while the R118A (equivalent to R133A) mutant displayed decreased activity (37). It was suggested that the importance of the first glycine (G114 or G129) in the CAPT motif is due to binding or positioning of the CDP-alcohol (37). This statement is further supported by a solved structure of AF2299, a representative CDP-AP from *Archaeoglobus fulgidus* (PDB: 4O6N), where the first glycine in the motif provides flexibility to TM2 for catalysis (39). Here, we made a proline substitution mutation, G129P, which almost abolished activity (Fig. 2.4), suggesting that the flexibility provided by this glycine is essential for catalysis of *C. albicans* Cho1. Furthermore, the arginine residue within the CAPT motif was shown to be important in binding and positioning of the CDP-alcohol substrate via electrostatic interactions (37, 39), but our R133A showed unchanged activity compared to HA1 (Fig. 2.2 and 3). However, a reversal of the charge by the R133E mutation significantly decreased activity compared to HA1 (Fig. 2.4), indicating the

arginine residue in the CAPT motif of *C. albicans* Cho1 potentially binds, or at least is in the proximity of, the CDP-DAG molecule, but that this interaction is not absolutely required. We hypothesize that the loss of the R133 residue can be compensated for by the adjacent positively charged R131 or K135 residue in the *C. albicans* Cho1 sequence. The four aspartic acid residues within the CAPT motif point to the same patch of electron density and likely participate in cofactor cation binding and catalysis that is shown in currently published structures (35, 38-41). These residues (D125, D128, D146 and D150, *C. albicans* Cho1 numbering) are also important in *C. albicans* Cho1 (Fig. 2.2 and 3), indicating a similar function.

In addition, we predicted a serine binding motif, X-V-L-C-G-L-X-R-L-A-R-F, based on sequence alignment from three different yeasts, which is present in all three fungal PS synthase sequences, but absent from all three PI synthase sequences (Fig. 2.5). Interestingly, a further alignment of 8 previously reviewed PS synthases with 7 PI synthase sequences from a variety of species including the *C. albicans* Cho1 sequence also generates part of the predicted serine binding motif (Fig. S2.4), especially the C-terminal section. Site-directed mutagenesis of the residues within the serine binding motif in the *C. albicans* Cho1 protein showed that three of the C-terminal four residues (R186A, L187A and F190A) produced an almost complete abolition of activity while R189A displayed significantly decreased activity (Figs. 2.6&2.7), supporting the hypothesis that these residues play roles in Cho1 catalytic function. Moreover, after this paper was accepted for publication, Centola et al published a structure of a phosphatidylserine synthase from archaea *Methanocaldococcus jannaschii* and showing this motif is involved in coordinating serine (23).

Furthermore, we have found that the decreased activity of the R189A mutant is due to the significantly decreased binding affinity for serine (as reflected by increased apparent K_M , Fig. 2.8B), suggesting the residue R189 is involved in serine binding. This is also supported by the position of residue R189 in the homology model of Cho1, which is in proximity to the CAPT motif (e.g., the distance of C α from R189 and D150 is 12.92Å), and thus could bind and position serine for catalysis (Fig. 2.9B). Further investigation will be required to determine if this interaction is occurring between R189 and serine in the fungal PS synthase. Finally, L184A demonstrated a significantly increased V_{max} , but also increased K_M for CDP-DAG (Fig. 2.8D). The similar specificity constants (k_{cat}/K_M) of L184A with respect to HA1 suggest that mutation L184A does not make Cho1 use either substrate more efficiently (Table 2.5), but rather the effect of increased V_{max} outcompetes that of an increased K_M , leading to a net outcome of increased activity. This also indicates that the turnover number (k_{cat}), rather than substrate binding (K_M), is the limiting factor for the catalysis of Cho1 protein. Currently, the function of residue L184 is unknown.

In order to determine the relative locations of the putative serine binding site and the CAPT motif, we produced a homology model of Cho1. The homology model of *C. albicans* PS synthase was built based on the phosphatidylinositolphosphate (PIP) synthase from *Renibacterium salmoninarum* (PDB: 5D92) and provided a preliminary view of what Cho1 might look like (Fig. 2.9). The model predicts a six-transmembrane domain protein structure where the CAPT and predicted serine binding motifs are within relatively close proximity to one another. Many of the residues within the CAPT motif are charged and have been found to be part of a hydrophilic face of the 2nd and 3rd transmembrane (TM2/3) domains of this protein, correlating well with the current structures (35, 38-41). The

predicted serine binding motif (yellow) is located on TM4 and is spatially in the interface of cytosolic and membrane-bound portions, possibly allowing serine entry into this site. This correlates well with the previous findings that the second small molecules for CDP-AP proteins (serine, in the example of Cho1) bind in a cavity formed by TM 4, 5 and 6 not deeply in the membrane (35, 38, 40). This, again, indicates that there are additional residues involved in serine binding.

We have demonstrated here, for the first time, the importance of the CAPT motif within the PS synthase from a medically relevant, pathogenic fungus. Furthermore, we have begun efforts to identify the binding site for the second substrate in this enzyme, serine, an area that is still relatively unstudied. We have produced a homology model of Cho1 that places both of the substrate binding sites in close proximity and lays the foundation for structural studies. These findings contribute not only to the general understanding of phospholipid synthesizing enzymes, but also provide crucial information on candidate locations in this protein where binding of small molecule drug candidates may interfere with substrate binding. However, a limitation of this study is that it did not investigate the impact of mutations on post-translational regulation of Cho1. For example, further experiments will be required to determine whether CAPT and serine binding mutants of Cho1 have different subcellular localizations compared to HA1, as membrane localization affects Cho1 function (23). In addition, phosphorylation has been shown to regulate *S. cerevisiae* Cho1 protein by inhibiting enzymatic activity, but retains normal Cho1 protein level during exponential and stationary growth phases (21, 49). In this study, the phosphorylation level variations among different mutants were not taken into account for the *in vitro* PS synthase assay as we do not know what effect phosphorylation of Cho1

has in *C. albicans*. The impact of variation was minimized by growing the different strains to a similar OD₆₀₀ of 1.5-2.0 in the early exponential phase, in which the PS synthesis activity was maximal (50).

Cho1 represents a promising drug target, so an additional, valuable data set will come from exploring how the mutants that impact enzyme catalysis affect virulence. This data should lead to a more precise definition of how much enzymatic inhibition is required to cause a loss of virulence and better direct future inhibitor studies.

Conflict of Interest

The authors declare no conflict of interest. The content is solely the responsibility of the authors and does not necessarily represent the official views of the National Institutes of Health.

Acknowledgements

The funding sources for this project are NIH-1 R01AI153599 (TBR) and NIH 1R21AI130895-01 (TBR). The funders had no role in study design, data collection and interpretation, or the decision to submit the work for publication. The authors would like to thank Dr. Melinda Hauser for her advice and suggestions regarding this project. We would also like to thank Drs. Hong Guo and Jerome Baudry for their assistance with the use of MOE, and Madison Steiner for the help with plasmid design. Finally, the authors would like to thank and remember the late Professor Billy Carver for his contributions to the early stages of this project, as well as his camaraderie and infectious personality.

References

1. Brown, G. D., Denning, D. W., Gow, N. A., Levitz, S. M., Netea, M. G., and White, T. C. (2012) Hidden killers: human fungal infections *Science translational medicine* 4, 165rv113 10.1126/scitranslmed.3004404
2. Kullberg, B., Filler, S., and Calderone, R. (2002) *Candida and candidiasis* ASM Press, Washington, DC,
3. Wisplinghoff, H., Bischoff, T., Tallent, S. M., Seifert, H., Wenzel, R. P., and Edmond, M. B. (2004) Nosocomial bloodstream infections in US hospitals: analysis of 24,179 cases from a prospective nationwide surveillance study *Clinical infectious diseases* 39, 309-317
4. Morrell, M., Fraser, V. J., and Kollef, M. H. (2005) Delaying the empiric treatment of *Candida* bloodstream infection until positive blood culture results are obtained: a potential risk factor for hospital mortality *Antimicrobial agents and chemotherapy* 49, 3640-3645
5. Pfaller, M., Neofytos, D., Diekema, D., Azie, N., Meier-Kriesche, H.-U., Quan, S.-P. *et al.* (2012) Epidemiology and outcomes of candidemia in 3648 patients: data from the Prospective Antifungal Therapy (PATH Alliance®) registry, 2004–2008 *Diagnostic microbiology and infectious disease* 74, 323-331
6. Holeman Jr, C. W., and Einstein, H. (1963) The toxic effects of amphotericin B in man *California medicine* 99, 90
7. Whaley, S. G., Berkow, E. L., Rybak, J. M., Nishimoto, A. T., Barker, K. S., and Rogers, P. D. (2016) Azole Antifungal Resistance in *Candida albicans* and Emerging Non-*albicans Candida* Species *Front Microbiol* 7, 2173 10.3389/fmicb.2016.02173
8. Ghannoum, M. A., and Rice, L. B. (1999) Antifungal Agents: Mode of Action, Mechanisms of Resistance, and Correlation of These Mechanisms with Bacterial Resistance *Clinical Microbiology Reviews* 12, 501-517 10.1128/cmr.12.4.501
9. Odds, F. C., Brown, A. J., and Gow, N. A. (2003) Antifungal agents: mechanisms of action *Trends in microbiology* 11, 272-279 10.1016/s0966-842x(03)00117-3
10. Chen, Y. L., Montedonico, A. E., Kauffman, S., Dunlap, J. R., Menn, F. M., and Reynolds, T. B. (2010) Phosphatidylserine synthase and phosphatidylserine decarboxylase are essential for cell wall integrity and virulence in *Candida albicans* *Mol Microbiol* 75, 1112-1132 10.1111/j.1365-2958.2009.07018.x
11. Braun, B. R., van Het Hoog, M., d'Enfert, C., Martchenko, M., Dungan, J., Kuo, A. *et al.* (2005) A human-curated annotation of the *Candida albicans* genome *PLoS Genet* 1, 36-57 10.1371/journal.pgen.0010001
12. Konarzewska, P., Wang, Y., Han, G.-S., Goh, K. J., Gao, Y.-G., Carman, G. M. *et al.* (2019) Phosphatidylserine synthesis is essential for viability of the human fungal pathogen *Cryptococcus neoformans* *The Journal of biological chemistry* 294, 2329-2339 10.1074/jbc.RA118.006738
13. Atkinson, K., Fogel, S., and Henry, S. A. (1980) Yeast mutant defective in phosphatidylserine synthesis *Journal of Biological Chemistry* 255, 6653-6661

14. Atkinson, K. D., Jensen, B., Kolat, A. I., Storm, E. M., Henry, S. A., and Fogel, S. (1980) Yeast mutants auxotrophic for choline or ethanolamine J Bacteriol 141, 558-564
15. Kovac, L., Gbelska, I., Poliachova, V., Subik, J., and Kovacova, V. (1980) Membrane mutants: a yeast mutant with a lesion in phosphatidylserine biosynthesis Eur J Biochem 111, 491-501 10.1111/j.1432-1033.1980.tb04965.x
16. Bae-Lee, M. S., and Carman, G. M. (1984) Phosphatidylserine synthesis in *Saccharomyces cerevisiae*. Purification and characterization of membrane-associated phosphatidylserine synthase J Biol Chem 259, 10857-10862
17. Carman, G. M., and Matas, J. (1981) Solubilization of microsomal-associated phosphatidylserine synthase and phosphatidylinositol synthase from *Saccharomyces cerevisiae* Can J Microbiol 27, 1140-1149
18. Carson, M. A., Atkinson, K. D., and Waechter, C. J. (1982) Properties of particulate and solubilized phosphatidylserine synthase activity from *Saccharomyces cerevisiae*. Inhibitory effect of choline in the growth medium Journal of Biological Chemistry 257, 8115-8121
19. Bailis, A. M., Poole, M. A., Carman, G. M., and Henry, S. A. (1987) The membrane-associated enzyme phosphatidylserine synthase is regulated at the level of mRNA abundance Molecular and Cellular Biology 7, 167-176 10.1128/mcb.7.1.167
20. Kelley, M. J., Bailis, A. M., Henry, S. A., and Carman, G. M. (1988) Regulation of phospholipid biosynthesis in *Saccharomyces cerevisiae* by inositol. Inositol is an inhibitor of phosphatidylserine synthase activity J Biol Chem 263, 18078-18085
21. Kinney, A. J., and Carman, G. M. (1988) Phosphorylation of yeast phosphatidylserine synthase in vivo and in vitro by cyclic AMP-dependent protein kinase Proc Natl Acad Sci U S A 85, 7962-7966
22. Poole, M. A., Homann, M. J., Bae-Lee, M. S., and Carman, G. M. (1986) Regulation of phosphatidylserine synthase from *Saccharomyces cerevisiae* by phospholipid precursors Journal of Bacteriology 168, 668-672 10.1128/jb.168.2.668-672.1986
23. Kohlwein, S. D., Kuchler, K., Sperka-Gottlieb, C., Henry, S. A., and Paltauf, F. (1988) Identification of mitochondrial and microsomal phosphatidylserine synthase in *Saccharomyces cerevisiae* as the gene product of the CHO1 structural gene J Bacteriol 170, 3778-3781
24. Kuchler, K., Daum, G., and Paltauf, F. (1986) Subcellular and submitochondrial localization of phospholipid-synthesizing enzymes in *Saccharomyces cerevisiae* J Bacteriol 165, 901-910
25. Davis, S. E., Tams, R. N., Solis, N. V., Wagner, A. S., Chen, T., Jackson, J. W. *et al.* (2018) *Candida albicans* cannot acquire sufficient ethanolamine from the host to support virulence in the absence of de novo phosphatidylethanolamine synthesis Infection and immunity 86, e00815-00817
26. Cassilly, C. D., Farmer, A. T., Montedonico, A. E., Smith, T. K., Campagna, S. R., and Reynolds, T. B. (2017) Role of phosphatidylserine synthase in shaping the

- phospholipidome of *Candida albicans* FEMS Yeast Res 17, 10.1093/femsyr/fox007
27. Mandal, S., Moudgil, M. n., and Mandal, S. K. (2009) Rational drug design European Journal of Pharmacology 625, 90-100 <https://doi.org/10.1016/j.ejphar.2009.06.065>
 28. Nikawa, J., Kodaki, T., and Yamashita, S. (1987) Primary structure and disruption of the phosphatidylinositol synthase gene of *Saccharomyces cerevisiae* J Biol Chem 262, 4876-4881
 29. Hjelmstad, R. H., and Bell, R. M. (1990) The sn-1,2-diacylglycerol cholinephosphotransferase of *Saccharomyces cerevisiae*. Nucleotide sequence, transcriptional mapping, and gene product analysis of the CPT1 gene J Biol Chem 265, 1755-1764
 30. Hjelmstad, R. H., and Bell, R. M. (1991) sn-1,2-diacylglycerol choline- and ethanolaminephosphotransferases in *Saccharomyces cerevisiae*. Nucleotide sequence of the EPT1 gene and comparison of the CPT1 and EPT1 gene products J Biol Chem 266, 5094-5103
 31. Tanaka, S., Nikawa, J., Imai, H., Yamashita, S., and Hosaka, K. (1996) Molecular cloning of rat phosphatidylinositol synthase cDNA by functional complementation of the yeast *Saccharomyces cerevisiae* *pis* mutation FEBS Lett 393, 89-92 10.1016/0014-5793(96)00858-7
 32. Matsumoto, K. (1997) Phosphatidylserine synthase from bacteria Biochim Biophys Acta 1348, 214-227 10.1016/s0005-2760(97)00110-0
 33. Dryden, S. C., and Dowhan, W. (1996) Isolation and expression of the *Rhodobacter sphaeroides* gene (*pgsA*) encoding phosphatidylglycerophosphate synthase J Bacteriol 178, 1030-1038 10.1128/jb.178.4.1030-1038.1996
 34. Matsuo, Y., Fisher, E., Patton-Vogt, J., and Marcus, S. (2007) Functional characterization of the fission yeast phosphatidylserine synthase gene, *pps1*, reveals novel cellular functions for phosphatidylserine Eukaryotic cell 6, 2092-2101 10.1128/ec.00300-07
 35. Gräve, K., Bennett, M. D., and Högbom, M. (2019) Structure of *Mycobacterium tuberculosis* phosphatidylinositol phosphate synthase reveals mechanism of substrate binding and metal catalysis Communications Biology 2, 175 10.1038/s42003-019-0427-1
 36. Delhaize, E., Hebb, D. M., Richards, K. D., Lin, J.-M., Ryan, P. R., and Gardner, R. C. (1999) Cloning and Expression of a Wheat (*Triticum aestivum*L.) Phosphatidylserine Synthase cDNA: OVEREXPRESSION IN PLANTS ALTERS THE COMPOSITION OF PHOSPHOLIPIDS Journal of Biological Chemistry 274, 7082-7088 10.1074/jbc.274.11.7082
 37. Williams, J. G., and McMaster, C. R. (1998) Scanning alanine mutagenesis of the CDP-alcohol phosphotransferase motif of *Saccharomyces cerevisiae* cholinephosphotransferase J Biol Chem 273, 13482-13487 10.1074/jbc.273.22.13482
 38. Nogly, P., Gushchin, I., Remeeva, A., Esteves, A. M., Borges, N., Ma, P. *et al.* (2014) X-ray structure of a CDP-alcohol phosphatidyltransferase membrane

- enzyme and insights into its catalytic mechanism *Nat Commun* 5, 4169
10.1038/ncomms5169
39. Sciara, G., Clarke, O. B., Tomasek, D., Kloss, B., Tabuso, S., Byfield, R. *et al.* (2014) Structural basis for catalysis in a CDP-alcohol phosphotransferase *Nat Commun* 5, 4068 10.1038/ncomms5068
 40. Clarke, O. B., Tomasek, D., Jorge, C. D., Dufresne, M. B., Kim, M., Banerjee, S. *et al.* (2015) Structural basis for phosphatidylinositol-phosphate biosynthesis *Nat Commun* 6, 8505 10.1038/ncomms9505
 41. Dufresne, M. B., Jorge, C. D., Timóteo, C. G., Petrou, V. I., Ashraf, K. U., Banerjee, S. *et al.* (2020) Structural and Functional Characterization of Phosphatidylinositol-Phosphate Biosynthesis in Mycobacteria *Journal of Molecular Biology*
 42. Ikushiro, H., Islam, M. M., Okamoto, A., Hoseki, J., Murakawa, T., Fujii, S. *et al.* (2009) Structural Insights into the Enzymatic Mechanism of Serine Palmitoyltransferase from *Sphingobacterium multivorum* *The Journal of Biochemistry* 146, 549-562 10.1093/jb/mvp100
 43. Ohsawa, T., Nishijima, M., and Kuge, O. (2004) Functional analysis of Chinese hamster phosphatidylserine synthase 1 through systematic alanine mutagenesis *The Biochemical journal* 381, 853-859 10.1042/bj20040443
 44. Kanfer, J., and Kennedy, E. P. (1964) Metabolism and Function of Bacterial Lipids: II. BIOSYNTHESIS OF PHOSPHOLIPIDS IN *ESCHERICHIA COLI* *Journal of Biological Chemistry* 239, 1720-1726
 45. Tams, R. N., Cassilly, C. D., Anaokar, S., Brewer, W. T., Dinsmore, J. T., Chen, Y.-L. *et al.* (2019) Overproduction of Phospholipids by the Kennedy Pathway Leads to Hypervirulence in *Candida albicans* *Frontiers in Microbiology* 10, 10.3389/fmicb.2019.00086
 46. Mignone, F., Gissi, C., Liuni, S., and Pesole, G. (2002) Untranslated regions of mRNAs *Genome biology* 3, 1-10
 47. Chen, T., Jackson, J. W., Tams, R. N., Davis, S. E., Sparer, T. E., and Reynolds, T. B. (2019) Exposure of *Candida albicans* β (1,3)-glucan is promoted by activation of the *Cek1* pathway *PLOS Genetics* 15, e1007892 10.1371/journal.pgen.1007892
 48. Fischl, A. S., Homann, M. J., Poole, M. A., and Carman, G. M. (1986) Phosphatidylinositol synthase from *Saccharomyces cerevisiae*. Reconstitution, characterization, and regulation of activity *Journal of Biological Chemistry* 261, 3178-3183
 49. Choi, H. S., Han, G. S., and Carman, G. M. (2010) Phosphorylation of yeast phosphatidylserine synthase by protein kinase A: identification of Ser46 and Ser47 as major sites of phosphorylation *J Biol Chem* 285, 11526-11536 10.1074/jbc.M110.100727
 50. Homann, M. J., Bailis, A. M., Henry, S. A., and Carman, G. M. (1987) Coordinate regulation of phospholipid biosynthesis by serine in *Saccharomyces cerevisiae* *Journal of Bacteriology* 169, 3276-3280 10.1128/jb.169.7.3276-3280.1987

51. KIYONO, K., MIURA, K., KUSHIMA, Y., HIKIJI, T., FUKUSHIMA, M., SHIBUYA, I. *et al.* (1987) Primary Structure and Product Characterization of the *Saccharomyces cerevisiae* CHO1 Gene That Encodes Phosphatidylserine Synthase1 *The Journal of Biochemistry* 102, 1089-1100
10.1093/oxfordjournals.jbchem.a122147
52. Okada, M., Matsuzaki, H., Shibuya, I., and Matsumoto, K. (1994) Cloning, Sequencing, and Expression in *Escherichia-Coli* of the *Bacillus-Subtilis* Gene for Phosphatidylserine Synthase *Journal of Bacteriology* 176, 7456-7461
53. Sohlenkamp, C., de Rudder, K. E., Röhrs, V., López-Lara, I. M., and Geiger, O. (2000) Cloning and characterization of the gene for phosphatidylcholine synthase *Journal of Biological Chemistry* 275, 18919-18925

Supplementary Figures

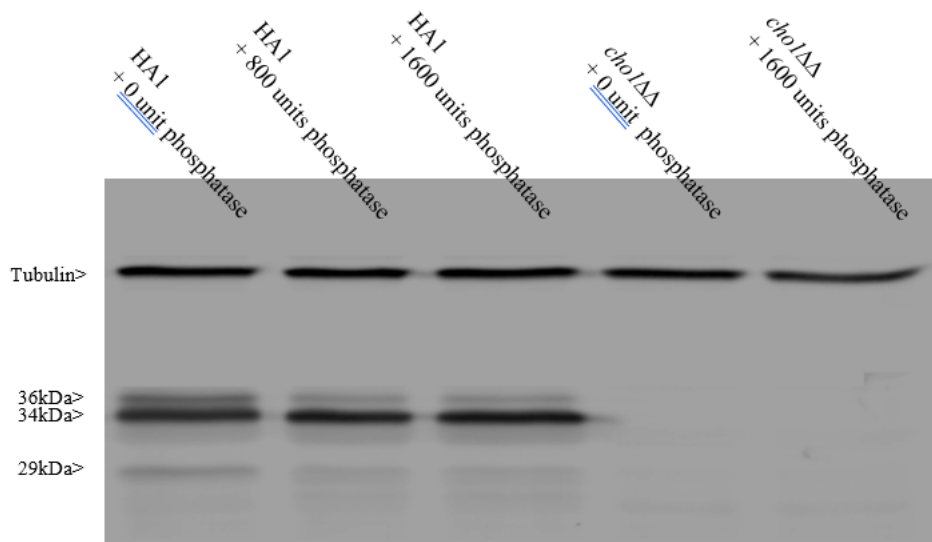


Figure S2.1. The 36 kDa and 29 kDa band of Cho1 protein contains phosphorylated population.

Proteins were extracted from HA1 and were subjected to Lambda phosphatase treatment (NEB #P0757) before Western blotting. The phosphatase concentrations are indicated in the figure. One unit is defined as the amount of phosphatase that hydrolyzes 1 nmol of p-Nitrophenyl Phosphate in 1 min at 30°C in a total reaction volume of 50 μ l. The total reaction time is 30 min.

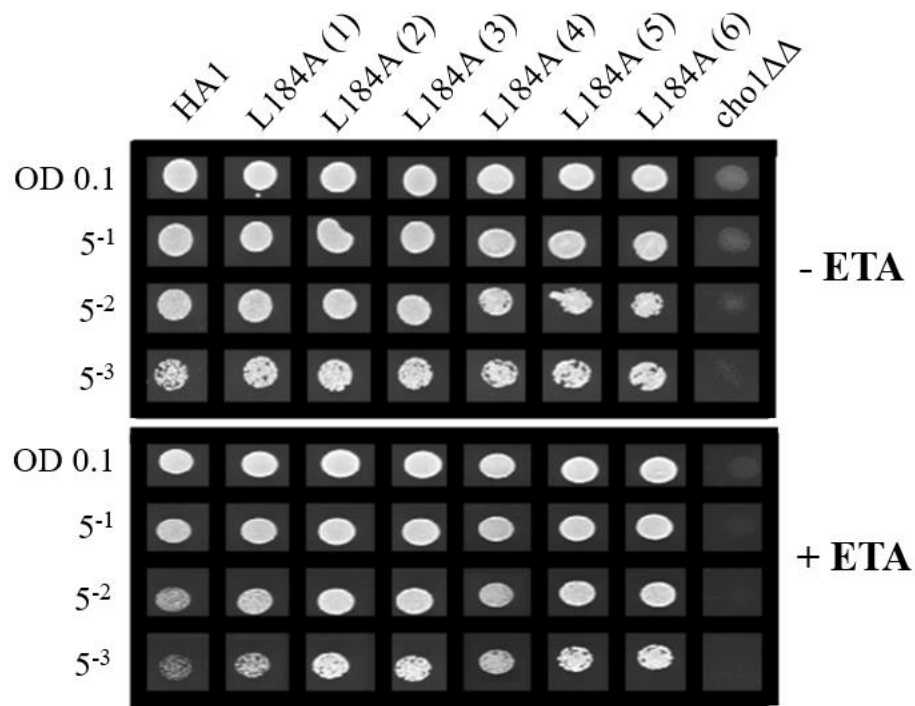


Figure S2.2. The elevated growth of L184A is not due to a spurious mutation. The growth of six L184A transformation colony candidates was measured in a spot dilution assay to rule out the possibility that a spurious mutation in the genome might account for the elevated growth of L184A. (+ETA, minimal medium +1 mM ethanolamine; -ETA, minimal medium).

Cho1 **D₁₂₅(X)₂D₁₂₈G₁₂₉(X)₂A₁₃₂R₁₃₃(X)₈G₁₄₂(X)₃D₁₄₆(X)₃D₁₅₀**

Cpt1 **D₁₁₀(X)₂D₁₁₃G₁₁₄(X)₂A₁₁₇R₁₁₈(X)₈G₁₂₇(X)₃D₁₃₁(X)₃D₁₃₅**

Figure S2.3. Alignment of CAPT motifs from *S. cerevisiae* Cpt1 and *C. albicans* Cho1
Alignment of CAPT motifs from *S. cerevisiae* Cpt1 and *C. albicans* Cho1 demonstrates the conserved nature of the amino acids within this proposed CDP-alcohol binding domain.

	Cho1_Candida---albicans	TT--VDVLF FLAFWVLCGLTR <u>LARFNIS</u> VNNIPKDK-HGKSQY-FEGLPIPTNLFWVGFMA
	PSS_Helicobacter_pylori	NFGRIGMAVSALFVIFGAI <u>RLARFNIS</u> TNTSDPY-----S-FIGIPIPA AAV VVLCV
	PSS_Bacillus_subtilis	TLPPFIGILCALTYISICGMLR L SKFNIEQ--SKLP-----T-FIGMPIPFAGMCLVILS
	PSS_Mycobacterium_leprae	TTP-VGNVAVLLYPVCVVLRLARFNALDDGTQP--AYTREF-FVGMPPAPAGAVSMIGLL
PS synthases	PSS_Mycobacterium_tuberculosis	KWP-VGNVVVLLYAVCVVLR L ARYNALQDDGTQP--AYAHEF-FVGMPPAPAGAVSMIGLL
	PSS_Mycobacterium_bovis	KWP-VGWWVLLYAVCVVLR L ARYNALQDDGTQP--AYAHEF-FVGMPPAPAGAVSMIGLL
	PSS_Schizosaccharomyces_pombe	TF--LDTVILSLFVLCGLTR L ARFNVSVNSIPKDG-SGKSQF-FEGTPIPTTSLVTVCG
	PSS_Methanocaldococcus_jannaschii	NL--ALISAIIFCLCGALR L ARFGILN---VK-----G-FIGLPIPAGALLVGFCA
	PSS_Saccharomyces_cerevisiae	TT--FDVMILSFFVLCGLAR L ARFNVTVAQLPKDSSTGSKSY-FEGLPMPPTTLALVLGMA
	CDIPT_RAT	LSMSLDVASHWLHLHSSVVR-----GSESHKM--IDL SGNPV LRIYYTSRPA L FTLCA
	CDIPT_HUMAN	ISMSLDVASHWLHLHSSVVR-----GSESHKM--IDL SGNPV LRIYYTSRPA L FTLCA
PI synthases	PIS_Schizosaccharomyces_pombe	LLVSLDLASHYMHMYSTLHC-----GASSHKT--VTKKHNM MLR LYYGNNKVLFI F CA
	CDIPT_Drosophila_melanogaster	LSIAIDVACHWLFMQTSVVV-----GRSSHKV--N--DNFIMR LYY QKDI-LTFMCC
	CDIPT_MOUSE	LSMSLDVASHWLHLHSSVVR-----GSESHKM--IDL SGNPV LRIYYTSRPA L FTLCA
	PIS_YEAST	LMLGLDITSHYMHMYASLSA-----GKTS HKS --VGE GES RLLHLYYTRRDVLF I CA
	PIS1_Arabidopsis_thaliana	SLLALDIASHWLQMYSTFLA-----GKSSHKD--VKD STSW LFR LYY GNRIFM CY CCV

Figure S2.4. Alignment of several previously reviewed PS synthase with PI synthase sequences from different species reveals part of the putative serine binding site in *C. albicans* Cho1.

A further alignment of 8 previously reviewed PS synthases with 7 previously reviewed PI synthase sequences from different species, in the presence of *C. albicans* Cho1, has generated a region in all PS synthases which is absent in all PI synthases (red box). The putative serine binding of *C. albicans* Cho1 is underlined.

**CHAPTER 3 SOLUBILIZATION, PURIFICATION, AND
CHARACTERIZATION OF THE HEXAMERIC FORM OF
PHOSPHATIDYLSERINE SYNTHASE FROM *CANDIDA ALBICANS***

Publication Note

A version of this chapter has been previously published by Yue Zhou, Jawhar H. Syed, Dmitry A. Semchonok, Edward Wright, Fotis L. Kyrilis, Farzad Hamdi, Panagiotis L. Kastritis, Barry D. Bruce and Todd B. Reynolds:

Zhou, Y., Syed, J. H., Semchonok, D. A., Wright, E., Kyrilis, F. L., Hamdi, F., ... & Reynolds, T. B. (2023). Solubilization, purification, and characterization of the hexameric form of phosphatidylserine synthase from *Candida albicans*. *Journal of Biological Chemistry*, 299(6).

Contribution in the paper: Conceived and designed the experiments: YZ, BDB, TBR. Performed the experiments: YZ, JS, DS, EW, FLK, FH. Analyzed the data: YZ, JS, DS, EW, BDB, FZ, TBR. Contributed reagents/materials/analysis tools: PLK, BDB, TBR. Wrote the paper: YZ, DS, EW, BDB, TBR. All authors contributed to the article and approved the submitted version.

Specifically, Dmitry, Fotis, Fazad, and Panagiotis did all the electron microscopy work. Analytical ultracentrifugation was done by Ed Wright. Hassan helped with the growth curves. Strain construction, solubilization/purification and all the other experiments were done by Yue Zhou. The paper was written by Yue Zhou, Dmitry, Ed and edited by the rest of the people.

Abstract

Phosphatidylserine (PS) synthase from *Candida albicans*, encoded by the *CHO1* gene, has been identified as a potential drug target for new antifungals against systemic candidiasis. Rational drug design or small molecule screening are effective ways to identify specific inhibitors of Cho1, but both will be facilitated by protein purification. Due to the transmembrane nature of Cho1, methods were needed to solubilize and purify the native form of Cho1. Here, we used six non-ionic detergents and three styrene maleic acids (SMAs) to solubilize an HA-tagged Cho1 protein from the total microsomal fractions. Blue native PAGE (BN-PAGE) and immunoblot analysis revealed a single band corresponding to Cho1 in all detergent-solubilized fractions, while two bands were present in the SMA2000-solubilized fraction. Our enzymatic assay suggests that digitonin- or DDM-solubilized enzyme has the most PS synthase activity. Pull-downs of HA-tagged Cho1 in the digitonin-solubilized fraction reveal an apparent MW of Cho1 consistent with a hexamer. Furthermore, negative-staining electron microscopy analysis and AlphaFold2 structure prediction modeling suggest the hexamer is composed of a trimer of dimers. We purified Cho1 protein to near-homogeneity as a hexamer using affinity chromatography and TEV protease treatment, and optimized Cho1 enzyme activity for manganese and detergent concentrations, temperature (24°C), and pH (8.0). The purified Cho1 has a K_m for its substrate CDP-diacylglycerol of 72.20 μM with a V_{max} of 0.079 $\text{nmol}/(\mu\text{g}\cdot\text{min})$ while exhibiting a sigmoidal kinetic curve for its other substrate serine, indicating cooperative binding. Purified hexameric Cho1 can potentially be used in downstream structure determination and small drug screening.

Introduction

The incidence of human systemic fungal infections has increased dramatically over the past 30 years, and this is partly due to an increase in the number of immunocompromised patients (1-3). *Candida* species are the leading cause of fungal infections in humans. Among *Candida spp.*, *Candida albicans* (*C. albicans*) is the most commonly isolated one, and it is capable of causing mucosal, cutaneous, and bloodstream infections (i.e., invasive mycoses) (1, 4, 5). In all cases, successful management of patients with systemic *Candida* infections requires antifungal therapy. Currently, three classes of antifungals are used against systemic *Candida* infection: azoles, echinocandins, and polyenes. Unfortunately, all of these antifungals have limitations, including rising drug resistance to azoles and echinocandins and toxicity of amphotericin B to patients (6-10). Therefore, new antifungal drug development is of utmost importance.

The phosphatidylserine (PS) synthase (gene name: *CHO1*) in *C. albicans* has been identified as a potential drug target due to its importance in fungal virulence, conservation among major fungal pathogens, and absence in humans (11-13). Rational drug design is one way to identify inhibitors of *C. albicans* Cho1 protein, and ligand or structure-based design approaches can be used (14). Given the limited known Cho1 ligands, structure-based design is more approachable for Cho1, which requires the identification of the substrate-binding pockets. Cho1 has two substrates, cytidyldiphosphate-diacylglycerol (CDP-DAG) and L-serine, from which it catalyzes the formation of the important phospholipid, phosphatidylserine. This catalytic activity has been observed in the mitochondria and endoplasmic reticulum (15-17). PS is then trafficked to other cellular compartments, such as the plasma membrane. Due to its CDP-

DAG binding site, Cho1 belongs to the CDP-alcohol phosphatidyltransferase (CDP-AP) protein family, which has a highly conserved CDP-alcohol phosphotransferase (CAPT) motif, D-(X)₂-D-G-(X)₂-A-R-(X)₂-N-(X)₅-G-(X)₂-L-D-(X)₃-D (18). The CAPT motif is utilized by CDP-AP enzymes to bind CDP-linked molecules and catalyze the formation of a phosphodiester bond between the CDP-linked molecule and a second small alcohol (13, 19-22). Several residues within the CAPT motif of *C. albicans* Cho1 have been previously characterized and shown to be essential for function (18). The binding pocket for serine, however, is not conserved among CDP-APs since serine is more specific to Cho1. Recently, the serine-binding pocket of the PS synthase in the archaea *Methanocaldococcus jannaschii* has been identified from its solved structure (23), and some critical serine-binding residues of *C. albicans* Cho1 protein have been identified by alanine scanning mutagenesis (18), providing new details of the serine-binding site in Cho1. However, there are a number of substantial differences between the *M. jannaschii* PS synthase and *C. albicans* Cho1. The Cho1 enzyme is predicted to have only 6 transmembrane domains, whereas the *M. jannaschii* PS synthase has 8, and there are several key residues that we have identified in Cho1 that do not have a clear role in the *M. jannaschii* PS synthase (18, 23). Thus, it is important to generate a specific structure for the fungal enzyme in order to further rational drug design approaches.

In addition, there have been only six CDP-AP enzymes within the protein family with solved structures (22-27), and all are from prokaryotes. Moreover, with the exception of *M. jannaschii* PS synthase, all of the others have six transmembrane domains. A homology model of *C. albicans* Cho1 was previously reported, and it was based on the phosphatidylinositolphosphate (PIP) synthase from *Renibacterium*

salmoninarum (18), which also has six transmembrane domains. The *M. jannaschii* PS synthase structure had also not yet been published at that time. However, due to the low amino acid sequence similarity between *C. albicans* Cho1 and the six existing CDP-APs with known structures, an atomic structure of Cho1 is needed for an unbiased and thorough structure-based design, which requires a relatively homogenous purified *C. albicans* Cho1 enzyme. AlphaFold2 is a powerful tool for structure prediction, but it has limitations such as low efficacy in predicting enzyme binding sites accurately for drug screening (28-31).

Small molecule screening is another way to identify inhibitors to Cho1. A compound, SB-224289, has been discovered from a previous whole-cell-based screening. Still, it was found to act only on Cho1-related physiological pathways instead of the enzyme itself, preventing further characterization and optimization (32). The major limitation of cell-based drug screening is that it typically fails to find inhibitors of enzymes with known molecular targets and mechanisms (14). In this regard, a target-based screen is more favorable, as it overcomes the limitations that can occur due to cellular entry. These issues can be resolved later through medicinal chemistry approaches. Thus, a successful purification scheme for functional *C. albicans* Cho1 enzyme is necessary.

PS synthase was first identified and purified to homogeneity in *Escherichia coli* (33-35). In contrast with the membrane-bound characteristics of Cho1 in yeasts, the *Escherichia coli* PS synthase is associated with ribosomes (36). The first fungal Cho1 homolog, from *Saccharomyces cerevisiae*, was identified in 1980 (37, 38), and characterization of the *S. cerevisiae* Cho1 enzyme included an understanding of its

regulation (39-41) and identification of its localization (15, 16). Solubilization and purification was also performed on *S. cerevisiae* Cho1, followed by the characterization of its enzyme kinetics (42-44). For *C. albicans* Cho1 enzyme, the structural gene and function were characterized in 2010 (11). Later, the Michaelis-Menten kinetics of the *C. albicans* Cho1 were biochemically determined using crude membranes from the wildtype and Cho1-overexpressor strains, which yielded a millimolar-scale K_m for serine and micromolar-scale K_m for CDP-DAG (18, 45).

In this study, we aimed to solubilize and purify functional Cho1 protein from its native host, *C. albicans*, and characterize its basic biochemical properties. Previously, Triton X-100 was used to solubilize *S. cerevisiae* Cho1, and subsequent purification was achieved using a lengthy process of CDP-diacylglycerol-Sepharose affinity chromatography followed by anion-exchange DE-53 chromatography, due to the lack of knowledge of the structural gene (43, 44). Even if some insights can be gained from the *S. cerevisiae* Cho1 solubilization/purification, detergent has to be carefully selected for *C. albicans* Cho1 because the phospholipid compositions of these two species are quite different, thus the optimal solubilization detergent and condition is not interchangeable (46-48). Moreover, since the original purification of *S. cerevisiae* Cho1 in the early 1980s, a number of improved detergents and solubilizing reagents have been created. For example, styrene maleic acid (SMA) copolymers have gained popularity in recent years for membrane protein solubilization as they maintain the original and stable lipid environment, and thus can be a substitute for detergents (47-50). In this work, several popular detergents and SMAs were screened and optimized to solubilize Cho1 from the crude membrane with high activity and homogeneity. The assessment of the solubilized

C. albicans Cho1 by blue-native (BN)-PAGE and several complementary approaches indicated that *C. albicans* Cho1, unlike *S. cerevisiae* Cho1 or any other CDP-APs, is a hexamer. The purified *C. albicans* Cho1 can be used for downstream applications such as small molecule screening or structure determination.

Results

Solubilization of *Candida albicans* Cho1 with different detergents and styrene-maleic acid (SMA) copolymers

Since Cho1 is a transmembrane protein, solubilization was conducted before protein purification. The *C. albicans* strain HA1 is a derivative of SC5314 and has a C-terminally HA₃-tagged Cho1 protein under the constitutively active *ENO1* promoter (18). This strain was used to express the Cho1 protein for solubilization. To determine the optimal detergent for solubilization, the total crude membrane was collected and solubilized using the detergents digitonin, n-Dodecyl- β -D- Maltopyranoside (DDM), n-Tetradecyl- β -D-Maltopyranoside (TDM), Triton X-100, the digitonin substitute (Glyco-Diosgenin, GDN) or Lauryl Maltose Neopentyl Glycol (LMNG), each at a final concentration of 1.5%. To check if the Cho1 protein was successfully solubilized from the membrane, as well as to measure the molecular weight (MW) of the native protein complex, the resulting solubilized detergent fractions were assessed by blue native polyacrylamide gel electrophoresis (BN-PAGE) followed by Western blotting against the HA epitope to identify the Cho1 complex. All six detergents led to formation of a single band representing the HA-tagged Cho1 (Figure 3.1A), confirming that these detergents could successfully solubilize Cho1 native membranes. However, the estimated MW of

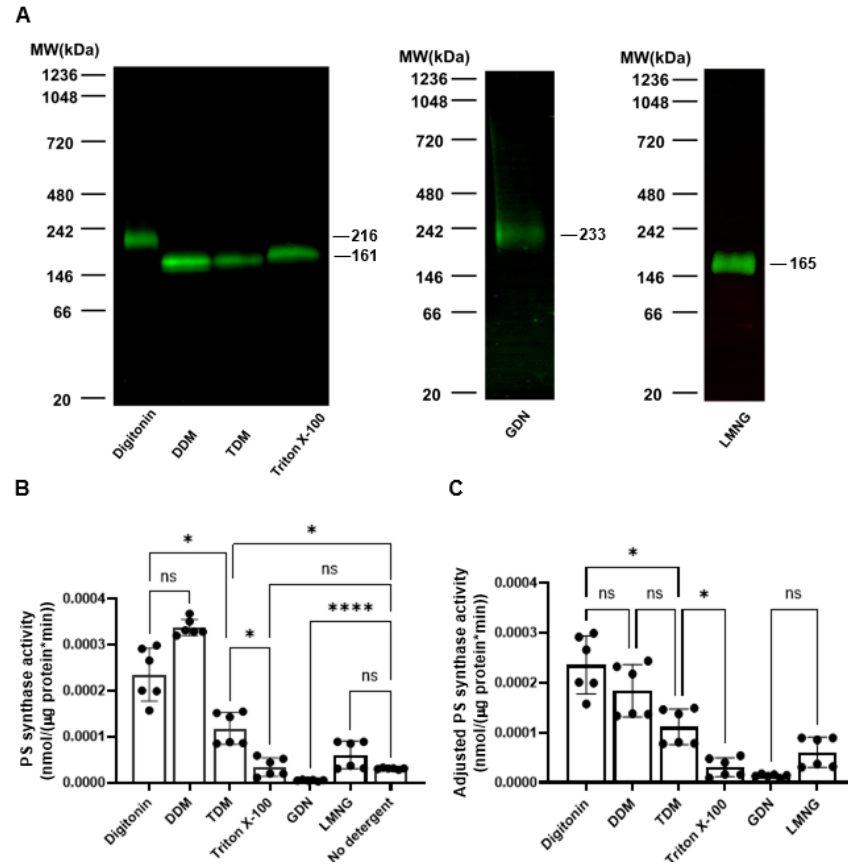


Figure 3.1. Solubilization of HAX3-tagged Cho1 using six popular non-ionic detergents. (A) Crude membrane was collected from the *cho1* $\Delta\Delta$ *P_{ENO1}-CHO1-HAX3* (HA1) strain. Digitonin, DDM, TDM, Triton X-100, GDN, or LMNG were used to solubilize Cho1 at a final concentration of 1.5%. The solubilized Cho1-HAX3 protein was detected by Western blotting of the BN-PAGE. For each solubilized fraction, (B) the PS synthase activity (nmol/(μ g protein*min)) and (C) adjusted PS synthase activity (nmol/(μ g protein*min)) were measured by an *in vitro* PS synthase assay. Crude membrane protein with no detergent was used as a control. Statistics were conducted using one-way ANOVA and Dunnett's T3 multiple comparisons test (ns=not significant, $p > 0.05$; *, $0.05 > p > 0.01$; ****, $p < 0.0001$). The activities were measured in duplicate with a total of six biological replicates as indicated. The bars represent the mean, and the error bars are \pm standard deviation (S.D.) values.

digitonin and GDN solubilized Cho1 is higher than the others, indicating a difference in [i] the conformation of the solubilized Cho1 protein, [ii] composition of residual bound phospholipids in the Cho1-micelle particle or [iii] the extent to which excess lipid interferes with protein migration in the protein-detergent micelles. These factors have been previously shown to affect protein migration during BN-PAGE (49).

The PS synthase activity of each detergent-solubilized Cho1 fraction was measured and compared to the original crude membrane prep (no detergent fraction) (Figure 3.1B). The PS synthase activity was calculated based on the incorporation L-[³H]-serine into the lipid phase following normalization to the protein quantity, as described previously (18, 45). Digitonin-, DDM-, and TDM-solubilized fractions showed significantly increased PS synthase activity compared to the crude membrane (Figure 1B). In contrast, Triton X-100- and LMNG-solubilized fractions have similar activity to the unextracted membranes, and the GDN-solubilized fraction had diminished activity. The DDM-solubilized fraction has the highest PS synthase activity and is followed by the digitonin fraction. The higher PS synthase activity in these two detergent fractions can be explained by [i] a higher solubilization rate (thus, more Cho1 protein molecules are present in the reaction), [ii] a solubilized conformation with higher enzyme activity, or [iii] both.

To help explain these observations, the adjusted PS synthase activity was calculated using PS synthase activity adjusted to the Cho1 protein level reflected on the immunoblots. This adjusted PS synthase activity could better represent the enzymatic activity of Cho1 in the solubilized fractions since the activity was further normalized to the Cho1 protein level in the solubilized fractions. In Figure 3.1C, the digitonin- and

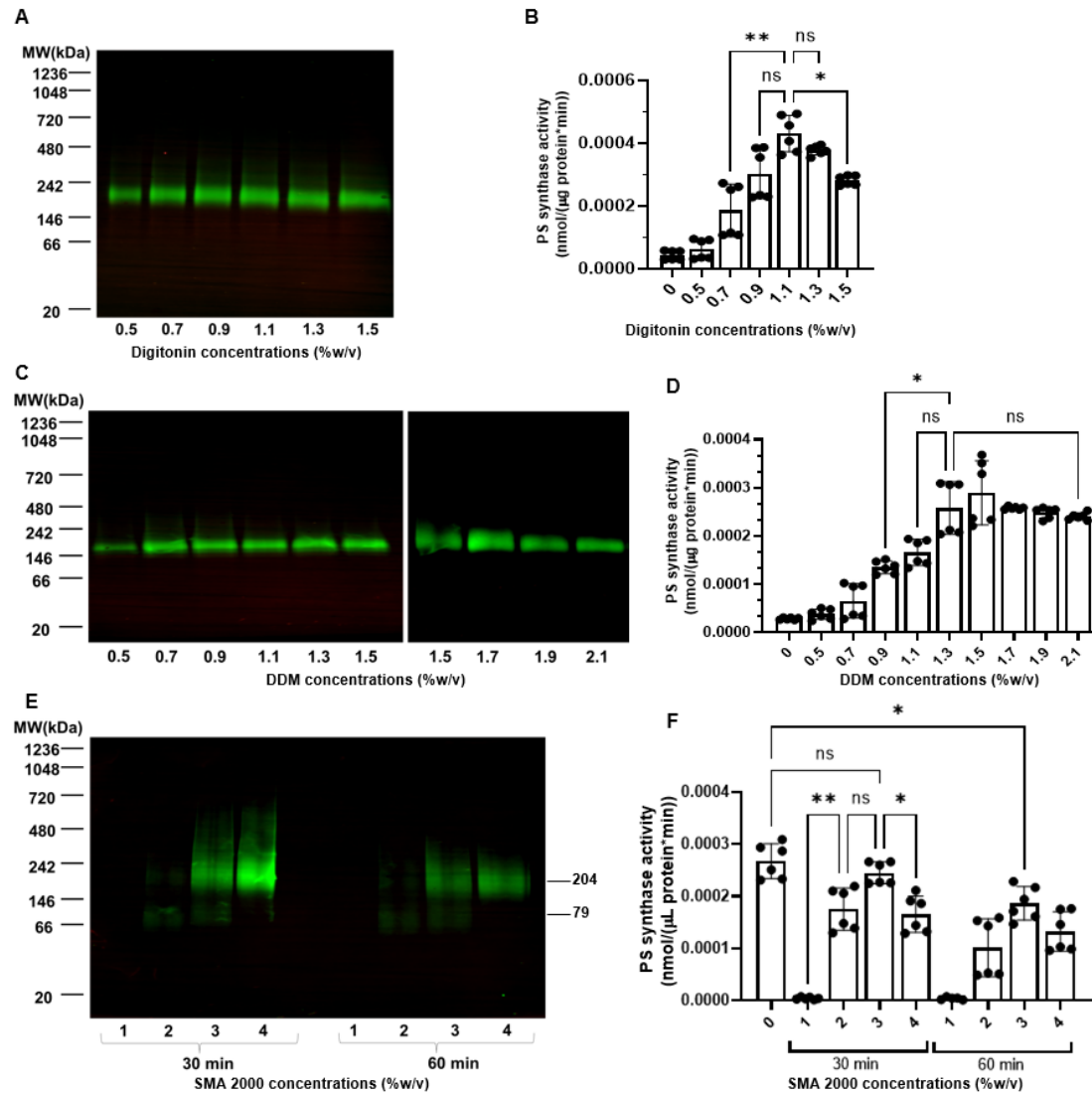
DDM-solubilized fractions showed similar levels of adjusted PS synthase activity as opposed to the slightly increased PS synthase activity in the DDM fraction, indicating that the high activity of PS synthase activity in the DDM fraction is due to a higher solubilization rate rather than a higher enzymatic activity. On the contrary, the lower PS synthase activities of Triton X-100, GDN- and LMNG-solubilized fraction are due to lower enzymatic activity of solubilized Cho1 in these detergents.

Based on these results, both digitonin and DDM were selected for further optimization. For this optimization, different concentrations of digitonin and DDM were used to solubilize the Cho1 protein. The resulting solubilized fractions were subjected to conformational (BN-PAGE) and activity checks. For digitonin, all six concentrations, 0.5%, 0.7%, 0.9%, 1.1%, 1.3%, and 1.5%, were able to solubilize Cho1 and 1.1% was determined to be the optimal concentration as its PS synthase activity is highest (Figure 3.2A&B). DDM's concentration was increased from 0.5% to 2.1% in 0.2% increments, and PS synthase activity remained unchanged at $\geq 1.3\%$ DDM (Figure 3.2C&D).

Styrene maleic acid (SMA) copolymers have gained popularity in the membrane protein field as they are a substitution for detergents to produce a SMALP (SMA Lipid Particle) that maintains a membrane protein's original and stable lipid environment (50-53). SMALPs are compatible with many biophysical approaches (50, 51, 54). Initially, SMA1000, 2000, and 3000 were used to solubilize Cho1 at concentrations of 2, 3, and 4% at 37° C, but only SMA2000 was able to solubilize Cho1 from the membrane (Figure S3.1). SMA2000 was further refined, and a range of 1-4% SMA2000 was used to optimize the solubilization conditions with either 30 or 60 min incubations (Figure 3.2E&F). Two bands (204 kDa and 79 kDa) of Cho1 were found at concentrations of 2-

Figure 3.2. Optimization of digitonin, DDM and styrene maleic acid (SMA) 2000 for solubilization and activity.

(A, C) HAx3-tagged Cho1 protein was solubilized in different (A) digitonin concentrations (0.5%, 0.7%, 0.9%, 1.1%, 1.3% and 1.5%) or (C) DDM concentrations (0.5%, 0.7%, 0.9%, 1.1%, 1.3%, 1.5%, 1.7%, 1.9% and 2.1%), and Cho1 levels for the different fractions were measured by Western blotting following BN-PAGE. (B, D) Fractions were also tested for PS synthase activity (nmol/(μ g protein*min)). Digitonin-solubilized fractions are shown in (B) and DDM-solubilized fractions are in (D). (E) SMA2000-solubilized HAx3-tagged Cho1 protein, at different times (30 or 60 min) and SMA concentrations (1%, 2%, 3% and 4%), was detected by Western blot. (F) The PS synthase activities of SMA 2000-solubilized fractions were measured and are presented as nmol/(μ L protein*min). Crude membrane protein with no detergent/SMA2000 was used as a control. Statistics were conducted using one-way ANOVA and Dunnett's T3 multiple comparisons test (ns=not significant, $p > 0.05$; *, $0.05 > p > 0.01$, **, $0.01 > p > 0.001$). The activities were measured in duplicate with a total of six biological replicates as indicated. The bars represent the mean and the error bars are \pm S.D. values.



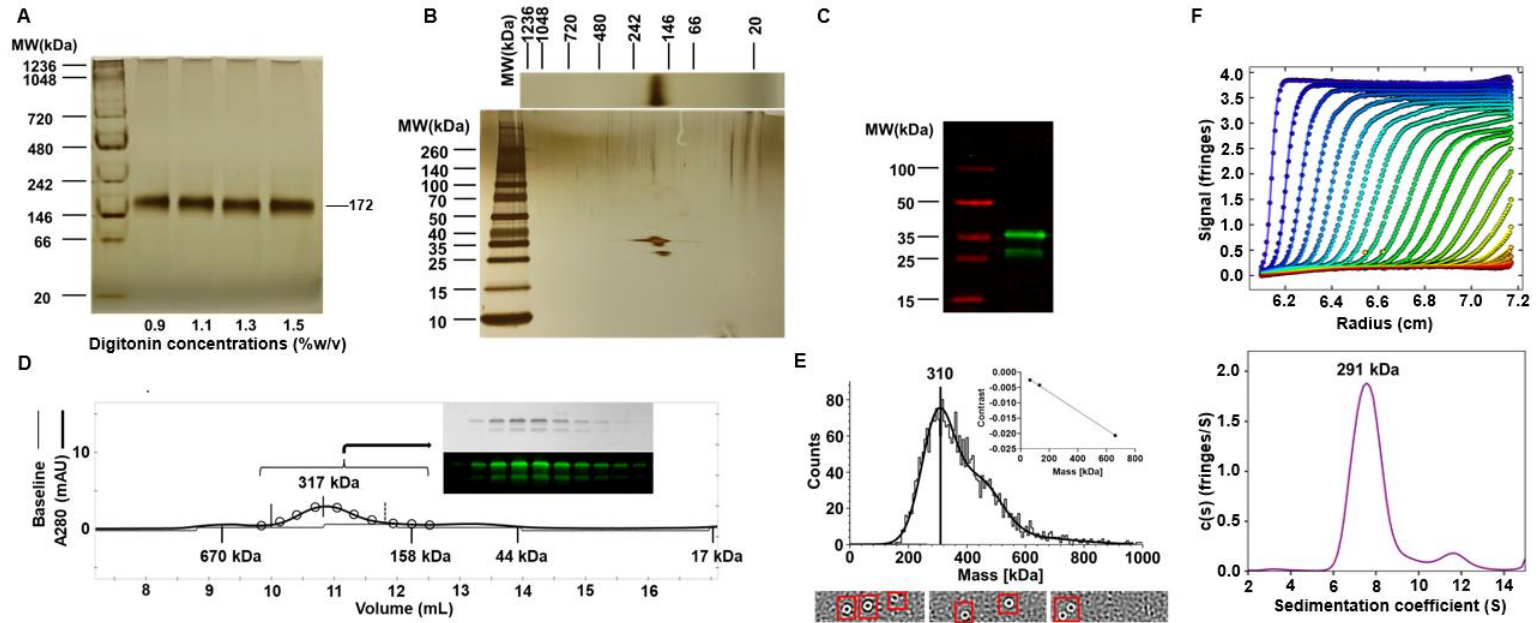
4% even if the lower band has much less protein, indicating two distinct protein species. Moreover, solubilization at 30 min had a higher yield than at 60 min, possibly due to protein degradation or dissociation of the SMALP complex. SMA2000 at 4% gave the highest protein yield after a 30 min solubilization (Figure 3.2E). In contrast, enzyme assays revealed that the 3% SMA2000 solubilized fraction had the highest PS synthase activity (Figure 3.2F). Since the protein concentrations in the SMA-solubilized fractions were not measurable due to interference of the SMA copolymers to protein concentration assays (data not shown), PS synthase activities for these fractions were normalized by the volume of the reaction (nmol/(μ L protein*min)). One explanation for the inconsistency between Cho1 band intensity and activity at 4% is that excessive SMA2000 in the this fraction may interfere with the activity, which offsets the high protein amount. The SMA2000 bands were much more diffuse than those in the detergent fractions. Since detergent fractions gave the greatest increases in activity and the clearest bands, further purification schemes were pursued with the detergents digitonin and DDM.

***Candida albicans* Cho1 appears as a hexamer**

Next, to assess the feasibility of purifying Cho1 from solubilized fractions, a small-scale pull-down was performed using anti-HA beads, and BN-PAGE measured pulled-down proteins from digitonin-solubilized membranes. As shown in Figure 3.3A, a single 172-kDa native complex containing Cho1 was found in the 0.9, 1.1, 1.3, and 1.5% digitonin fractions, indicating high purity. To check the protein composition of this native complex, a 2nd dimensional SDS-PAGE was performed on the gel strip of the 1.1% digitonin fraction from the BN-PAGE (Figure 3.3B). This 2nd-dimensional SDS-PAGE, which should break up complexes into individual components, revealed several bands. To

Figure 3.3. The solubilized native Cho1 complex appears to be a hexamer.

(A) BN-PAGE of the pulled-down HAx3-tagged Cho1 protein from the solubilized fractions of 0.9%, 1.1%, 1.3%, 1.5% digitonin. (B) The 2nd dimensional SDS-PAGE of the BN-PAGE gel strip from 1.1% digitonin. These BN-PAGE gels were stained with PierceTM silver stain kit, and MW of different bands (kDa) were estimated based on the protein ladder as indicated. (C) SDS-PAGE and Western blot of the pulled-down HAx3-tagged Cho1 protein showed three bands at 36 kDa, 29 kDa and 27 kDa, representing the bands from (B). (D) Size exclusion chromatography of pulled-down HAx3-tagged Cho1 protein. The estimated molecular weights of Cho1 and different protein markers are indicated. The protein profile was assessed by the eluted fractions (circles) on silver-stained SDS-PAGE (inset figure, top) or Western blotting with anti-HA antibody (inset figure, bottom). (E) Histogram of trajectory counts detected in a mass photometry movie (n = 1 movie, 1 min) of pulled-down HAx3-tagged Cho1 protein. Contrast–mass calibration curve of the measurement is shown in the inset (BSA, 66 kDa and 132 kDa; Thyroglobulin, 660 kDa). Three frames with Cho1-digitonin-micelles (highlighted in red squares) are shown under the histogram. (F) Sedimentation velocity analytical ultracentrifugation (SV-AUC) analysis of the oligomeric state of Cho1. SV-AUC interference profile for Cho1 sedimenting at 50,000 rpm at 20°C. The raw data (circles) and best fit using the continuous c(s) distribution model (lines) in SEDFIT are shown on the top. Every fourth scan is shown for clarity. The c(s) distribution plot for the data in the top panel is shown on the bottom. The peak at 7.7S accounts for over 85% of the total signal. This peak corresponds to a MW of 291 kDa as calculated in SEDFIT using the buffer density and viscosity, protein partial specific volume and best fit frictional coefficient.



determine whether these bands represent Cho1, the same pulled-down sample was subjected to Western blotting against the HA tag (Figure 3.3C). It revealed one upper band (36 kDa) and two lower bands (29 and 27 kDa), corresponding to the bands on the 2nd dimensional SDS-PAGE based on MW, contained the HA tag. This result indicates that the 172-kDa native complex corresponds to Cho1, suggesting this native complex is made of only Cho1 protein instead of interactions with other proteins. The multiple bands of Cho1 on the SDS-PAGE have been reported previously, and it is suggested that the lower bands are the proteolytic product of the full-length upper band (16, 18, 55). Interestingly, based on the MW of the Cho1 complex (172 kDa) and monomeric HA-tagged Cho1 (27, 29, 36 kDa), the native complex is likely to be a hexamer. In order to measure the molecular mass of the native Cho1 protein and test if Cho1 forms a hexamer by complementary approaches, the pull-downed Cho1 protein was analyzed by size-exclusion chromatography (Figure 3.3D) and mass photometry (Figure 3.3E), both of which suggested an ~310 kDa form. Moreover, analytical ultracentrifugation also indicated the MW of the pull-downed Cho1 protein to be 291 kDa (Figure 3.3F). Unlike BN-PAGE which converts membrane proteins into water-soluble protein upon binding G250 dye (56), these approaches examine the molecular mass of the native Cho1-digitonin-micelle particle. Since it is hard to determine how much digitonin monomers are associated with Cho1, the mass of an empty digitonin micelle (124kDa, (57)) was subtracted from the Cho1-digitonin-micelle particle, and the estimated molecular weight of the Cho1 protein alone from these independent approaches is close to the ~180kDa, as we saw in the native gels, again supporting a hexamer.

For DDM-solubilized fractions, the anti-HA pull-downs in the 0.9%, 1.1%, 1.3%, and 1.5% solubilized particles were subjected to BN-PAGE followed by a 2nd dimensional SDS-PAGE as described above (Figure S3.2). Even though the 168-kDa complex is present at the highest abundance, multiple bands of other molecular weights are also observed on the BN-PAGE. Given that the molecular weight of monomeric Cho1 ranges from 27 to 36 kDa, the various bands are likely to correspond to different oligomeric states of Cho1 because the differences among them are close to the multiples of ~30 kDa, with the hexamer form (168 kDa) being the most abundant. This is also supported by the 2nd dimensional SDS-PAGE, which only shows bands corresponding to Cho1 in the native complexes. However, since different oligomers exist in the DDM-solubilized fraction, digitonin was chosen as the detergent for the solubilization and subsequent purification as it gives a more consistent oligomeric state.

Affinity tag construction and protein purification of *Candida albicans* Cho1

To achieve a large-scale purification, codon-optimized glutathione S-transferase (GST), maltose-binding protein (MBP), and octa-histidine (Hisx8) tags were C-terminally attached to the existing HAx3 tag of Cho1. A Tobacco Etch Virus (TEV) protease recognition site, ENLYFQG, was inserted between the Cho1 protein and the HAx3 tag to permit the removal of the HA epitope & C-terminal affinity tags after purification. All three versions of the tagged Cho1 protein were expressed from the constitutively active *ENO1* promoter in *C. albicans*, and immunoblotting confirmed their expression (Figure 3.4A). To determine the best tag for purification, the enzyme activities of these three different affinity tagged Cho1 proteins were measured by both *in vivo* and *in vitro* assays.

Growth in conditions that require PS synthesis were used as a proxy for *in vivo* activity. Loss of the *CHO1* gene leads to poor growth in general because Cho1 forms PS, which is the first phospholipid in the *de novo* pathway, and is a substrate for synthesizing the essential phospholipid, phosphatidylethanolamine (PE). The *cho1ΔΔ* mutant exhibits perturbed growth in general, but especially in minimal media, which lacks ethanolamine (11, 18). Cell growth can be partially restored by supplementing the media with exogenous ethanolamine, which is consumed in the Kennedy salvage pathway to make PE. Hence, *in vivo* Cho1 activity correlates with cell growth in the minimal media lacking ethanolamine. Therefore, growth curves and spot dilution assays in minimal media were used to measure the growth of strains bearing the three versions of Cho1 (Figure 3.4B-D) to determine how well each functioned in providing the needed phospholipids. A strain lacking Cho1 (*cho1ΔΔ*) served as a negative control, while the HA1 strain was used as a positive control. Cells with the Cho1-GST tag grew similarly to HA1 in all conditions, while Cho1-MBP did not grow similarly to HA1 and was closer to the *cho1ΔΔ* mutant. This suggests that the MBP tag interferes with the Cho1 function in the cell, unlike the GST tag. In contrast, the Hisx8 tagged Cho1 could complement the growth of the *cho1ΔΔ* mutant and unexpectedly even caused the strain to grow slightly faster than the HA1 strain. This was more evident during growth in minimal media without ethanolamine (Figure 3.4B-D), suggesting that the Hisx8 tag may improve the activity of Cho1 compared to the HA tag alone *in vivo*.

To measure the *in vitro* activity of these three new Cho1 constructs, the PS synthase activity assay was performed. Instead of the solubilized fraction, crude membranes were used in the reaction as described in Experimental Procedures. The

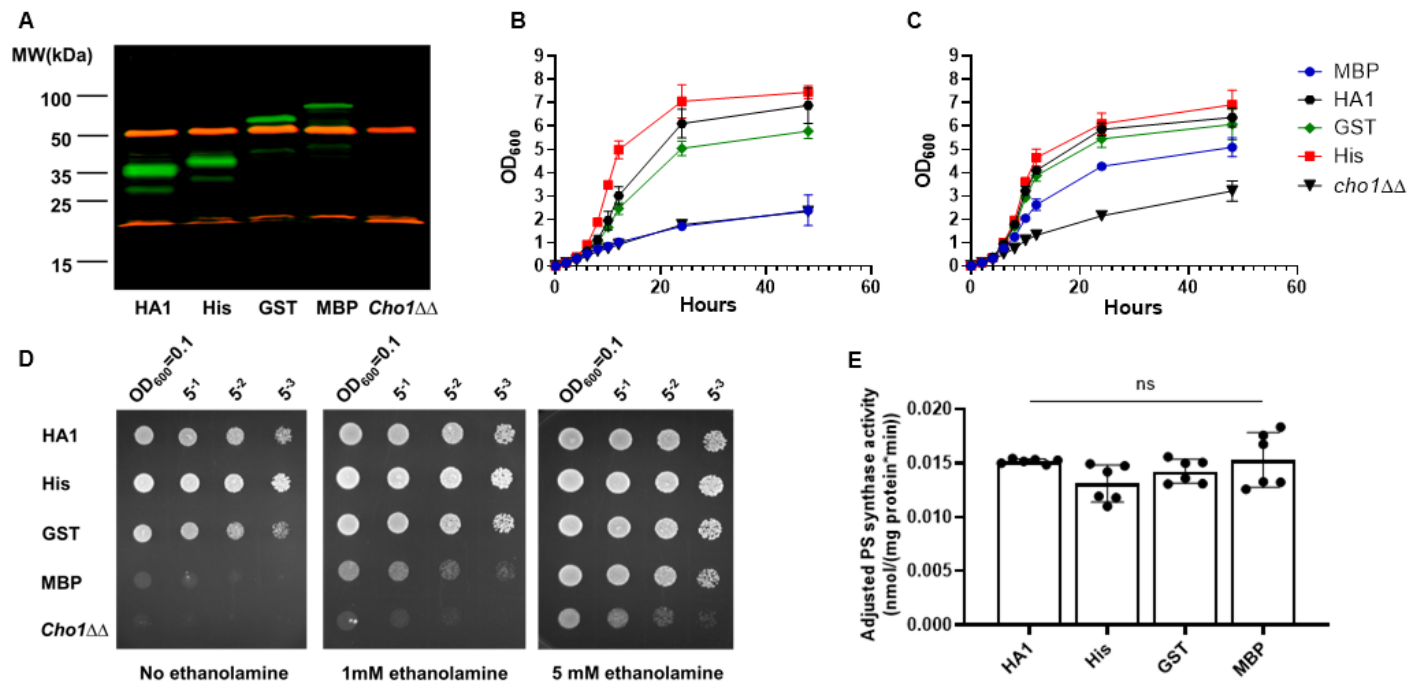


Figure 3.4. His-, GST- and MBP-tagged Cho1 construct express active enzyme. (A) Membranes containing Cho1 protein were extracted from the HA1, *cho1*ΔΔ *P*_{ENO1}-*CHO1*-ENLYFQG-HA_{x3}-His_{x8} (His_{x8}-tagged Cho1), *cho1*ΔΔ *P*_{ENO1}-*CHO1*-ENLYFQG-HA_{x3}-GST (GST-tagged Cho1), *cho1*ΔΔ *P*_{ENO1}-*CHO1*-ENLYFQG-HA_{x3}-MBP (MBP-tagged Cho1), and *cho1*ΔΔ negative control strains, fractionated by SDS-PAGE and Western blotted with anti-HA (green) and anti-tubulin (red) antibodies. Different bands corresponding to Cho1 appear at their expected MW. (B-D) *In vivo* activities of Cho1 with different tags were assessed via growth curves in the absence (B) and presence (C) of 1mM ethanolamine, and (D) corresponding spot dilution assays on agar plates. (E) Adjusted PS synthase activities (nmol/(mg protein*min)) of the crude membrane fractions from different Cho1 strains were measured. Statistics were conducted using one-way ANOVA and Dunnett's T3 multiple comparisons test (ns=not significant, $p > 0.05$). The activities were measured in duplicate with a total of six biological replicates as indicated. The bars represent the mean and the error bars are \pm S.D. values.

adjusted PS synthase activity (nmol/ (mg protein*min)) was then calculated from the PS synthase activity normalized to Cho1 expression via Western blotting, which reflects the intrinsic enzymatic activity of Cho1 with different tags. Contrary to the *in vivo* growth assay results, there is no significant difference in the adjusted PS synthase activities among these different versions of Cho1 (Figure 3.4E). The full explanation for why there was not a clear correlation between growth and *in vitro* activity for the different Cho1 constructs is unknown. However, the low *in vivo* activity of MBP-tagged Cho1 protein could be due to decreased expression, as supported by the Western blotting results (Figure 3.4A). The reasons for the difference between Cho1-His and Cho1-GST are unknown, but the better growth of the Cho1-His strain suggested it would be better for large-scale purification.

In addition, Hisx8-tagged Cho1 was optimal due to its more specific binding/elution conditions, and a large-scale pilot purification was conducted using chromatography with cobalt resin, as described in Experimental Procedures. Initially, the elution fraction contained several bands on the BN-PAGE, and only one corresponded to Cho1 (Figure S3.3). TEV protease was used to treat the concentrated elution overnight to clear the elution further and cleave the affinity tag. The resulting mixture was passed over fresh cobalt beads to remove non-specifically bound protein and cleaved tags. Figure 3.5A lane 2 shows a single 185-kDa protein band on the BN-PAGE after the second affinity chromatography, indicating high purity of the tag-free native Cho1 complex. This complex separated into 30kDa and 23kDa bands on the 2nd dimensional SDS-PAGE (Figure 3.5B), consistent with Figure 3.3 and the previous findings that *Saccharomyces cerevisiae* PS synthase separates into 30kDa and 23kDa bands on SDS-PAGE (16, 55).

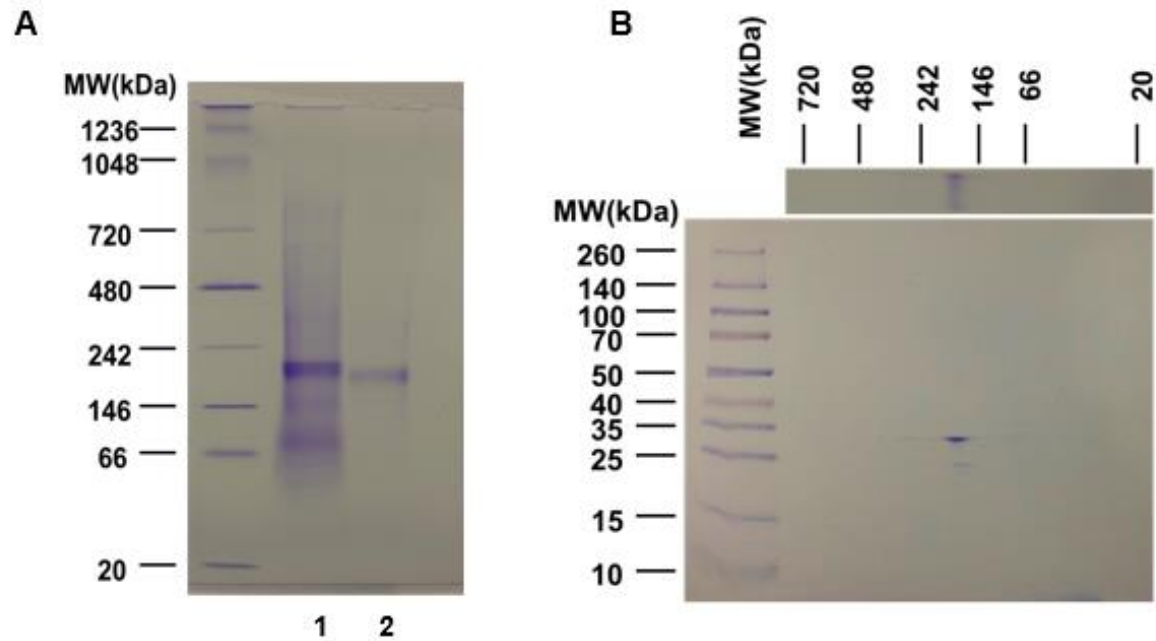


Figure 3.5. Tag-free hexameric Cho1 was purified to homogeneity using affinity chromatography and AcTEV treatment.

(A) BN-PAGE gel of the purified hexameric Hisx8-tagged Cho1 protein prior to tag removal (lane 1), and after AcTEV treatment and second purification for the tag-free version (lane 2). (B) Second dimensional SDS-PAGE of lane 2 from the BN-PAGE in (A) shows bands corresponding to Cho1 based on MW. All gels were stained with Coomassie blue R250 dye.

passed over fresh cobalt beads to remove non-specifically bound protein and cleaved tags. Figure 3.5A lane 2 shows a single 185-kDa protein band on the BN-PAGE after the second affinity chromatography, indicating high purity of the tag-free native Cho1 complex. This complex separated into 30kDa and 23kDa bands on the 2nd dimensional SDS-PAGE (Figure 3.5B), consistent with Figure 3.3 and the previous findings that *Saccharomyces cerevisiae* PS synthase separates into 30kDa and 23kDa bands on SDS-PAGE (16, 55).

Enzymology properties and kinetics of *Candida albicans* Cho1

The enzymological properties of the purified Cho1 complex were then tested, and the specific activities were measured in different conditions. The optimal temperature of the Cho1 complex appeared to be 24°C, although this was not significantly different than activity at 30°C or 20°C (Figure 3.6A). This is surprising since *C. albicans* is a human fungal pathogen and lives in an environment of 37°C. The optimal manganese cofactor concentration was between 0.5-1.0 mM and decreased above 1.0 mM, and the pH optimum is around 8.0 (Figure 3.6B&C). These enzymological properties of *C. albicans* Cho1 are consistent with those of the *S. cerevisiae* Cho1 homolog previously reported (44). For detergents used in the reaction, Triton X-100 was shown previously to stimulate the activity of *Saccharomyces cerevisiae* Cho1, and the Triton X-100-CDP-diacylglycerol micelle also serves as a substrate in this reaction (44, 58). *C. albicans* Cho1 activity was tested in different detergent concentrations. Even if the molar concentration of CDP-DAG was unchanged, the addition of detergents to the reaction dilutes the surface concentration of CDP-DAG in a mixed micelle (59), so the mole fraction (mol %) of CDP-DAG was also calculated (Figure 3.6D&E, blue triangles). By

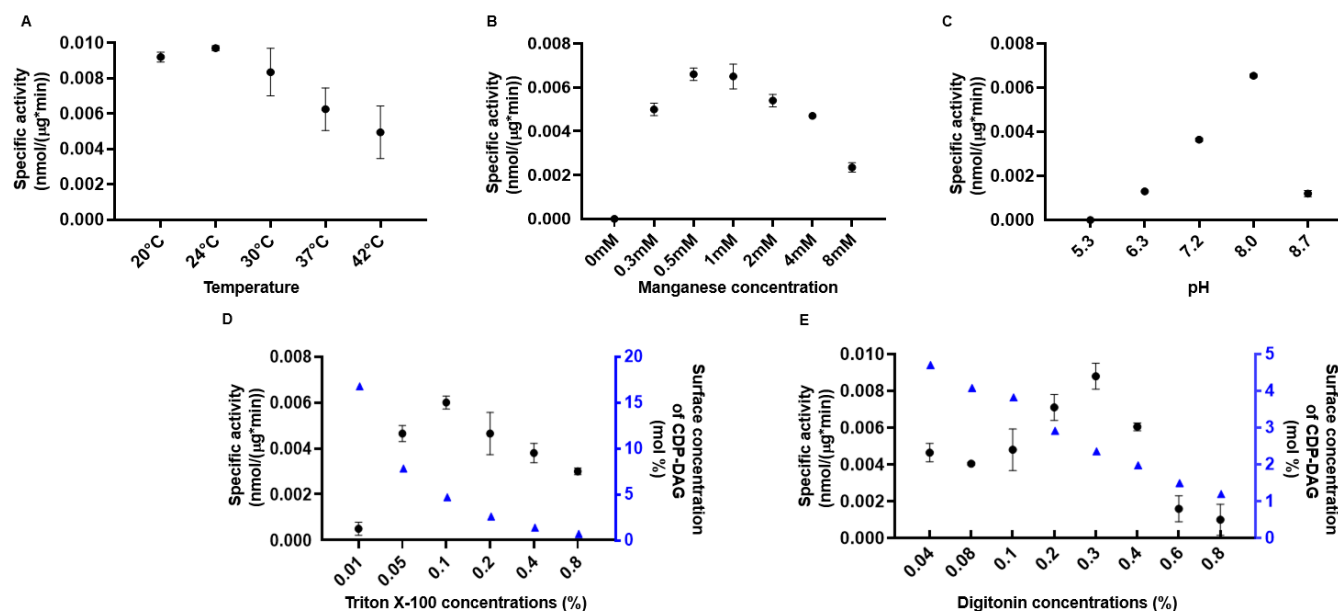


Figure 3.6. Effects of temperature, manganese concentration, pH and detergents on purified hexameric Cho1 enzyme activity. (A) Temperature, (B) manganese concentrations, (C) pH, (D) Triton X-100 concentrations, and (E) digitonin concentrations were varied as indicated, and specific activities (black filled circle, nmol/(µg*min)) of purified Cho1 under each condition were measured as described in the Experimental Procedures. The surface concentrations of CDP-DAG (blue filled triangle) in mixed micelles (mol %) were also calculated and shown in (D) and (E). The specific activities were measured in two biological replicates, and data points are shown as the mean ± S.D. values.

varying the Triton X-100 concentration from 0.01% to 0.8%, we identified the optimal Triton X-100 concentration as 0.1%, and the Cho1 activity decreases at higher concentrations probably due to the drop in CDP-DAG surface concentration (Figure 3.6D). Besides Triton X-100, digitonin was used as the solubilization detergent, which is also involved in the reaction. Surprisingly, when different concentrations were tested in the reaction, digitonin was found to stimulate the activity of Cho1, even with the decrease in the surface concentrations of CDP-DAG, with the greatest efficiency observed at 0.3% (Figure 3.6E).

In addition, the kinetics of the purified Cho1 complex were measured. For determining the K_m and V_{max} of CDP-DAG, serine was kept constant at 19 mM, and the specific activities of Cho1 were measured at CDP-DAG concentrations of 25, 75, 100, 150, 200, 250, 300, and 400 μM with a surface concentration between 4.5-5.3 mol % (Figure 3.7A). The K_m for CDP-DAG was estimated at $72.20 \pm 15.82 \mu\text{M}$, while the V_{max} was found to be $0.079 \pm 0.006 \text{ nmol}/(\mu\text{g}\cdot\text{min})$. This K_m is very close to that of the partially purified *S. cerevisiae* PS synthase, which is 60 μM (44). For serine, the CDP-DAG concentration was fixed at 300 μM , and the serine concentration was varied between 0.25 and 15 mM, and the specific activities were measured and plotted against the serine concentrations. This kinetic curve fits better into a sigmoidal curve, indicating some cooperativity in serine binding (Figure 3.7B). The Hill slope for cooperativity was estimated to be 1.83 ± 0.22 and the V_{max} to be $0.088 \pm 0.007 \text{ nmol}/(\mu\text{g}\cdot\text{min})$. The K_{half} , which represents the substrate concentration when the enzyme reaches half of the V_{max} in

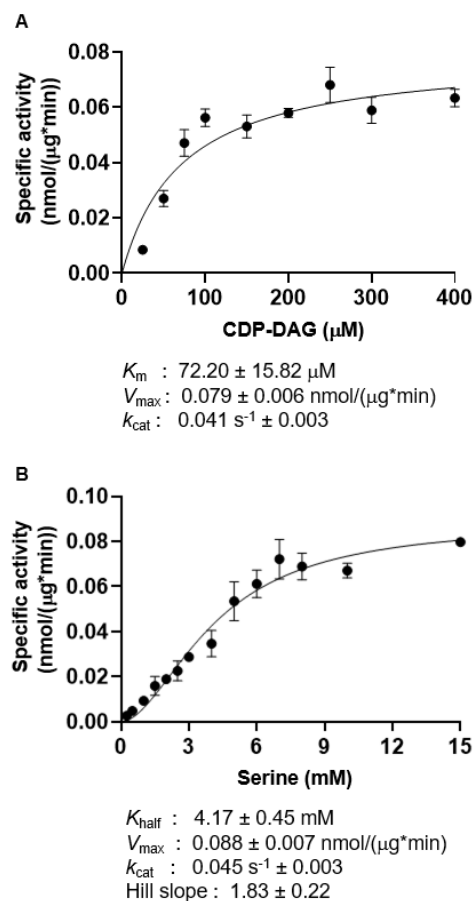


Figure 3.7. Kinetic curves suggest a cooperative serine binding in the purified hexameric Cho1. (A) Kinetics curve for CDP-DAG. Serine was kept constant at 19 mM, and the specific activities of purified hexameric Cho1 were plotted against various CDP-DAG concentrations (surface concentration 4.5-5.3 mol %). (B) Kinetics curve for serine. CDP-DAG was kept at 300 μM (surface concentration 5 mol%), and the specific activities of purified hexameric Cho1 were plotted against various serine concentrations. The specific activities were measured in three biological replicates, and data points are shown as the mean \pm S.D. values.

the allosteric sigmoidal substrate-velocity curve, was estimated to be 4.17 ± 0.45 mM. In both cases, the k_{cat} is estimated between 0.041-0.045 s^{-1} .

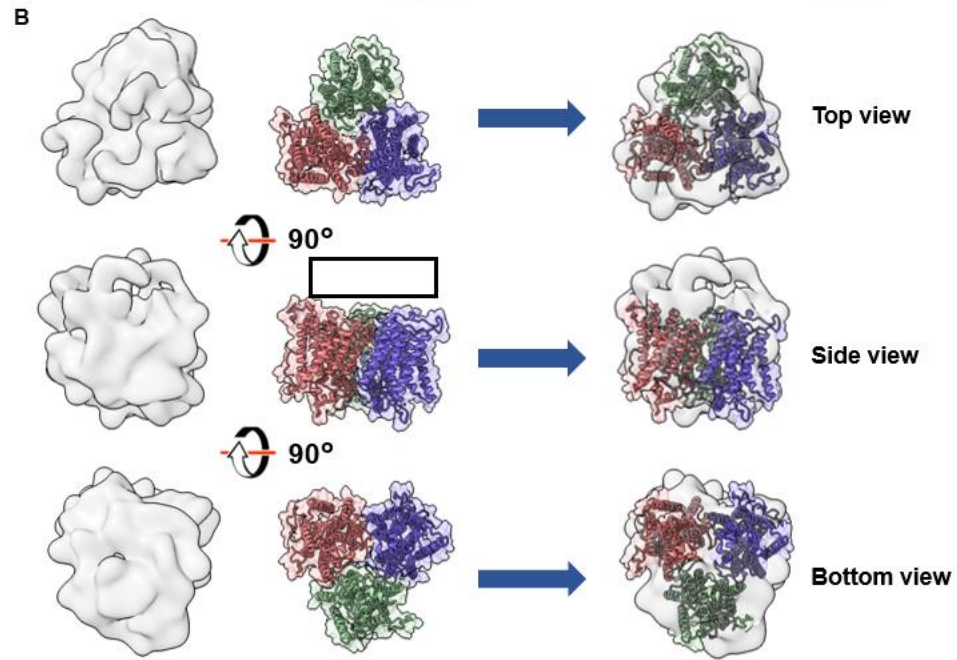
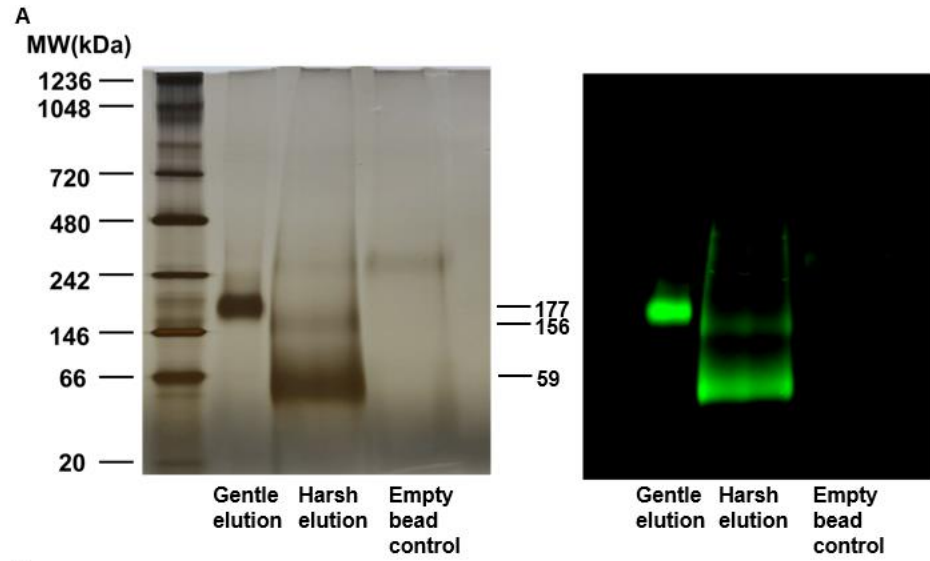
***Candida albicans* Cho1 is very likely to be a trimer of dimers**

To date, all of the experimentally reported structures of membrane-bound CDP-alcohol utilizing phospholipid synthases are dimers (22-27). In contrast, data from the BN-PAGE, as well as other MW estimation techniques (Figure 3.3), suggest that Cho1 is found in a larger complex. When further examined by SDS-PAGE, the high-molecular-weight Cho1 contains only bands corresponding to Cho1 (Figure 3.3A-C, Figure 3.5), so this complex represents a higher oligomeric state of Cho1, and the molecular weight suggests a hexamer (185 kDa as a complex and 30 kDa as a monomer). However, the organization of this hexamer was unclear.

To test whether the higher oligomer of Cho1 can be broken into smaller oligomers, anti-HA beads were used to pull down the Cho1 complex. This was eluted by either using excess HA peptide or 50 mM NaOH followed by 1M Tris-HCl (pH=8.5). HA peptide exchange is a gentle way to elute proteins from anti-HA beads. In contrast, NaOH plus Tris-HCl is a harsh way that also disrupts loose protein associations. The pull-down products from two elution methods and a control group in which the anti-HA beads have no bound proteins and are eluted with NaOH were assessed on the BN-PAGE and a subsequent immunoblot. The gentle elution results in a higher protein oligomer (Figure 3.8A), but the harsh elution leads to two bands on the BN-PAGE, one at 59 kDa and the other at 156 kDa. These bands both correspond with Cho1 protein, as evidenced by immunoblotting (Figure 3.8A). Since the MW of monomeric HAX3-Cho1 is 36 kDa, the 59 kDa band is likely a dimeric form of Cho1, while the 156 kDa bands represent a

Figure 3.8. Hexameric Cho1 is likely made of a trimer of dimers.

(A) BN-PAGE gel (left) and a subsequent Western blot of the same gel (right) are shown for Cho1 that was eluted from HA protein purification resin with either synthetic HA peptide (gentle elution) or NaOH followed by 1M TrisHCl pH=8.5 (harsh elution). A protein-free resin control was eluted using the harsh elution. MW of different bands (kDa) were estimated from the protein ladder and indicated. (B) The *ab-initio* 3D density map of pulled-down Cho1 built from negative staining electron microscopy (left lane) fits well with the predicted trimer of Cho1 dimers (middle lane) in three different views. A black box indicates the region of the deleted fifty amino acid residues from the N-terminus of Cho1.



trimer of dimers. These results strongly support the native oligomer as a hexamer composed of a trimer of more stable dimers.

To gain insights into the shape of the hexameric Cho1 complex, negative staining electron microscopy and single-particle image analysis was performed on the Cho1 complex following the pull-down. It is well known that detergent micelles present in the sample can produce background noise in the negative staining micrographs and significantly distort the interpretation of small membrane proteins (60). However, the digitonin micelle with an apparent mass of 124 kDa (57) is smaller than the Cho1-digitonin micelle complex (~300 kDa, Figure 3.3), so the larger particles were intentionally collected for analysis. A total of 564,320 particles were picked and 2D classified, resulting in a 2D class average (Figure S3.4A&B). The best particles, chosen by size and signal, led to five 3D density maps built as described in the Experimental Procedures (Table S3.1, Figure S3.4C). Among the five, density map iv has evident contours and reveals discrete features, and thus was selected for analysis (Figure 3.8B, left lane). In the meantime, a dimeric form of the Cho1 structure was predicted using AlphaFold2 software (Figure S3.5A). The predicted structure's N-terminal 50 amino acid residues were deleted due to their intrinsically disordered nature and low prediction confidence score (Figure S3.5B).

A predicted trimer of the dimeric Cho1 complexes was simulated by the HSYMDOCK docking web server (Figure 3.8B, middle lane) (61). It was then fitted with the 3D density map generated from the negative staining electron microscopy (Figure 3.8B, right lane). As shown, the 3D density map fits well with the predicted trimer of Cho1 dimers in the top and side views, given that the N-terminal region of Cho1 was omitted in the predicted

trimer-of-dimers structure (Figure 3.8B, right lane). The bottom perspective shows additional density in the 3D map absent in the trimer-of-dimers structure, which can be explained by the bound digitonin micelle and residual bound phospholipids. In sum, the 3D density map generated here is believed to represent the overall shape of a trimer of Cho1 dimers in a complex.

Discussion

Here, we have developed and optimized solubilization and purification methods for the membrane-bound Cho1 protein from *C. albicans*. Several detergents were used to solubilize Cho1, and digitonin stands out among them, as the Cho1 protein was purified in a single conformation after being solubilized by digitonin (Figure 3.3A&3.5A). However, it is noticeable that the digitonin-solubilized Cho1 complex has a higher MW than Cho1 solubilized by other detergents (Figure 3.1A, Figure 3.2A&3.2C). It is possible that this difference is due to Cho1 being solubilized in a different conformation or being found within a different lipid-detergent micelle. However, another possibility is that digitonin might conserve the interaction between Cho1 and an unknown protein(s) in the crude solubilization fraction due to the very mild solubilization property of digitonin (49, 62). This is supported by the observation that in digitonin, the solubilized Cho1 complex from the crude fraction has a higher MW than Cho1 from pull-down reactions (216kDa vs. 172 kDa, Figure 3.1A&3.3A). The decrease in MW (~44kDa) during the pull-down process could represent a loss of the unknown protein(s). The interaction(s) between Cho1 and unknown proteins in the crude fraction may not be preserved by other detergents and may be lost even for digitonin during the purification process.

Another advantage of digitonin is that it not only retains but also stimulates the enzymatic activity of Cho1 (Figures 3.2B&3.6E). This is interesting because, unlike Triton X-100, which was used to dissolve the substrate CDP-DAG and was previously shown to provide a surface for catalysis (58), digitonin served to solubilize Cho1 and keep Cho1 in the micelle. In contrast, the synthetic substitute of digitonin, GDN, despite having a similar steroid-based structure as digitonin (63-65), failed to maintain PS synthase activity after solubilization (Figure 3.1B&C). Currently, we do not have an explanation for the stimulant effect of digitonin, and further experiments are required to explain this stimulant effect.

Since *C. albicans* Cho1 uses CDP-DAG as one of the substrates and has the CAPT motif, it belongs to the CDP-alcohol phosphatidyltransferase family (18). So far, six protein members within this family have solved crystal structures, all of which are dimers (22-27). Here, we show for the first time that *C. albicans* Cho1 forms hexamers based on MW from BN-PAGE (Figure 3.3&5). It has previously been shown that the migration of solubilized proteins on BN-PAGE can be affected by the choice of detergent, detergent concentration, and micelle lipid composition, thus skewing the MW estimation (49). To account for this, six different non-ionic detergents, both mild and harsh, were used to solubilize Cho1, which led to protein bands of a similar high MW for Cho1 and suggested hexamers in each case (Figure 3.1A). Also, the concentration of digitonin and DDM were varied from 0.5%-1.5% and 0.5%-2.1%, respectively, which will change the micelle lipid compositions, but only single bands corresponding with hexamers appeared in the BN-PAGE (Figure 3.2A&C). In addition, size-exclusion chromatography, mass photometry and analytical ultracentrifugation have also indicated

the MW of native Cho1 protein alone is 180 kDa (Figure 3.3D-F), once the micelle MW is subtracted. These results taken altogether suggest that Cho1 forms hexamers.

Furthermore, a harsh elution of Cho1 from the anti-HA beads with NaOH and 1M Tris-HCl indicated that the hexamer species is made of Cho1 dimers (Figure 3.8A). Thus, we have concluded that Cho1 forms a trimer-of-dimers in the native environment (Figure 3.8). The SMALP 2000 solubilization fraction further supports this, producing both a hexamer and a dimer based on the MW (Figure 3.2E). Since SMALP 2000 solubilizes proteins in the native environment, this points to the existence of both Cho1 hexamers and dimers in the native membrane, with the hexamer being more abundant. We have further shown the likely presence of a simulated trimer of Cho1 dimers in the sample via negative staining electron microscopy (Figure 3.8B and Fig S3.4). Together, those results suggest that *C. albicans* Cho1 forms hexamers and is highly likely a trimer-of-dimers. The explanations for the oligomer state discrepancy between *C. albicans* Cho1 and structures of other CDP-alcohol phosphatidyltransferases include: (i) the loose association between three Cho1 dimers may be broken during the crystallization process, or (ii) the eukaryotic *C. albicans* Cho1 has evolved a higher oligomer state compared to the six solved prokaryotic counterparts.

Finally, a surprising finding is the sigmoidal velocity-substrate concentration curve for serine, indicating that Cho1 cooperatively binds serine. Both high and low K_m values have been reported previously for both crude and purified *S. cerevisiae* PS synthase (42, 44, 66, 67), and Kiyono et al. observed a serine K_m of 0.14 mM at low L-serine concentrations and 9.5 mM at high L-serine concentrations in both microsomal and partially purified *S. cerevisiae* PS synthase (17). All those results together suggest

potential cooperativity in the serine-binding of PS synthase. We do not know whether cooperativity occurs within one protomer or between protomers. Interestingly, two serine-binding pockets were identified in the PS synthase structure of *Methanocaldococcus jannaschii* (Figure S3.6). Still, the authors later considered one serine-binding pocket (Figure S3.6, serine 1) an experimental artifact due to the less optimal position for reaction (23). However, binding the less optimal serine likely facilitates binding the optimal serine for catalysis. Thus, the cooperative serine binding is present within one protomer. However, since *M. jannaschii* PS synthase is the first and only PS synthase with a solved structure, and due to the distant phylogenetic relationship between *M. jannaschii* and *C. albicans*, there is limited information available and a solved *C. albicans* Cho1 structure will give insight into this question. Here, we have developed the solubilization and purification methods for hexameric *C. albicans* Cho1, which can be used for small molecule screening or structure determination.

Experimental Procedures

Strain construction and media

This study used the HA1 *Candida albicans* strain to solubilize Cho1. This strain was previously created and expressed a HAx3-tagged Cho1 protein from a strong constitutive promoter, as described in (18). The yeast strains constructed in this study are also listed in Table 3.1. Media used in this study include YPD (1% yeast extract, 2% peptone, 2% dextrose) and minimal medium (0.67% yeast nitrogen base, 2% dextrose \pm 1 mM ethanolamine).

Table 3.1. Strains used and produced in this study

Organism	Strain	Plasmid	Genotype
<i>Candida albicans</i>	HA1	pCDC4	<i>cho1ΔΔ_{PENO1}-CHO1-HAx3</i>
<i>Candida albicans</i>	YZ81	pYZ79	<i>cho1ΔΔ_{PENO1}-CHO1-ENLYFQG-HAx3-Hisx8</i>
<i>Candida albicans</i>	YZ88	pYZ84	<i>cho1ΔΔ_{PENO1}-CHO1-ENLYFQG-HAx3-GST</i>
<i>Candida albicans</i>	YZ89	pYZ85	<i>cho1ΔΔ_{PENO1}-CHO1-ENLYFQG-HAx3-MBP</i>

To create new constructs, site-directed mutagenesis was performed on the plasmid pCDC4 (18), harboring gene *CHO1-HAx3*, to generate a TEV protease recognition site (ENLYFQG) between the *CHO1* and *HAx3* gene using a primer-based method (Table 3.2, YZO 67&68). The *CHO1-ENLYFQG-HAx3* gene was PCR-amplified with a forward primer (YZO 64) and a reverse primer (YOZ 66) that added a Hisx8 tag at the end of the existing HAx3 tag. The following amplification product was then cloned into the plasmid pBT1, which contains the constitutive *ENO1* promoter (P_{ENO1}) and the *SAT1* marker (68), to create the plasmid pYZ79. *Candida albicans* codon-optimized glutathione S-transferase (GST) and maltose-binding protein (MBP) genes purchased from Genscript were fused to the *CHO1-ENLYFQG-HAx3* gene by replacing the existing Hisx8 tag in pYZ79 via amplification by PCR with the appropriate primers (Table 3.2) to create plasmids pYZ84 and pYZ85, respectively. Plasmids pYZ79, pYZ84, and pYZ85 were linearized with *MscI* restriction enzyme (within the P_{ENO1} sequence) and then were electroporated into the *cho1ΔΔ* *Candida albicans* strain (11). The transformants were selected on the YPD plates containing 100 μg/ml nourseothricin. Colony PCR was performed on six candidates for each gene construct to ensure the successful integration under the P_{ENO1} promoter on the chromosomal DNA, and no spurious mutations occurred during the transformation.

Spot dilution assay and growth curves

Spot dilution assays and growth curves were conducted as described in (18).

Table 3.2. Primers used in this study

Primer name	Sequence	Function/Mutation
YZO 67	atctcaaaatctttaaattcctaaccagcggccgtgaaaattttatttca aggttcatacccatcacgatgttctctgactat	Adding TEV protease recognition site (ENLYFQG)
YZO 68	ggatcctgcatagtcgggacgtcatagggatagccggcatagtcagga acatcgtatgggtatgaaccttgaataataaatttcaac	Adding TEV protease recognition site (ENLYFQG)
YZO 64	aaaagcggccgcatgtcagactcatcagctaccgggttctccaagcacc aagagtcagcaattgtatcagattcagaaggag	Adding Hisx8 tag to the existing HA tag
YZO 66	aaagagctcctatccaccgtgatggtgatggtgatggcggcc ggagcgtaatctggaacgtcatatggataggatcctgcatagtcgggac g	Adding Hisx8 tag to the existing HA tag
YZO 69	tatccctatgacgtcccggactatgcaggatcctatccatgacgttccag attacgtcggccgcttatgtccctatactaggttattgg	Replacing the existing Hisx8 tag with a GST tag
YZO 70	tttgagctcctatccacctttggaggatggtgccaccacca	Replacing the existing Hisx8 tag with a GST tag
YZO 71	tatccctatgacgtcccggactatgcaggatcctatccatag	Replacing the existing Hisx8 tag with an MBP tag
YZO 72	tttgagctcctatccaccttctcgttcagctttttgta	Replacing the existing Hisx8 tag with an MBP tag

PS synthase assay

The PS synthase assay was used to measure the enzymatic activity of the Cho1 protein. Cells were lysed as previously described to isolate membranes containing PS synthase using a French press (45). Then the crude membranes were collected by centrifugation at 3,000 x g to remove intact cells. The remaining supernatant was centrifuged at 27,000 x g for 30 min to pellet the cellular membranes. The reaction was then set up as described in (18), with the adjustment of 30°C as the reaction temperature. Briefly, PS synthase activity was measured by counting the total radioactivity of L-[³H]-serine in the chloroform phase (phosphatidylserine), normalized to the protein amount (0.5 mg crude membrane protein) as measured by the Bio-Rad protein assay and dividing it by the reaction time (30 min). The reagents were added to final concentrations of 50 mM Tris-HCl (pH=8.0), 1mM MnCl₂, 0.1% Triton X-100, 0.1 mM CDP-DAG, 0.5 mM L-serine (spiked with 5% (by volume) L-[³H]-serine (30 Ci/mmol)), 5% glycerol and 1mM BME, at a total volume of 100 μL. For the solubilized fractions, 50 μL volume was used in each reaction, and the protein concentration of each solubilized fraction was measured using the Pierce™ detergent compatible Bradford assay kit. To calculate the adjusted PS synthase activity, PS synthase activity was normalized to the relative densitometry values of the Cho1 bands from each sample run on a Western blot as described in (18) and expressed as nmol/(μg protein*min). The specific activity was measured using the same conditions (unless otherwise indicated) with 1-2 μg purified Cho1 protein. Specific activity was calculated based on the slope of linear PS production, from at least three time points, within 30 min, representing the initial velocity.

Western blot

Western blots of the Cho1 protein fractionated on SDS-PAGE gels were conducted as described in (18). PVDF membranes were used for BN-PAGE gels, and the wet transfer was done in 1X NuPAGE™ Transfer buffer at 25 V and 4° C for 1 hour. The subsequent membrane was de-stained in 100% methanol before blotting. The blotting procedure is the same as the SDS-PAGE membrane described in (18).

Cell lysis, solubilization, and purification

Candida albicans strains were grown in YPD to OD₆₀₀ between 6.5-8.0 for solubilization and purification. The cells were centrifuged and lysed, as previously described (45). Cell lysates used for large-scale purification were supplemented with 10 µg/mL leupeptin, pepstatin A, and 10 mM PMSF. The crude membranes were clarified by centrifugation at 3,000 x g for 10 min to remove unbroken cells. Then the supernatant was recentrifuged at 100,000 x g for 60 min to pellet the cellular membranes. The crude membranes were resuspended in 50 mM Tris-HCl (pH=8.0), 2 mM MnCl₂, 30 mM MgCl₂, 10 mM KCl, 10% glycerol, and 2 mM BME to a final protein concentration of 10 mg/mL as measured by Bio-Rad, protein assay dye before solubilization by detergents. For SMA solubilization, the crude membrane was resuspended in a modified buffer: 50 mM Tris-HCl (pH=8.8), 125 mM KCl, 10% glycerol, and 10 mM BME. Detergents or SMAs (Cray Valley) were dissolved in H₂O and added to the crude membrane prepared to the final concentration indicated. The solubilization was carried out at 4° C (for detergents) or 37° C (for SMAs) for 60 min or the time otherwise indicated, which was then cleared through centrifugation at 100,000 x g for at least 30 min. The subsequent supernatant was considered the solubilized fraction.

Protein pull-downs were performed with Pierce™ anti-HA magnetic beads. Following solubilization, 50 µL of anti-HA magnetic beads were applied to the solubilization fraction and gently mixed for 30 min at room temperature. The beads were washed twice with 500 µL TBS + 0.1% digitonin, followed by a final wash of H₂O + 0.05% digitonin. The bound protein was eluted using a solution of 2 mg/mL HA synthetic peptide (Thermo Scientific™) + 0.05% digitonin for gentle elution. For harsh elution, 100 µL of 50 mM NaOH + 0.05% digitonin buffer was used, followed by adding 50 µL 1M Tris, pH 8.5 + 0.05% digitonin.

Protein column purification was performed using HisPur™ cobalt resin (Thermo Scientific™). Briefly, HisPur™ Cobalt Resin was prepacked on the chromatography column and washed with 10 bead-bed volumes of washing solution (50 mM Tris-HCl (pH=7.0), 15mM imidazole and 0.1% digitonin). Solubilized fractions, from 1% digitonin or other indicated conditions, were gently loaded and run through the pre-washed beads via gravity. The flow-through fraction was again loaded on the column twice for maximum binding. Then at least 6 column volumes of washing solution were used to wash out non-specifically bound proteins. Elution was performed using 6x column volumes of the elution buffer (50 mM Tris-HCl (pH=8.0), 150 mM imidazole, and 0.05% digitonin or other detergents). The elution fraction was concentrated to 500 µL and exchanged with 4 mL dilution buffer (50 mM Tris-HCl (pH=8.0), 0.1% digitonin) in the Pierce™ Protein Concentrator PES (10K MWCO, 5-20 mL) twice, and again concentrated to ~500 µL final volume. The protein concentration of the final buffer-exchanged sample was measured using the Pierce™ detergent compatible Bradford assay

kit. To cleave the His-tag, AcTEV™ protease (Invitrogen™) was applied at the ratio of 1 μL: 30 μg protein of the buffer-exchanged sample in the presence of 2 mM DTT. The cleavage reaction was carried out overnight at 4° C. Following cleavage, the sample was applied to fresh pre-washed HisPur™ cobalt resin to remove any non-specifically bound protein, free His-tags, and the uncleaved Cho1 protein. The final protein concentration was measured using the Pierce™ detergent compatible Bradford assay kit, and the cleaved protein was used for specific activity determination.

Blue native (BN)-PAGE and 2nd dimensional SDS-PAGE

The NativePAGE™ system was used for the BN-PAGE. 0.5%-1% NativePAGE™ G-250 sample additive, 1X NativePAGE™ Sample Buffer, and 2 μg solubilized protein (2 μL for SMA-solubilized fractions and 14 μL for purified protein) were mixed and loaded on the NativePAGE™ 4 to 16%, Bis-Tris gel. NativeMark™ unstained protein standard (Invitrogen™) was used as the protein ladder for MW estimation. The gel was run at 4° C with pre-chilled buffers, with NativePAGE™ dark blue cathode buffer at 70 V for 50 min and NativePAGE™ light blue cathode buffer at 150 V till the dye reached the gel front. The gels were then analyzed by Western blot (as mentioned above), Coomassie Blue R250 staining, or silver staining.

The 2nd dimensional SDS-PAGE was performed using the Novex™ system. Briefly, the gel strip was cut from the 1st dimension NativePAGE™ gel and equilibrated in the 1X NuPAGE® LDS sample buffer with 50 mM DTT for at least 30 min. The gel strip was then transferred to an alkylating solution containing 1X NuPAGE® LDS Sample Buffer with 50 mM N,N-Dimethylacrylamide (DMA), rocking for 30 min. The gel strip was then transferred to the quenching solution with 1X NuPAGE® LDS Sample

Buffer with 5 mM DTT and 20% ethanol. Then, the prepared gel strip was mounted to the 2D well of Tris-Glycine Novex™ 4 to 20% mini protein gel and run at 110V till the dye reached the gel front. For analysis, the resulting 2D gel was subjected to Coomassie Blue R-250 or silver staining.

Size-exclusion chromatography

Pull-downed Cho1 was subjected to size-exclusion chromatography. All buffers and samples were filter through 0.22 µm filters. A Superdex 200 10/300 GL column (Cytiva) was attached to an NGC chromatography system Quest 10 plus (Bio-Rad) for the analysis. To equilibrate the column, 1.5 column volumes of water followed by 1.5 column volumes of elution buffer (50 mM Tris-HCl (pH=8.0) + 0.04% digitonin) were run through the column at a flow rate of 0.5 mL/min. The pull-downed Cho1 sample or gel filtration standards (Bio-Rad, #1511901) were then manually injected in the sample loop. The elution buffer was used to elute the injected sample at a flow rate of 0.4 mL/min. Fraction collection was enable from 0.16-1 column volumes and each fraction had 0.3 mL. Fractions with peaks revealed by the A280 detection were analyzed by SDS-PAGE and immunoblotting.

Sedimentation Velocity Analytical Ultracentrifugation

Sedimentation velocity experiments were carried out in a Beckman XL-I analytical ultracentrifuge using an An-60Ti rotor. Sample volumes of 400 µL were loaded into charcoal-filled Epon double-sector cells with a 12 mm pathlength. Samples were equilibrated for 1 h at 20 °C prior to the run. Other experimental conditions included a rotor speed of 50,000 rpm and a temperature of 20 °C. Sedimentation was monitored using the interference optical system scanning every two minutes. Data were

fit to a continuous [c(s)] distribution model using SEDFIT (version 16.1c) (69). The protein partial specific volume, buffer density, and buffer viscosity were calculated using SEDNTERP (version 3.0.4) (70).

Mass Photometer

Mass photometry experiments were performed on a Refeyn One^{MP} using the pull-downed Cho1 in the 50 mM Tris-HCl (pH=8.0) + 0.05% digitonin buffer. Each experiment consisted of 6,000 frames collected over 60 seconds. Data analysis was carried out using DiscoverMP (version 2.5.0, Refeyn). Mass photometry contrast was converted to mass values using a standard curve generated using BSA (monomer), BSA (dimer) and thyroglobulin (dimer).

Electron microscopy

First, 5 μ L of the pulled-down sample with a total protein concentration of 0.03 mg/mL was applied to the glow-discharged (PELCO easyGlowTM, 15 mA, 25 s) Quantifoil 100 Carbon Support Films grid: Cu 300 and left on the grid for 45s (Table S3.1). The excess sample was removed by blotting. Then, 5 μ l of 2% uranyl acetate was applied to the grid and was rapidly removed by blotting after 30 s. Next, the washing step included the application of 5 μ l 2% uranyl acetate on the grid and removed immediately. After drying out, the grids were loaded in the 200 kV Thermo Scientific Glacios using an autoloader under cryo-EM conditions.

Electron microscopy data acquisition

Image acquisition was performed on the 200 kV Thermo Scientific Glacios in bright field imaging mode. Movies were recorded using a Thermo Scientific Falcon 3EC

Direct electron Detector in linear mode at a nominal magnification of 92,000, corresponding to a pixel size of 1.567 Å/pix with 8 frames at a dose of 30 e-/Å² per frame and an exposure time of 30 s per movie (Table S3.1).

Image processing

The dataset of Cho1 protein images was derived from 4,946 movies. The raw movie files were imported into SCIPION 3.0 (71) for the following processing steps. The movies were motion corrected using the MotionCor2-1.4.7 protocol (72), and the CTF estimation was done by the Gctf -1.06 protocol (73). A total of 574,190 particles were extracted after manual/auto Xmipp particle picking. After multiple rounds of 2D classification using the cryoSPARC v.3.2 protocol (74), the main protein complex with apparent features was sorted. The particles for the defined 2D classes were subjected to the cryoSPARC v.3.2 *ab initio* protocol with five categories. Then, the 3D Heterogeneous refinement using 5 *ab initio* 3D maps obtained at the previous step was followed using cryoSPARC v.3.2. The best-resulting 3D class containing 54,899 particles was subjected to a 3D non-uniform refinement (74). As a result, a final 3D map was obtained. The resulting 3D map underwent rigid fitting using a structure from AlphaFold2 prediction software (75) in ChimeraX (76).

Statistical analysis and molecular weight (MW) estimation on the gels

All the statistical analyses were performed with GraphPad Prism 9.1 software. The PS synthase activities were compared using Brown-Forsythe and Welch ANOVA tests (unequal SDs). All MW estimates were conducted in the band analysis tool of the Quantity One software (Bio-Rad).

Acknowledgments

The authors would like to thank Dr. Andrew Wagner and Elise Phillips for their help with primer design and making media. This work was funded in part by NIH grant R01AI153599 (TBR). For TEM usage, the authors are grateful for funding from the Federal Ministry for Education and Research (BMBF, ZIK program) (03Z22HN23, 03Z22HI2 and 03COV04), the European Regional Development Funds (EFRE) for Saxony-Anhalt (ZS/2016/04/78115), the Deutsche Forschungsgemeinschaft (DFG) (391498659, RTG 2467) and the Martin-Luther University of Halle-Wittenberg.

References

1. Kullberg, B., Filler, S., and Calderone, R. (2002) *Candida and candidiasis* ASM Press, Washington, DC
2. Brown, G. D., Denning, D. W., Gow, N. A., Levitz, S. M., Netea, M. G., and White, T. C. (2012) Hidden killers: human fungal infections *Science translational medicine* 4, 165rv113 10.1126/scitranslmed.3004404
3. Cassone, A., and Cauda, R. (2012) *Candida* and candidiasis in HIV-infected patients: where commensalism, opportunistic behavior and frank pathogenicity lose their borders *Aids* 26, 1457-1472
4. Morrell, M., Fraser, V. J., and Kollef, M. H. (2005) Delaying the empiric treatment of *Candida* bloodstream infection until positive blood culture results are obtained: a potential risk factor for hospital mortality *Antimicrobial agents and chemotherapy* 49, 3640-3645
5. Wisplinghoff, H., Bischoff, T., Tallent, S. M., Seifert, H., Wenzel, R. P., and Edmond, M. B. (2004) Nosocomial bloodstream infections in US hospitals: analysis of 24,179 cases from a prospective nationwide surveillance study *Clinical infectious diseases* 39, 309-317
6. Pfaller, M., Neofytos, D., Diekema, D., Azie, N., Meier-Kriesche, H.-U., Quan, S.-P. *et al.* (2012) Epidemiology and outcomes of candidemia in 3648 patients: data from the Prospective Antifungal Therapy (PATH Alliance®) registry, 2004–2008 *Diagnostic microbiology and infectious disease* 74, 323-331
7. Holeman Jr, C. W., and Einstein, H. (1963) The toxic effects of amphotericin B in man *California medicine* 99, 90
8. Ghannoum, M. A., and Rice, L. B. (1999) Antifungal Agents: Mode of Action, Mechanisms of Resistance, and Correlation of These Mechanisms with Bacterial Resistance *Clinical Microbiology Reviews* 12, 501-517 10.1128/cmr.12.4.501
9. Odds, F. C., Brown, A. J., and Gow, N. A. (2003) Antifungal agents: mechanisms of action *Trends in microbiology* 11, 272-279 10.1016/s0966-842x(03)00117-3
10. Whaley, S. G., Berkow, E. L., Rybak, J. M., Nishimoto, A. T., Barker, K. S., and Rogers, P. D. (2016) Azole Antifungal Resistance in *Candida albicans* and Emerging Non-*albicans Candida* Species *Front Microbiol* 7, 2173 10.3389/fmicb.2016.02173
11. Chen, Y. L., Montedonico, A. E., Kauffman, S., Dunlap, J. R., Menn, F. M., and Reynolds, T. B. (2010) Phosphatidylserine synthase and phosphatidylserine decarboxylase are essential for cell wall integrity and virulence in *Candida albicans* *Mol Microbiol* 75, 1112-1132 10.1111/j.1365-2958.2009.07018.x
12. Braun, B. R., van Het Hoog, M., d'Enfert, C., Martchenko, M., Dungan, J., Kuo, A. *et al.* (2005) A human-curated annotation of the *Candida albicans* genome *PLoS Genet* 1, 36-57 10.1371/journal.pgen.0010001
13. Konarzewska, P., Wang, Y., Han, G.-S., Goh, K. J., Gao, Y.-G., Carman, G. M. *et al.* (2019) Phosphatidylserine synthesis is essential for viability of the human fungal pathogen *Cryptococcus neoformans* *The Journal of biological chemistry* 294, 2329-2339 10.1074/jbc.RA118.006738

14. Mandal, S., Moudgil, M. n., and Mandal, S. K. (2009) Rational drug design European Journal of Pharmacology 625, 90-100
<https://doi.org/10.1016/j.ejphar.2009.06.065>
15. Kuchler, K., Daum, G., and Paltauf, F. (1986) Subcellular and submitochondrial localization of phospholipid-synthesizing enzymes in *Saccharomyces cerevisiae* J Bacteriol 165, 901-910
16. Kohlwein, S. D., Kuchler, K., Sperka-Gottlieb, C., Henry, S. A., and Paltauf, F. (1988) Identification of mitochondrial and microsomal phosphatidylserine synthase in *Saccharomyces cerevisiae* as the gene product of the CHO1 structural gene J Bacteriol 170, 3778-3781
17. KIYONO, K., MIURA, K., KUSHIMA, Y., HIKIJI, T., FUKUSHIMA, M., SHIBUYA, I. *et al.* (1987) Primary Structure and Product Characterization of the *Saccharomyces cerevisiae* CHO1 Gene That Encodes Phosphatidylserine Synthase1 The Journal of Biochemistry 102, 1089-1100
[10.1093/oxfordjournals.jbchem.a122147](https://doi.org/10.1093/oxfordjournals.jbchem.a122147)
18. Zhou, Y., Cassilly, C. D., and Reynolds, T. B. (2021) Mapping the Substrate-Binding Sites in the Phosphatidylserine Synthase in *Candida albicans* Frontiers in Cellular and Infection Microbiology 11, 10.3389/fcimb.2021.765266
19. Nikawa, J., Tsukagoshi, Y., Kodaki, T., and Yamashita, S. (1987) Nucleotide sequence and characterization of the yeast PSS gene encoding phosphatidylserine synthase Eur J Biochem 167, 7-12
[10.1111/j.1432-1033.1987.tb13297.x](https://doi.org/10.1111/j.1432-1033.1987.tb13297.x)
20. Hjelmstad, R. H., and Bell, R. M. (1991) sn-1,2-diacylglycerol choline- and ethanolaminephosphotransferases in *Saccharomyces cerevisiae*. Nucleotide sequence of the EPT1 gene and comparison of the CPT1 and EPT1 gene products J Biol Chem 266, 5094-5103
21. Hjelmstad, R. H., and Bell, R. M. (1990) The sn-1,2-diacylglycerol cholinephosphotransferase of *Saccharomyces cerevisiae*. Nucleotide sequence, transcriptional mapping, and gene product analysis of the CPT1 gene J Biol Chem 265, 1755-1764
22. Gräve, K., Bennett, M. D., and Högbom, M. (2019) Structure of *Mycobacterium tuberculosis* phosphatidylinositol phosphate synthase reveals mechanism of substrate binding and metal catalysis Communications Biology 2, 175
[10.1038/s42003-019-0427-1](https://doi.org/10.1038/s42003-019-0427-1)
23. Centola, M., van Pee, K., Betz, H., and Yildiz, Ö. (2021) Crystal structures of phosphatidyl serine synthase PSS reveal the catalytic mechanism of CDP-DAG alcohol O-phosphatidyl transferases Nat Commun 12, 6982
[10.1038/s41467-021-27281-w](https://doi.org/10.1038/s41467-021-27281-w)
24. Nogly, P., Gushchin, I., Remeeva, A., Esteves, A. M., Borges, N., Ma, P. *et al.* (2014) X-ray structure of a CDP-alcohol phosphatidyltransferase membrane enzyme and insights into its catalytic mechanism Nat Commun 5, 4169
[10.1038/ncomms5169](https://doi.org/10.1038/ncomms5169)
25. Sciara, G., Clarke, O. B., Tomasek, D., Kloss, B., Tabuso, S., Byfield, R. *et al.* (2014) Structural basis for catalysis in a CDP-alcohol phosphotransferase Nat Commun 5, 4068
[10.1038/ncomms5068](https://doi.org/10.1038/ncomms5068)

26. Clarke, O. B., Tomasek, D., Jorge, C. D., Dufresne, M. B., Kim, M., Banerjee, S. *et al.* (2015) Structural basis for phosphatidylinositol-phosphate biosynthesis *Nat Commun* 6, 8505 10.1038/ncomms9505
27. Dufresne, M. B., Jorge, C. D., Timóteo, C. G., Petrou, V. I., Ashraf, K. U., Banerjee, S. *et al.* (2020) Structural and Functional Characterization of Phosphatidylinositol-Phosphate Biosynthesis in Mycobacteria *Journal of Molecular Biology*
28. Akdel, M., Pires, D. E. V., Pardo, E. P., Jänes, J., Zalevsky, A. O., Mészáros, B. *et al.* (2022) A structural biology community assessment of AlphaFold2 applications *Nat Struct Mol Biol* 29, 1056-1067 10.1038/s41594-022-00849-w
29. Schauerl, M., and Denny, R. A. (2022) AI-Based Protein Structure Prediction in Drug Discovery: Impacts and Challenges *Journal of Chemical Information and Modeling* 62, 3142-3156 10.1021/acs.jcim.2c00026
30. Jones, D. T., and Thornton, J. M. (2022) The impact of AlphaFold2 one year on *Nat Methods* 19, 15-20 10.1038/s41592-021-01365-3
31. Scardino, V., Di Filippo, J. I., and Cavasotto, C. N. (2023) How good are AlphaFold models for docking-based virtual screening? *iScience* 26, 105920 10.1016/j.isci.2022.105920
32. Cassilly, C. D., Maddox, M. M., Cherian, P. T., Bowling, J. J., Hamann, M. T., Lee, R. E. *et al.* (2016) SB-224289 Antagonizes the Antifungal Mechanism of the Marine Depsipeptide Papuamide A *PLoS One* 11, e0154932 10.1371/journal.pone.0154932
33. Kanfer, J., and Kennedy, E. P. (1964) Metabolism and Function of Bacterial Lipids: II. BIOSYNTHESIS OF PHOSPHOLIPIDS IN *ESCHERICHIA COLI* *Journal of Biological Chemistry* 239, 1720-1726
34. Ohta, A., Waggoner, K., Louie, K., and Dowhan, W. (1981) Cloning of genes involved in membrane lipid synthesis. Effects of amplification of phosphatidylserine synthase in *Escherichia coli* *Journal of Biological Chemistry* 256, 2219-2225
35. Raetz, C., Larson, T., and Dowhan, W. (1977) Gene cloning for the isolation of enzymes of membrane lipid synthesis: phosphatidylserine synthase overproduction in *Escherichia coli* *Proceedings of the National Academy of Sciences* 74, 1412-1416
36. Raetz, C. R., and Kennedy, E. P. (1972) The association of phosphatidylserine synthetase with ribosomes in extracts of *Escherichia coli* *J Biol Chem* 247, 2008-2014
37. Atkinson, K., Fogel, S., and Henry, S. A. (1980) Yeast mutant defective in phosphatidylserine synthesis *Journal of Biological Chemistry* 255, 6653-6661
38. Atkinson, K. D., Jensen, B., Kolat, A. I., Storm, E. M., Henry, S. A., and Fogel, S. (1980) Yeast mutants auxotrophic for choline or ethanolamine *J Bacteriol* 141, 558-564
39. Poole, M. A., Homann, M. J., Bae-Lee, M. S., and Carman, G. M. (1986) Regulation of phosphatidylserine synthase from *Saccharomyces cerevisiae* by phospholipid precursors *Journal of Bacteriology* 168, 668-672 10.1128/jb.168.2.668-672.1986

40. Bailis, A. M., Poole, M. A., Carman, G. M., and Henry, S. A. (1987) The membrane-associated enzyme phosphatidylserine synthase is regulated at the level of mRNA abundance *Molecular and Cellular Biology* 7, 167-176
10.1128/mcb.7.1.167
41. Kelley, M. J., Bailis, A. M., Henry, S. A., and Carman, G. M. (1988) Regulation of phospholipid biosynthesis in *Saccharomyces cerevisiae* by inositol. Inositol is an inhibitor of phosphatidylserine synthase activity *J Biol Chem* 263, 18078-18085
42. Carman, G. M., and Matas, J. (1981) Solubilization of microsomal-associated phosphatidylserine synthase and phosphatidylinositol synthase from *Saccharomyces cerevisiae* *Can J Microbiol* 27, 1140-1149
43. Bae-Lee, M., and Carman, G. M. (1990) Regulation of yeast phosphatidylserine synthase and phosphatidylinositol synthase activities by phospholipids in Triton X-100/phospholipid mixed micelles *J Biol Chem* 265, 7221-7226
44. Bae-Lee, M. S., and Carman, G. M. (1984) Phosphatidylserine synthesis in *Saccharomyces cerevisiae*. Purification and characterization of membrane-associated phosphatidylserine synthase *J Biol Chem* 259, 10857-10862
45. Cassilly, C. D., Farmer, A. T., Montedonico, A. E., Smith, T. K., Campagna, S. R., and Reynolds, T. B. (2017) Role of phosphatidylserine synthase in shaping the phospholipidome of *Candida albicans* *FEMS Yeast Res* 17, 10.1093/femsyr/fox007
46. Zinser, E., Sperka-Gottlieb, C., Fasch, E.-V., Kohlwein, S. D., Paltauf, F., and Daum, G. (1991) Phospholipid synthesis and lipid composition of subcellular membranes in the unicellular eukaryote *Saccharomyces cerevisiae* *Journal of bacteriology* 173, 2026-2034
47. Goyal, S., and Khuller, G. (1992) Phospholipid composition and subcellular distribution in yeast and mycelial forms of *Candida albicans* *Journal of medical and veterinary mycology* 30, 355-362
48. Mouhib, M., Benediktsdottir, A., Nilsson, C. S., and Chi, C. N. (2021) Influence of Detergent and Lipid Composition on Reconstituted Membrane Proteins for Structural Studies *ACS Omega* 6, 24377-24381 10.1021/acsomega.1c02542
49. Crichton, P. G., Harding, M., Ruprecht, J. J., Lee, Y., and Kunji, E. R. (2013) Lipid, detergent, and Coomassie Blue G-250 affect the migration of small membrane proteins in blue native gels: mitochondrial carriers migrate as monomers not dimers *J Biol Chem* 288, 22163-22173 10.1074/jbc.M113.484329
50. Dörr, J. M., Koorengel, M. C., Schäfer, M., Prokofyev, A. V., Scheidelaar, S., Van Der Crujisen, E. A. *et al.* (2014) Detergent-free isolation, characterization, and functional reconstitution of a tetrameric K⁺ channel: the power of native nanodiscs *Proceedings of the National Academy of Sciences* 111, 18607-18612
51. Knowles, T. J., Finka, R., Smith, C., Lin, Y.-P., Dafforn, T., and Overduin, M. (2009) Membrane proteins solubilized intact in lipid containing nanoparticles bounded by styrene maleic acid copolymer *Journal of the American Chemical Society* 131, 7484-7485
52. Orwick-Rydmark, M., Lovett, J. E., Graziadei, A., Lindholm, L., Hicks, M. R., and Watts, A. (2012) Detergent-free incorporation of a seven-transmembrane

- receptor protein into nanosized bilayer Lipodisq particles for functional and biophysical studies *Nano letters* 12, 4687-4692
53. Long, A. R., O'Brien, C. C., Malhotra, K., Schwall, C. T., Albert, A. D., Watts, A. *et al.* (2013) A detergent-free strategy for the reconstitution of active enzyme complexes from native biological membranes into nanoscale discs *BMC biotechnology* 13, 1-10
 54. Brady, N. G., Li, M., Ma, Y., Gumbart, J. C., and Bruce, B. D. (2019) Non-detergent isolation of a cyanobacterial photosystem I using styrene maleic acid alternating copolymers *RSC advances* 9, 31781-31796
 55. Kinney, A. J., and Carman, G. M. (1988) Phosphorylation of yeast phosphatidylserine synthase in vivo and in vitro by cyclic AMP-dependent protein kinase *Proc Natl Acad Sci U S A* 85, 7962-7966
 56. Wittig, I., Braun, H.-P., and Schagger, H. (2006) Blue native PAGE *Nature Protocols* 1, 418-428 10.1038/nprot.2006.62
 57. Bamber, L., Harding, M., Butler, P. J. G., and Kunji, E. R. S. (2006) Yeast mitochondrial ADP/ATP carriers are monomeric in detergents *Proceedings of the National Academy of Sciences* 103, 16224-16229 doi:10.1073/pnas.0607640103
 58. Carman, G., and Dowhan, W. (1979) Phosphatidylserine synthase from *Escherichia coli*. The role of Triton X-100 in catalysis *The Journal of biological chemistry* 254, 8391-8397 10.1016/S0021-9258(19)86903-X
 59. Carman, G. M., Deems, R. A., and Dennis, E. A. (1995) Lipid Signaling Enzymes and Surface Dilution Kinetics ($\#x2217$;) *Journal of Biological Chemistry* 270, 18711-18714 10.1074/jbc.270.32.18711
 60. Gewering, T., Januliene, D., Ries, A. B., and Moeller, A. (2018) Know your detergents: A case study on detergent background in negative stain electron microscopy *J Struct Biol* 203, 242-246 10.1016/j.jsb.2018.05.008
 61. Yan, Y., Tao, H., and Huang, S.-Y. (2018) HSYMDOCK: a docking web server for predicting the structure of protein homo-oligomers with Cn or Dn symmetry *Nucleic acids research* 46, W423-W431
 62. Zhang, Q., and Cherezov, V. (2019) Chemical tools for membrane protein structural biology *Current opinion in structural biology* 58, 278-285
 63. Chae, P. S., Rasmussen, S. G., Rana, R. R., Gotfryd, K., Kruse, A. C., Manglik, A. *et al.* (2012) A new class of amphiphiles bearing rigid hydrophobic groups for solubilization and stabilization of membrane proteins *Chemistry—A European Journal* 18, 9485-9490
 64. Magnani, F., Serrano-Vega, M. J., Shibata, Y., Abdul-Hussein, S., Lebon, G., Miller-Gallacher, J. *et al.* (2016) A mutagenesis and screening strategy to generate optimally thermostabilized membrane proteins for structural studies *Nat Protoc* 11, 1554-1571 10.1038/nprot.2016.088
 65. Laguerre, A., Löhr, F., Henrich, E., Hoffmann, B., Abdul-Manan, N., Connolly, P. J. *et al.* (2016) From Nanodiscs to Isotropic Bicelles: A Procedure for Solution Nuclear Magnetic Resonance Studies of Detergent-Sensitive Integral Membrane Proteins *Structure* 24, 1830-1841 10.1016/j.str.2016.07.017
 66. Carson, M. A., Atkinson, K. D., and Waechter, C. J. (1982) Properties of particulate and solubilized phosphatidylserine synthase activity from

- Saccharomyces cerevisiae. Inhibitory effect of choline in the growth medium
Journal of Biological Chemistry 257, 8115-8121
67. Nikawa, J.-I., and Yamashita, S. (1981) Characterization of phosphatidylserine synthase from saccharomyces cerevisiae and a mutant defective in the enzyme Biochimica et Biophysica Acta (BBA) - Lipids and Lipid Metabolism 665, 420-426 [https://doi.org/10.1016/0005-2760\(81\)90254-X](https://doi.org/10.1016/0005-2760(81)90254-X)
 68. Tams, R. N., Cassilly, C. D., Anaokar, S., Brewer, W. T., Dinsmore, J. T., Chen, Y.-L. *et al.* (2019) Overproduction of Phospholipids by the Kennedy Pathway Leads to Hypervirulence in Candida albicans Frontiers in Microbiology 10, 10.3389/fmicb.2019.00086
 69. Schuck, P. (2000) Size-distribution analysis of macromolecules by sedimentation velocity ultracentrifugation and lamm equation modeling Biophysical journal 78, 1606-1619
 70. Philo, J. S. (2023) SEDNTERP: a calculation and database utility to aid interpretation of analytical ultracentrifugation and light scattering data European Biophysics Journal 1-34
 71. De la Rosa-Trevín, J., Quintana, A., Del Cano, L., Zaldívar, A., Foche, I., Gutiérrez, J. *et al.* (2016) Scipion: A software framework toward integration, reproducibility and validation in 3D electron microscopy Journal of structural biology 195, 93-99
 72. Zheng, S. Q., Palovcak, E., Armache, J.-P., Verba, K. A., Cheng, Y., and Agard, D. A. (2017) MotionCor2: anisotropic correction of beam-induced motion for improved cryo-electron microscopy Nature methods 14, 331-332
 73. Zhang, K. (2016) Gctf: Real-time CTF determination and correction Journal of structural biology 193, 1-12
 74. Punjani, A., Rubinstein, J. L., Fleet, D. J., and Brubaker, M. A. (2017) cryoSPARC: algorithms for rapid unsupervised cryo-EM structure determination Nature methods 14, 290-296
 75. Jumper, J., Evans, R., Pritzel, A., Green, T., Figurnov, M., Ronneberger, O. *et al.* (2021) Highly accurate protein structure prediction with AlphaFold Nature 596, 583-589
 76. Pettersen, E. F., Goddard, T. D., Huang, C. C., Meng, E. C., Couch, G. S., Croll, T. I. *et al.* (2021) UCSF ChimeraX: Structure visualization for researchers, educators, and developers Protein Science 30, 70-82

Supplementary Figures

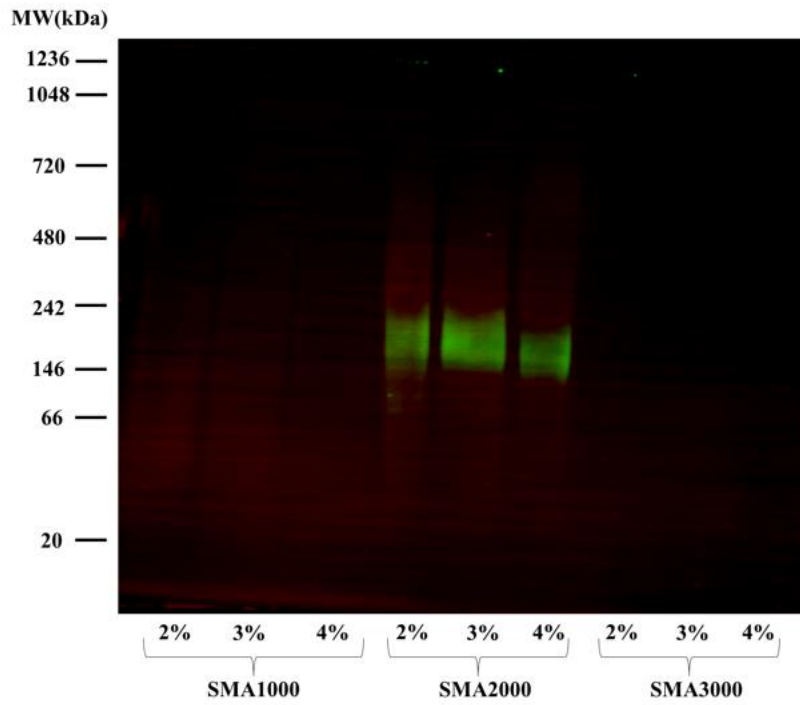


Figure S3.1. HAx3-tagged Cho1 protein was solubilized in SMA1000, 2000 and 3000 at 2%, 3% and 4% for 2 hours, and the resulting solubilized fractions were detected by Western blotting following BN-PAGE.

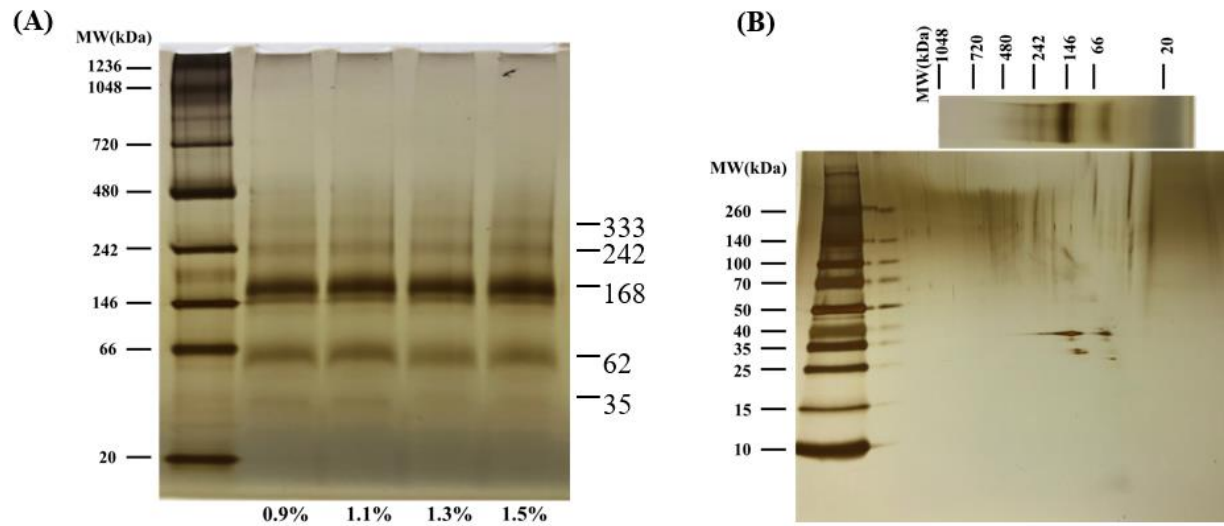


Figure S3.2. (A) BN-PAGE of the pulled-down HAx3-tagged Cho1 protein from the solubilized fractions of 0.9%, 1.1%, 1.3%, 1.5% DDM. (B) The 2nd dimensional SDS-PAGE of the BN-PAGE gel strip from 1.1% DDM. All gels were stained with Pierce™ silver stain kit, and MW of different bands (kDa) were estimated from protein ladders and indicated.

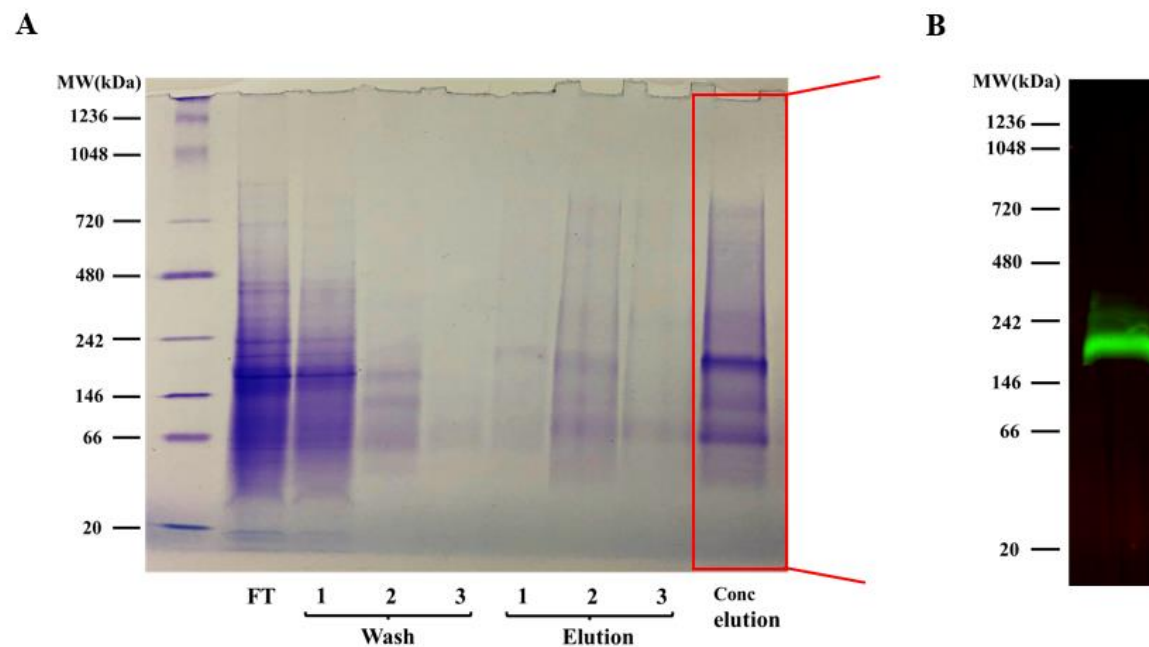


Figure S3.3.(A) BN-PAGE gel of cobalt resin flowthrough (FT), washes 1, 2, & 3, and elutions 1, 2, & 3 and the concentrated combined elution fractions (Conc. Elution), all stained with Coomassie blue R250 dye. (B) Western blotting of the concentrated elution on the BN-PAGE using anti-HA antibody

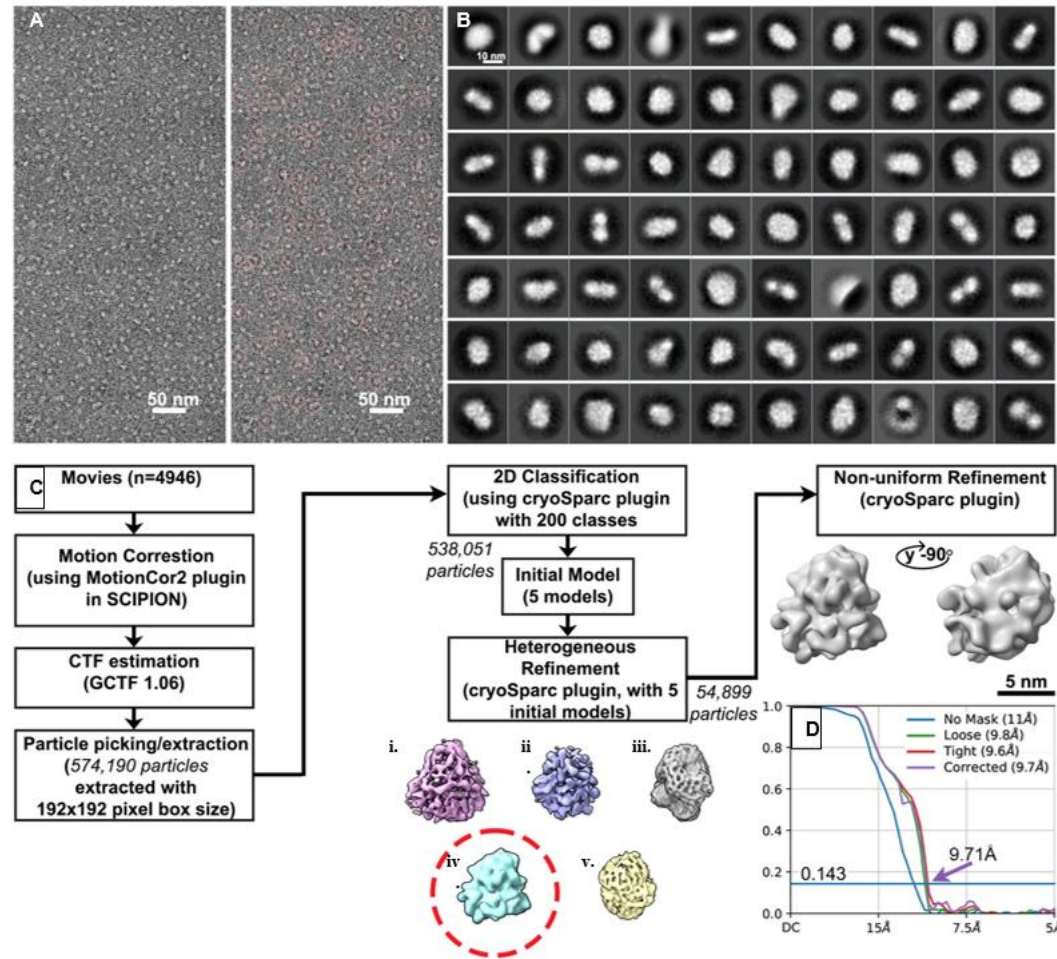


Figure S3.4. Data processing pathway for the negative staining TEM of the Cho1 micelles (A) Representative negatively stained TEM micrograph (4,956 in total) of the Cho1 complex (left). All particles picked from that micrograph are marked with pink circles (right). (B) Representative reference-free 2D class averages. (C) Overview of the negative staining TEM workflow for the Cho1 complex dataset. Red circle shows the 3D model that was chosen for further analysis. (D) The gold-standard Fourier Shell Correlation (FSC) curve. Based on the FSC=0.143 criterion, the resolution of the full map is 9.7 Å.



Figure S3.5. The structure prediction model of the Cho1 dimer using AlphaFold2 (A), and the refined Cho1 dimer with the deletion of N-terminal 50 amino acids is shown in (B).

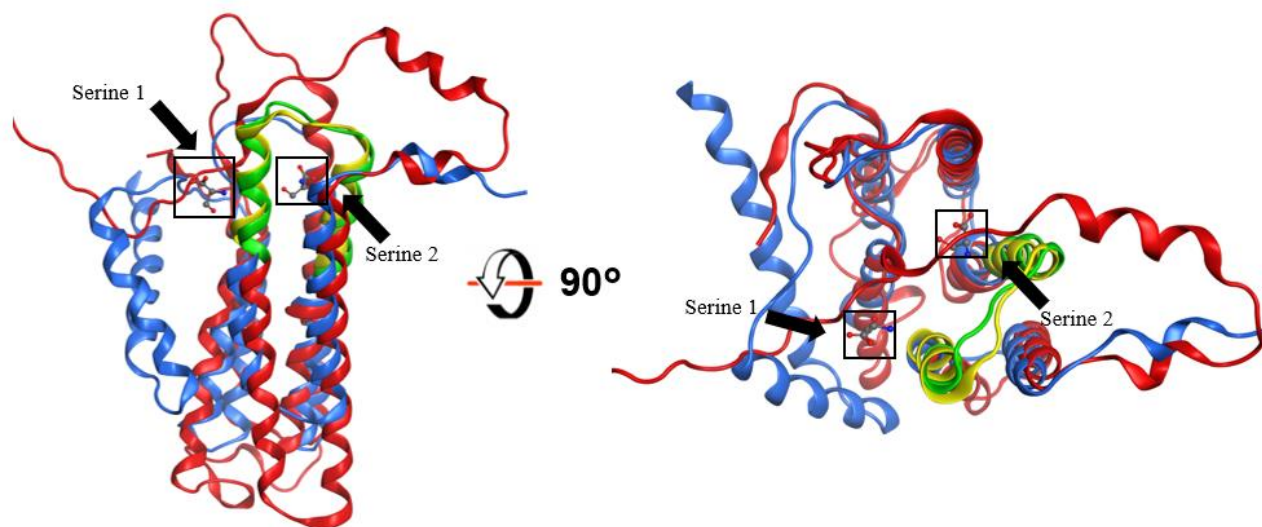


Figure S3.6. Superposition of AlphaFold2-predicted Cho1 structure (red) with *Methanocaldococcus jannaschii* PS synthase structure (blue, PDB: 7B1L) at two different views. The conserved CAPT motif was shown as green in the predicted Cho1 structure and yellow in *Methanocaldococcus jannaschii* PS synthase structure. The two bound serine are from *Methanocaldococcus jannaschii* PS synthase structure. Serine 1 was claimed to be an experimental artifact.

**CHAPTER 4 IDENTIFICATION OF SMALL MOLECULE
INHIBITORS TO CANDIDA ALBICANS PHOSPHATIDYLSERINE
SYNTHASE VIA A TARGET-BASED SCREEN**

Author list: Yue Zhou, Gregory A. Phelps, Mikayla M. Mangrum, Jemma McLeish, Elise K. Phillips, Jinchao Lou, Christelle F. Ancajas, Jeffrey M. Rybak, Peter M. Oelkers, Richard E. Lee, Michael D. Best, and Todd B. Reynolds

Contribution in the paper: Conceived and designed the experiments: YZ, GAP, JMR, REL, TBR. Performed the experiments: YZ, GAP, MMM, JM, JMR, EKP, JL, CFA. Analyzed the data: YZ, GAP, TBR. Contributed reagents/materials/analysis tools: JMR, REL, MDB, TBR. Wrote the original draft: YZ. Writing & Editing: YZ, GAP, PMO, CFA, TBR. All authors contributed to the article and approved the submitted version.

All small molecules were handled by Greg. Plate design and analysis were conducted by Greg. The *Manduca* experiment was performed by Jemma. The protein purification and optimization in the reaction and characterization of the drugs *in vivo* were carried out by Yue. The paper is written by me, Greg and Jemma, and edited by the others.

Abstract

Systemic infections by *Candida spp.* are associated with high mortality rates, partly due to limitations in current antifungals, highlighting the need for novel drugs and drug targets. The fungal phosphatidylserine synthase, Cho1, from *Candida albicans* is a logical antifungal drug target due to its importance in virulence, absence in the host and conservation among fungal pathogens. Inhibitors of Cho1 could serve as lead compounds for drug development, so we developed a target-based screen for inhibitors of purified Cho1. This enzyme condenses serine and cytidyldiphosphate-diacylglycerol (CDP-DAG) into phosphatidylserine (PS) and cytidylmonophosphate (CMP). Accordingly, we developed an *in vitro* nucleotidase-coupled malachite green-based high throughput assay for purified *C. albicans* Cho1 that monitors CMP production as a proxy for PS synthesis. Over 7,300 molecules curated from repurposing chemical libraries were interrogated in primary and dose-responsivity assays using this platform. The screen had a promising average Z' score of ~ 0.8 , and seven compounds were identified that inhibit Cho1. Three out of these, ebselen, LOC14, and CBR-5884, exhibited inhibitory effects against *C. albicans* cells, with fungicidal inhibition by ebselen and fungistatic inhibition by LOC14 and CBR-5884. Furthermore, CBR-5884 was shown to disrupt *in vivo* Cho1 function by inducing phenotypes consistent with the *cho1* $\Delta\Delta$ mutant, including a reduction of cellular PS levels. Kinetics curves and computational docking suggest that CBR-5884 competes with serine for binding of Cho1 with a K_i of $1,550 \pm 245.6$ nM, thus this compound has the potential for development into an antifungal compound.

Introduction

Candida species are the most commonly isolated fungal pathogens of humans (1, 2). *Candida* has been associated with mucosal infections, such as vulvovaginal infections in 51% of women or oropharyngeal infections in 27% of HIV+ patients, even when on anti-retroviral (ART) therapy (3, 4). In addition, these species are responsible for ~27% of bloodstream infections associated with a central line (1, 2, 5). *Candida* bloodstream infections pose a considerable threat to public health, with a mortality rate of approximately 40% (1, 2, 6, 7). *Candida albicans* (*C. albicans*) is the most commonly isolated species within *Candida* species (1, 2, 8). Currently, there are only three classes of antifungal drugs in common use (azoles, polyenes, and echinocandins) for treating systemic *Candida* infections. However, their effectiveness is hindered by rising drug resistance to azoles and echinocandins and toxicity profile of the polyene amphotericin B (9-13). Therefore, there is a pressing need to develop novel antifungal drugs.

Central in the phospholipid synthetic pathway in fungi is the phosphatidylserine (PS) synthase reaction (CDP-diacylglycerol—serine O-phosphatidyltransferase; EC 2.7.8.8) mediated by Cho1. This enzyme has been identified as a potential drug target due to the observation that [i] removal of Cho1 in *Candida albicans* prevents it from causing disease in mouse models of systemic or oral infection (14, 15), and this enzyme is also crucial for the growth of the major fungal pathogen *Cryptococcus neoformans* (16); [ii] Cho1 is not present in humans, indicating that specific inhibitors targeting this enzyme should not have toxic effects on humans (17), and [iii] *CHO1* is highly conserved

across various fungal species, suggesting that inhibitors of this enzyme would have broad spectrum anti-fungal effects (16, 17). Hence, inhibitors to Cho1 would be excellent lead compounds for antifungal drug development.

The fungal Cho1 enzyme was first characterized in the yeast *Saccharomyces cerevisiae*. This included descriptions of cellular localization in the endoplasmic reticulum and mitochondrial outer membranes (18-20), activity regulation (21-23) and protein purification (24, 25). Cho1 catalyzes the formation of PS from cytidyldiphosphate-diacylglycerol (CDP-DAG) and L-serine, and it belongs to the CDP-alcohol phosphatidyltransferase (CDP-AP) protein family. The CDP-AP proteins employ the highly conserved CDP-alcohol phosphotransferase (CAPT) motif, D-(X)₂-D-G-(X)₂-A-R-(X)₂-N-(X)₅-G-(X)₂-L-D-(X)₃-D, to bind CDP-linked molecules and facilitate the formation of a phosphodiester bond between the CDP-linked molecule and another small alcohol (16, 26-30), specifically, CDP-DAG and serine for Cho1. However, it is important to note that the binding pocket for serine, unlike the CAPT motif, is not conserved among CDP-AP proteins. Previous studies have identified and characterized several crucial residues within the CAPT motif and the putative serine-binding site of *C. albicans* Cho1 through alanine scanning mutagenesis (26, 31). Additionally, valuable insights have been provided into the serine-binding pocket from the atomic structure of the PS synthase from the archaean *Methanocaldococcus jannaschii* (32). Differences between the *M. jannaschii* PS synthase and *C. albicans* Cho1 are apparent by the presence of specific residues in *C. albicans* Cho1 that play important roles, yet lack clear counterparts in the *M. jannaschii* PS synthase (26, 32).

Besides the characterization of the substrate-binding residues, the *C. albicans* Cho1 has also been solubilized and purified as a hexameric protein (33), distinct from all the CDP-AP enzymes with solved structures (30, 32, 34-40), which are dimers. The hexameric *C. albicans* Cho1 can be separated into a trimer of stable dimers, indicating the hexamer might be [i] an early oligomer state, since Cho1 was solubilized from the early-to-mid log phase of *C. albicans* or [ii] species-specific (33). Furthermore, purified Cho1 enzyme was optimized for activity and was shown to have a K_m for CDP-DAG of 72.20 μM with a V_{max} of 0.079 $\text{nmol}/(\mu\text{g}\cdot\text{min})$ while exhibiting a sigmoidal kinetic curve for its other substrate serine, indicating cooperative binding (33). This sigmoidal kinetic could potentially reconcile the contradicting high and low K_m values reported previously for *S. cerevisiae* PS synthase (22, 25, 41-43). The mechanism underlying the cooperative binding of serine is currently unknown.

Rational drug design is one way to discover compounds to a drug target protein. This can be achieved through either ligand-based or structure-based design methods (44). However, since there is a scarcity of known Cho1 ligands, and the atomic structure of *C. albicans* Cho1 has not yet been solved, employing rational drug design to identify Cho1-specific inhibitors is challenging. On the contrary, small molecule screening is an alternative way to identify inhibitors to Cho1 independent of structural information. Two whole-cell screens have been carried out to identify Cho1 inhibitors, but neither has been successful (45, 46). One identified the compound SB-224289, but it was discovered that SB-224289 only affects Cho1-associated physiological pathways (45). The other screen identified bleomycin, but this again impacts phospholipid related physiologies rather than

Cho1 itself (46). Thus, to carry out identification of a Cho1 inhibitor, a target-based screen was developed. This approach is enabled by the purification of Cho1, and is favorable because molecules identified will show direct inhibition on the target. Potential issues such as the cellular entry of molecules identified from target-based screening can be resolved later through medicinal chemistry approaches.

Cho1 activity has been measured in crude membrane preps (26, 31, 45, 47) and as a purified form (33, 48), using a radioactive substrate. However, that methodology is inconsistent with a high throughput screen. Here, we have adapted a non-radioactive assay with an easy setup and colorimetric readout (49), which detects the byproduct cytidine monophosphate (CMP) released from Cho1, to measure its activity in the presence of screening molecules. Using this assay, approximately 7,300 molecules were interrogated in a primary screen from a set of curated repurposing libraries to reveal one compound, CBR-5884, that stood out as it displayed an inhibitory effect on Cho1 both *in vitro* and in live *C. albicans* cells.

Results

A malachite-green-based nucleotidase-coupled assay was used to screen for inhibitors of purified Cho1 protein

A expression cassette plasmid carrying the strong, constitutive promoter for translational elongation factor 1 (P_{TEF1}) fused upstream of the *C. albicans* *CHO1* gene was integrated into the genome at the *TEF1* locus to ensure a strong and stable expression level (50). Then, Cho1 was solubilized and purified from the microsomal fraction of *Candida albicans* as described in the Materials and Methods section. A blue native

PAGE indicated the Cho1 protein was successfully purified as a hexameric form of ~180 kDa to relative homogeneity (Figure 4.1A), consistent with findings in (33). The purified Cho1 was used for small molecule screening.

A malachite green-based nucleotidase-coupled assay was used to measure the PS synthesis activity of Cho1 (Figure 4.1B). Cho1 catalyzes the production of PS and cytidine monophosphate (CMP) from CDP-DAG and serine, where CMP can then be recognized and cleaved by the nucleotidase CD73 to release inorganic phosphate, which is subsequently detected by malachite green. To test whether this malachite green-based assay can reflect Cho1 activity, a time-course test was performed with a fixed amount of purified Cho1 in the presence of substrates (Figure 4.1C). The OD₆₂₀ signal increased as the reaction proceeded until it plateaued at 200 min, suggesting that the assay is suitably dynamic assay to probe Cho1 activity (Figure 4.1C). Based on this data, a fixed time of 180 minutes was chosen for the screen.

As no effective inhibitors of Cho1 have been identified to date, a highly potent and selective inhibitor of the second step of the assay (nucleotidase CD73) was examined as a positive control (51). This compound, AB-680, exhibited an IC₅₀ value of 1.82 nM in the malachite-green assay (Figure S4.1A). A concentration of 1 μM AB-680 was used in the screen, and was compared to DMSO and no protein wells, which served as negative controls. Reactions with AB-680 showed similar color as the no protein control in the 384-well plate (Figure 4.1D), and the measured OD₆₂₀ signal was four-fold less in the presence of the AB-680 (Figure 4.1E). Thus, AB-680 can be used as a positive control for selecting inhibitors in the primary screen. In order to eliminate false positives that are

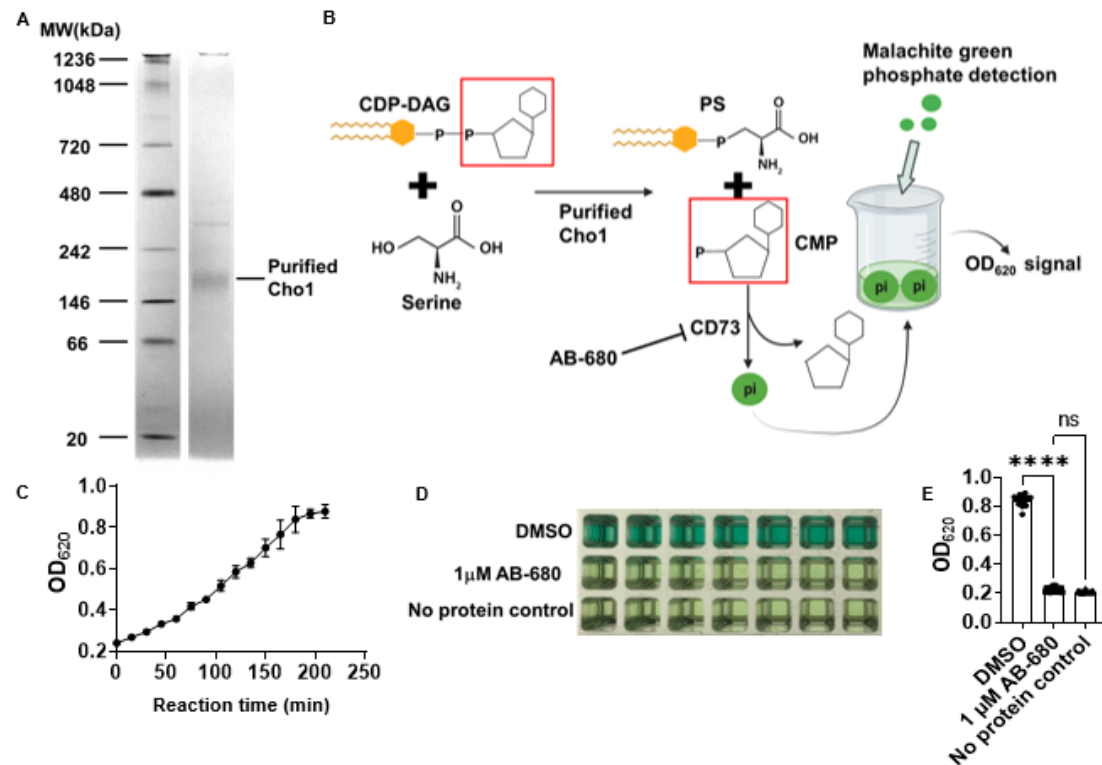


Figure 4.1. A malachite-green-based nucleotidase-coupled assay measures the activity of purified Cho1 protein. (A) Blue native PAGE gel of the purified hexameric tag-free Cho1 protein. Purified Cho1 and protein ladder with known MW are indicated. The gel was stained with Coomassie Blue R-250. (B) Schematic representation of the malachite-green-based nucleotidase-coupled assay. Cho1 synthesizes PS from CDP-DAG (cytidine diphosphate diacylglycerol) and serine. This releases PS and CMP (cytidine monophosphate). The phosphate from CMP is cleaved by the nucleotidase CD73 to release inorganic phosphate, which can be bound by the malachite green reagent and measured colorimetrically at OD₆₂₀. AB-680 is a potent inhibitor of CD73, and can thus inhibit the reaction. (C) OD₆₂₀ signal from the malachite green reagent that was added to the reaction shown in (B) at different time points after the reaction started. Reactions were set up with the same conditions and stopped by adding malachite green at the time indicated. The dots represent the mean of four replicates, and the error bars are \pm standard deviation (S.D.) values. (D) Inhibition of the nucleotidase-coupled assay by AB-680 is shown for a series of replicates and (E) is quantified for a total of 21 replicates. Statistics were conducted using one-way ANOVA using Tukey's multiple comparisons test (ns=not significant, ****, $p < 0.0001$).

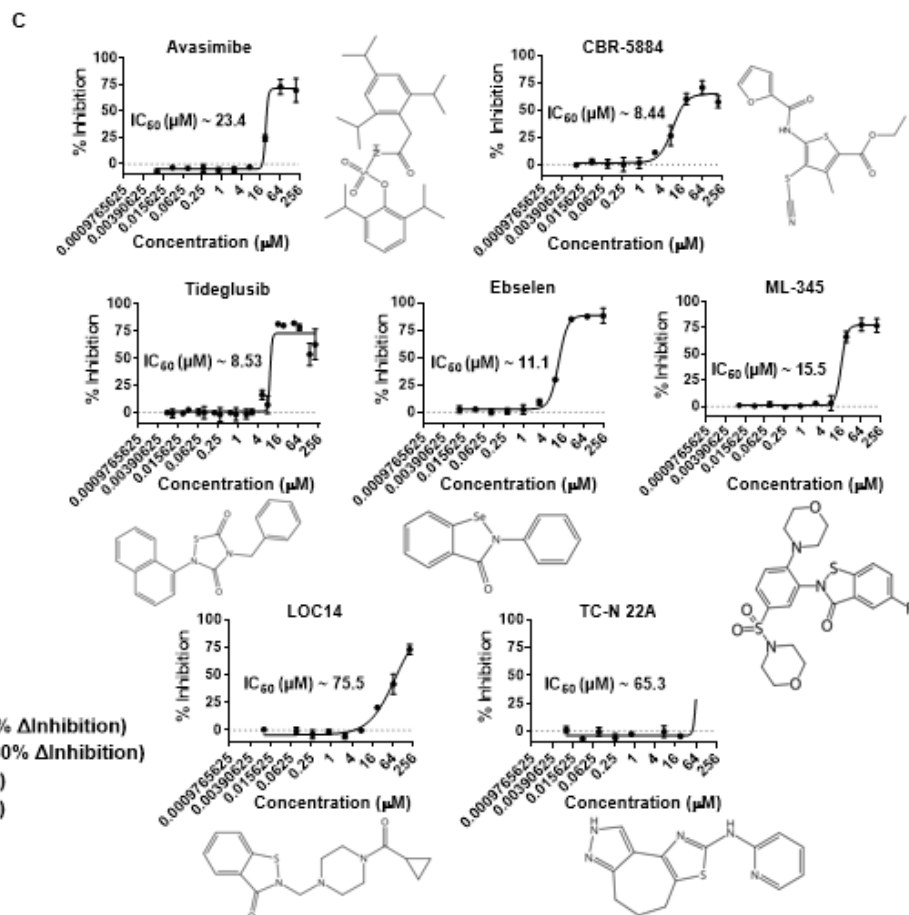
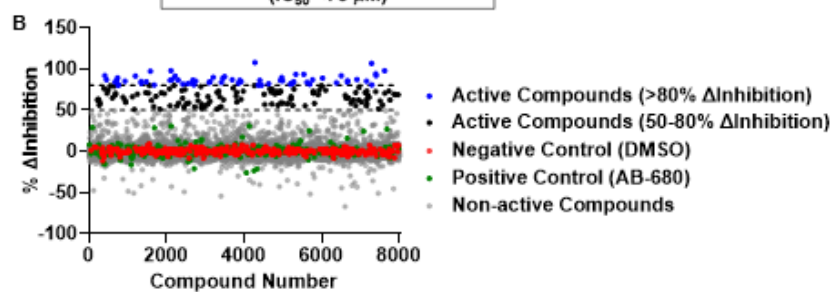
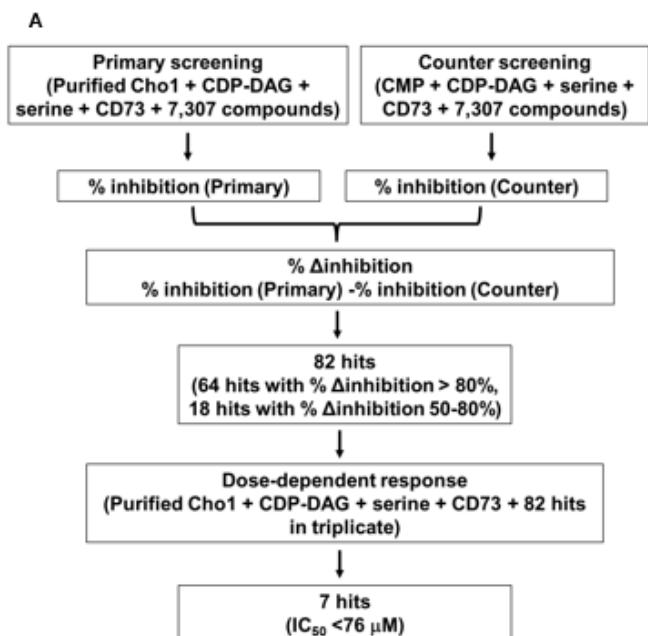
actually inhibiting the nucleotidase CD73, a counter screen was developed where Cho1 was replaced with CMP, but CD73 was still present so that we could detect direct inhibitors of the nucleotidase.

Seven Cho1-specific inhibitors were identified from the high throughput small molecule screen

The screen interrogated 7,307 molecules from three curated repurposing libraries in the primary screen and counter screen (which were run concurrently) at a final concentration of 100 μ M each (Figure 4.2A). The primary screen had an average Z' score of ~ 0.8 (Figure S4.1B), indicating a good signal to noise ratio (52). To prioritize hit compounds and eliminate false positives, % Δ inhibition was calculated by subtracting the % inhibition from the counter screen (Figure S4.1D) from that of the primary screen (Figure S4.1C) for each molecule (Figure 4.2B). All compounds with $>80\%$ Δ inhibition and selected molecules of limited structural liabilities with 50-80% Δ inhibition, a total of 82 molecules, were advanced for dose-response assessment using the same screening platform, which once again yielded results of high quality (Z' of 0.83; Figure S4.1E). Compounds exerting dose-dependent activity were then further triaged by manual inspection to exclude pan assay interference compounds (PAINS), which tend to react nonspecifically with numerous biological targets (53). Finally, seven molecules exerting IC_{50} values $\leq 76 \mu$ M were identified, of which CBR-5884, ML-345, ebselen and tideglusib were most potent possessing $IC_{50} \leq 20 \mu$ M (Figure 4.2C). These molecules, in

Figure 4.2. Seven Cho1-specific inhibitors were identified from the high-throughput malachite green screen.

(A) Flowchart for the primary and counter screen and the calculation of % Δ inhibition. (B) The dot plot of % Δ inhibition for all the compounds, including controls, used in the screen. Reaction with DMSO and AB-680 were used as 0% Δ inhibition (negative) and 100% Δ inhibition (positive) controls, respectively. The two dotted lines from the Y-axis indicate 80 and 50% Δ inhibition, respectively. (C) Dose-response curve and structure of the seven non-pan-assay interference (non-PAINS) compounds identified from the screen. The dots represent the mean of three replicates, and the error bars are \pm standard deviation (S.D.) values. Best-fit IC_{50} values (in μ M) were shown in each graph.



addition to avasimibe and LOC14 were selected for further investigation. The TC-N 22A molecule was not easily available and was not pursued.

Ebselen, LOC14 and CBR-5884 showed inhibitory effects on *C. albicans* cells

To further validate the inhibitory effects of the six molecules on Cho1, a radioactive PS synthase assay was conducted on Cho1 in the presence of these compounds. Unlike the malachite green-based assay, the radioactive PS synthase assay directly measures the incorporation of L-[³H]-serine into PS in the lipid phase (26, 33, 47). The radioactive PS synthase assay was performed on purified Cho1 in the presence of the six compounds at 100 μ M, and all six molecules were shown to totally inhibit Cho1 (Figure 4.3A), consistent with the screening results.

We then tested the effects of the six compounds on live cells. Since PS is the lipid precursor for making phosphatidylethanolamine (PE), an essential phospholipid, via the *de novo* pathway, disabling PS production will stop cell growth in minimal media lacking ethanolamine, which is used to make PE via the salvage (Kennedy) pathway (14, 26). To test the inhibitory effects of the compounds on live cells, wildtype *C. albicans* strain SC5314 was grown with avasimibe, CBR-5884, tideglusib, ebselen, ML-345 and LOC14 in minimal media at 30°C for 24 hours, along with a *cho1* $\Delta\Delta$ strain as a control (Figure 4.3B). The concentration of the compounds varied from 7.9 to 500 μ M. It is worth noting that avasimibe, tideglusib and CBR-5884 precipitated at high concentrations, indicating a low solubility (Figure S4.2A). Among all compounds, avasimibe, tideglusib and ML-345 did not affect cell growth even at 500 μ M, indicating they do not have an inhibitory effect on *Candida albicans* cells under our assay conditions (Figure 4.3B). Ebselen, LOC14 and CBR-5884, on the contrary, caused cell growth perturbation at different concentrations,

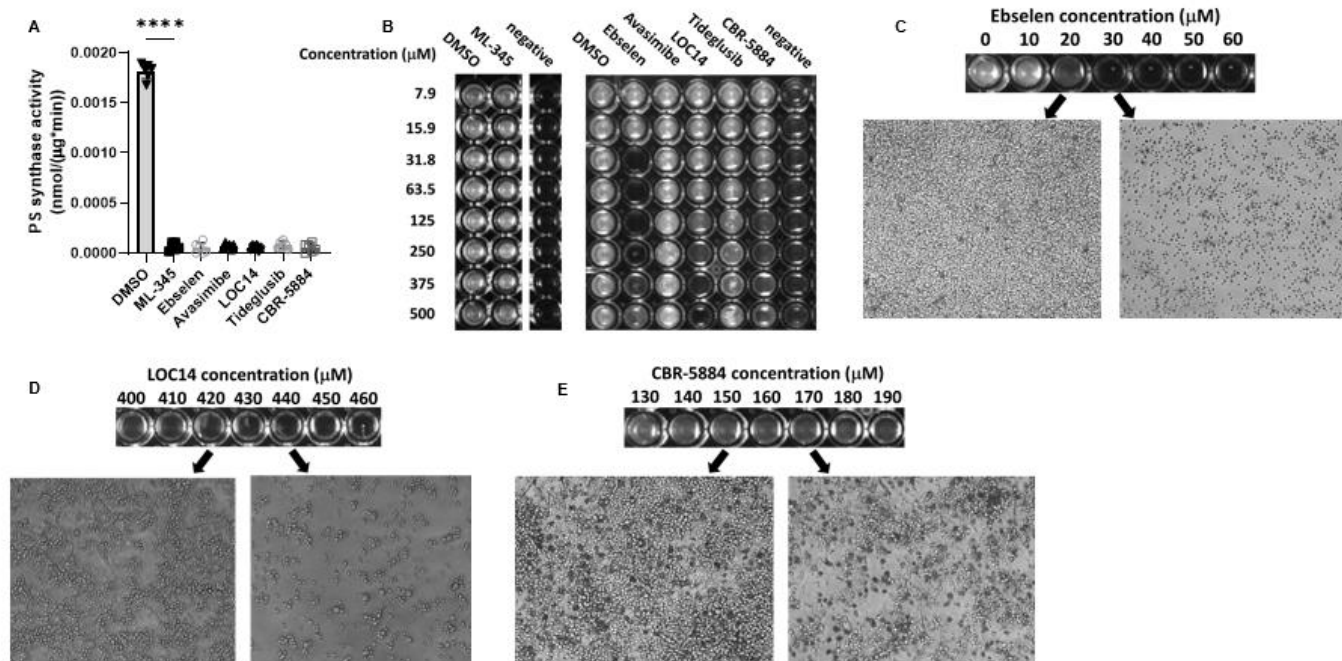


Figure 4.3. Ebselen, LOC14 and CBR-5884 inhibited cell growth of *C. albicans*.

(A) The PS synthase activity of purified Cho1 was measured by L-[^3H]-serine incorporation into PS in the presence of different inhibitors at 100 μM or equivalent DMSO, and are presented as nmol/(μg protein*min). Statistics were conducted using one-way ANOVA and Dunnett's T3 multiple comparisons test (****, 0.0001 > p). The activities were measured in duplicate with a total of six biological replicates as indicated. The bars represent the mean and the error bars are \pm S.D. values. (B) Wildtype *C. albicans* was grown in minimal media for 24 hours with DMSO or different inhibitors at the concentrations indicated, and the *cho1 $\Delta\Delta$* strain in DMSO was used as a control (shown as “negative”). (C-E) Inverted microscopy (400x) was used to visualize cell treated with (C) ebselen (D) LOC14 and (E) CBR-5884 under the concentrations indicated for 24 hours.

suggesting that they have an inhibitory effect (Figure 4.3B). This is consistent with the radioactive PS synthase assay done on the crude membrane containing Cho1, in which only ebselen, CBR-5884 and LOC14 decreased PS production on the native crude membranes (Figure S4.3).

To further characterize the inhibitory effects of ebselen, LOC14 and CBR-5884 on live cells, wildtype *C. abicans* SC5314 was incubated with these compounds in a dosage series with 10 μM increments to determine a more accurate minimal inhibitory concentration (MIC) value. Ebselen at 30 μM was shown to inhibit cell growth, and cells were smaller than normal wild-type cells when viewed in the microscope (Figure 4.3C). LOC14 and CBR-5884, on the contrary, showed significantly decreased cell density at 440 μM and 170 μM , respectively (Figures 4.3D&4.3E), but not abnormally small cells. To determine if the inhibitory effects are fungistatic or fungicidal, cells grown for 24 hours in minimal media with these compounds were plated, and colony forming units (CFUs) were counted. Ebselen showed no colonies after incubation at 30 μM , consistent with the small cell phenotype and suggesting it has a fungicidal effect (Figure 4.4A). In contrast, cells incubated with 430 μM LOC14 and 170 μM CBR-5884 exhibited similar CFUs as the pre-incubation, indicative of a fungistatic effect (Figures 4.4B&C). The inhibitory effect of CBR-5884 can be alleviated by ethanolamine supplementation

We then tested if the effects of ebselen, LOC14 and CBR-5884 on cells are pleiotropic or mainly caused by perturbed Cho1 function. Other than the *de novo* pathway where Cho1 is involved, PE can also be synthesized via the Kennedy salvage pathway, which requires exogenous ethanolamine. Hence, if the decreased cell growth in the

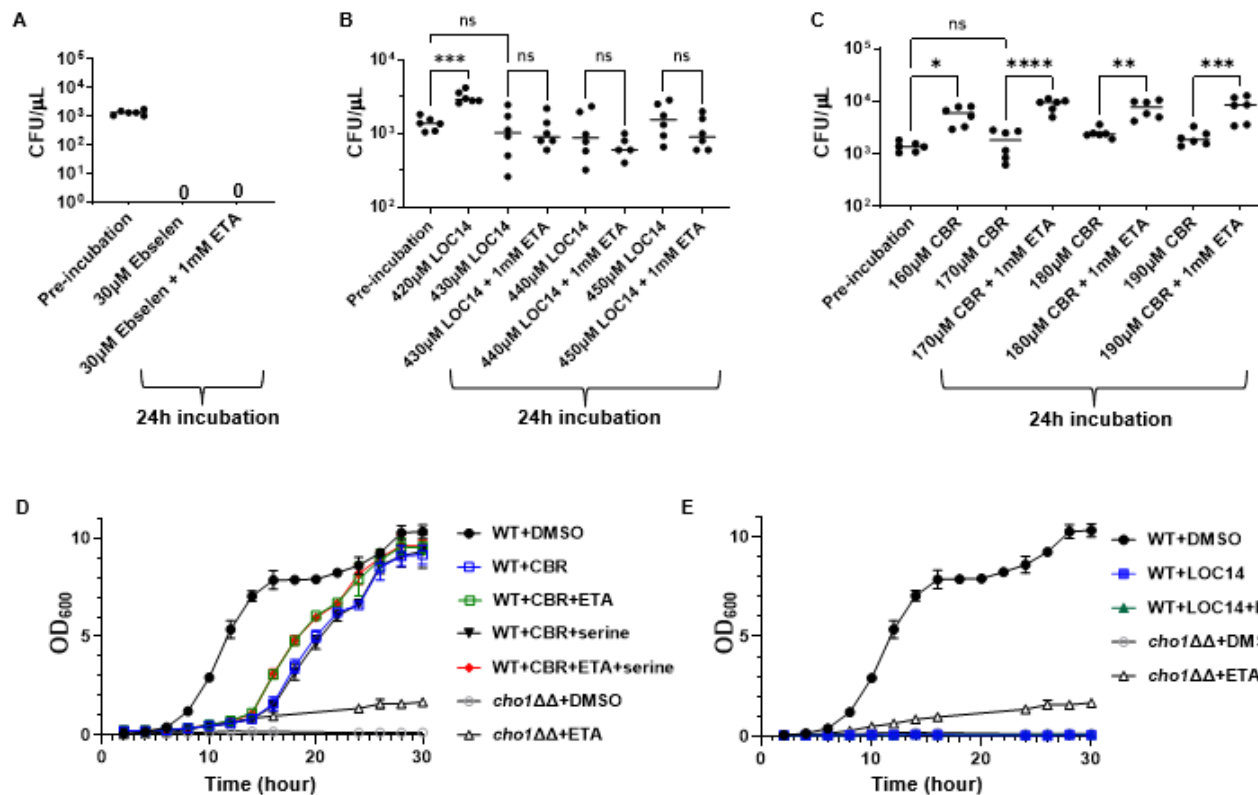


Figure 4.4. Ethanolamine supplementation can mitigate the inhibitory impact of CBR-5884. (A-C) Colony forming units (CFUs) from cells treated with different concentrations of (A) ebselen, (B) LOC14 and (C) CBR-5884, \pm 1 mM ethanolamine (ETA) supplement, for 24 hours compared to pre-incubation. Statistics were conducted using one-way ANOVA and Tukey's multiple comparisons test (ns=not significant, $p > 0.05$; *, $0.05 > p > 0.01$, **, $0.01 > p > 0.001$). Six biological replicates were tested in each treatment. (D) Growth curves of wildtype *C. albicans* in the presence of 170 μ M CBR-5884 or equivalent DMSO, with the addition of 1 mM ethanolamine (ETA) or 5 mM serine or both, from 0 to 30 hours. The *cho1* $\Delta\Delta$ strain was also included as a control. The dots represent the mean values of six replicates, and the error bars are \pm standard deviation (S.D.) values. (E) Growth curves of wildtype *C. albicans* in the presence of 430 μ M LOC-5884 or equivalent DMSO, with the addition of 1 mM ethanolamine (ETA), from 0 to 30 hours. The *cho1* $\Delta\Delta$ strain was also included as a control. The dots represent the mean values of six replicates, and the error bars are \pm standard deviation (S.D.) values.

presence of the compounds is restored by ethanolamine supplementation, the inhibitory effect is likely due to Cho1 inhibition. For this, *C. albicans* cells were again grown with ebselen, LOC14 and CBR-5884 in minimal media supplemented with 1 mM ethanolamine. Although ethanolamine did not rescue cells with ebselen or LOC14, cells treated with CBR-5884 generated significantly higher CFUs upon addition of ethanolamine (Figures 4.4A-C). This result suggests that the inhibitory effect of ebselen and LOC14 on the cells are not solely caused by Cho1 inhibition, while CBR-5884 is more directly targeting Cho1.

To gain insight into the dynamic, inhibitory properties of these molecules, growth curves were determined with wildtype cells grown in the minimal media \pm ethanolamine, in the presence of CBR-5884 or LOC14. Ebselen was not pursued in the growth curve assay due to its fungicidal effect. The *cho1* $\Delta\Delta$ strain was used as a control for loss of Cho1 activity. Given that CBR-5884 is a selective inhibitor of phosphoglycerate dehydrogenase for *de novo* serine synthesis in cancer cells (54), and to make sure that the growth perturbation is not due to serine starvation, 5 mM serine was also added to the media \pm ethanolamine. As shown in Figure 4.4D, cells grown in media + ethanolamine and + ethanolamine/serine grew similarly, while those grown in minimal media and minimal media + serine had similarly reduced growth. This suggests that serine did not help the cells recover from the inhibition from CBR-5884, which likely indicates [i] CBR-5884 does not target *C.albicans* phosphoglycerate dehydrogenase or [ii] the CBR-5884 inhibition of *C. albicans* phosphoglycerate dehydrogenase is not the major cause of diminished growth. Cells with ethanolamine supplementation grew better than those in minimal media alone, especially from 12 to 24 hours, consistent with Figure 4.4C.

Growth rates during log phase (Figure S4.2B) and lag phase duration (Figure S4.2C) were estimated from the growth curves, and they showed that the addition of ethanolamine increased the growth rate and decreased the lag time. All these results again support the hypothesis that CBR-5884 targets Cho1 *in vivo*. All strain groups caught up with growth after a 24-hour incubation (Figure 4.4D), suggesting that CBR-5884 loses its effect over time.

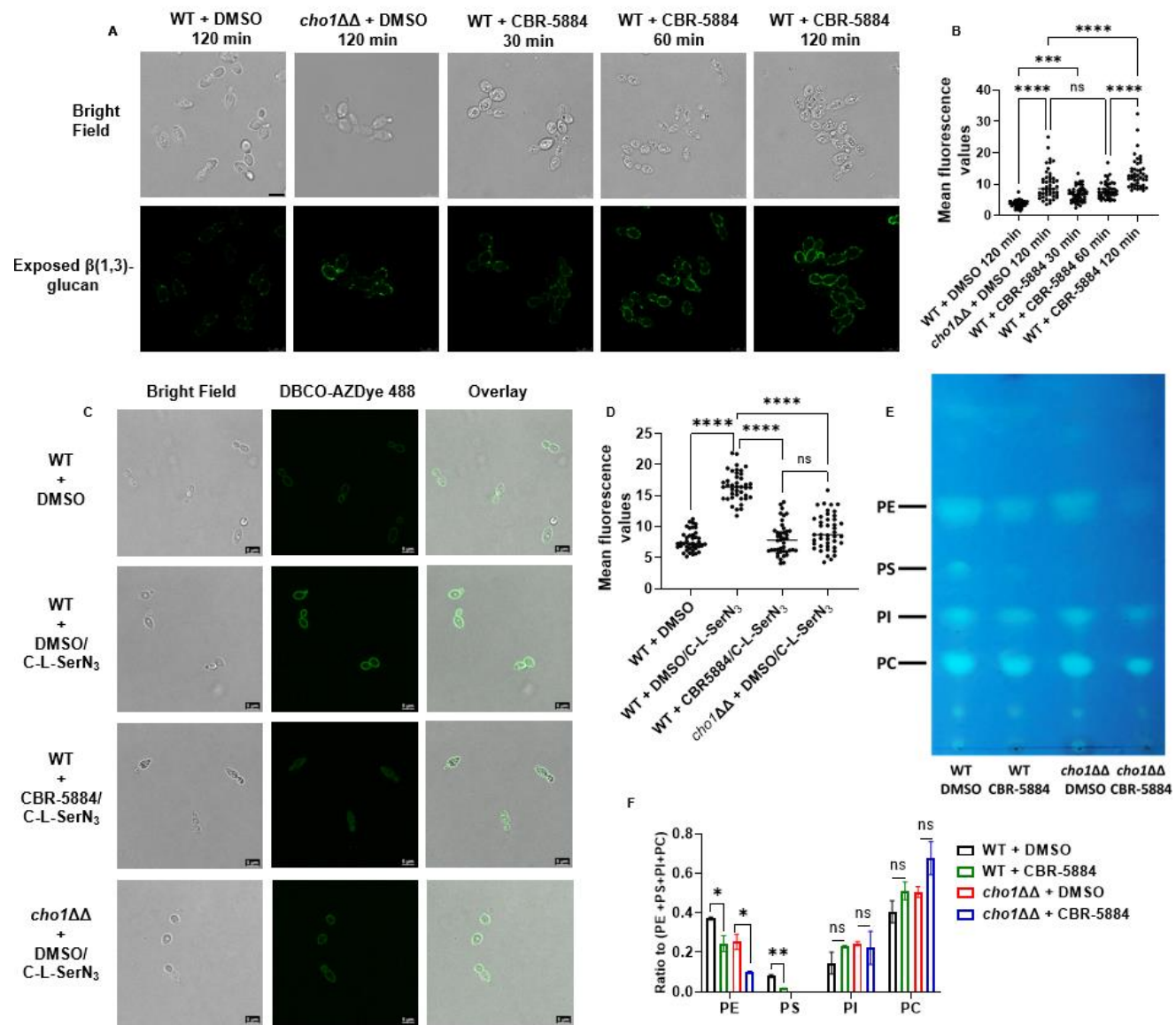
In contrast, LOC14 was also subjected to growth curve determination but no cells grew, in the presence or absence of ethanolamine (Figure 4.4E). This corroborates with Figure 4.4B that the inhibition by LOC14 is not acting solely on Cho1. Since the goal was a Cho1-specific inhibitor, ebselen and LOC14 were not pursued further.

CBR-5884 interferes with PS synthesis *in vivo*

It has been determined previously that deletion of Cho1 leads to increased exposure (unmasking) of cell wall $\beta(1-3)$ -glucan, rendering cells are more prone to be targeted by the immune system (14, 55). Here, we tested whether the CBR-5884 could induce unmasking. Wildtype *C. albicans* cells were grown in YPD supplemented with DMSO or CBR-5884 for 30, 60 and 120 min, along with *cho1* $\Delta\Delta$ strain, and exposed $\beta(1-3)$ -glucan was stained and visualized through confocal microscopy. The *cho1* $\Delta\Delta$ strain exhibited increased unmasked foci, compared to WT strain in DMSO, consistent with previous findings that disruption of Cho1 leads to increased unmasking (Figure 4.5A) (55). Similarly, CBR-5884 treatment showed increased unmasking after 30-min incubations, and the unmasking became more obvious at 60- and 120-min treatment. The mean fluorescence values confirmed that 30-min CBR-5884 treatment is sufficient to induce significantly increased unmasking compared to wildtype *C. albicans*, and 120-min

Figure 4.5 CBR-5884 interferes with *in vivo* PS synthesis.

(A) CBR-5884 induces cell wall $\beta(1,3)$ -glucan exposure. Exposed cell wall $\beta(1,3)$ -glucan of wildtype *C. albicans* treated with 170 μM CBR-5884 or equivalent DMSO control for time indicated are shown. Exposed $\beta(1,3)$ -glucan is shown as green fluorescence and the corresponding cells are shown in the bright field as well. (B) Quantification of the mean fluorescence from (A). Forty-six cells from at least 10 images were used for the quantification and shown. Statistics were conducted using one-way ANOVA and Tukey's multiple comparisons test (ns=not significant, $p > 0.05$; ****, $0.0001 > p$). (C) CBR-5884 interferes with the incorporation of C-L-SerN₃ probe into the cell membrane. A final concentration of 1.5 mM C-L-SerN₃ was added to wildtype *C. albicans* and *cho1* $\Delta\Delta$ cells grown with and without 170 μM CBR-5884. The cells were then stained with the DBCO-AZ Dye 488 to allow click-tagging, followed by microscopy. Corresponding brightfield and overlay images were also shown. Wildtype *C. albicans* grown without the C-L-SerN₃ probe was included as a control for background fluorescence. (D) Quantification of the mean fluorescence from (C). Forty cells from at least 10 images were used for the quantification and shown. Statistics were conducted using one-way ANOVA and Tukey's multiple comparisons test (ns=not significant, $p > 0.05$; ****, $0.0001 > p$). (E) Thin layer chromatography (TLC) plate of phospholipids extracted from wildtype and *cho1* $\Delta\Delta$ *C. albicans* treated with 170 μM CBR-5884 or equivalent DMSO. The positions of PS (phosphatidylserine), PE (phosphatidylethanolamine), PI (phosphatidylinositol) and PC (phosphatidylcholine) are indicated based on standards. (F) The ratio of the phospholipid to total (PE+PS+PI+PC) phospholipids for strains in (E). The quantification was done in ImageJ software from two TLC plates. Statistics were conducted using unpaired two-tailed t test (ns=not significant, $p > 0.05$; *, $0.05 > p > 0.01$, **, $0.01 > p > 0.001$).



treatment could induce more unmasking than *cho1* $\Delta\Delta$ strain (Figure 4.5B). This could be because CBR-5884 inhibition causes a sudden loss of Cho1 function that the cells have not yet adjusted to, whereas a *cho1* $\Delta\Delta$ mutant has adjusted its metabolism to the loss of PS. Alternatively, it may indicate an off-target effect. It is also interesting to note that there are dark structures in the cells under the bright field when treated with CBR-5884, which are absent in wildtype or *cho1* $\Delta\Delta$ strains without CBR-5884. We currently do not have evidence to explain the identity or formation of these structures, but speculate that they represent fragmented vacuoles that serve in detoxification (56).

In order to further measure the impact of CBR-5884 on PS synthesis *in vivo*, an assay for fluorescence-based labeling of PS via biorthogonal tagging using a clickable serine probe was utilized. This probe consists of a serine analogue carrying an azide tag for click chemistry, C-L-SerN₃, and can be incorporated into live cell membranes by infiltrating lipid metabolism to produce azide-tagged PS analogues that can be post-labeled via click-tagging with fluorophores to localized/quantify PS in cells (57, 58). Wildtype *C. albicans* was grown in YPD to early log phase before C-L-SerN₃ was added, along with CBR-5884 or DMSO (Figure 4.5C). The *cho1* $\Delta\Delta$ strain and no probe control were also included for background fluorescence, and mean fluorescence of each group was quantified (Figure 4.5D). In the absence of CBR-5884, C-L-SerN₃ labels the cell membrane of wildtype *C. albicans* with stronger fluorescence compared to no probe or *cho1* $\Delta\Delta$ strains (Figures 4.5C&D), indicating C-L-SerN₃ was converted into PS as previously described (57). However, in the presence of CBR-5884, the fluorescence is

significantly diminished on the periphery of the cell (Figures 4.5C&D). This indicates that CBR-5884 inhibits *in vivo* PS production.

Finally, a direct biochemical test for PS levels was performed by thin layer chromatography (TLC) in cells treated with CBR-5884. Wildtype *C. albicans* and *cho1* $\Delta\Delta$ strains were grown in the presence and absence of CBR-5884, and the four major phospholipid species are shown in Figure 4.5E and quantified in Figure 4.5F. Consistently, the relative PS level in wildtype *C. albicans* strain treated with CBR-5884 significantly dropped compared to the DMSO treatment (Figures 4.5E&F), indicating that CBR-5884 interferes with PS production. Interestingly, the relative PE levels also significantly decreased in strains treated with CBR-5884, especially in the *cho1* $\Delta\Delta$ strain without PS as a precursor (Figures 4.5E&F). This potentially indicates that CBR-5884 may independently impact PE production.

CBR-5884 acts as a competitive inhibitor that occupies the serine binding site of Cho1

To investigate the molecular mechanism by which CBR-5884 inhibits Cho1, purified Cho1 specific activity was assayed with varying concentrations of serine and CDP-DAG in the presence of CBR-5884. Serine was varied from 4 to 32 mM, CDP-DAG was kept at 200 μ M, and several concentrations of CBR-5884 were tested (Figure 4.6A). The pattern of inhibition fits with competitive inhibition and a low K_i value of $1,550 \pm 245.6$ nM. Next, serine was held at a sub-saturating concentration of 20 mM or a saturating concentration of 32 mM, and CDP-DAG was varied from 25 to 300 μ M. At the lower serine concentration, the inhibition of CBR-5884 on Cho1 activity was observed

Figure 4.6 CBR-5884 may function as a competitive inhibitor occupying the serine binding site of Cho1.

(A) Kinetics curve for serine in the presence of CBR-5884. CDP-DAG was kept constant at 200 μM (4.8 mol %), and the specific activities of purified hexameric Cho1 were plotted against various serine concentrations (4, 8, 16, 24, 32 mM) in the presence of 0, 100, 250, 500, 1000, 2000 nM CBR-5884. The curves best fit for competitive inhibition with a K_i value of 1550 ± 245.6 nM. The dots in all curves represent the mean values of two replicates, and the error bars are \pm standard deviation (S.D.) values. (B) Kinetics curve for CDP-DAG in the presence of CBR-5884. Serine was kept constant at 20 mM, and the specific activities of purified hexameric Cho1 were plotted against various CDP-DAG concentrations (25, 50, 100, 200, 300 μM , 4.2 – 5.0 mol %) in the presence of 0, 100, 250, 500 and 1000 nM CBR-5884. (C) Kinetics curve for CDP-DAG in the presence of CBR-5884 with 32 mM serine. Specific activities of purified hexameric Cho1 were plotted against various CDP-DAG concentrations in the presence of 0, 100, 250, 500, 1000 and 2000 nM CBR-5884. (D) Computational docking of serine and CBR-5884 into Cho1 AlphaFold structure. Top 5 poses of CBR-5884 (green) and serine (black) are shown within the active site of Cho1. CDP-DAG is shown as cyan and the conserved CAPT motif of Cho1 is highlighted in dark blue. (E) A model for the inhibition mechanism of CBR-5884 to Cho1. Cho1 follows a sequential bi-bi reaction, in which it has to bind CDP-DAG prior to serine for catalysis. In the presence of CBR-5884, CDP-DAG-bound Cho1 could either bind serine for reaction or CBR-5884 for no reaction.

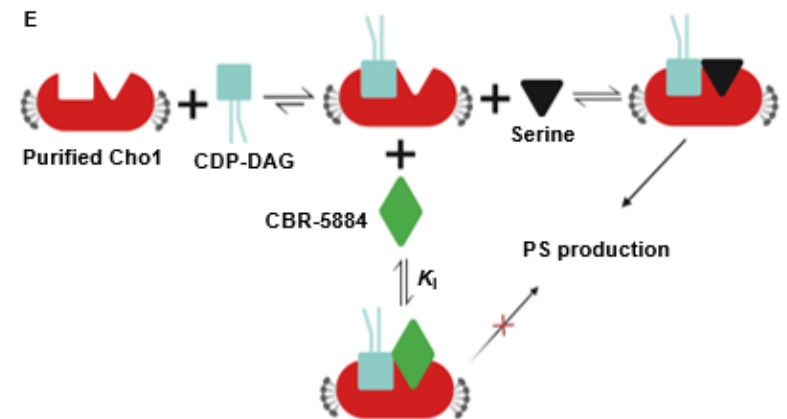
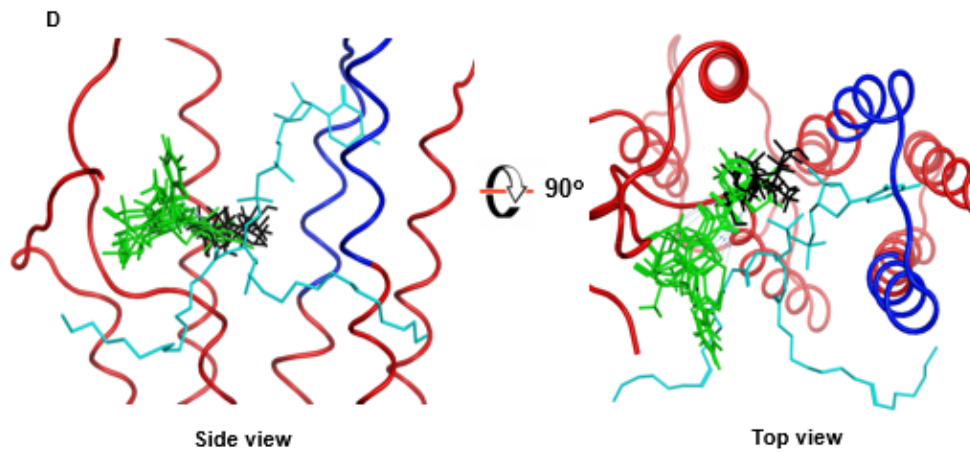
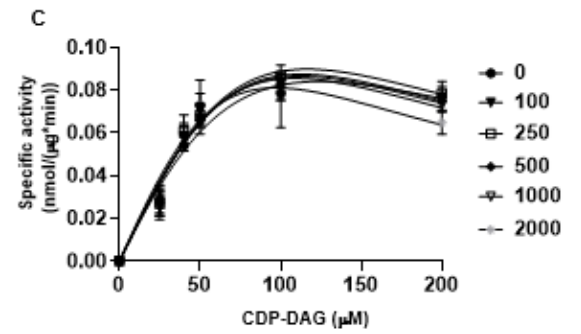
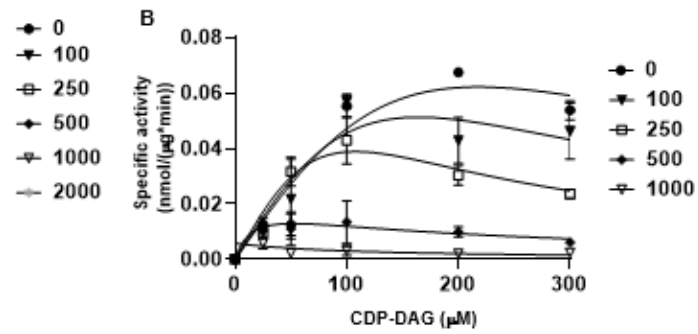
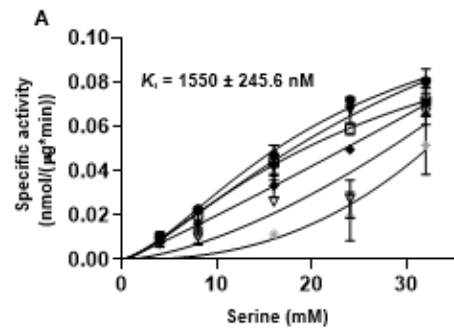


(Figure 4.6B), but the inhibition was overcome under saturating serine concentrations (Figure 4.6C). These results suggest that CBR-5884 inhibits Cho1 by competing for serine and can be outcompeted with a high serine concentration. It is interesting that CDP-DAG inhibits Cho1 activity at high concentrations, especially in the presence of CBR-5884 (Figure 4.6B). This substrate inhibition from CDP-DAG has been reported previously (22, 59).

To gather more insight for the serine competition, we computationally docked CBR-5884 into the active site of *C. albicans* Cho1. Since fungal PS synthases follow the ordered sequential bi-bi reaction mechanism where Cho1 binds CDP-DAG before serine for catalysis (25), we first generated a predicted CDP-DAG-bound *C. albicans* Cho1 structure by superposing *C. albicans* Cho1 AlphaFold model with the CDP-DAG-bound PS synthase from *Methanocaldococcus jannaschii* (PDB: 7B1L) (Figure S4.4A) (32).

The CDP-alcohol phosphotransferase (CAPT) binding motif, which is known to bind and catalyze CDP-DAG, is conserved and aligned between the *C. albicans* Cho1 and *M. jannaschii* PS synthase structures, so we hypothesized that the CDP-DAG from *M. jannaschii* PS synthase interacts with *C. albicans* Cho1 in a very similar manner, and thus is incorporated in the *C. albicans* Cho1 for docking. Next, we simulated and combined all the possible active site pockets from the CDP-DAG-bound *C. albicans* Cho1, and docked CBR-5884 and L-serine into these possible sites (Figure S4.4B). A total of 20,000 initial poses of CBR-5884 and serine were generated and then refined to 5 top poses with the highest docking scores (Figure 4.6D). All five CBR-5884 poses have overlap with the serine poses, with a higher docking score of -11.48 ± 0.12 kcal/mol

compared to the serine docking score of -6.72 ± 0.08 kcal/mol. This, corroborates the low K_i value and suggests that CBR-5884 likely competes with serine to occupy the serine binding pocket in Cho1. Here, we generated a scheme for CBR-5884 inhibition (Figure 4.6E). Following the first step in the sequential bi-bi reaction where Cho1 binds CDP-DAG, either CBR-5884 or serine can dock into the active site. The catalysis will occur if serine enters, and will not if CBR-5884 occupies the site. Since CBR-5884 is favored by Cho1, serine can only outcompete CBR-5884 at a high concentration.

Discussion

Here, we adapted a malachite green-based nucleotidase-coupled assay to screen for and identify inhibitors targeting *C. albicans* Cho1 (49). Since the amount of phosphate released is directly proportional to the CMP, and thus PS produced in the reaction, this method can be used to measure Cho1 activity in real time (Figure 4.1C). It is worth mentioning that besides CMP, the nucleotidase CD73 is known to cleave AMP to release phosphate in various studies (60-62), and given that this assay is suitable for 384-well plates or even 1536-well plates, it may potentially be applied to any enzyme producing AMP/CMP.

Ebselen, LOC14 and CBR-5884 stood out among seven Cho1-specific inhibitors due to their inhibitory effects on the *C. albicans* cell growth (Figure 4.3). Ebselen is an organo-selenium compound originally developed as a glutathione peroxidase mimic that acts on the cholesterol ester hydroperoxides and phospholipid hydroperoxides (63), and it has garnered significant attention in recent years due to its diverse therapeutic applications due to its anti-inflammatory, antioxidant and anticancer activity (64-69). In

addition, ebselen has exhibited notable *in vitro* and *in vivo* antifungal activity against a range of fungal pathogens, including *Candida* spp., *Fusarium* spp., *Aspergillus fumigatus* and *Cryptococcus neoformans* (70-72). Studies have shown that ebselen effectively inhibits fungal growth by targeting many key enzymes (73-78). Here, we have demonstrated again that ebselen inhibits wildtype *C. albicans* growth (Figures 4.3&4.4). The inhibition of purified Cho1 by ebselen is potent, with an IC₅₀ of 11.1 μM (Figure 4.2C), but the inhibition on Cho1 is very likely not the main cause for ebselen's inhibition of *C. albicans* growth, since ethanolamine cannot bypass the drug (Figure 4.4). Currently, we do not know the mechanism of ebselen's inhibition on Cho1, but given the tendency for ebselen to interact with cysteine residues (79), we hypothesize that ebselen might interact with residue C182, located in the putative serine-binding site of Cho1 (26), thus disrupting activity. Ebselen's promiscuous nature limits its clinical applicability.

Conversely, the antifungal effects of LOC14 and CBR-5884 are less well studied. LOC14 is a potent, non-covalent and reversible inhibitor for protein disulfide isomerase that has a neuroprotective effect in corticostriatal brain culture (80). In addition, LOC14 displayed promising effects against Huntington's disease (81) and can be used in a new anti-influenza therapeutic strategy (82). Here, we showed that LOC14 inhibits Cho1 activity (Figure 4.3), however, the *in vivo* inhibition is not likely conveyed through Cho1 (Figure 4.4). In contrast, CBR-5884 is an inhibitor of phosphoglycerate dehydrogenase, blocking *de novo* serine synthesis in cells, and is selectively toxic to cancer cell lines with high serine biosynthetic activity such as melanoma and breast cancer lines (54). Here, CBR-5884 was shown to not only inhibit purified Cho1 (Figures 4.2&4.6), but also

inhibit live cell growth by acting on the Cho1 *in vivo* (Figures 4.3-4.5). To our knowledge, this is the first paper showing the antifungal effects of LOC14 and CBR-5884.

CBR-5884 was then determined to be a competitive inhibitor of Cho1 with a K_i of 1550 ± 245.6 nM via kinetic analysis (Figure 4.6). Interestingly, in non-saturating serine concentrations (Figure 4.6B), the kinetic curves decreased in height and shifted to the left in the presence of increasing concentration of CBR-5884, indicating a decreasing K_m and V_{max} , mimicking an uncompetitive inhibition where the inhibitor binds to substrate-bound enzyme complex. This suggests that CBR-5884 is able to compete with serine by binding CDP-DAG-bound Cho1, and it cannot compete with CDP-DAG to bind to empty Cho1. The V_{max} of Cho1 in this study is estimated to be 0.128 ± 0.029 nmol/($\mu\text{g} \cdot \text{min}$), which is close to 0.088 ± 0.007 nmol/($\mu\text{g} \cdot \text{min}$) as described in (33). Also, it is worth mentioning that the curves where CDP-DAG was held constant and serine was varied follow a sigmoidal shape, which is consistent with previous finding that serine-binding may be cooperative (33), but the underlying mechanism is not clear. One small discrepancy has to be pointed out that the K_{half} of serine in this study is determined to be 21.88 ± 6.97 mM, which is five time higher than the 4.17 ± 0.45 mM from (33). The increased K_{half} may be explained by the presence of DMSO in this study, as DMSO has been shown to increase K_m in some enzymes (83-85).

CBR-5884 and serine were also docked onto the predicted CDP-DAG-bound Cho1 structure, and CBR-5884 was found to overlap with serine in the pocket (Figure 4.6D). A detailed ligand interaction map has shown that CBR-5884 almost shielded the

b-phosphorus of the CDP-DAG where the nucleophilic attack occurs (30, 35), and also some CBR-5884 poses directly interact with residues R186 and F190 in Cho1 (Figure S4.5), which are part of the putative serine-binding site and are shown to be essential for Cho1 activity (26). This indicates again that CBR-5884 inhibits Cho1 by competing with serine.

Our data strongly suggest that CBR-5884 inhibits Cho1 *in vivo*, however, Cho1 may not be the only cellular target of CBR-5884. This compound causes cells to become more unmasked than the *cho1* $\Delta\Delta$ mutant (Figure 4.5B). This could be due to sudden drop in PS caused by the compound compared with the *cho1* $\Delta\Delta$ mutant, which has adjusted to the change. However, it could also be due to inhibition of another target. In addition, in TLC analysis, it was revealed that CBR-5884 decreased PS and also impacted relative PE levels similarly to that seen in a *cho1* $\Delta\Delta$ mutant (Figures 4.5E&F). However, the CBR-5884 compound caused a greater decrease in PE levels in the *cho1* $\Delta\Delta$ mutant than that observed in wild-type or untreated *cho1* $\Delta\Delta$ cells. The compound also decreases growth of the *cho1* $\Delta\Delta$ strain in rich YPD media (Figure S4.6), suggesting that it has an additional target besides PS synthase. Since the *cho1* $\Delta\Delta$ strain cannot use PS as the precursor to make PE, the PE is made primarily via the Kennedy pathway, which requires CDP-ethanolamine phosphotransferase (14, 86). Cho1 and CDP-ethanolamine phosphotransferase belong to the same protein family and both use the CDP-alcohol phosphotransferase (CAPT) binding motif (29, 87, 88), so it is possible that CBR-5884 also inhibits CDP-ethanolamine phosphotransferase activity. Interestingly, PI synthase

also has the CAPT motif and binds CDP-DAG (89, 90), but the PI levels were not strongly affected (Figure 4.5E&F). Thus, the impact would be more specific ethanolamine phosphotransferase in this case.

This cross-reactivity could potentially be addressed by medicinal chemistry to synthesize analogs more specific for Cho1 and act at lower IC₅₀ so such a high concentration is not required, which could decrease off-target effects more likely. Moreover, the compounds could potentially be made more specific for Cho1. Importantly, we have novel proof of principle for successful pharmacological inhibition of a uniquely fungal enzyme central to phospholipid metabolism. Future rational drug design study will optimize CBR-5884 to be more specific for Cho1, as well as increase the solubility and potency of the compound in live cells.

Materials and Methods

Strain construction and media

This study used a *C. albicans* strain derived from SC5314 that was disrupted for *CHO1*, but had the gene complemented back with an affinity-tagged version. This strain *cho1ΔΔ P_{TEF1}-CHO1-ENLYFQG-HAx3-HISx8*, was made in this study and used to solubilize and purify Cho1. This strain expressed a Hisx8-tagged Cho1 protein from a strong constitutive promoter *P_{TEF1}*. To create this strain, a plasmid was generated that carried the tagged *CHO1* gene. This plasmid had a hygromycin B resistance gene, *CaHygB*, as a marker to go into strains. To make the plasmid pKE333, first the *CaHygB* marker cassette was amplified from the *CaHygB*-flipper plasmid (91) using primers

YZO113 & YZO114 having *NheI* and *MscI* cut site, respectively (Table 4.1). The *CaHygB* cassette was ligated into pKE4 plasmid (50), digested with *NheI* and *MscI*, to create the plasmid pKE4 - *CaHygB* (pKE333). Then, the *CHO1-ENLYFQG-HAx3-HISx8* gene, with the 3'UTR region was amplified from pYZ79 (33) using primers YZO110 & YZO111 and ligated into pKE333 to create the plasmid pYZ107. Plasmid pYZ107 was linearized with *PmlI* restriction enzyme (within the *P_{TEF1}* sequence) and electroporated into the *cho1ΔΔ* strain (14). Transformants were selected on YPD plates containing 600 µg/ml hygromycin B. Colony PCR was performed on six candidates for each gene construct to ensure the successful integration under the *P_{TEF1}* promotor on the chromosomal DNA, and no spurious mutations occurred during the transformation. Media used in this study include YPD (1% yeast extract, 2% peptone, 2% dextrose) and minimal medium (0.67% yeast nitrogen base W/O amino acids, 2% dextrose ± 1 mM ethanolamine).

Cell lysis, protein solubilization and purification

The *C. albicans* strain with His-tagged Cho1 expressed from *P_{TEF1}* was grown in YPD till the OD₆₀₀ reached between 7 and 8, then cells were lysed using a French press, as described in (47). Crude membranes were collected and solubilized with 1.5% digitonin as described in (33). His-tagged Cho1 was firstly purified via gravity affinity chromatography as describe in (33), and was further cleared by size exclusion chromatography (Superdex 200 10/300 GL column (Cytiva) attached to an NGC chromatography system Quest 10 plus (Bio-Rad)). The column was equilibrated with 1.5 column volumes of H₂O and 1.5 column volumes of elution buffer (50 mM Tris-HCl

Table 4.1. Primers used in this study

Primer name	Sequence	Purpose
YZO 110	aaaa <u>ATCGATATGTCAGACTCATCAGCTACCGGGTT</u> CTCC	F primer to clone <i>CHO1-ENLYFQG-HAx3-HISx8</i> gene into plasmid pKE333 (<i>ClaI</i> cut site underlined)
YZO 111	aaaa <u>ACGCGTACAGAACCAGAATTATTGTTTCAATT</u> GGGA	R primer to clone <i>CHO1-ENLYFQG-HAx3-HISx8</i> gene into plasmid pKE333 (<i>MluI</i> cut site underlined)
YZO 113	aaaa <u>GCTAGCCGTCAAACTAGAGAATAATAAAGA</u> AAACG	F primer to clone <i>CaHygB</i> gene into pKE4 to create pKE333 (<i>NheI</i> cut site underlined)
YZO 114	aaaa <u>TGGCCACTGCAGAGGACCACCTTTGATTGTAA</u> ATAG	R primer to clone <i>CaHygB</i> gene into pKE4 to create pKE333 (<i>MscI</i> cut site underlined)

(pH=8.0) + 0.04% digitonin) with a flow rate of 0.5 mL/min. Samples loaded onto the above column consisted of a concentrated Cho1 eluted from affinity chromatography that was filtered through 0.22 μ m filters that was then manually injected in the sample loop. The injected sample was eluted at a flow rate of 0.4 mL/min. Fractions containing Cho1 were pooled and subjected to AcTEV treatment, and then run through another round of affinity chromatography to remove impurities as described in (33). The resulting sample was loaded and checked on the blue-native PAGE for purity, oligomer state and homogeneity.

High-throughput malachite green screen

The Bioactives library was purchased from Selleck in 2014, and the remaining libraries (anti-infectives, FDA-approved Drug, and mechanism of action collections) were assembled from compounds available at the Chemical Biology and Therapeutics Department at St. Jude Children's Research Hospital (PMID: 33453364). All compounds were dissolved in DMSO and 100 nL was transferred to a 384-well clear bottom plate (ThermoFisher Scientific, cat# 265203) using a Beckman Echo 650 acoustic liquid handler. Equal volumes of either the selective CD73 nucleotidase inhibitor AB680 at a final concentration of 1 μ M (MedChemExpress, cat# HY-125286) or DMSO were used as positive and negative controls, respectively. A total of 30-35 ng of purified Cho1 protein was used in each reaction in 50 mM Tris-HCl (pH=8.0) for primary screening, combined with 100 μ M CDP-DAG (Avanti, cat# 870510), 5 mM serine, 0.4 ng CD73 nucleotidase (R&D systems, cat# EA002), 1 mM $MnCl_2$, 0.1% APX-100 and 0.1% digitonin, in a total volume of 10 μ L. Counter screen reactions were set up by replacing

only the purified Cho1 with 150 μ M CMP, with all other component remaining constant. The 10 μ L primary and counter screening reactions were delivered to each well of 384-well assay plate containing pre-aliquoted compounds from the library using a Multidrop Combi (ThermoFisher Scientific). This resulted in a DMSO concentration of 1%. After media transfer, assay plates were incubated for 3 hours at 30 °C. Plates were then removed and 32 μ L of malachite green mixture (6 μ L malachite A (2% (w/v) ammonium molybdate and 20% (v/v) sulfuric acid in H₂O) + 20 μ L H₂O + 6 μ L malachite B (0.1% (w/v) malachite green oxalate and 0.5% (w/v) polyvinyl alcohol in H₂O)) were added to each well via a MultiDrop Combi and incubated for an additional 10 minutes at room temperature. After incubation, plates were briefly centrifuged at 500 xg and absorbance at 620 nm was then measured using a Cytation7 plate reader (Biotek, Winooski, VT). Raw absorbance values of the compounds were normalized to DMSO (0% inhibition) and AB680 (100% inhibition) from both primary and counter screens, and % Δ inhibition was calculated by subtracting % inhibition from primary by % inhibition from counter screen. Z-factors for each plate were calculated using the in-house program RISE (Robust Investigation of Screening Experiments). All non-PAINs compounds that had >80% Δ inhibition progressed to dose-response testing (82 total compounds). Dose-response experiments were performed in triplicate as described above using a 10-point, threefold serial dilution with the top concentration for each compound tested being 200 μ M (Range: 0.010161-200 μ M). The absorbance at 620 nm was then measured using a PHERAstar FS multilabel reader (BMG, Cary, NC). Raw values were once again normalized to DMSO (0% inhibition) and AB680 (100% inhibition) and Z-factors for

each plate were calculated using RISE. The concentration of test compounds that inhibited protein by 50% (IC₅₀ value) as measured by the malachite green assay was computed using nonlinear regression-based fitting of inhibition curves using [inhibitor] vs. response-variable slope model in GraphPad Prism version 9.5.0 (GraphPad Software, La Jolla California USA).

Assay for metabolic labeling of PS using probe C-L-SerN₃

The C-L-SerN₃ probe ((*S*)-1-((3-azidopropyl)amino)-3-hydroxy-1-oxopropan-2-aminium chloride) was synthesized as described in (57). Cells grown overnight in YPD were washed three times in H₂O and inoculated into minimal media at a starting OD₆₀₀ of 0.05. Cells were shaken for 5 hours before 1.5 mM C-L-SerN₃ probe was added, along with 170 μM CBR-5884 or equivalent DMSO. Cells were then incubated for another 5 hours before being washed three times with H₂O, and 5% BSA in 1xPBS was used to treat cells for 20 min. The BSA was then removed, and cells were washed three times with 1xPBS, and then resuspended to OD₆₀₀ = 0.6 in 1 mL PBS + 1 μM AZDye 488 DBCO (Click chemistry tools, cat# 1278-1). Cells were covered with aluminum foil and rocked for 1 hour, and the dye was removed by centrifuging at 5,000 xg. Cells were washed with shaking at 1,000 rpm three times in 1xPBS, and resuspended in 200 μL Fluoromount-G mounting medium (cat# 00-4958-02). For each treatment, 10 μL of cell was added to a glass slide and 3 μL fresh Fluoromount-G mounting medium was used to mix the sample. Then, a Leica SP8 white light laser confocal microscope was used for imaging. The samples were excited using light at a wavelength of 488 nm, and the resulting fluorescence was captured within the range of 498 to 550 nm using a HyD detector. The

settings for laser strength, gain, and offset were maintained consistently throughout the experiment. Images of treated cells were taken after applying a zoom factor of 3. A total of 40 cells from at least 10 images were used for the quantification in ImageJ software.

Fluorescence imaging of unmasked $\beta(1-3)$ -glucan

Wildtype and *cho1* $\Delta\Delta$ cells were grown in YPD overnight (~16 hours), and back diluted to fresh YPD with $OD_{600} = 0.1$. The cells were then shaken at 225 rpm for 3 hours before 170 μ M CBR-5884 or equivalent DMSO were added. The cells were further shaken for 30, 60, 120 mins before the exposed $\beta(1-3)$ -glucan staining. The cells were stained as previously described (55, 92) with the exception that goat anti-mouse antibody conjugated to Alexa Fluor® 488 (Jackson ImmunoResearch) was used as the secondary antibody. For imaging, *Candida* cells were resuspended in 200 μ L of Fluoromount-G mounting medium and visualized with a Leica SP8 white light laser confocal microscope. The pictures were taken through Leica Application Suite X office software.

MIC plates tests and growth curves

MIC plate assays and growth curves were conducted in minimal media or minimal media supplemented with 1 mM ethanolamine (ETA). Wildtype SC5314 and *cho1* $\Delta\Delta$ strains were grown in YPD overnight and washed three times with H₂O before inoculation. The starting OD_{600} is 0.05 for both plate assays and growth curves. For MIC plates, both wildtype and *cho1* $\Delta\Delta$ strains were grown in flat-bottom 96-well plates at a final volume of 200 μ L, in the presence of different compounds or DMSO as indicated at 30°C. Leica light inverted microscope was then used to visualize growth after 24-hour incubation. In the meantime, cells grown in different compounds were subjected to live

cell counting. Cell cultures from flat-bottom 96-well plates after 24-hour incubation were diluted 100 to 10,000 times before plating on the minimal media, and the total colony forming unit (CFU) was kept within 200 for each plate. A total of six replicates were done in each condition.

The growth curves with different treatments were built from 2 hours to 30 hours with OD₆₀₀ measurement every two hours. A final concentration of 170 μ M CBR-5884, 430 μ M LOC14 and 5 mM serine was added into each group as indicated. Each curve was built in duplicates with six biological replicates. Growth rate (h^{-1}) and lag time (h) were calculated using GraphPad Prism software.

PS synthase assay

Enzymatic activity of Cho1 in the presence of the compounds was measured in the radioactive PS synthase assay. For purified Cho1, the procedure was fully described in (33). Briefly, 1-2 μ g of purified Cho1 was added in the reaction containing 50 mM Tris-HCl (pH = 8.0), 1 mM MnCl₂, 0.1% Triton X-100, 0.04% digitonin, 0.1 mM (4.7 mol %) 16:0 CDP-DAG (Avanti, cat# 870510) and 0.5 mM L-serine (spiked with 5% (by volume) L-[³H]-serine (15 Ci/mmol)) at a total volume of 100 μ L, in the presence of 100 μ M compounds or equivalent DMSO solvent. The reaction was conducted at 30 °C for 30 min and synthesized [³H]PS was measured using liquid scintillation counter. For crude membrane samples, crude membrane from wildtype and *cho1* $\Delta\Delta$ strains was collected and assayed as described in (33) with the exception that 2 mM L-serine (spiked with 5% (by volume) L-[³H]-serine (15 Ci/mmol)) was used in each reaction. A final concentration of 1 mM compounds was used for the crude membrane samples.

For the kinetic curves, the specific activity was measured in the reaction containing 50 mM Tris-HCl (pH = 8.0), 1 mM MnCl₂, 0.025-0.3% Triton X-100 and 0.033-0.07% digitonin with 0.75 to 1.5 µg purified Cho1 protein. The concentrations of 18:1 CDP-DAG (Avanti, cat# 870520) and serine were indicated in the graphs, and the mol % of CDP-DAG was kept between 4.2 – 5.0% for the curve where CDP-DAG was varied (Figures 4.6B & 4.6C) and at 4.8% (200 µM) for the curve where serine was varied (Figures 4.6A). The reaction was stopped at 20, 40 and 60 min, and specific activity was calculated based on the slope of linear PS production, representing the initial velocity.

Thin layer chromatography

Wildtype SC5314 and *cho1ΔΔ* strains grown overnight in YPD were inoculated into fresh YPD at OD₆₀₀ of 0.1 and were shaken for another 3 hours. Then, 170 µM CBR-5884 or equivalent DMSO solvent was added to both wildtype and *cho1ΔΔ* cultures, and cells were shaken for another 2 hours. Then, cells were washed with 1xPBS three times and normalized to a total OD₆₀₀ of 1. The phospholipids were extracted with hot ethanol method as described in (14). Whatman 250 µm silica gel aluminum backing plate (discontinued) was treated and separation of phospholipid was carried out as described in (93). Phospholipid standards PI, PE, PS and PC were purchased from Avanti. The quantification of the phospholipids was done in ImageJ software.

Computational docking

The computational docking was conducted in Molecular Operating Environment software (MOE, Chemical Computing Group, Ltd, Montreal, Canada). A CDP-DAG-bound *C. albicans* Cho1 structure was generated by superposing the *C. albicans* Cho1 AlphaFold model with the CDP-DAG-bound PS synthase from *Methanocaldococcus jannaschii* (PDB: 7B1L) (32). Structures from CBR-5884 and serine were introduced into the structure, and the system was quickly prepped and energy-minimized for docking. Potential docking sites were predicted by “site finder” function in MOE and all the sites having above 0 possibilities are combined for docking (Figure S4.4B). Both serine and CBR-5884 molecules were docked into the potential sites 20,000 times, and triangle matcher placement (scored by London dG) and rigid receptor refinement (scored by GBVI/WSA dG) were used to pick the top fives poses. The ligand interaction map was also generated in MOE.

Statistical analysis and molecular weight (MW) estimation on the gels

All the statistical analyses were performed with GraphPad Prism 9.1 software. The PS synthase activities were compared using ordinary (equal SDs) or Brown-Forsythe and Welch ANOVA tests (unequal SDs). Blue native PAGE and Coomassie Blue R-250 staining were conducted as described in (33) and all MW estimates were conducted in the band analysis tool of the Quantity One software (Bio-Rad).

Acknowledgments

The authors would like to thank Dr. Glen E. Palmer and Dr. Brian M. Peters from the University of Tennessee Health Science Center for their pKE4 and *CaHygB*-flipper plasmids. Reese Saho, a summer undergraduate student from Ohio Northern University, also helped with setting up the PS synthase assay. We also thank him for his work.

References

1. Morrell, M., Fraser, V. J., and Kollef, M. H. (2005) Delaying the empiric treatment of *Candida* bloodstream infection until positive blood culture results are obtained: a potential risk factor for hospital mortality *Antimicrobial agents and chemotherapy* 49, 3640-3645
2. Wisplinghoff, H., Bischoff, T., Tallent, S. M., Seifert, H., Wenzel, R. P., and Edmond, M. B. (2004) Nosocomial bloodstream infections in US hospitals: analysis of 24,179 cases from a prospective nationwide surveillance study *Clinical infectious diseases* 39, 309-317
3. Patel, P. K., Erlandsen, J. E., Kirkpatrick, W. R., Berg, D. K., Westbrook, S. D., Loudon, C. *et al.* (2012) The changing epidemiology of oropharyngeal candidiasis in patients with HIV/AIDS in the era of antiretroviral therapy *AIDS research and treatment* 2012,
4. Benedict, K., Singleton, A. L., Jackson, B. R., and Molinari, N. A. M. (2022) Survey of incidence, lifetime prevalence, and treatment of self-reported vulvovaginal candidiasis, United States, 2020 *BMC Women's Health* 22, 147
5. Novosad, S. A., Fike, L., Dudeck, M. A., Allen-Bridson, K., Edwards, J. R., Edens, C. *et al.* (2020) Pathogens causing central-line-associated bloodstream infections in acute-care hospitals—United States, 2011–2017 *Infection Control & Hospital Epidemiology* 41, 313-319
6. Brown, G. D., Denning, D. W., Gow, N. A., Levitz, S. M., Netea, M. G., and White, T. C. (2012) Hidden killers: human fungal infections *Science translational medicine* 4, 165rv113 10.1126/scitranslmed.3004404
7. Bustamante, C. I. (2005) Treatment of *Candida* infection: a view from the trenches! *Current opinion in infectious diseases* 18, 490-495
8. Kullberg, B., Filler, S., and Calderone, R. (2002) *Candida* and candidiasis ASM Press, Washington, DC,
9. Gow, N. A., Johnson, C., Berman, J., Coste, A. T., Cuomo, C. A., Perlin, D. S. *et al.* (2022) The importance of antimicrobial resistance in medical mycology *Nat Commun* 13, 5352
10. Pfaller, M., Neofytos, D., Diekema, D., Azie, N., Meier-Kriesche, H.-U., Quan, S.-P. *et al.* (2012) Epidemiology and outcomes of candidemia in 3648 patients: data from the Prospective Antifungal Therapy (PATH Alliance®) registry, 2004–2008 *Diagnostic microbiology and infectious disease* 74, 323-331
11. Holeman Jr, C. W., and Einstein, H. (1963) The toxic effects of amphotericin B in man *California medicine* 99, 90
12. Ghannoum, M. A., and Rice, L. B. (1999) Antifungal Agents: Mode of Action, Mechanisms of Resistance, and Correlation of These Mechanisms with Bacterial Resistance *Clinical Microbiology Reviews* 12, 501-517 10.1128/cmr.12.4.501
13. Whaley, S. G., Berkow, E. L., Rybak, J. M., Nishimoto, A. T., Barker, K. S., and Rogers, P. D. (2016) Azole Antifungal Resistance in *Candida albicans* and Emerging Non-*albicans Candida* Species *Front Microbiol* 7, 2173 10.3389/fmicb.2016.02173

14. Chen, Y. L., Montedonico, A. E., Kauffman, S., Dunlap, J. R., Menn, F. M., and Reynolds, T. B. (2010) Phosphatidylserine synthase and phosphatidylserine decarboxylase are essential for cell wall integrity and virulence in *Candida albicans* *Mol Microbiol* 75, 1112-1132 10.1111/j.1365-2958.2009.07018.x
15. Davis, S. E., Tams, R. N., Solis, N. V., Wagner, A. S., Chen, T., Jackson, J. W. *et al.* (2018) *Candida albicans* cannot acquire sufficient ethanolamine from the host to support virulence in the absence of de novo phosphatidylethanolamine synthesis *Infection and immunity* 86, e00815-00817
16. Konarzewska, P., Wang, Y., Han, G.-S., Goh, K. J., Gao, Y.-G., Carman, G. M. *et al.* (2019) Phosphatidylserine synthesis is essential for viability of the human fungal pathogen *Cryptococcus neoformans* *The Journal of biological chemistry* 294, 2329-2339 10.1074/jbc.RA118.006738
17. Braun, B. R., van Het Hoog, M., d'Enfert, C., Martchenko, M., Dungan, J., Kuo, A. *et al.* (2005) A human-curated annotation of the *Candida albicans* genome *PLoS Genet* 1, 36-57 10.1371/journal.pgen.0010001
18. Kohlwein, S. D., Kuchler, K., Sperka-Gottlieb, C., Henry, S. A., and Paltauf, F. (1988) Identification of mitochondrial and microsomal phosphatidylserine synthase in *Saccharomyces cerevisiae* as the gene product of the CHO1 structural gene *J Bacteriol* 170, 3778-3781
19. Kuchler, K., Daum, G., and Paltauf, F. (1986) Subcellular and submitochondrial localization of phospholipid-synthesizing enzymes in *Saccharomyces cerevisiae* *J Bacteriol* 165, 901-910
20. Gaigg, B., Simbeni, R., Hrastnik, C., Paltauf, F., and Daum, G. (1995) Characterization of a microsomal subfraction associated with mitochondria of the yeast, *Saccharomyces cerevisiae*. Involvement in synthesis and import of phospholipids into mitochondria *Biochimica Et Biophysica Acta (BBA)-Biomembranes* 1234, 214-220
21. Poole, M. A., Homann, M. J., Bae-Lee, M. S., and Carman, G. M. (1986) Regulation of phosphatidylserine synthase from *Saccharomyces cerevisiae* by phospholipid precursors *Journal of Bacteriology* 168, 668-672 10.1128/jb.168.2.668-672.1986
22. Carson, M. A., Atkinson, K. D., and Waechter, C. J. (1982) Properties of particulate and solubilized phosphatidylserine synthase activity from *Saccharomyces cerevisiae*. Inhibitory effect of choline in the growth medium *Journal of Biological Chemistry* 257, 8115-8121
23. Letts, V. A., and Henry, S. A. (1985) Regulation of phospholipid synthesis in phosphatidylserine synthase-deficient (chol) mutants of *Saccharomyces cerevisiae* *J Bacteriol* 163, 560-567
24. Letts, V. A., Klig, L. S., Bae-Lee, M., Carman, G. M., and Henry, S. A. (1983) Isolation of the yeast structural gene for the membrane-associated enzyme phosphatidylserine synthase *Proceedings of the National Academy of Sciences* 80, 7279-7283 10.1073/pnas.80.23.7279
25. Bae-Lee, M. S., and Carman, G. M. (1984) Phosphatidylserine synthesis in *Saccharomyces cerevisiae*. Purification and characterization of membrane-associated phosphatidylserine synthase *J Biol Chem* 259, 10857-10862

26. Zhou, Y., Cassilly, C. D., and Reynolds, T. B. (2021) Mapping the Substrate-Binding Sites in the Phosphatidylserine Synthase in *Candida albicans* *Frontiers in Cellular and Infection Microbiology* 11, 10.3389/fcimb.2021.765266
27. Nikawa, J., Tsukagoshi, Y., Kodaki, T., and Yamashita, S. (1987) Nucleotide sequence and characterization of the yeast PSS gene encoding phosphatidylserine synthase *Eur J Biochem* 167, 7-12 10.1111/j.1432-1033.1987.tb13297.x
28. Hjelmstad, R. H., and Bell, R. M. (1991) sn-1,2-diacylglycerol choline- and ethanolaminephosphotransferases in *Saccharomyces cerevisiae*. Nucleotide sequence of the EPT1 gene and comparison of the CPT1 and EPT1 gene products *J Biol Chem* 266, 5094-5103
29. Hjelmstad, R. H., and Bell, R. M. (1990) The sn-1,2-diacylglycerol cholinephosphotransferase of *Saccharomyces cerevisiae*. Nucleotide sequence, transcriptional mapping, and gene product analysis of the CPT1 gene *J Biol Chem* 265, 1755-1764
30. Gräve, K., Bennett, M. D., and Högbom, M. (2019) Structure of Mycobacterium tuberculosis phosphatidylinositol phosphate synthase reveals mechanism of substrate binding and metal catalysis *Communications Biology* 2, 175 10.1038/s42003-019-0427-1
31. Zhou, Y., and Reynolds, T. (2021) Identification of the substrate-binding sites in the phosphatidylserine synthase from *Candida albicans* *The FASEB Journal* 35, <https://doi.org/10.1096/fasebj.2021.35.S1.02666>
32. Centola, M., van Pee, K., Betz, H., and Yildiz, Ö. (2021) Crystal structures of phosphatidyl serine synthase PSS reveal the catalytic mechanism of CDP-DAG alcohol O-phosphatidyl transferases *Nat Commun* 12, 6982 10.1038/s41467-021-27281-w
33. Zhou, Y., Syed, J. H., Semchonok, D. A., Wright, E., Kyrilis, F. L., Hamdi, F. *et al.* (2023) Solubilization, purification, and characterization of the hexameric form of phosphatidylserine synthase from *Candida albicans* *Journal of Biological Chemistry* 299, 10.1016/j.jbc.2023.104756
34. Nogly, P., Gushchin, I., Remeeva, A., Esteves, A. M., Borges, N., Ma, P. *et al.* (2014) X-ray structure of a CDP-alcohol phosphatidyltransferase membrane enzyme and insights into its catalytic mechanism *Nat Commun* 5, 4169 10.1038/ncomms5169
35. Sciara, G., Clarke, O. B., Tomasek, D., Kloss, B., Tabuso, S., Byfield, R. *et al.* (2014) Structural basis for catalysis in a CDP-alcohol phosphotransferase *Nat Commun* 5, 4068 10.1038/ncomms5068
36. Clarke, O. B., Tomasek, D., Jorge, C. D., Dufresne, M. B., Kim, M., Banerjee, S. *et al.* (2015) Structural basis for phosphatidylinositol-phosphate biosynthesis *Nat Commun* 6, 8505 10.1038/ncomms9505
37. Dufresne, M. B., Jorge, C. D., Timóteo, C. G., Petrou, V. I., Ashraf, K. U., Banerjee, S. *et al.* (2020) Structural and Functional Characterization of Phosphatidylinositol-Phosphate Biosynthesis in Mycobacteria *Journal of Molecular Biology*

38. Wang, L., and Zhou, M. (2023) Structure of a eukaryotic cholinephosphotransferase-1 reveals mechanisms of substrate recognition and catalysis *Nat Commun* 14, 2753 [10.1038/s41467-023-38003-9](https://doi.org/10.1038/s41467-023-38003-9)
39. Wang, Z., Yang, M., Yang, Y., He, Y., and Qian, H. (2023) Structural basis for catalysis of human choline/ethanolamine phosphotransferase 1 *Nat Commun* 14, 2529 [10.1038/s41467-023-38290-2](https://doi.org/10.1038/s41467-023-38290-2)
40. Yang, B., Yao, H., Li, D., and Liu, Z. (2021) The phosphatidylglycerol phosphate synthase PgsA utilizes a trifurcated amphipathic cavity for catalysis at the membrane-cytosol interface *Current Research in Structural Biology* 3, 312-323 <https://doi.org/10.1016/j.crstbi.2021.11.005>
41. Nikawa, J.-I., and Yamashita, S. (1981) Characterization of phosphatidylserine synthase from *Saccharomyces cerevisiae* and a mutant defective in the enzyme *Biochimica et Biophysica Acta (BBA) - Lipids and Lipid Metabolism* 665, 420-426 [https://doi.org/10.1016/0005-2760\(81\)90254-X](https://doi.org/10.1016/0005-2760(81)90254-X)
42. Carman, G. M., and Matas, J. (1981) Solubilization of microsomal-associated phosphatidylserine synthase and phosphatidylinositol synthase from *Saccharomyces cerevisiae* *Can J Microbiol* 27, 1140-1149
43. KIYONO, K., MIURA, K., KUSHIMA, Y., HIKIJI, T., FUKUSHIMA, M., SHIBUYA, I. *et al.* (1987) Primary Structure and Product Characterization of the *Saccharomyces cerevisiae* CHO1 Gene That Encodes Phosphatidylserine Synthase1 *The Journal of Biochemistry* 102, 1089-1100 [10.1093/oxfordjournals.jbchem.a122147](https://doi.org/10.1093/oxfordjournals.jbchem.a122147)
44. Mandal, S., Moudgil, M. n., and Mandal, S. K. (2009) Rational drug design *European Journal of Pharmacology* 625, 90-100 <https://doi.org/10.1016/j.ejphar.2009.06.065>
45. Cassilly, C. D., Maddox, M. M., Cherian, P. T., Bowling, J. J., Hamann, M. T., Lee, R. E. *et al.* (2016) SB-224289 Antagonizes the Antifungal Mechanism of the Marine Depsipeptide Papuamide A *PLoS One* 11, e0154932 [10.1371/journal.pone.0154932](https://doi.org/10.1371/journal.pone.0154932)
46. Pokharel, M., Konarzewska, P., Roberge, J. Y., Han, G.-S., Wang, Y., Carman, G. M. *et al.* (2022) The Anticancer Drug Bleomycin Shows Potent Antifungal Activity by Altering Phospholipid Biosynthesis *Microbiology Spectrum* 10, e00862-00822 [doi:10.1128/spectrum.00862-22](https://doi.org/10.1128/spectrum.00862-22)
47. Cassilly, C. D., Farmer, A. T., Montedonico, A. E., Smith, T. K., Campagna, S. R., and Reynolds, T. B. (2017) Role of phosphatidylserine synthase in shaping the phospholipidome of *Candida albicans* *FEMS Yeast Res* 17, [10.1093/femsyr/fox007](https://doi.org/10.1093/femsyr/fox007)
48. Zhou, Y., Bruce, B., and Reynolds, T. (2022) Solubilization and purification of phosphatidylserine synthase from *Candida albicans* *The FASEB Journal* 36, <https://doi.org/10.1096/fasebj.2022.36.S1.L7431>
49. Wu, Z. L., Ethen, C. M., Prather, B., Machacek, M., and Jiang, W. (2011) Universal phosphatase-coupled glycosyltransferase assay *Glycobiology* 21, 727-733 [10.1093/glycob/cwq187](https://doi.org/10.1093/glycob/cwq187)
50. Willems, H. M. E., Bruner, W. S., Barker, K. S., Liu, J., Palmer, G. E., and Peters, B. M. (2017) Overexpression of *Candida albicans* Secreted Aspartyl Proteinase 2

- or 5 Is Not Sufficient for Exacerbation of Immunopathology in a Murine Model of Vaginitis Infection and immunity 85, 10.1128/iai.00248-17
51. Lawson, K. V., Kalisiak, J., Lindsey, E. A., Newcomb, E. T., Leleti, M. R., Debien, L. *et al.* (2020) Discovery of AB680: A Potent and Selective Inhibitor of CD73 *J Med Chem* 63, 11448-11468 10.1021/acs.jmedchem.0c00525
 52. Zhang, J.-H., Chung, T. D. Y., and Oldenburg, K. R. (1999) A Simple Statistical Parameter for Use in Evaluation and Validation of High Throughput Screening Assays *Journal of Biomolecular Screening* 4, 67-73 10.1177/108705719900400206
 53. Baell, J. B., and Nissink, J. W. M. (2018) Seven Year Itch: Pan-Assay Interference Compounds (PAINS) in 2017—Utility and Limitations *ACS Chemical Biology* 13, 36-44 10.1021/acscchembio.7b00903
 54. Mullarky, E., Lucki, N. C., Beheshti Zavareh, R., Anglin, J. L., Gomes, A. P., Nicolay, B. N. *et al.* (2016) Identification of a small molecule inhibitor of 3-phosphoglycerate dehydrogenase to target serine biosynthesis in cancers *Proc Natl Acad Sci U S A* 113, 1778-1783 10.1073/pnas.1521548113
 55. Davis, S. E., Hopke, A., Minkin, S. C., Montedonico, A. E., Wheeler, R. T., and Reynolds, T. B. (2014) Masking of $\beta(1-3)$ -Glucan in the Cell Wall of *Candida albicans* from Detection by Innate Immune Cells Depends on Phosphatidylserine Infection and immunity 82, 4405-4413 10.1128/iai.01612-14
 56. Weber, R. W. S. (2002) Vacuoles and the fungal lifestyle *Mycologist* 16, 10-20 [https://doi.org/10.1017/S0269-915X\(02\)00611-0](https://doi.org/10.1017/S0269-915X(02)00611-0)
 57. Ancajas, C. F., Alam, S., Alves, D. S., Zhou, Y., Wadsworth, N. M., Cassilly, C. D. *et al.* (2023) Cellular Labeling of Phosphatidylserine Using Clickable Serine Probes *ACS Chemical Biology* 18, 377-384 10.1021/acscchembio.2c00813
 58. Ancajas, C. F., Carr, A. J., Lou, J., Sagar, R., Zhou, Y., Reynolds, T. B. *et al.* (2023) Harnessing Clickable Acylated Glycerol Probes as Chemical Tools for Tracking Glycerolipid Metabolism *Chemistry – A European Journal* 29, e202300417 <https://doi.org/10.1002/chem.202300417>
 59. Antonsson, B. E. (1994) Purification and characterization of phosphatidylinositol synthase from human placenta *Biochemical Journal* 297, 517-522
 60. Antonioli, L., Pacher, P., Vizi, E. S., and Haskó, G. (2013) CD39 and CD73 in immunity and inflammation *Trends in molecular medicine* 19, 355-367
 61. Cardoso, A. M., Schetinger, M. R. C., Correia-de-Sá, P., and Sévigny, J. (2015) Impact of ectonucleotidases in autonomic nervous functions *Autonomic Neuroscience* 191, 25-38
 62. Duarte-Araújo, M., Nascimento, C., Timóteo, M. A., Magalhães-Cardoso, M. T., and Correia-de-Sá, P. (2009) Relative contribution of ecto-ATPase and ecto-ATPDase pathways to the biphasic effect of ATP on acetylcholine release from myenteric motoneurons *Br J Pharmacol* 156, 519-533 10.1111/j.1476-5381.2008.00058.x
 63. Maiorino, M., Roveri, A., and Ursini, F. (1992) Antioxidant effect of ebselen (PZ 51): Peroxidase mimetic activity on phospholipid and cholesterol hydroperoxides

- vs free radical scavenger activity Archives of biochemistry and biophysics 295, 404-409 [https://doi.org/10.1016/0003-9861\(92\)90534-4](https://doi.org/10.1016/0003-9861(92)90534-4)
64. Maiorino, M., Roveri, A., Coassin, M., and Ursini, F. (1988) Kinetic mechanism and substrate specificity of glutathione peroxidase activity of ebselen (PZ51) *Biochem Pharmacol* 37, 2267-2271 10.1016/0006-2952(88)90591-6
 65. Parnham, M., and Sies, H. (2000) Ebselen: prospective therapy for cerebral ischaemia *Expert Opinion on Investigational Drugs* 9, 607-619 10.1517/13543784.9.3.607
 66. Liang, Q., Shen, N., Lai, B., Xu, C., Sun, Z., Wang, Z. *et al.* (2019) Electrical Stimulation Degenerated Cochlear Synapses Through Oxidative Stress in Neonatal Cochlear Explants *Front Neurosci* 13, 1073 10.3389/fnins.2019.01073
 67. Haritha, C. V., Sharun, K., and Jose, B. (2020) Ebselen, a new candidate therapeutic against SARS-CoV-2 *Int J Surg* 84, 53-56 10.1016/j.ijssu.2020.10.018
 68. Nakamura, Y., Feng, Q., Kumagai, T., Torikai, K., Ohigashi, H., Osawa, T. *et al.* (2002) Ebselen, a glutathione peroxidase mimetic seleno-organic compound, as a multifunctional antioxidant. Implication for inflammation-associated carcinogenesis *J Biol Chem* 277, 2687-2694 10.1074/jbc.M109641200
 69. Jin, Z., Du, X., Xu, Y., Deng, Y., Liu, M., Zhao, Y. *et al.* (2020) Structure of Mpro from SARS-CoV-2 and discovery of its inhibitors *Nature* 582, 289-293 10.1038/s41586-020-2223-y
 70. Venturini, T. P., Chassot, F., Loreto É, S., Keller, J. T., Azevedo, M. I., Zeni, G. *et al.* (2016) Antifungal activities of diphenyl diselenide and ebselen alone and in combination with antifungal agents against *Fusarium* spp *Med Mycol* 54, 550-555 10.1093/mmy/myv120
 71. Thangamani, S., Eldesouky, H. E., Mohammad, H., Pascuzzi, P. E., Avramova, L., Hazbun, T. R. *et al.* (2017) Ebselen exerts antifungal activity by regulating glutathione (GSH) and reactive oxygen species (ROS) production in fungal cells *Biochimica et Biophysica Acta (BBA)-General Subjects* 1861, 3002-3010
 72. Sakita, K. M., Capoci, I. R. G., Conrado, P. C. V., Rodrigues-Vendramini, F. A. V., Faria, D. R., Arita, G. S. *et al.* (2021) Efficacy of Ebselen Against Invasive Aspergillosis in a Murine Model *Front Cell Infect Microbiol* 11, 684525 10.3389/fcimb.2021.684525
 73. Marshall, A. C., Kidd, S. E., Lamont-Friedrich, S. J., Arentz, G., Hoffmann, P., Coad, B. R. *et al.* (2019) Structure, Mechanism, and Inhibition of *Aspergillus fumigatus* Thioredoxin Reductase *Antimicrob Agents Chemother* 63, 10.1128/aac.02281-18
 74. Marshall, M. O., and Kates, M. (1974) Biosynthesis of Nitrogenous Phospholipids in Spinach Leaves *Canadian Journal of Biochemistry* 52, 469-482 10.1139/o74-071
 75. Billack, B., Pietka-Ottlik, M., Santoro, M., Nicholson, S., Młochowski, J., and Lau-Cam, C. (2010) Evaluation of the antifungal and plasma membrane H⁺-ATPase inhibitory action of ebselen and two ebselen analogs in *S. cerevisiae* cultures *J Enzyme Inhib Med Chem* 25, 312-317 10.3109/14756360903179419
 76. Chan, G., Hardej, D., Santoro, M., Lau-Cam, C., and Billack, B. (2007) Evaluation of the antimicrobial activity of ebselen: Role of the yeast plasma

- membrane H⁺-ATPase *Journal of Biochemical and Molecular Toxicology* 21, 252-264 <https://doi.org/10.1002/jbt.20189>
77. Azad, G. K., Singh, V., Mandal, P., Singh, P., Golla, U., Baranwal, S. *et al.* (2014) Ebselen induces reactive oxygen species (ROS)-mediated cytotoxicity in *Saccharomyces cerevisiae* with inhibition of glutamate dehydrogenase being a target *FEBS Open Bio* 4, 77-89 10.1016/j.fob.2014.01.002
 78. Azad, G. K., Balkrishna, S. J., Sathish, N., Kumar, S., and Tomar, R. S. (2012) Multifunctional Ebselen drug functions through the activation of DNA damage response and alterations in nuclear proteins *Biochem Pharmacol* 83, 296-303 10.1016/j.bcp.2011.10.011
 79. Terentis, A. C., Freewan, M., Sempértegui Plaza, T. S., Raftery, M. J., Stocker, R., and Thomas, S. R. (2010) The selenazal drug ebselen potently inhibits indoleamine 2,3-dioxygenase by targeting enzyme cysteine residues *Biochemistry* 49, 591-600 10.1021/bi901546e
 80. Kaplan, A., Gaschler, M. M., Dunn, D. E., Colligan, R., Brown, L. M., Palmer, A. G., 3rd *et al.* (2015) Small molecule-induced oxidation of protein disulfide isomerase is neuroprotective *Proc Natl Acad Sci U S A* 112, E2245-2252 10.1073/pnas.1500439112
 81. Zhou, X., Li, G., Kaplan, A., Gaschler, M. M., Zhang, X., Hou, Z. *et al.* (2018) Small molecule modulator of protein disulfide isomerase attenuates mutant huntingtin toxicity and inhibits endoplasmic reticulum stress in a mouse model of Huntington's disease *Hum Mol Genet* 27, 1545-1555 10.1093/hmg/ddy061
 82. Chamberlain, N., Korwin-Mihavics, B. R., Nakada, E. M., Bruno, S. R., Heppner, D. E., Chapman, D. G. *et al.* (2019) Lung epithelial protein disulfide isomerase A3 (PDIA3) plays an important role in influenza infection, inflammation, and airway mechanics *Redox Biol* 22, 101129 10.1016/j.redox.2019.101129
 83. Chen, Q. X., Liu, X. D., and Huang, H. (2003) Inactivation kinetics of mushroom tyrosinase in the dimethyl sulfoxide solution *Biochemistry (Mosc)* 68, 644-649 10.1023/a:1024665709631
 84. Milčić, N., Stepanić, V., Crnolatac, I., Findrik Blažević, Z., Brkljača, Z., and Majerić Elenkov, M. (2022) Inhibitory Effect of DMSO on Halohydrin Dehalogenase: Experimental and Computational Insights into the Influence of an Organic Co-solvent on the Structural and Catalytic Properties of a Biocatalyst *Chemistry – A European Journal* 28, e202201923 <https://doi.org/10.1002/chem.202201923>
 85. Ostermeier, L., Oliva, R., and Winter, R. (2020) The multifaceted effects of DMSO and high hydrostatic pressure on the kinetic constants of hydrolysis reactions catalyzed by α -chymotrypsin *Physical Chemistry Chemical Physics* 22, 16325-16333
 86. Cassilly, C. D., and Reynolds, T. B. (2018) PS, It's Complicated: The Roles of Phosphatidylserine and Phosphatidylethanolamine in the Pathogenesis of *Candida albicans* and Other Microbial Pathogens *J Fungi (Basel)* 4, 10.3390/jof4010028
 87. McMaster, C. R., and Bell, R. M. (1994) Phosphatidylcholine biosynthesis in *Saccharomyces cerevisiae*. Regulatory insights from studies employing null and

- chimeric sn-1,2-diacylglycerol choline- and ethanolaminephosphotransferases J Biol Chem 269, 28010-28016
88. Williams, J. G., and McMaster, C. R. (1998) Scanning alanine mutagenesis of the CDP-alcohol phosphotransferase motif of *Saccharomyces cerevisiae* cholinephosphotransferase J Biol Chem 273, 13482-13487
10.1074/jbc.273.22.13482
 89. Paulus, H., and Kennedy, E. P. (1960) The enzymatic synthesis of inositol monophosphatide Journal of Biological Chemistry 235, 1303-1311
 90. Fischl, A. S., and Carman, G. M. (1983) Phosphatidylinositol biosynthesis in *Saccharomyces cerevisiae*: purification and properties of microsome-associated phosphatidylinositol synthase Journal of Bacteriology 154, 304-311
 91. Liu, J., Vogel, A. K., Miao, J., Carnahan, J. A., Lowes, D. J., Rybak, J. M. *et al.* (2022) Rapid Hypothesis Testing in *Candida albicans* Clinical Isolates Using a Cloning-Free, Modular, and Recyclable System for CRISPR-Cas9 Mediated Mutant and Revertant Construction Microbiol Spectr 10, e0263021
10.1128/spectrum.02630-21
 92. Chen, T., Jackson, J. W., Tams, R. N., Davis, S. E., Sparer, T. E., and Reynolds, T. B. (2019) Exposure of *Candida albicans* β (1,3)-glucan is promoted by activation of the Cek1 pathway PLOS Genetics 15, e1007892
10.1371/journal.pgen.1007892
 93. Vaden, D. L., Gohil, V. M., Gu, Z., and Greenberg, M. L. (2005) Separation of yeast phospholipids using one-dimensional thin-layer chromatography Analytical biochemistry 338, 162-164

Supplementary Figures

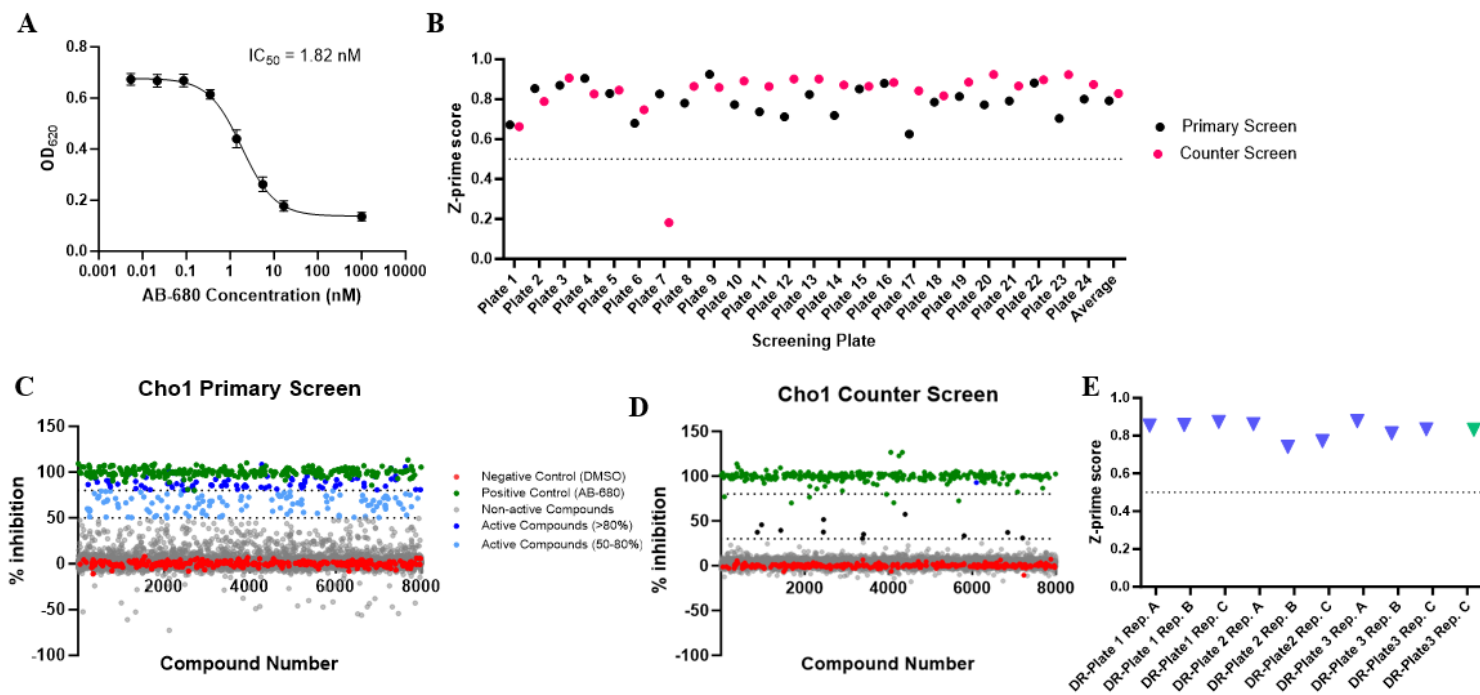


Figure S4.1. (A) Dose-response curve of AB-680 compound. The dots represent the mean of nine replicates, and the error bars are \pm standard deviation (S.D.) values. (B) Z-prime scores of plates in the primary and counter screens. (C) Z-prime scores of plates in the dose-response curves for the second-round screen.

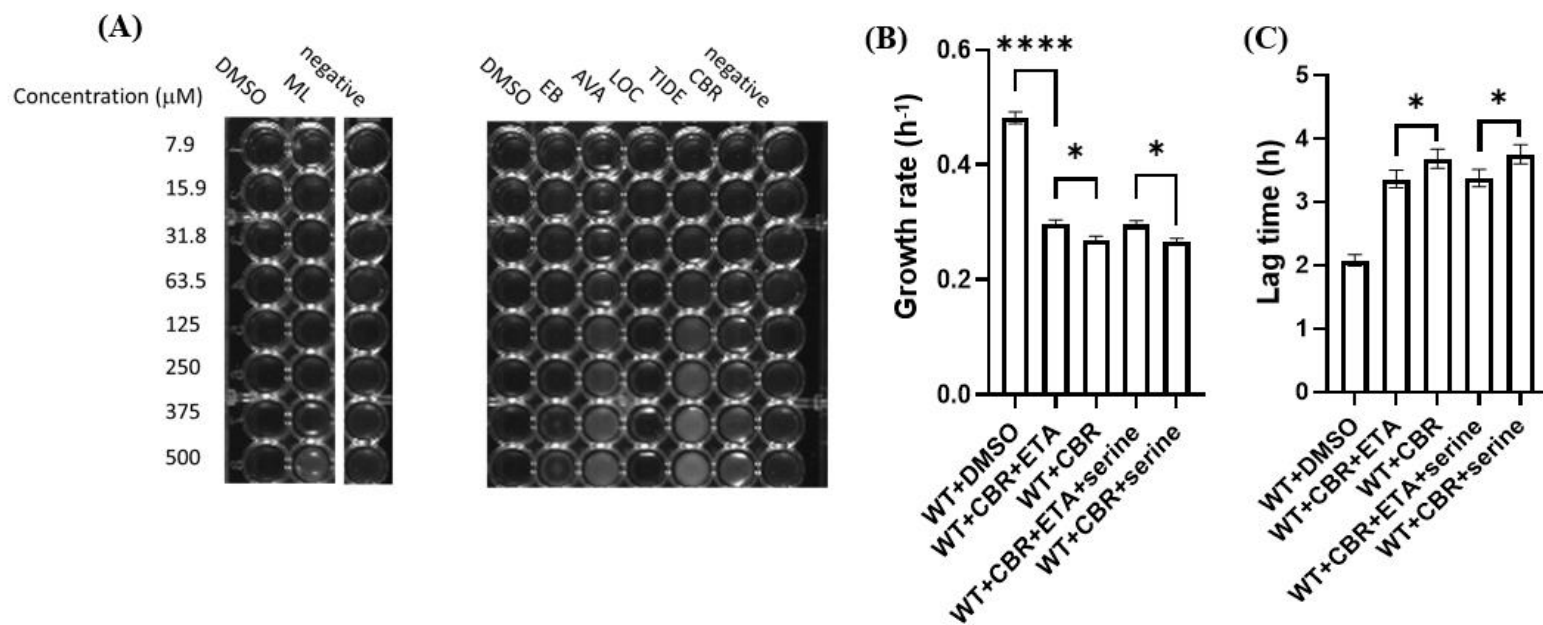


Figure S4.2. (A) Avasimibe, tideglusib and CBR-5884 precipitated at high concentrations; (B, C) The growth rate (h^{-1}) (B) and lag time (h) (C) were calculated from Figure 4D. Statistics were conducted using one-way ANOVA and Tukey's multiple comparisons test (ns=not significant, $p > 0.05$; *, $0.05 > p > 0.01$, ****, $0.0001 > p$).

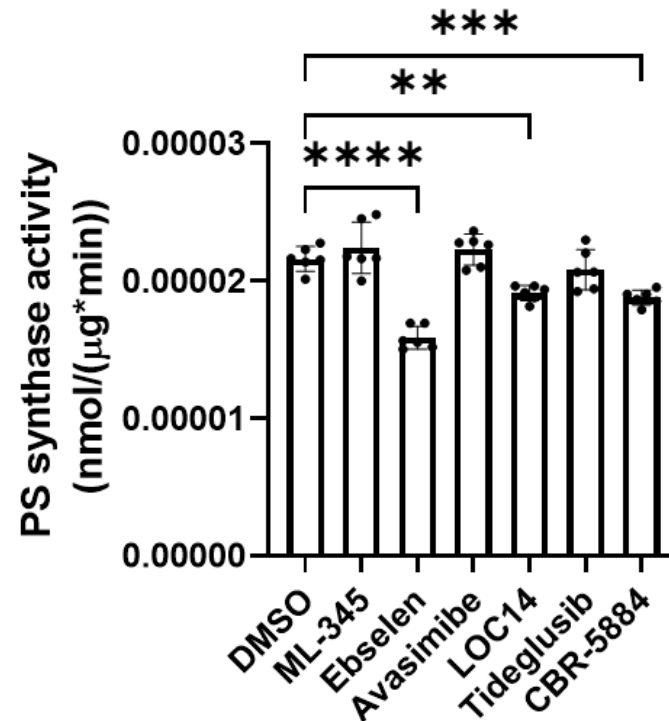


Figure S4.3. The PS synthase activity of crude membrane containing Cho1 was measured by L-[³H]-serine incorporation into PS in the presence of different inhibitors at 1 mM, and are presented as nmol/(μg protein*min). Statistics were conducted using one-way ANOVA and Dunnett's T3 multiple comparisons test (**, 0.01 > p > 0.001; ***, 0.001 > p > 0.0001; ****, 0.0001 > p). The activities were measured in duplicate with a total of six biological replicates as indicated. The bars represent the mean values and the error bars are ± S.D. values.

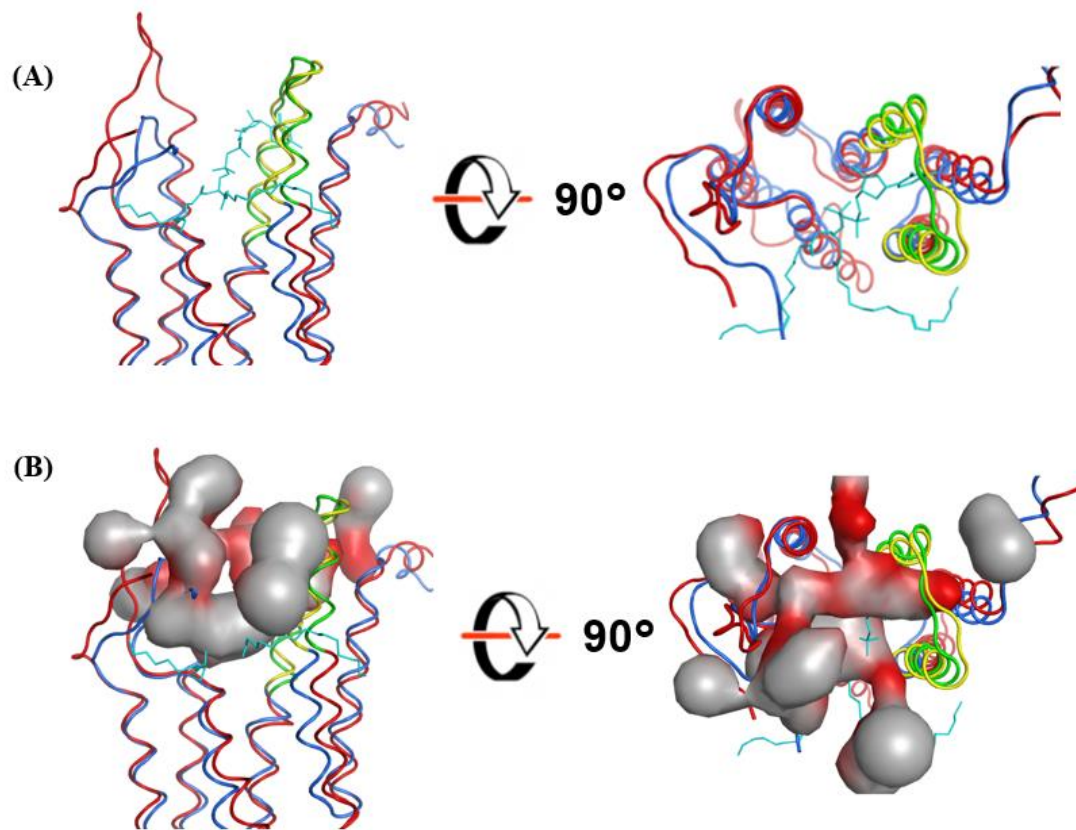
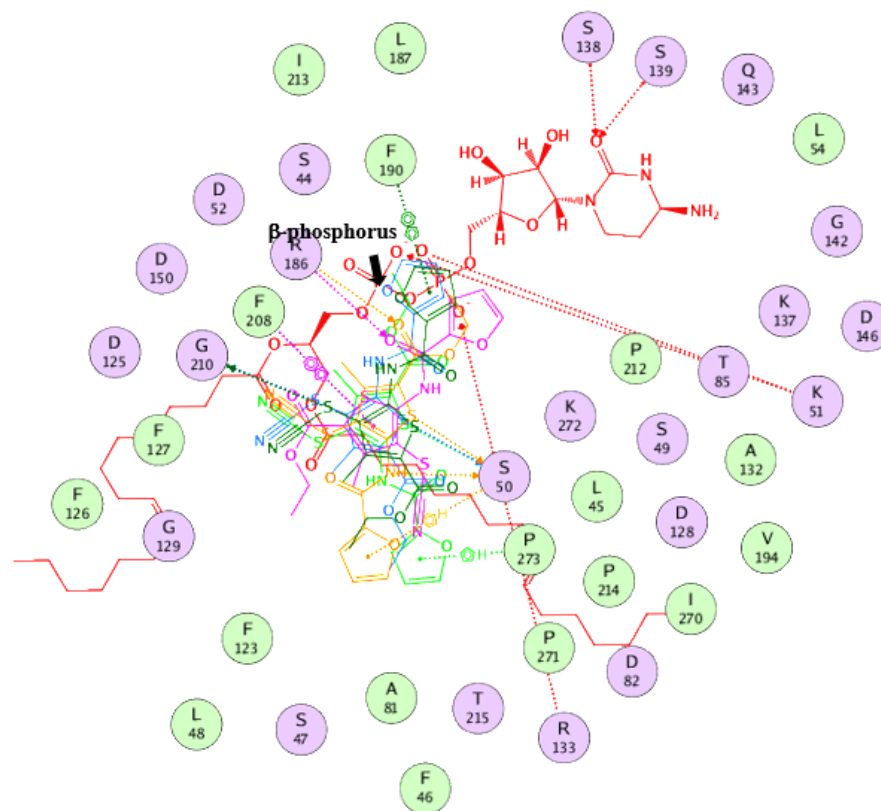


Figure S 4.4. (A) Superposition of *C. albicans* AlphaFold Cho1 model (red) with *Methanocaldococcus jannaschii* PS synthase (blue) (PDB: 7B1L). The conserved CAPT site are highlighted as green and yellow, respectively. CDP-DAG (cyan) is *Methanocaldococcus jannaschii* PS synthase (PDB: 7B1L). (B) All the possible active site pockets predicted from *C. albicans* Cho1 using MOE are shown as pocket surfaces.



CBR-5884 MOE(S) = -11.48 ± 0.12 kcal/mol
Serine MOE(S) = -6.72 ± 0.08 kcal/mol

Figure S4.5. Overlay of ligand interactions between top five poses of CBR-5884 with *C. albicans* AlphaFold Cho1 model. The bound CDP-DAG is also shown and the β -phosphorus is indicated. Dotted lines indicate interactions. Docking scores MOE(S) of serine and CBR-5884 were shown.

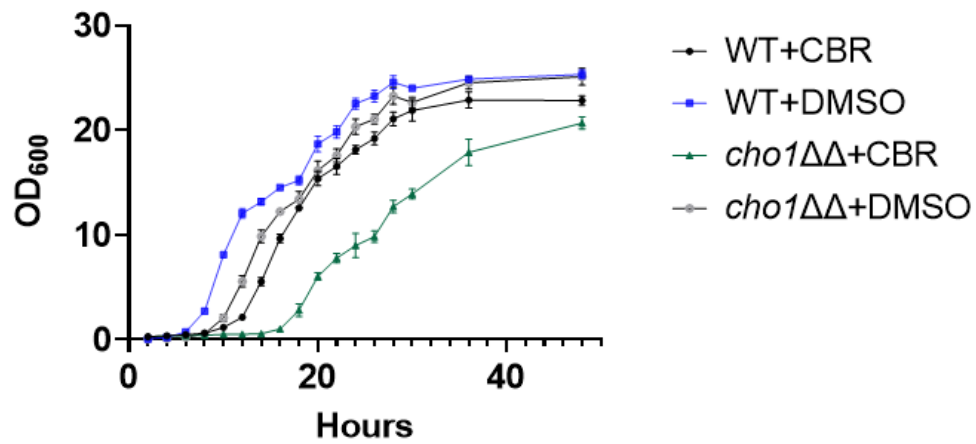


Figure S4.6. Growth curve of wildtype and *cho1ΔΔ* *C. albicans* strains in the presence of 170 μ M CBR-5884 or equivalent DMSO in YPD from 0 to 48 hours. The dots represent the mean values of six replicates, and the error bars are \pm standard deviation (S.D.) values

CHAPTER 5 FUTURE DIRECTIONS

Introduction

My Ph.D. project involves studying a membrane-bound enzyme called phosphatidylserine (PS) synthase or Cho1, which is a promising drug target for treating *Candida* infections. A large amount of data have been presented in chapters 2-4. These results came from the experiments that worked, but there are a number of unpublished results from approaches which were less successful that may potentially be helpful in thinking of future directions. Here, the results from the main chapters will be discussed, and the “omitted” details of unpublished work and some future directions will be discussed.

Additional serine-binding residues have been predicted using AlphaFold Cho1 structure

My Ph.D. began by investigating certain predicted substrate-binding residues of *Candida albicans* PS synthase via site-directed mutagenesis. As a result, some critical substrate-binding were identified and characterized. In Chapter Two, it was shown that almost all the conserved residues in the CDP-alcohol phosphotransferase (CAPT) motif are involved in activity, and a large proportion of the putative serine-binding site residues are also involved in the Cho1 function. Since the CAPT motif is conserved in the protein family, where some human homologs exist, targeting the CAPT motif for drug development can be risky. This left the serine-binding site as a more attractive target for characterization. The fact that the CBR-5884 molecule competes with serine for binding Cho1 and is relative specific for Cho1 strengthens this claim. Therefore, characterization of the whole serine binding site, including additional residues involved in serine binding, could be very informative.

The putative serine binding site was predicted by amino acid sequence alignment. The AlphaFold predicted structure of Cho1, which came out after the publication of my chapter two could be used to improve the prediction of new residues. To facilitate this, an amino acid sequence alignment of 100 different fungal PS synthases was performed to identify conserved residues, and the rationale is that since these fungal PS synthases are closely related and are all capable of binding serine, some of the conserved residues should be critical for serine binding. Besides the residues previously characterized, we have found an additional 28 conserved residues from the alignment that might be essential for protein functions. To narrow down targets from the alignment, we will start with residues that are proximal to the potential serine binding pocket in the 3D structure. This potential serine binding pocket was predicted by superposing the existing *Methanocaldococcus jannaschii* PS synthase structure (PDBID: 7POW) on *C. albicans* Cho1 from Alpha Fold. Due to the conservation between the active sites, the bound serine from *M. jannaschii* PS synthase is very likely to mimic that from the *C. albicans* Cho1. Therefore, only residues conserved among the 100 fungal PS synthase alignment, within 10 Å distance from the serine molecule will be chosen for further characterization. A total of seven residues fulfill this requirement, and they are S139, Q143, E144, S147, N191, S193 and V194. So far, mutants S139A, Q143A, E144A, S147A, N191A and S193A have been made and tested for *in vitro* PS synthase activity. V194A is being generated now. All of those mutations need to be tested for growth curve and spot dilution assay, and interesting ones need to be characterized for the kinetics, either on the crude membrane or the purified form.

Enzymatic kinetic curves were possible with the R189A and L184A mutants because they they did not completely lose activities. Many mutants that have been made totally lost activity, and thus are not measurable for the kinetics curves. However, loss of activity could indicate a loss of catalytic activity or substrate-binding ability, which the kinetic curves alone cannot clarify, so a binding assay needs to be developed. Isothermal calorimetry (ITC) and surface plasmon resonance (SPR) are two ways to measure binding. ITC requires a large amount of purified Cho1 protein and thus is very tedious and expensive, and SPR requires labeling of the purified Cho1 and the setup of the experiment can take up to months (plus we do not have an SPR machine on campus), so a more straightforward method is needed. Here, we propose a saturation binding assay inspired by “sigma receptor binding assays” published in 2016 by Uyen B. Chu and Arnold E. Ruoho. Briefly, the crude membrane containing different PS synthase mutants will be incubated with a range of [³H]-serine concentrations in 96-well plates. Then, the incubated membrane samples will be filtered through glass fiber filter papers and washed several times to eliminate abundant unbound substrate. The retained radioactivity on the filter will be subjected to liquid scintillation spectroscopy for radioactivity. The level of radioactivity could give us an estimate of the total binding of [³H]-serine to the membrane. The crude membrane from the *cho1Δ/Δ* strain will be used as a nonspecific binding control for the assay. The specific binding data will be calculated as total binding data subtracted by nonspecific binding. The specific binding data will then be analyzed by nonlinear regression analysis for single-site binding using Prism software to yield an apparent K_d , which directly indicates the substrate-binding affinity of different mutants. However, if the crude membrane protein fails to generate reliable specific binding results,

we could also potentially subject the purified Cho1 to this saturation binding assay, which requires much less protein compared to ITC.

Besides the potential serine-binding residues, three conserved residues from the sequence alignment, I96, L148 and L151, are located on the interface between the two protomers in the Cho1 dimer, and thus are very likely to be involved in the dimerization of Cho1. The alanine mutants of these three residues are being made. Once I96A, L148A and L151A are made, they will be solubilized using either digitonin or SMA 2000 before being pulled down, and then run on the Blue Native PAGE to check oligomer states. Lower oligomers are expected to be seen if these residues are involved in dimerization.

Enzymatic characterization of different Cho1 oligomers can potentially answer the biological meaning of oligomerization

Chapter Three is more focused on solubilizing and purifying the membrane-bound Cho1 protein, which is challenging due to the low abundance of membrane proteins in the membrane and the need to solubilize them in the enzymatically active form. For the solubilization process, six detergents, as well as three styrene maleic acids, were tested and it turned out that digitonin was the best solubilizing reagent to retain Cho1 activity and conformation. Cho1 was purified as a hexameric form, which is unique because all the other members of this family with solved structures are dimers. We have three hypotheses for the higher oligomeric state of purified Cho1. First, the hexameric form of *C. albicans* Cho1 could be fungal-specific because all eight structures from the same protein family are from prokaryotes, with no fungal counterpart available. The special fungal phospholipid profile could promote the formation of hexamers, which could be preserved by detergents. Second, the hexameric form of *C. albicans* Cho1 could result

from the overexpression cassette we used to express Cho1. We can test this by purifying Cho1 from a non-overexpressor strain and checking the oligomer state. We now have an antibody to Cho1. The third possibility is that the hexameric Cho1 complex could be a pre-oligomer. Our biochemical and negative staining TEM data suggested that the hexameric Cho1 is likely made of a trimer of dimers. Since we harvested the membrane from cells in log phase ($OD_{600} = 6-8$) instead of the stationary phase, which others have done, it is likely the hexameric Cho1 form is a pre-processed form, which dissociates into dimers during the stationary phase. This can be tested by harvesting membranes from cells at different growth stages, solubilizing Cho1 from those membranes, and comparing the oligomer states.

Furthermore, it is interesting to compare the specific activities of Cho1 of different oligomer states. Cho1 exhibits cooperative binding for serine. Cho1 could function as a monomer, but it also forms dimers and tetramers. The cooperative serine binding pattern could result from the cooperativity among different protomers within the oligomer. Currently, Cho1 hexamers can be broken into dimers upon adding a basic solution, but there is currently no method to dissociate the dimers into monomers that are still functional. One possible method for getting different Cho1 oligomers is to pull down Cho1 from the DDM-solubilized fraction, as different oligomers exist in the DDM-solubilized fraction. The SMA2000 solubilized fraction also had two Cho1 species, one corresponds to a dimer and the other to a hexamer, which can also be used for this purpose. Then, size exclusion chromatography can be used to separate different oligomers, followed by the *in vitro* PS synthase assay for specific activity. This will

answer a very fundamental biological question of whether the oligomerization of Cho1 is necessary.

Purification yield for Cho1 can be further increased

In Chapter Four, over 7,300 bioactive small molecules with known biological targets were screened against purified Cho1 to identify potential inhibitors of PS synthase using a high-throughput assay. To increase the protein purification yield, protein expression and solubilization and purification methods were further optimized. When two copies of *CHO1* were simultaneously expressed from from P_{TEF2} and P_{ENO1} promoters in the same cell, and the expression of Cho1 was much higher, but the PS synthase activity per mg membrane protein decreased significantly (data not shown). This is very likely due to misfolding of protein or deprivation of essential lipids per Cho1 protein on the crude membrane due to the overexpression. Also, it is worth mentioning that *C. albicans* has many proteins with internally consecutive histidine residues that interfere with the affinity chromatography purification. If possible, another expression system (e.g., insect cells) could be used to solve these issues.

To improve solubilization, the digitonin concentration was changed from 1% to 1.5% for a higher solubilization rate. However, due to the gentle nature of digitonin, the unsolubilized fraction still has a lot of PS synthase activity. DDM has a higher solubilization rate and also retained Cho1 activity, but different oligomers exist in the pulled-down sample as shown in Chapter Three. Also, efforts are needed to optimize the affinity chromatography, size exclusion chromatography, and TEV protease treatment used for DDM-treated samples, as initial attempts failed to purify Cho1 from DDM-solubilized fractions. In the meantime, since only six detergents have been screened for

solubilization, more detergents could be tried for a cheaper (digitonin is very expensive) and more complete solubilization, which can also be compatible with our purification scheme.

It is worth pointing out that the C-terminally attached affinity tag interferes with Cho1 activity as indicated by a lower specificity activity of tag-uncleaved Cho1 compared to the tag-free Cho1, so a tag cleavage is necessary for purifying active Cho1. Both TEV and thrombin proteases have been tried for the tag cleavage. TEV protease recognizes amino acid sequence (ENLYFQ/G), and cleaves the protein between Q and G, while thrombin recognizes (LVPR/GS) and cleaves between R and G. It was shown that purified Cho1 with the thrombin recognition site residues after cleavage (LVPR) has low specific activity compared to that with the TEV leftover residues (ENLYFQ). This can be potentially explained by the net positive charge of the thrombin site leftover (LVPR) compared to the net negative charge of the TEV site leftover (ENLYFQ), but the underlying mechanism is unknown. However, both thrombin and TEV have low protease activity at 4°C, which is the temperature for the tag cleavage. Here, I propose the 3C protease to be used for the tag cleavage in the future. The recognition site of 3C protease is (LEVLFG/GP), and cleaves between Q and G. The cleavage leftover has a net negative charge similar to TEV, and most importantly, its optimal working temperature is 4°C and could also resist detergent interference. With all these benefits, 3C protease could help increase the purification yield.

The first identified Cho1 inhibitor, CBR-5884, can be further optimized

For the screening, a nucleotidase-coupled malachite green-based assay was designed to detect inhibitors that target *C. albicans* Cho1. The phosphate released from

the reaction directly correlates with the amount of CMP, indicating the level of PS generated, allowing us to measure Cho1 activity in real-time. Using the nucleotidase inhibitor AB-680 as a positive control produced a four-fold difference in the signals between the positive and negative controls, resulting in promising average Z' scores of approximately 0.8. Given this assay's compatibility with 384-well or even 1536-well plates, it could potentially be employed for any enzyme that produces CMP as a main or side product.

The small molecule screening identified seven inhibitors that completely inhibit Cho1, and one molecule, CBR-5884, is particularly interesting because it inhibits not only purified Cho1 but also its function *in vivo*, thus being an on-target inhibitor. However, CBR-5884 also reduced PE production, but only in the absence of *CHO1*, which may potentially act on CDP-ethanolamine phosphotransferase (Ept1). To test this, we can simply modify the existing *in vitro* PS synthase assay to measure the activity of *C. albicans* Ept1 in the presence of CBR-5884. *CaEpt1* catalyzes two reactions--- it catalyzes CDP-ethanolamine and DAG into PE, and also catalyzes CDP-choline and DAG into PC. Since radioactive labeled CDP-ethanolamine is not commercially available without a very expensive synthesis step, we can probe the activity of Ept1 by measuring the incorporation of [³H]CDP-choline into [³H]PC in the absence and presence of CBR-5884. This will tell us whether CBR-5884 inhibits *CaEpt1* or not.

Further characterizations have shown that CBR-5884 is a competitive inhibitor of Cho1 for serine with a K_i of $1.55 \pm 0.25 \mu\text{M}$, and it is the first inhibitor of PS synthase discovered to our knowledge. Despite the low micro-molar K_i value for purified Cho1, the MIC of CBR-5884 in *C. albicans* cells is very high (170 μM). This indicates that (1)

CBR-5884 has poor cell permeability and thus requires modification or a special delivery method (e.g., liposome delivery), or (2) CBR-5884 interacts with the native membrane surrounding Cho1 in a way that decreases its potency. Optimization of the CBR-5884 molecule is required in each scenario, which requires an understanding of interactions between CBR-5884 and Cho1. For this, crosslinking compounds can be used to covalently attach CBR-5884 to purified Cho1, followed by trypsin digest and mass spectrometry to identify the residues directly interacting with CBR-5884. Moreover, fragments and derivatives of CBR-5884 can be synthesized and tested for potency. CBR-5884 is made of furan, acetamide, thiophene, thiocyanate and ethyl acetate moieties, which can be fragmented or combined in different ways to determine the effective structure. For example, in the detailed CBR-5884/Cho1 interaction (Figure S4.5), three of the five top poses predicted the furan group protruding towards/overlapping with the β -phosphorus of CDP-DAG, which is known to interact with the catalytic core D150 of Cho1. This suggests that the furan group can be replaced with bulkier function groups (e.g., benzene ring) for stronger inhibition. In addition, residue F208 is predicted to form π - π interaction with the thiophene group of CBR-5884. This can be validated by mutating F208 to alanine and checking the inhibition of CBR-5884 on the resulting mutant. The information from the CBR-5884 derivatives, combined with the interacting residues, will provide an overview of the ligand/protein binding map.

One CBR-5884 derivative, F0882-0799, has been tested on purified Cho1 and it showed inhibition at a much higher concentration (data not shown). This F0882-0799 compound does not have the thiocyanate moiety and also has the ethyl acetate tail in a different conformation. Currently, we do not know whether it is the thiocyanate, ethyl

acetate, or both that lead to the decrease in the inhibition, but the fact that this CBR-5884 derivative inhibited Cho1 strengthens the claim that the CBR-5884 is a reversible inhibitor and fits into the active site pocket for inhibition. Besides CBR-5884, more Cho1-specific inhibitors can be identified through a larger-scale screening. A large number of inhibitors will provide essential information on the pharmacophore, and thus aid in rational drug design or *in silico* screening.

Structural work on Cho1 using cryo-EM

Besides these, efforts have also been made to determine the structure of the hexameric Cho1 through a collaboration with Dr. Melanie Ohi from the University of Michigan. A low-resolution density map has been generated from TEM using the pulled-down Cho1, which shows the overall shape of the protein. However, when a large quantity of purified Cho1 protein was subjected to cryo-EM, the inference from the digitonin micelles prevented from getting a high-resolution structure. Therefore, we decided to put purified Cho1 into the lipid nanodisc and remove all the digitonin. After purification of Cho1 via affinity chromatography and size exclusion chromatography, MSP1E3D1 scaffold protein was used, and digitonin was slowly removed using dialysis. The lipid nanodiscs will simultaneously form with and without Cho1. Thus, Cho1-containing lipid nanodisc was purified and concentrated by another size exclusion chromatography followed by affinity chromatography. The purified Cho1-containing lipid nanodiscs showed high homogeneity on negative staining electron microscopy and a following 2D class analysis. However, initial cryo-EM screening on the Cho1-containing lipid nanodisc was not successful, probably due to the fact that the sample was not freshly made. More trials and optimizations have to be done, given that the lipid nanodisc

approach is promising so far. In the future, one improvement can be made on the lipid compositions in the lipid nanodisc. Currently, a stoichiometry of 9:1 detergent-solubilized POPC and cholesterol at a final concentration of 10 mM was used for the lipid nanodisc construction, and the Cho1 lost ~30% activity in the lipid nanodisc. It was previously suggested that phosphatidic acid (PA) and PI significantly stimulated Cho1 activity due to the negative charges, so incorporation of these two phospholipids in the lipid nanodisc would potentially increase Cho1 activity in the nanodisc. More studies are required to identify the optimal ratios of these phospholipids in the sense that they both form a solid lipid nanodisc and also retain/stimulate Cho1 activity.

Conclusion

Combining the small molecule screening and structure biology, a new class of antifungal targeting *C. albicans* Cho1 can be developed. Good luck to whomever take this project after I leave.

**APPENDIX RECONSTITUTION OF PURIFIED HEXAMERIC
CHO1 FROM *CANDIDA ALBICANS* INTO LIPID NANODISC FOR
STRUCTURE DETERMINATION**

This section was included as an Appendix because the story is largely incomplete, and significant amount of work is required to make it a real chapter. However, it provides information for further researchers to complete the story.

Contributing author list: Yue Zhou, Jacquelyn Roberts, Melanie D. Ohi and Todd B. Reynolds

Introduction

Systemic infections by *Candida spp.* are associated with high mortality rates. Limitations in the current antifungals fail to mitigate the high mortality, so a new class of antifungals is in demand. In this regard, the phosphatidylserine synthase from *Candida albicans*, a membrane protein encoded by the *CHO1* gene, has been identified as a potential drug target for new antifungals. Inhibitors of Cho1 could be used as lead compounds for drug development. Rational drug design is one way to develop specific inhibitors, but the lack of Cho1 protein structure prevents an effective and insightful drug design. Previously, Cho1 has been solubilized and purified as a hexamer to relative homogeneity (as shown in Chapter three) for structure determination via cryo-electron microscopy (cryo-EM). However, we failed to obtain a structure of high resolution due to the high flexibility of the purified Cho1 and the inference of detergent micelles (data not shown). Therefore, we decided to reconstitute the purified hexameric Cho1 into lipid nanodisc. In this appendix, the detailed protocols and results for reconstructing Cho1 lipid nanodisc are described.

Method

Reconstructing purified Cho1 into MSP1E3D1 lipid nanodisc

Cho1 was first purified using affinity chromatography coupled with size-exclusive chromatography (SEC) as described in Chapter four. Fractions containing Cho1 protein from SEC were combined and concentrated prior to lipid nanodisc reconstitution. Phospholipid POPC and cholesterol, dissolved in chloroform, were aliquot into glass tube at a stoichiometry of 9:1, dried with nitrogen gas, and then solubilized in 50 mM Tris-

HCl (pH=8.0) with 2% digitonin to a final concentration of 10 mM. To dissolve the lipids, the mixture was vortexed for 30 seconds to ensure thorough mixing. Following this, mixture was sat at room temperature (RT) for a minimum of 30 minutes, followed by another vortex for 30 seconds. Then, a water bath sonication was performed until the lipids fully dissolved into the solution. Probe sonication can also be used to help solubilizing phospholipid in the solution (be careful not to take the glass tube because it will shatter).

Once the lipids are dissolved in solution as reflected by a relatively clear appearance, purified Cho1, lipids, and MSP1E3D1 (non-histagged, Cube Biotech # 26162) were combined at a predetermined molar ratio of Cho1:MSP:lipids = 1:2:300 for a final volume of 500 μ L. These components were combined and incubated on ice for 1 hour. Then, the mixture was slowly dialyzed against 50 mM Tris-HCl (pH=8.0). The first dialysis was done in a 500 mL buffer for three hours, and the buffer was changed to fresh, and sample was then dialyzed overnight. Next morning, the mixture was loaded on SEC to separate the Cho1-filled nanodiscs from the empty ones (Figure A1A). All SEC fractions containing Cho1-filled nanodiscs were combined and purified again via affinity chromatography. The purified Cho1-filled nanodiscs were checked on SDS-PAGE for successful lipid nanodisc constitution and purity prior to negative staining electron microscopy.

Results and Discussion

Following nanodisc formation and purification, Cho1-filled nanodiscs were checked on SDS-PAGE (Figure A1B). As shown, SEC separation was not able to remove

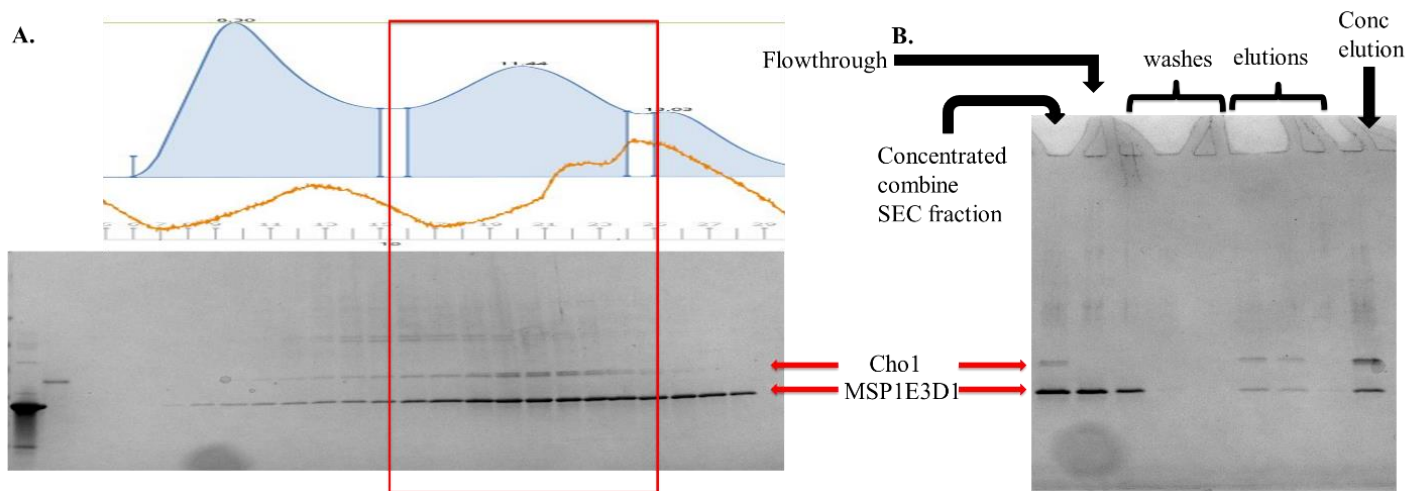


Figure A1. Purified Cho1 was successfully reconstituted into lipid nanodisc.

(A) Size exclusion chromatography and corresponding fractions on the SDS-PAGE shows co-elution of Cho1 and MSP1E3D1. (B) SDS-PAGE gel of each step in the affinity chromatography purification of Cho1-filled nanodiscs.

all the empty lipid nanodiscs from the mixture as reflected by a high ratio of MSP1E3D1 to Cho1 protein in the SEC fractions, as Cho1-filled nanodisc should have 1:1 ratio of MSP1E3D1 and Cho1, so affinity chromatography is necessary. The elution from the affinity chromatography then yielded a 1:1 ratio of Cho1 and MSP1E3D1 bands on SDS-PAGE, indicating high purity. The purified Cho1-containing lipid nanodiscs was checked using negative staining TEM and showed high homogeneity on a following 2D class analysis and 3D reconstruction (Figure A2), thus suitable for cryo-EM analysis.

However, the activity of Cho1 in the lipid nanodisc decreased compared to the micelle form (Figure A3), so a further optimization in the lipid composition in the nanodisc is required. Also, the Cho1-filled lipid nanodisc dissembled after one freeze and thaw (data not shown), so fresh sample preparation is always needed for cryo-EM in the future.

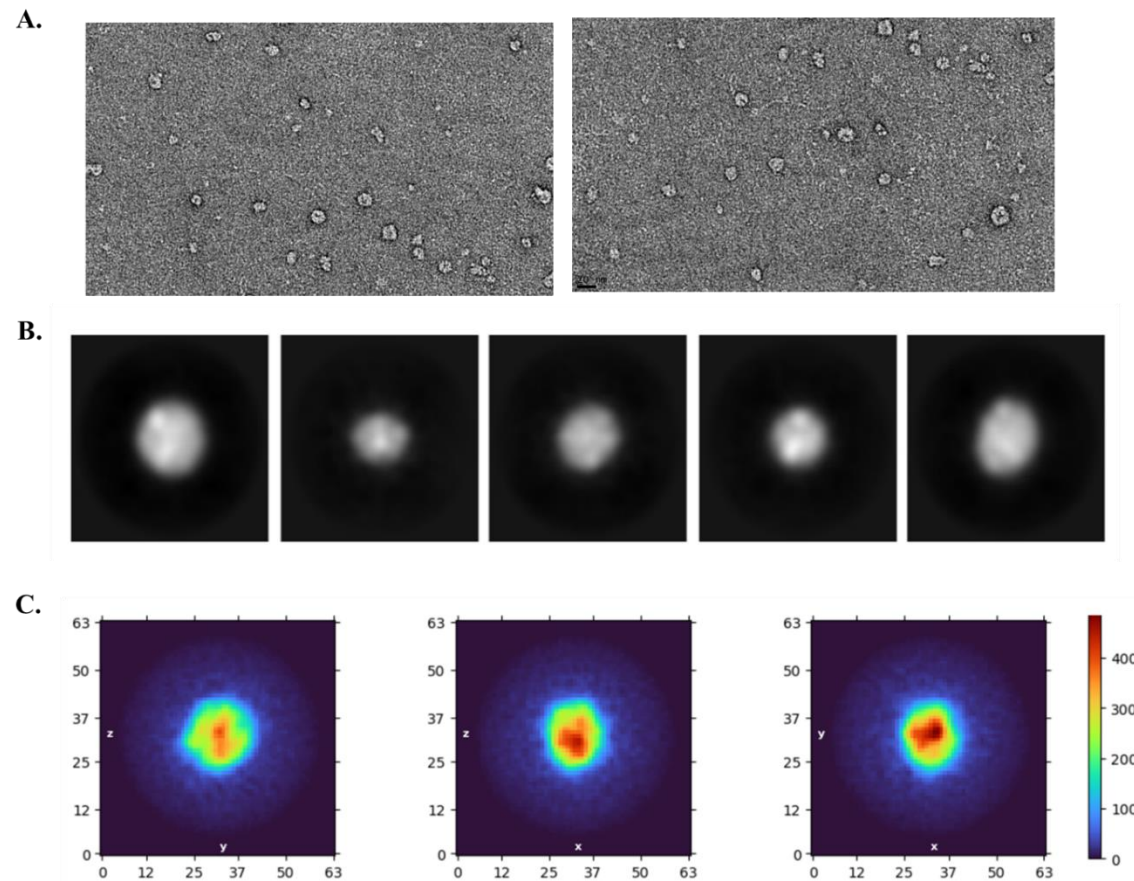


Figure A2. Purified Cho1-filled nanodiscs showed high homogeneity

(A) Purified Cho1-filled nanodisc under negative staining electron microscopy (twenty-fold dilution). (B) 2D averages of Cho1-filled nanodiscs in negative stain. (C) Low-resolution *ab initio* 3D reconstructions of negatively stained Cho1-filled nanodiscs. The red areas in the center of the round nanodiscs show the presence of Cho1.

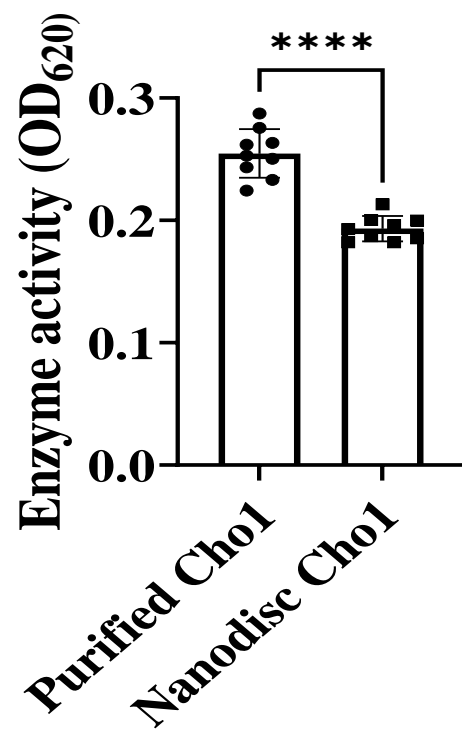


Figure A3. Enzyme activity of Cho1 in the micelle form and Cho1 in the lipid nanodiscs measured by malachite green.

VITA

Yue Zhou (Aeric) was born in Zhengzhou, Henan province, China, on 21 October 1992. He attended high school at the prestigious Zhengzhou No.1 high school, and won the 72nd place among over 5,000 participants in the Science Olympiad competition of biology in 2010. He graduated in 2011, moved to Xianyang, Sha'an Xi province and attended the Northwest Agriculture & Forestry University, where he completed a bachelor's degree in engineering with a major in Viticulture and Enology. Following graduation, he went to the California State University, Fresno, to start research in microbiology and biochemistry under Dr. Hwan Youn, where he completed the degree of Master of Science with a major in Biology. He then moved to the University of Tennessee, Knoxville, to continue his research in microbiology and biochemistry with guidance from Dr. Todd Reynolds. During graduate school, he enjoyed lifting weights and traveling with his wife Yiqun (Yuki) Liu whenever possible. After he failed his 1st attempt in the prelim, he brought Charlie Wagner to his family, who is a cute Pembroke Welsh corgi. He completed his Doctor of Philosophy degree in Microbiology in October 2023, right before his 31st birthday.